



The
University
Of
Sheffield.

**Synthesis and characterisation of analogous linear and highly
branched poly(n-butyl methacrylate)s for cell-polymer
interaction *in vitro***

Ohood Yousef Alyamani

Submitted for the degree of Master of Philosophy

Department of Chemistry

April 2018

ACKNOWLEDGEMENTS

Firstly, I thank God for giving me the strength and patience to finish this work. There are numerous people who have contributed to my success during my period of research studying at the Universities of Sheffield and Bradford. I would like to thank all these people here to show my appreciation for their energy, effort, patience and time in helping to finish this work.

I am grateful to my supervisor, Prof. Stephen Rimmer, for giving me the opportunity to work with him and to conduct research in his research group, and for sharing his knowledge about science.

From the University of Sheffield, I would like to thank all staff in the Chemistry Department. Special thanks go to Dr. Kayleigh, who was the first person to teach me the basics of cell culture work. I am also thankful to our technical assistants, Rob Hanson, Simon Thorpe and Jennifer Louth for helping me with analytical analysis and mass spectroscopy, and thanks also to all other lab colleagues. I would also like to thank Dr. Nicola Green for helping and training me in the use of confocal microscopy in the Kroto Imaging Facility Department.

From the University of Bradford, I would like to thank Dr. Colin Grant for helping me to analyse the mechanical properties of polymers using atomic force microscopy (AFM). I would also like to thank Dr. Maria Katsikogianni for training me to use contact angles and for teaching me how to calculate the surface energy of polymer surfaces. My thanks also go to Dr. Thomas Swift for his help and for providing helpful information about DOSY-NMR. I would also like to thank Dr. Richard Telford for introducing me to thermal analysis (DSC and TGA) techniques. I would like to express my thanks to Prof. Vladimir Botchkarev and his research groups for allowing me to do cell culture work in his laboratory.

My sincere thanks go to Al-Baha University and the Saudi Embassy in London for providing the funding which allowed me to undertake this research.

I would like to acknowledge my husband Saeed and daughter Jana for their support, help, patience and love; without their help I could not have come so far. Finally, I send my thanks to my parents in my home country for supporting me throughout my PhD study.

ABSTRACT

Human cell adhesion to synthetic biomaterial substrates is the main form of technology supporting cell therapy or regenerative tissues. Therefore, *n*-butyl methacrylate-based polymers were synthesised with two architectures. Highly branched polymers were synthesised by a combination of RAFT and SCVP polymerisation employing 4-vinylbenzyl-pyrrolocarbodithoate as the chain transfer agent (CTA) and a 4,4'-azobiscyanovaleric acid (ACVA) initiator. These polymers were modified to carboxylic acid by using an excess of ACVA. Linear polymers were produced by reacting *n*-BMA with a co-monomer 4-divinyl benzoic acid and ACVA as an initiator via free radical polymerisation. Both architectures were subjected to the change of these acidic functionalities to amines via the addition of an excess of primary alkyl diamine. A variety of analytical techniques were used to analyse all of the polymer architectures with varying functionalities. ¹H- and ¹³C-NMR spectroscopy, elemental analysis and FTIR were conducted to provide valuable data with regards to polymer characterisation. The molar mass and molecular weight distribution of the polymers were measured in pure THF solvent at 30°C using size-exclusion chromatography (SEC). Furthermore, NMR diffusion-ordered spectroscopy (1H NMR-DOSY) was used to evaluate the success of the polymerisation without any side reaction and to determine the hydrodynamic radius and intrinsic viscosity of the polymers.

The physico-chemical and thermal properties of linear and highly branched (*n*-butyl methacrylate) polymers were obtained. The glass transition temperature, T_g , of the polymers was determined by differential scanning calorimetry (DSC) and the degradation rate of the polymers was determined by thermogravimetric analysis (TGA). Mechanical properties such as the topography and stiffness of the acidic polymer surfaces have been analysed via atomic force microscopy (AFM). The behaviour of polymers when coated on glass coverslip substrates was determined by measuring water sessile drop contact angles, whilst the surface free energy (SFE) of the polymers was also calculated by measuring contact angles in three different probe solvents. Two methods for SFE were compared: the Owen and Wendt method is used to obtain the dispersive and polar components, and the Lifshitz-van der Waals acid-base method has been used to obtain apolar, acid and base components in the contact angle experiments. A

comparison of morphology and roughness values on polymer coated coverslips had been carried out using AFM.

Glass coverslips were dip-coated using a solution of PBMA-based coating materials with a 5 mg/ml polymer concentration and placed onto well-plates for studying cell adhesion and cell number *in vitro*. The effect of specific polymer functionalities and architectures on three types of cells was assessed in the cell culture: human renal epithelial cells (HREpCs), human dermal fibroblast cells (HDFCs) and a human lung carcinoma epithelial cell line (A549). It was found that the three-different type of cells behaved differently with each polymer. The PBMA with acid functionality provided a good surface for the adhesion of HDF cells, while PBMA with a different primary alkyl amine functionality provided a good surface for the adhesion of HREp cells. However, A549, as a cancer cell line, adhered well to all polymer surfaces.

The relationship between surface wettability of polymer substrates and the measured cell viability, under metabolic activity and cell number assays was determined. Further, the correlation between the two different approaches to calculating surface free energy components and cell adhesion results was investigated. However, a strong correlation between the components of the surface energy and cell behaviour could not be founded.

Overall, this work provides knowledge on how functional polymers influence cell adhesion and on the compatibility of these biomaterials with specific types of cells.

TABLE OF CONTENTS

ACKNOWLEDGEMENTS	I
ABSTRACT.....	II
TABLE OF CONTENTS	IV
LIST OF FIGURES	X
LIST OF TABLES	XIV
LIST OF SCHEMES	XVI
LIST OF ABBREVIATIONS	XVIII
1 CHAPTER ONE: AIM AND THESIS OUTLINE.....	1
1.1 MOTIVATION.....	1
1.2 SCOPE OF PROJECT.....	3
1.3 OBJECTIVES	4
1.4 THESIS OUTLINE	5
2 CHAPTER TWO: LITERATURE REVIEW (POLYMERS AND CELL ADHESION)	6
2.1 INTRODUCTION TO POLYMERS	6
2.1.1 Polymer architectures	6
2.1.2 Polymerisation techniques.....	9
2.1.2.1 Step growth polymerisation.....	9
2.1.2.2 Chain growth polymerisation	9
2.1.2.3 Ionic polymerisation.....	9
2.1.2.4 Conventional radical polymerisation.....	10
2.1.2.5 Reversible deactivated radical polymerisation	12
2.1.3 Synthesis of branched polymers.....	14

2.1.4 RAFT polymerisation.....	21
2.1.5 End group modification via RAFT polymerisation.....	24
2.2 INTRODUCTION TO CELL ADHESION	27
2.2.1 Biomaterials and biocompatibility	27
2.2.2 Protein adsorption and cell adhesion on biomaterial surfaces.....	29
2.2.3 Properties of material surface on cells.....	32
2.2.3.1 Surface wettability (hydrophobic / hydrophilic surface)	33
2.2.3.2 Surface charge	34
2.2.3.3 Surface topography and roughness.....	35
2.2.3.4 Surface stiffness	36
2.2.4 Epithelial and fibroblast cells	37
3 CHAPTER THREE: POLY(N-BUTYL METHACRYLATE) OF VARYING ARCHITECTURE AS A PROTOTYPICAL SYSTEM FOR PROMOTING EPITHELIALISATION	41
3.1 INTRODUCTION	41
3.2 RESULTS AND DISCUSSION	45
3.2.1 Chain transfer agent of 4-vinylbenzyl-pyrrol carbodithioate	45
3.2.2 Highly branched poly(<i>n</i> -butyl methacrylate) with pyrrole end group.....	47
3.2.3 Functionalised highly branched poly(butyl methacrylate) with an acid end group	53
3.2.4 Diamine addition to HB-PBMA with acid end group	58
3.2.5 Linear analogue poly(<i>n</i> -butyl methacrylate) with acid ends	62
3.2.6 Coupling of linear butyl methacrylate copolymers to diamine	68
3.2.7 Diffusion ordered NMR spectroscopy.....	70
3.3 CONCLUSION	76

3.4	EXPERIMENTAL	77
3.4.1	Synthesis of RAFT agent of 4-vinylbenzyl-pyrrolocarbodithioate	77
3.4.2	RAFT polymerisation of <i>n</i> -butyl methacrylate using 4-vinylbenzyl pyrrolocarbodithioate as the chain transfer agent	78
3.4.3	Conversion of the pyrrole-carbodithioate end group to carboxylic acid in HB P(BMA)	79
3.4.4	Highly branched poly (<i>n</i> -butyl methacrylate) with amine ends	80
3.4.5	Conventional free radical polymerisation of <i>n</i> -butyl methacrylate and 4-vinyl benzoic acid	82
3.4.6	Linear poly(<i>n</i> -butyl methacrylate) with amine functionality	83
3.5	INSTRUMENTATION	85
3.5.1	Freeze-pump-thaw polymerisation	85
3.5.2	Nuclear magnetic resonance spectroscopy	85
3.5.3	Infrared spectroscopy	85
3.5.4	Size exclusion chromatography (SEC).....	85
3.5.5	Elemental analysis	85
3.6	APPENDIXES	86
4	CHAPTER FOUR: THERMAL, PHYSICAL AND MECHANICAL PROPERTIES OF POLYMERS	91
4.1	INTRODUCTION	91
4.2	RESULTS AND DISCUSSION	94
4.2.1	Thermal analysis.....	94
4.2.1.1	TGA measurements	94
4.2.1.2	DSC measurements	96
4.2.1	Investigating the wettability of polymer surfaces via contact angles.....	99

4.2.2 Surface free energy of polymers.....	103
4.2.2.1 Theory of dispersion-polar approach.....	103
4.2.2.2 Theory of acid-base approach	104
4.2.2.3 Calculating SFE by dispersion-polar approach	106
4.2.2.4 Calculating SFE by Lifshitz-van der Waals (acid-base) approach	107
4.2.3 Surface morphology and roughness for polymers.....	109
4.2.4 Topography and mechanical properties of carboxylic polymers	112
4.3 CONCLUSION	115
4.4 EXPERIMENTAL.....	118
4.4.1 Thermal gravimetric analysis	118
4.4.2 Differential scanning calorimetry.....	118
4.4.3 Contact angle measurements and Surface free energy determination.....	118
4.4.4 Atomic force microscopy	118
4.5 APPENDIXES	120
5 CHAPTER FIVE: STUDIES OF CELL/BIOMATERIAL INTERACTION OF HUMAN CELLS WITH POLY (BUTYL METHACRYLATE)S.....	124
5.1 INTRODUCTION	124
5.2 RESULTS.....	127
5.2.1 Cell viability assay	127
5.2.2 Determination number of cells	131
5.2.3 Cytotoxicity assay	137
5.2.4 Immunofluorescence	140
5.2.5 Polymer architecture (linear and branched) impact on cell adhesion.....	147
5.3 DISCUSSION	149

5.4	CONCLUSION	156
5.5	EXPERIMENTAL	157
5.5.1	Equipment and reagents	157
5.5.2	Cell culture	158
5.5.2.1	Human renal epithelial cells (HREps) culture	158
5.5.2.2	Human dermal fibroblast cells (HDFs) culture	158
5.5.2.3	Human carcinoma epithelial lung cells (A549) culture	159
5.5.3	Sub-culturing of cells	159
5.5.4	Cryopreservation of cells (cell freezing)	160
5.5.5	Thawing of cells	160
5.5.6	Cell counting protocol	160
5.5.7	Preparing test material	161
5.5.7.1	Polymer solution	161
5.5.7.2	Sterilising glass coverslips:	161
5.5.8	DAPI and phalloidin- TRITC staining	161
5.5.9	Cell viability, determination number of cells and cytotoxicity methods.....	162
5.5.9.1	Alamar Blue® assay	162
5.5.9.2	PicoGreen assay	163
5.5.9.3	LDH cytotoxicity assay	164
5.5.10	Statistical analysis	165
5.6	INSTRUMENTATION	166
5.6.1	Optical microscopy	166
5.6.2	Confocal microscopy	166

6	RELATIONSHIP BETWEEN SURFACE PROPERTIES (WETTABILITY AND SURFACE FREE ENERGY) OF SYNTHESISED POLYMERS AND CELL BEHAVIOUR	167
6.1	INTRODUCTION	167
6.2	RESULTS AND DISCUSSION.....	168
6.2.1	Correlation between surface wettability and cell behaviour	168
6.2.2	Correlation between surface free energy components and cell behaviour	170
6.2.2.1	Human renal epithelial cells	171
6.2.2.2	Human dermal fibroblast cells.....	172
6.2.2.3	Human carcinoma epithelial lung cells	174
6.3	CONCLUSION	178
7	CONCLUSION AND FUTURE WORK.....	179
7.1	SUMMARY AND CONCLUSION.....	179
7.2	FUTURE WORK	182
8	REFERENCES	184

LIST OF FIGURES

Figure 1.1- Overview of the project.....	2
Figure 2.1- The architecture of copolymers: (a) statistical, (b) alternating, (c) block, (d) graft	6
Figure 2.2- Example of branched polymer architectures: (a) star, (b) brush, (c) pom-pom, (d) dendrigraft, (e) highly/ hyperbranched, (f) dendrimers ¹⁹	7
Figure 2.3- The RAFT branching monomer: (a) synthesised by Yang et al., and (b and c) synthesised by Carter et al binding the dithioester as the chain's terminal group ¹⁹	17
Figure 2.4- Illustration of the differences viscosity of different polymer architectures (image copied without modification ⁶⁸)	18
Figure 2.5- Differences in hydrodynamic volume between linear and branched polymers in solution.....	19
Figure 2.6- Example of a universal calibration of SEC (image copied without modification ⁷⁰)	20
Figure 2.7- General RAFT agent structure	23
Figure 2.8- The location of the polymer in RAFT polymerisation, showing the α and ω ends	25
Figure 2.9- The organisation of an epithelial sheet (this figure was adapted from reference ¹⁶⁴ and produced using the Servier Medical Art software).....	40
Figure 3.1- The conversion of lysine to allysine via lysyl oxidase in the ECM	44
Figure 3.2- Proton NMR of 4-vinylbenzyl-pyrrole carbodithioate in chloroform-d solvent...45	45
Figure 3.3- ¹³ C-NMR spectrum of 4-vinylbenzyl-pyrrole carbodithioate in chloroform-d solvent	46
Figure 3.4- ¹ H-NMR spectra of highly branched poly(butyl methacrylate)	49
Figure 3.5- FT-IR of highly branched poly(butyl methacrylate) HB-PBMA-2	52
Figure 3.6- SEC results of HB-PBMA with pyrrole functionalities	52
Figure 3.7- ¹ H-NMR spectrum of highly branched with carboxylic end group (HB-PBMA:COOH-2)	54

Figure 3.8- FTIR spectra showing the differences between HB-PBMA-2 before and after functionalisation.....	55
Figure 3.10- Molar mass distribution of highly branched polymers before and after functionalities.....	56
Figure 3.11- ¹ H-NMR spectra of aminated HB- PBMA:1,4-DAB.....	60
Figure 3.12- FTIR spectra of acidic HB-PBMA-2 after amination with primary alkyl amine.....	61
Figure 3.13- ¹ H-NMR spectra of analogue linear poly(butyl methacrylate-co-vinyl benzoic acid).....	65
Figure 3.14- FTIR spectra of linear P(BMA-co-vinyl benzoic acid) P(BMA)-2.....	66
Figure 3.15- SEC results of L-P(BMA-co-VBA).....	67
Figure 3.16- Solid FTIR of aminated linear poly(butyl methacrylate) P(BMA)-2.....	68
Figure 3.17- Examples of 2D DOSY spectra of (left) HB-PBMA:pyrrole, (middle) HB-PBMA:COOH and (right) L-PBMA:COOH.....	72
Figure 3.18- Diffusion coefficient distributions obtained from DOSY analysis.....	73
Figure 3.19- ¹ H-NMR DOSY analysis of R _H distribution (left) HB-PBMA:pyrrole, (middle) HB-PBMA:COOH and (right) L-PBMA:COOH.....	74
Figure 4.1- TGA graphs of poly(butyl methacrylate)s with varying architectures and functionalities.....	94
Figure 4.2- DSC thermograms for polymers. The top response for each sample was for the second heating cycle, while the bottom response was for the first heating cycle.....	98
Figure 4.3- Wettability of different polymer surfaces with drop imaging of highly branched polymers by water contact angles using the sessile drop method.....	100
Figure 4.4- Wettability of different polymer surfaces with drop imaging of linear polymers by water contact angles using the sessile drop method.....	101
Figure 4.5- AFM height images of (top) HB-PBMA:pyrrole film, (middle) HB-PBMA:COOH film and (bottom) HB-PBMA:1,6DAH film -(scan size 5µm x 5µm).....	110
Figure 4.6- AFM height images of (top) pure-PBMA film, (middle) L-PBMA:COOH film and (bottom) L-PBMA:1,6DAH film -(scan size 5µm x 5µm).....	111
Figure 4.7- The results of roughness values of polymers.....	112

Figure 4.8- AFM height images of (top) L-PBMA:COOH film and (bottom) HB-PBMA:COOH - (scan size 5 μ m x 5 μ m).....	113
Figure 4.9- Moduli of linear and highly branched polymer films as a function of temperature. Axis logarithmic.....	114
Figure 5.1- Structures of the different architectures of poly (n-butyl methacrylate), which are used as the substrates for cell adhesion.....	126
Figure 5.2- Results of AlamarBlue assay for HREp cells on poly(butyl methacrylate)s with different functionalities and architectures.....	128
Figure 5.3- Results of AlamarBlue assay for A549 cells on poly(butyl methacrylate)s with different functionalities and architectures.....	129
Figure 5.4- Results of AlamarBlue assay for HDF cells on poly(butyl methacrylate)s with different functionalities and architectures.....	130
Figure 5.5- PicoGreen results for HREpCs after incubation on PBMA with different functionalities and architectures (a) number of cells (b) quantity of DNA.....	132
Figure 5.6- PicoGreen results for A549 cells after incubation on P(BMA) with different functionalities and architectures (a) total number of DNA (b) number of cells.....	134
Figure 5.7- PicoGreen results for HDFCs after incubation on P(BMA) with different functionalities and architectures (a) number of cells (b) quantity of DNA.....	136
Figure 5.8- The percentage of cytotoxicity from the LDH assay in HREp cells after exposure to different polymer materials for 72 hours.....	138
Figure 5.9- The percentage of cytotoxicity from the LDH assay in A549 cells after exposure to different polymer materials for 72 hours.....	139
Figure 5.10- The percentage of cytotoxicity from the LDH assay in HDF cells after exposure to different polymer materials for 72 hours.....	140
Figure 5.11- Immunofluorescence micrographs of HREp cells on different polymer coatings stained with TRITC-phalloidin for actin (red) and DAPI for nucleus (blue).....	142
Figure 5.12- Immunofluorescence micrographs of A549 cells on different polymer coatings stained with phalloidin-TRITC for actin (red) and DAPI.....	144
Figure 5.13- Immunofluorescence micrographs of HDF cells on different polymer coatings stained with phalloidin-TRITC for actin (red) and DAPI for nucleus (blue).....	146

Figure 5.14- The results of two architectures of the same functionality in cell adhesion (a) HREp cells, (b) A549 cells and (c) HDF cells	147
Figure 5.15- Standard curves for PicoGreen assay derived from lambda DNA standards, and known cells concentrations	163
Figure 6.1- Relationship between the human renal epithelial (left) cell number and (right) metabolic activity assays with surface wettability	168
Figure 6.2- Relationship between the human dermal fibroblast (left) cell number and (right) metabolic activity assays with surface wettability	169
Figure 6.3- Relationship between the human carcinoma epithelial “A549” (left) cell number and (right) metabolic activity assays with surface wettability	169
Figure 6.4- Spearman’s correlation between the number of human renal epithelial cells and the total surface energy ($\gamma Sd - p$), its dispersive (γSd) and polar(γSd) components, according to the “dispersion-polar” approach	171
Figure 6.5- Spearman correlation between the number of human renal epithelial cells and the total surface energy ($\gamma SLW - AB$), its electron acceptor ($\gamma S +$), electron donor ($\gamma S -$), and polar(γSAB) components, according to the “Lifshitz-van der Waals acid-base” approach	172
Figure 6.6- Spearman’s correlation between the number of human dermal fibroblast cells and the total surface energy ($\gamma Sd - p$), its dispersive (γSd) and polar(γSd) components, according to the “dispersion-polar” approach	173
Figure 6.7- Spearman’s correlation between the number of human dermal fibroblast cells and the total surface energy ($\gamma SLW - AB$), its electron acceptor ($\gamma S +$), electron donor ($\gamma S -$), and polar (γSAB) components, according to the “Lifshitz-van der Waals acid-base” approach	174
Figure 6.8- Spearman’s correlation between the number of human carcinoma cells and the total surface energy ($\gamma Sd - p$), its dispersive (γSd) and polar(γSd) components, according to the “dispersion-polar” approach	175
Figure 6.9- Spearman’s correlation between the number of human carcinoma cells and the total surface energy ($\gamma SLW - AB$), with its electron acceptor ($\gamma S +$), electron donor ($\gamma S -$), and polar (γSAB) components, according to “Lifshitz-van der Waals acid-base” approach	176

LIST OF TABLES

Table 2.1- The three main classes of RAFT chain transfer agent ⁸¹	23
Table 2.2- The processing of cell adhesion in vitro ¹²⁰	32
Table 3.1- Elemental analysis for the chain transfer agent of theoretical and actual compounds	46
Table 3.2- Result of SCVP RAFT polymerisation reaction of BMA in the presence of CTA determined by ¹ H-NMR spectroscopy	50
Table 3.3- SEC results for highly branched polymers before and after functionalities.....	55
Table 3.4- Summary of theoretical and actual elemental analysis for poly(butyl methacrylate) with pyrrole and acid end groups	57
Table 3.5- The theoretical and actual CHN elements before and after amination reaction.....	62
Table 3.6- Predication of reactivity ratio of p(BMA-co-VBA)	63
Table 3.7- Result of copolymerisation reaction of BMA and 4-VBA determined by ¹ H-NMR spectroscopy	66
Table 3.8- Elemental analysis of linear P(BMA) before and after amination with different primary alkyl amine	69
Table 3.9- The values of the logarithms of self-diffusion coefficients of all polymers.....	73
Table 3.10- Hydrodynamic radius (R _H) and intrinsic viscosity (IV) calculated using DOSY, M _n calculated form SEC.....	75
Table 3.11- Summary of reagent quantities used in RAFT polymerisation of n-butyl methacrylate	79
Table 3.12- Summary of reagents used in the coupling of highly branched PBMA to diamine	81
Table 3.13- Summary of reagent quantities used in free radical copolymerisation of n-butyl methacrylate and 4-vinylbenzoic acid.....	82
Table 3.14- Summary of reagents used in the coupling of linear PBMA to diamine.....	84
Table 4.1- TGA data for the polymers.....	96

Table 4.2- Glass transition temperatures of different polymers	98
Table 4.3- Contact angle measurements on poly(butyl methacrylate)s with different architectures and functionality coated on coverslips as substrates	102
Table 4.4- Surface tension properties (mJ/m-2) of the three probe liquids	106
Table 4.5- Total surface-free energy (γ_{total}) of P(BMA) polymers, its dispersion (γ_{Sd}) and polar (γ_{Sp}) components	106
Table 4.6- Total surface-free energy (γ_{total}) of poly (n-butyl methacrylate) polymers, its polar (γ_{SAB}) and non-polar (γ_{SLW}) components, electron donor (γ_{S-}) and electron acceptor (γ_{S+}).....	108
Table 4.7- Elastic modulus of L-PBMA:COOH and HB-PBMA:COOH \pm SD at the various temperatures	114
Table 5.1- List of equipment used	157
Table 5.2- List or reagents used.....	157

LIST OF SCHEMES

Scheme 2.1- General mechanism and rate coefficient of conventional radical polymerisation	11
Scheme 2.2- The mechanism of reversible termination (RT) in RDRP	13
Scheme 2.3- The mechanism of degenerative chain transfer (DT) in RDRP	13
Scheme 2.4- The mechanism of self-condensing vinyl polymerisation (SCVP) ²⁷	16
Scheme 2.5- Mechanism of RAFT polymerisation (I = initiator, M = monomer, R = radical) that can initiate polymerisation (P_n and P_m = polymer chains) ^{27, 79}	22
Scheme 2.6- Mechanism of radical-induced removal thiocarbonylthio via radical cross-coupling from RAFT polymerisation ⁸⁸	25
Scheme 3.1- General scheme of synthesis of highly branched poly(butyl methacrylate) with pyrrole, acid and amine functionalities	43
Scheme 3.2- General scheme of synthesis of linear poly(butyl methacrylate) with acid and amine functionalities	43
Scheme 3.3- Synthesis of the chain transfer agent 4-vinylbenzyl-pyrrole carbodithioate	45
Scheme 3.4- RAFT polymerisation of n-butyl methacrylate with a pyrrole end using ACVA as the initiator and dioxane as the solvent.....	47
Scheme 3.5- Reaction mechanism for the synthesis of highly branched polymers via RAFT-SCVP copolymerisation ¹⁹²⁻¹⁹³	48
Scheme 3.6- Functionalisation of HB-PBMA with acid end group using an excess of ACVA	53
Scheme 3.7- Amination of highly branched poly(n-butyl methacrylate)	58
Scheme 3.8- Mechanism of amide formation between carboxylic acid and amine with EDC as a coupling agent in an aqueous system	59
Scheme 3.9- Free radical polymerisation of linear analogue P(BMA-co-4-VBA)	62
Scheme 3.10- Possible propagation step sequences in free radical copolymerisation of P(BMA-co-4-VBA).....	63

Scheme 3.11- Amination of linear butyl methacrylate with acid end group using different diamines	68
Scheme 4.1- Two radicals terminated by a disproportionation in FRP	95
Scheme 4.2- Two radicals terminated by combination (coupling) in FRP	95
Scheme 5.1- Reduction of Resazurin to Resorufin via mitochondrial dehydrogenase.....	162
Scheme 5.2- Schematic of the principle of LDH cytotoxicity assay mechanism.....	164

LIST OF ABBREVIATIONS

%	Percent
[η] or [IV]	Intrinsic viscosity
μg	Microgram
μl	Microliter
μm	Micrometre
1,2-DAE	1,2-diaminoethane
1,3-DAP	1,3-diaminopropane
1,4-DAB	1,4-diaminobutane
1,6-DAH	1,6-diaminohexane
4-VBA	4-vinyl benzoic acid
4-VBPC	4-Vinylbenzyl pyrrole carbodithioate
A549	Human lung adenocarcinoma epithelial cell line
AB	AlamarBlue
ACVA	4-4'-Azobis(4-cyanovaleric acid)
AFM	Atomic force microscopy
ANOVA	Analysis of variance
ATRP	Atom transfer radical polymerisation
ATCC	American type culture collection
CA	Contact angle
CDCl_3	Deuterated chloroform
cm^{-1}	Wavenumber
CS_2	Carbon disulphide
CTA	Chain transfer agent
d	Doublet
\mathcal{D}	Dispersity

DAPI	(4',6-Diamidino-2-Phenylindole, Dihydrochloride)
D_{br}	Degree of branching
DCC	N,N'-Dicyclohexylcarbodiimide
DCM	Dichloromethane
dd	Doublet of doublets
DMEM	Dulbecco's modified Eagle's medium
DMEM	Dulbecco's modified Eagle's Medium
DMF	Dimethyl formamide
DMSO	Dimethyl sulfoxide
DOSY	Diffusion-ordered NMR spectroscopy
D (S)	Diffusion constant of solvent
DSC	Differential scanning calorimeter
D (P)	Diffusion constant of polymer
DT	Degenerative chain transfer
d-THF	Deuterated THF
EDC	1-Ethyl-3-(3-dimethylaminopropyl)carbodiimide
EDTA	Ethylenediaminetetraacetic acid
f	Initiator efficiency
FBS	Fetal bovine serum
FDA	Food and drug administration
FT-IR	Fourier transform infra-red spectroscopy
g	Gram
HB-PBMA	Highly branched poly(butyl methacrylate)
HBP	Highly branched polymers
HDFCs	Human dermal fibroblast cells
HREpCs	Human renal epithelial cells
ITP	Iodine-mediated polymerisation

ITS-A	Insulin-transferrin-selenium-A supplement
IUPAC	International union of pure and applied chemistry
J	Coupling constant
K	Mark-Houwink parameter
K_B	Boltzmann constant
K_x	x= rate coefficient of reaction. p: propagating rate, t: overall termination rate, tc: termination by combination rate, td: termination by decomposition rate, ini: initiation rate, dec: decomposition rate, da: deactivation rate in RT mechanism, ac: activation rate in RT mechanism, ex: exchange rate in DT mechanism, add: addition rate in RAFT mechanism, -add: reserve addition rate of RAFT, β : fragmentation rate of RAFT, $-\beta$: reserve fragmentation rate of RAFT
LDH	Lactate dehydrogenase activity
L-PBMA	Linear poly(butyl methacrylate)
m	Multiplet
MES	2-(<i>N</i> -morpholino)ethanesulfonic acid
mg	Milligram
ml	Millilitre
Mn	Number average molecular weight
mol	Mole
Mw	Weight average molecular weight
MWD	Molecular weight distribution
NaH	Sodium hydride
<i>n</i> -BMA	Butyl methacrylate
NMP	Nitroxide-mediated polymerisation
NMR	Nuclear magnetic resonance
P(BMA-co-VBA)	Poly(butyl methacrylate-co-vinyl benzoic acid)
PBS	Phosphate buffer saline

PnBMA	Poly(<i>n</i> -butyl methacrylate)
ppm	Parts per million
PRE	Persistent radical effect
r	Spearman correlation coefficients
RAFT	Reversible addition –fragmentation chain transfer polymerisation
RB	Repeating unit per branch
RDRP	Reversible deactivation radical polymerisation
R _H	Hydrodynamic radius
RI	Refractive index
RP	Radical polymerisation
RT	Reversible termination
s	Singlet
SDS	Sodium dodecyl sulphate
SEC	Size exclusion chromatography
SEF	Surface free energy
t	Triplet
TCP	Tissue culture polystyrene
<i>T_g</i>	Glass temperature
TGA	Thermogravimetric analysis
THF	Tetrahydrofuran
TRITC	Isothiocyanate
α	alpha
γ	Electron donor (Lewis base)
γ ⁺	Electron acceptor (Lewis acid)
γ _{AB}	Surface energy of polar
γ _L	Surface energy of liquid
γ _{LW}	Surface energy of non-polar

γ_s	Surface energy of solid
δ	Chemical shift in (ppm)
θ	Contact angle
ω	Omega
V_H	Hydrodynamic volume
OW	Owen and Wendt (dispersion-polar) approach
LW-AB	Lifshitz-van der Waals (Van Oss-Chaudhey-Good/ acid-base) approach

1 CHAPTER ONE: AIM AND THESIS OUTLINE

1.1 MOTIVATION

In the present day, many synthetic materials are utilised in modern technologies including biological and medical applications. The innovative use of biomaterials in the design of new therapies and the launch of novel products is a current topic of research. Polymeric biomaterials are a large class of biomaterials that have been manufactured and applied for use in many applications. The use of synthetic biomaterials is popular due to their modifiable properties and the fact that these materials have been well researched and studied¹⁻². They can be used as surface coatings to increase the biocompatibility of interacting surfaces. Also, in medical applications they can be used to decrease the probability of body rejection of otherwise immunogenic devices³. Understanding cell behaviour in polymeric biomaterials environments is critical for current and future nanobiotechnology fields including tissue engineering, cell biology and regenerative medicine. Polymeric biomaterials are thus of great interest, but much remains to be discovered and in particular little is known of the effects of architecture of functional coatings on biological properties.

Highly branched polymers (HBP) are defined in this thesis as polymers with branches on branches and with runs of linear segments, following the precedent of Voit and Lederer⁴. The term is used here to distinguish these materials from other branched polymers such as graft polymers and copolymers and hyperbranched polymers. The term hyperbranched is extensively used in the literature but it is considered here that the term implies much higher degrees of branching approaching branches on every repeat unit. Notwithstanding these comments it is accepted that IUPAC currently refers to highly branched polymers as defined here as branched polymers; polymers with at least one branched point. HBPs have very attractive properties due to their topological structure and physiochemical properties including the presence of many functional end groups and ease of synthesis. Therefore, HBPs afford unique advantages in biological and biomedical applications. For example, they have been used for drug delivery and release, gene transfection, and targeting. In bioimaging and diagnosis they are used as fluorescent probes and MRI contrast agents. In tissue engineering they are used for biomineralization of calcium carbonate and silica. Frey and colleagues synthesised hyperbranched poly(glycerol) (HPG) through anionic ring opening multi-branching polymerisation and utilised it in a variety of biological and medical applications⁵. HPG has favourable hydrophilicity properties and high chemical stability in addition to an excellent

biocompatibility and very low or absent immunogenicity. These characteristics of HPG and its derivatives give high potential for use in diagnostics, therapy and other medical applications such as surface attachments for protein-resistance and bioconjugation with peptides.

In recent decades, functional polymers have attracted increasing attention in cell-polymer interactions. Lim *et al.* synthesised hyperbranched poly(amino ester) with tertiary amino group for efficient transfection of DNA with low toxicity ⁶. In another research study Tian *et al.* reported the successful synthesis of an inherently biodegradable cationic hyperbranched copolymer with poly(ethylenimine) PEI as backbone and poly(ethylene glycol) PEG and poly(γ -benzyl L-glutamate) PBLG as hyperbranched stars for drug and gene delivery ⁷. These polymers display favourable bio-interactions that may be indicative of the positive inclusion of the amine functional group in increasing cell adhesion. Other functional groups such as carboxylic acid also might have positive affects in biocompatibility. MacNeil *et al.* utilised electrospinning techniques for polymer fabrication with acid functionality that can be used for drug release and tissue regeneration ⁸. MacNeil *et al.* observed that a polymer containing 3% acid promoted the attachment of keratinocytes and osteoblast-like cells ⁹⁻¹⁰. The purpose of this introduction is to review the work performed on the synthesis of polymers and to examine the behaviour of these polymers as substrates in maintaining cells *in vitro* for biological processing. A brief outline behind this research is shown in Figure 1.1 below:

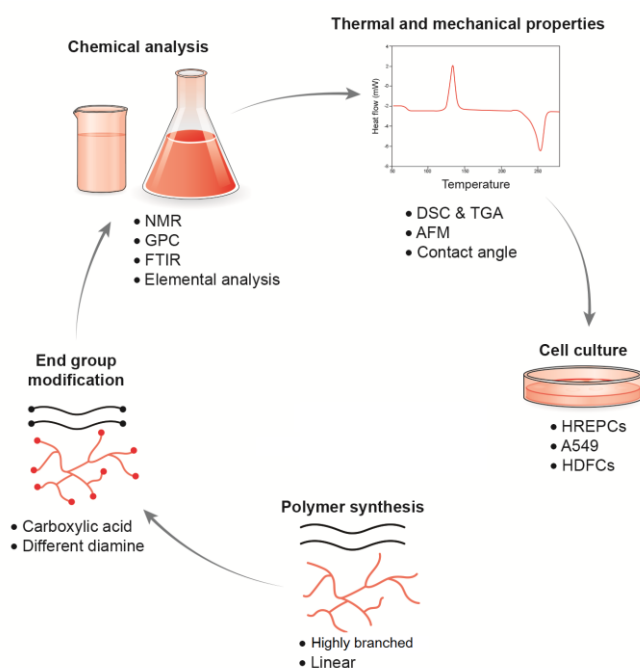


Figure 1.1- Overview of the project

1.2 SCOPE OF PROJECT

The main aim of this project is to develop and synthesise a new surface coating material based on methacrylate polymers to enhance its surface interaction with cell adhesion. This work is based on earlier work done within the Rimmer and MacNeil groups¹¹⁻¹², which showed that primary alkyl amine-enhanced hydrogel provides a suitable substrate for epithelial cell growth. Essentially, the hypothesis of the work is that coatings that reliably provide alkyl amine functionality would also support epithelial cell growth. Regarding the related ideas, poly(*n*-butyl methacrylate) (PnBMA), with its complex architectures and different functionalities, will be synthesised using reversible addition fragmentation chain transfer (RAFT) polymerisation to produce highly branched polymer and free radical polymerisation to create a linear polymer. The polymer materials with primary amine and acid functional groups will be synthesised in order to compare their behaviour with cell cultures.

The copolymer of highly branched poly(butyl methacrylate) (HB-PBMA) will be prepared with 4-vinylbenzyl-pyrrole carbodithioate as a chain transfer agent (CTA) using RAFT polymerisation., following the previous work of Carter *et al*¹³⁻¹⁴. These polymers will react with an excess of ACVA to create carboxylic acid functional groups, and then to amine end groups, again following and modifying the previous work¹⁵⁻¹⁶.

The copolymer of linear poly(butyl methacrylate) (L-PBMA) polymers will be synthesised with vinyl benzoic acid (4-VBA) to generate a carboxylic acid functionality using free radical polymerisation. The carboxylic end group of these materials will be modified to different amine functionalities.

The set of polymers will be analysed and characterised using techniques including NMR, SEC, FTIR and elemental analysis. NMR DOSY will be used to evaluate the success of the polymerisation without any side reactions and to determine the hydrodynamic radius and intrinsic viscosity of the polymers.

The thermal properties of the polymers will be studied using TGA and DSC measurements to show the degradation rate and glass transition of these materials, respectively. The surface behaviour of these polymers after coating on glass coverslips will be characterised by sessile drop contact angle measurements to evaluate the wettability and surface free energy components of the polymeric substrates. Atomic force microscopy (AFM) will be used to

characterise the topography and stiffness of linear and branched polymers with carboxylic acid functionalities, owing to insufficient time to analyse the remaining polymers. Further, the AFM also will be used to show the morphology and average roughness values of some polymers that coated on coverslips.

The purpose for the synthesis of these polymers is to examine the behaviour of these materials as substrates in maintaining cells *in vitro* for biological processing. Polymers will be used to coat glass coverslips to observe the effects of functional groups and architectures on growing cells by culturing epithelial and fibroblast cells on those materials.

Finally, the relationship between surface wettability of polymer substrates and cell culture work will be investigated. In addition, the correlation between cell adhesion and surface energy components will be considered.

1.3 OBJECTIVES

1. Synthesise HB-PBMA using RAFT polymerisation and analogue copolymers of linear poly(butyl methacrylate-co-vinyl benzoic acid) PBMA-co-VBA using conventional free radical polymerisation.
2. Conversion of end group in HB-PBMA and L-PBMA-co-VBA to diamine or acid functionalities.
3. Study the thermal, mechanical and surface properties of these polymer materials.
4. Study the interaction of the new polymers with different types of human epithelial and fibroblast cultured cells *in vitro*.
5. Establish the correlation between cell viability assay with wettability and surface energy components.

1.4 THESIS OUTLINE

Chapter 2 gives a brief introduction to polymers, highly branched polymers and their synthesis via the SCVP RAFT polymerisation method. It also reviews cell adhesion and its mechanism on biomaterial surfaces.

Chapter 3 explores the synthesis of 4-vinylbenzyl-pyrrole carbodithioate as a chain transfer agent in RAFT polymerisation. HB-P(BMA-*co*-CTA) and L-P(BMA-*co*-VBA) were produced and functionalised with amine or acid end groups. In addition, these species were analysed via NMR, SEC, FTIR and elemental analysis.

Chapter 4 investigates the thermal physical and mechanical properties of PBMA with linear and highly branched architectures and different functionalities. The thermal properties were investigated by DSC and TGA analysis. The topographies of L-PBMA and HB-PBMA with acidic functionalities were imaged and their elastic moduli evaluated, the average roughness's of polymer coated coverslips was determined via AFM. Moreover, contact angle was used to study the wettability of the polymers as coating materials and to calculate their surface energy.

Chapter 5 studies the correlation between synthesised PBMA and different architectures and functionalities with three types of human cells *in vitro*. Functional assay was undertaken via Alamarblue assay, whilst cell number was determined by PicoGreen assay; LDH assay was used to assess cell cytotoxicity on the various polymers. Furthermore, qualitative analysis was observed under confocal microscopy using DAPI-TRITC staining. Further, investigations into the correlation between surface free energy components with cell viability and number of adherent cells were undertaken.

Chapter 6 studies the relationship between surface wettability and surface free energy components of polymers with functional assays for cell adhesion.

Chapter 7 gives the overall conclusions to the present study and provides suggestions for future work according to its results.

2 CHAPTER TWO: LITERATURE REVIEW (POLYMERS AND CELL ADHESION)

2.1 INTRODUCTION TO POLYMERS

2.1.1 Polymer architectures

Polymers are large molecules composed of many repeated units termed monomers. The simplest polymers are formed from bifunctional monomers; these create a linear polymer chain. Homopolymers contain one type of monomer is used and copolymers contain two or more different monomers. The classification of copolymers is dependent on the distribution of the monomers within the polymer chain; namely, they are classified into statistical, alternating, block or graft copolymers, as illustrated in Figure 2.1.

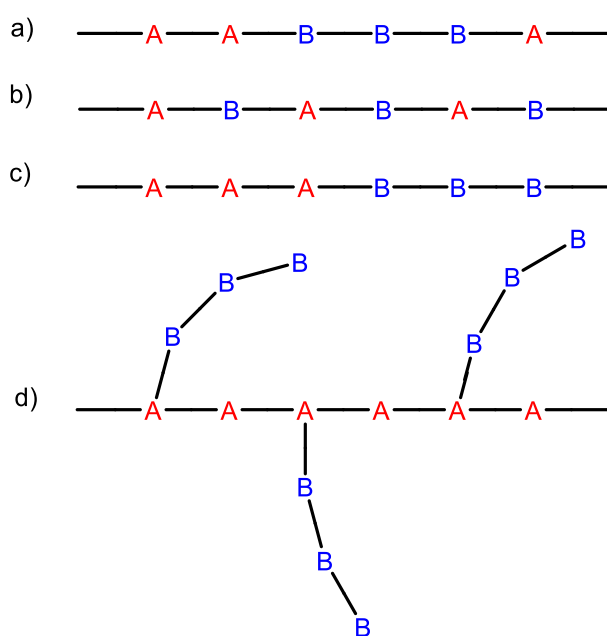


Figure 2.1- The architecture of copolymers: (a) statistical, (b) alternating, (c) block, (d) graft

Polyfunctional monomers can create complex structural architectures such as branched or cross-linked polymers, which can yield more complicated structures including stars, dendrimers, combs and pom-poms¹⁷.

Polymer properties and processing depend on composition, molecular weight, dispersity, as well as architecture. Polymer architectures plays an important role in the behaviour of materials under different conditions.

Linear polymers are macromolecules which have two chain ends and are considered the simplest type of polymers. The processing of these polymers and their underlying principles

has been investigated for many years¹⁷. A current challenge for polymer chemists, physicists and engineers is to gain a greater understanding of branching polymers.

The interest in branched polymers of a variety of architectures has grown rapidly over the past 15 years¹⁸. Branched polymers can provide a range of desirable properties as compared to linear polymers, such as low solution viscosity with better solubility, tuneable solution behaviour, critical phase behaviour and high levels of terminal functionality^{4,17,19}. Figure 2.2 illustrates some of the different branching architectures that provide different physical and chemical properties with a diverse range of applications.

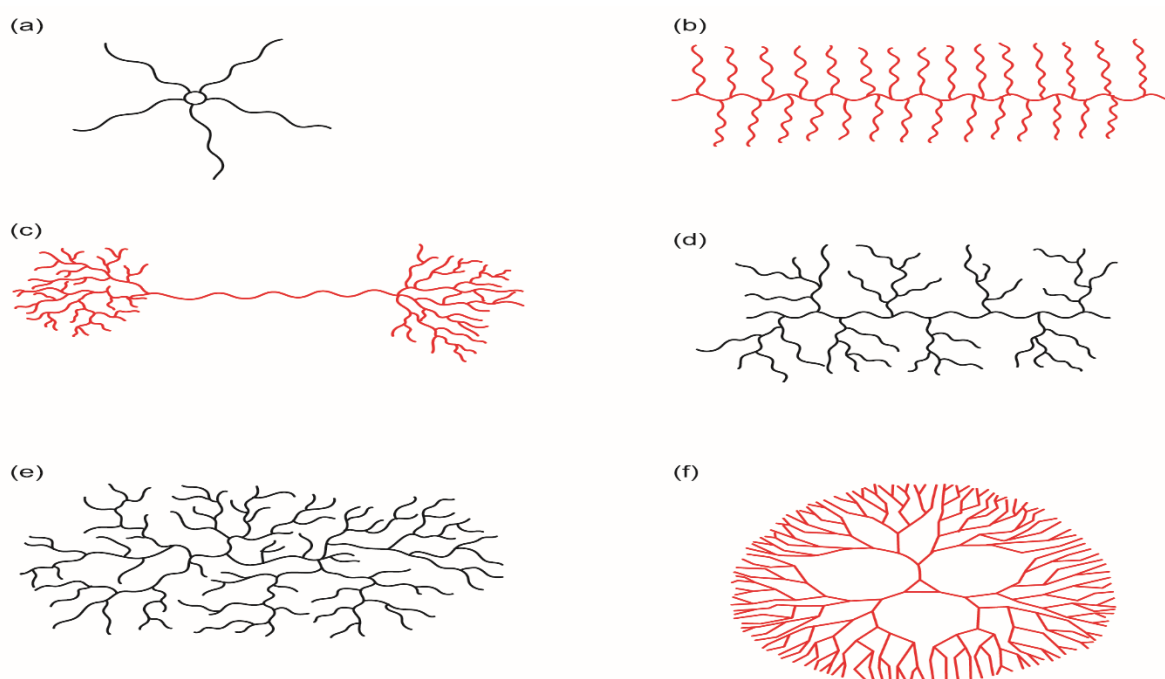


Figure 2.2- Example of branched polymer architectures: (a) star, (b) brush, (c) pom-pom, (d) dendrigraft, (e) highly/hyperbranched, (f) dendrimers¹⁹

There are benefits associated with the perfectly branched architecture of dendrimers. They exist as single molecular species with high degrees of branching. They have a large quantity of functional groups on the surface of the molecule, excellent solubility and very low solution viscosity. These factors make dendrimers ideal candidates for a wide range of applications, from catalyst support to drug delivery. One shortcoming of dendrimers is that they are challenging to produce, since they require complex synthesis that involves many purification steps. Their preparation is a highly expensive procedure that is not suited to being scaled up^{14, 19-20}. Therefore, highly branched polymers (HBPs) are more attractive alternative architectures to explore with analogous properties to dendrimers. Many practical and potential

applications have already been determined for HBPs – for instance, coatings, resins²¹⁻²², flow improvers or viscosity modifiers. Biomedical applications include their use as drug delivery devices, utilising the “cavities” formed in densely branched structures²³⁻²⁵ and the use of HBPs as host–guest systems³.

HBPs are in between the analogues of conventional linear polymers and dendrimers. They are macromolecules with a tree-like architecture, and they have different performance properties to linear polymers²⁰. First, HBPs, when compared to linear polymers, have the benefits of a low softening point and solution viscosity, elevated solubility, exhibit easy chemical modification of terminal groups, and have few chain entanglements. HBPs are capable of possessing large numbers of functional terminal groups, which can be further modified to suit specific applications. On the other hand, there are disadvantages to these materials, including irregular branching and uneven statistical functional group distribution throughout the macromolecule²⁶. They also tend to have broad molecular weight distributions. Polydisperse branched polymers tend to be difficult to characterise, sometimes requiring time-consuming fractionation steps in order to obtain full characterisation. Moreover, from branched polymers to dendrimers, HBPs consist of dendritic units, linear units and terminal units and dendrimers composed of dendritic and terminal units. HBPs display less perfect branching than dendrimers, as illustrated in Figure 2.2; indeed, they actually exhibit lower degrees of branching (D_{br}) than 1, though generally more than 0.4¹⁸. Polymers with a D_{br} less than 0.4 possess greater linear character, namely segmented hyperbranched polymers (SHPs)²⁷. HBPs have repeating units between two branching points and peripheral functional groups as typical features. However, the SHPs have been defined as having long linear chains dispersed between every two branching points and their functional groups may be located on the periphery of the polymer structure²⁸. As mentioned previously here we refer to these as highly branched. The degree of branching is the total number of dendritic and terminal units divided by the sum of all units, as defined by Frey²⁹⁻³⁰.

The subsequent section of this research discusses the criteria considered in the synthesis of polymers, starting with an overall assessment of polymerisation methods, and will later focus on the synthesis of HBPs.

2.1.2 Polymerisation techniques

To produce specific polymer structural designs, a variety of polymerisation methods have been employed, including step growth polymerisation and chain growth polymerisation, depending on the mechanism of polymerisation.

2.1.2.1 Step growth polymerisation

In step growth polymerisation, polymers are formed from bifunctional or multifunctional monomers, which first react to form dimers, then trimers, then longer oligomers, ending ultimately in long chain polymers with high molecular weights. Two well-known examples of polymers which have been produced by step growth polymerisation are Nylon (polyamide), which is formed from the reaction of dicarboxylic acid with diamine, and polyethylene terephthalic (PET) from the reaction of ethylene glycol with terephthalic acid. This mechanism depends on a long-term reaction to achieve polymers of high molecular weight, due to all monomers are able to react at any time.³¹

2.1.2.2 Chain growth polymerisation

Chain growth is another polymerisation technique where unsaturated (vinyl) monomers are used. Polymers are formed by addition of monomers to a growing chain, which occurs via the activation of a double bond via ionic or free radical initiators to produce a kinetic chain. The polymerisation mechanism of chain growth includes three different steps: initiation, propagation and termination. In chain-reaction polymerisations, the formation of high molecular weight species occurs immediately after the beginning of the reaction, *i.e.*, at low monomer conversion rates and is constant during the reaction. Increasing the reaction time only increases the polymer molecules, *i.e.*, increasing the polymer yield but not their size, which remains almost constant³¹.

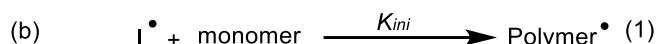
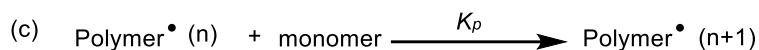
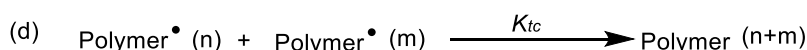
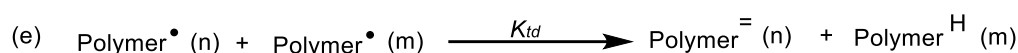
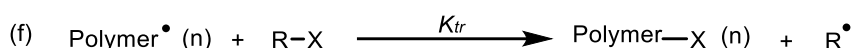
2.1.2.3 Ionic polymerisation

Ionic polymerisation involves both cationic and anionic techniques, where polymerisation proceeds through a kinetic chain mechanism. In this method, the formation and stabilisation of a carbonium ion for cationic polymerisation, or carbanion for anionic polymerisation, depends on the nature of the -R group in the vinyl monomer $\text{CH}_2=\text{CHR}$ ³². For this reason, there is a limit to the types of monomers which can be polymerised using ionic polymerisation methods due to the requirements of electronics in terms of charge stability. To

obtain successful cationic polymerisation, it is important to include electron-donating groups to have the positive charge delocalization stabilized across the π -orbitals of the double bond, while an electron-withdrawing substituent is similarly necessary in anionic polymerisation. Additional disadvantages of ionic polymerisation include the necessity of severe reaction conditions involving catalysts in very high concentrations, very low temperatures and extremely dry solvents³³, in addition to rapid reaction rates and generally poor reproducibility.

2.1.2.4 Conventional radical polymerisation

Conventional radical polymerisation (RP) is an extensively utilised commercial and research procedure. It can be used with an extensive range of monomers such as methacrylate, styrene, methacrylamides, butadiene and vinyl acetate. It has numerous advantageous properties including insensitivity to functional groups, such as OH, NR₂, COOH, CONR₂, and the associated reaction conditions (bulk, solution, emulsion, miniemulsion, suspension) can be modified. In addition, it is now possible to control polymer structure and design. However, the method lacks versatility in the regulation of polymer architecture. This is unfortunate as three-dimensional dendritic polymers, which include dendrimers and highly branched polymers, have unusual and significant properties in terms of shape and functionality³². The RP mechanism is presented in Scheme 2.1 and briefly described in the following.

Initiation & radical formation**Propagation****Termination****combination****disproportionation****Transfer**

X= halogen or hydrogen

Scheme 2.1- General mechanism and rate coefficient of conventional radical polymerisation

Scheme 2.1 shows that the initiation step can be divided into two different processes. In reaction (a), the initiator decomposes (such as thermally, chemically, photochemically) (reaction-rate coefficient: k_{dec}), while the initiator efficiency, f , gives the percentage of decomposing initiator that provides the initiating radical, I^\bullet . In reaction (b) (K_{ini}), the initiating radical reacts with the monomer molecule and initiates a growing polymer chain, $\text{Polymer}^\bullet(1)$. In reaction (c) (K_p), the addition of successive monomers to polymer^\bullet leads to the propagation of the chain. This propagation is ultimately stopped via a termination step with two Polymer^\bullet . For the termination reaction, there are two possible mechanisms, which are a combination reaction (Reaction d, K_{tc}) and a disproportionation reaction (Reaction e, K_{td}). The combination reaction gives one polymer ($n+m$) via the formation of a covalent bond between two radicals, while the disproportionation reaction yields two polymers, one with an unsaturated polymer species, $\text{Polymer}^= (n)$ and another with a saturated polymer species, $\text{Polymer}^H (m)$. The rate coefficient of the termination reaction is given by the following equation:

$$k_t = k_{tc} + k_{td}$$

For optimal radical polymerisation, the presented reactions are all assumed to be irreversible, whereas their rate coefficients remain constant and do not depend on quantities such as chain length or monomer conversion. Moreover, the propagation step only involves the monomer molecules, while the radical concentration remains constant throughout the polymerisation.

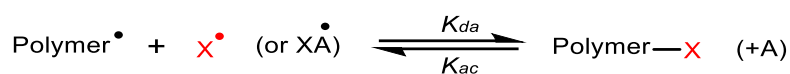
During the polymerisation process, non-ideal reactions can lead to a transfer of the radical function of polymer[•] onto other molecules, as seen in step (f) in Scheme 2.1. This reaction plays an important role in the mechanism of RDRPs, in which agents are added to the system so as to induce (reversible) transfer reactions, which will be presented in more detail below.

2.1.2.5 Reversible deactivated radical polymerisation

Reversible deactivated radical polymerisation (RDRP), previously known as living or controlled polymerisation, is where the active polymer chain end is a free radical. The names ‘living’ and ‘controlled’ are discouraged by IUPAC because radical polymerisation cannot be a truly living process due to the unavoidable termination reaction between two radicals³⁴. RDRP offers numerous benefits, including the ability to control molecular weight, polydispersity, it can be used for a range of monomers, and can be used in the synthesis of well-defined macromolecular architectures, for example block or star copolymers³⁵. Although RDRP is a highly active area of the research, it has some drawbacks including a limited range of usable monomers, expensive reagents or the need to synthesise special additives, it requires the removal of certain unwanted chemical groups after polymerisation, and special polymerisation conditions and a high reaction temperature are required³⁶⁻³⁷.

RDRP depends on reversible activation of dormant species (Polymer-X) to propagate the radical (Polymer[•]), or in the other words, reversible deactivation of (Polymer[•]) with a capping agent (X) to form the dormant species (Polymer-X)³⁸. In order to ensure the growth of all chains is equal and thus that a narrow molecular weight distribution (MWD) is obtained, a high activation–deactivation frequency is important for a successful RDRP. There are two main mechanisms of reversible deactivation, namely (1) reversible termination (RT) and (2) degenerative (or reversible) chain transfer (DT)³⁹, as described below.

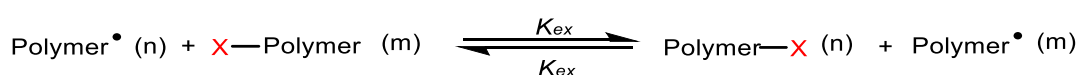
The general mechanism of reversible termination (RT) is shown in Scheme 2.2 below and is briefly described in the following.



Scheme 2.2- The mechanism of reversible termination (RT) in RDRP

In this mechanism, a reversible termination reaction X^\bullet or (XA^\bullet) is deactivated by Polymer^\bullet . The RT system is based on the persistent radical effect (PRE) where, in this kind of reaction, various radicals compete in secondary reactions. The long-lived (persistent) radicals fail to undergo self-termination, only reacting in cross-couplings. This shows the high significance of the product distribution's cross-coupling products⁴⁰. Unlike Polymer^\bullet , there is no irreversible self-termination process for the persistent radical X^\bullet or (XA^\bullet) . This results in the build-up of X^\bullet , thereby enhancing the likelihood of Polymer^\bullet reacting with X^\bullet in a reversible manner instead of in an irreversible manner with another Polymer^\bullet . Examples of this mechanism are the nitroxide-mediated polymerisation (NMP) where X = nitroxyl group, as first reported by Georges *et al.*⁴¹ in 1993, and the atom transfer radical polymerisation (ATRP) with X = Cl, Br and A = transition-metal complex, as first observed in 1995 by Matyjaszewski *et al.*⁴² and Sawamoto *et al.*⁴³

Another mechanism of reversible deactivation is degenerative or reversible chain transfer (DT), which is shown in Scheme 2.3 below.



Scheme 2.3- The mechanism of degenerative chain transfer (DT) in RDRP

In this mechanism, the transfer of X from another polymer-X is through a deactivated Polymer^\bullet ; generally, this process is reversible chain transfer. The most common examples of this mechanism are reversible addition-fragmentation chain transfer (RAFT) with X = thiocarbonylthio group, as first reported in 1998 by Rizzardo *et al.*³⁶, whilst another example is iodine-mediated polymerisation (ITP) with X = I, as first observed in 1995 by Matyjaszewski *et al.*⁴⁴. Based on this context, the RAFT procedure is named for the distinctive technique of successive addition and fragmentation, resulting in a moderately steady intermediate radical. By contrast, ITP involves direct transfer of the iodine atom from one given chain to another. The principles of RAFT are explained in more detail in section 2.1.4.

2.1.3 Synthesis of branched polymers

In 1940, Flory determined the molecular weight distribution of hyperbranched polymers via statistical mechanics and developed the concept of the degree of branching⁴⁵. Flory further explained the history of hyperbranched polymers synthesised by polycondensation of the AB_n structure, where A and B are different functional groups, which led to polydispersity and a unique hyperbranched architecture that avoids gelation⁴⁶. The term “hyperbranched polymer” was first used by Kim and Webster in 1988, when they generated hyperbranched polyphenylene from the synthesis of the polycondensation reaction of (3,5-dibromophenyl)boronic acid. Subsequently, HBPs have attracted the interest of both scientists and engineers due to their distinctive characteristics and potential applications in different areas.

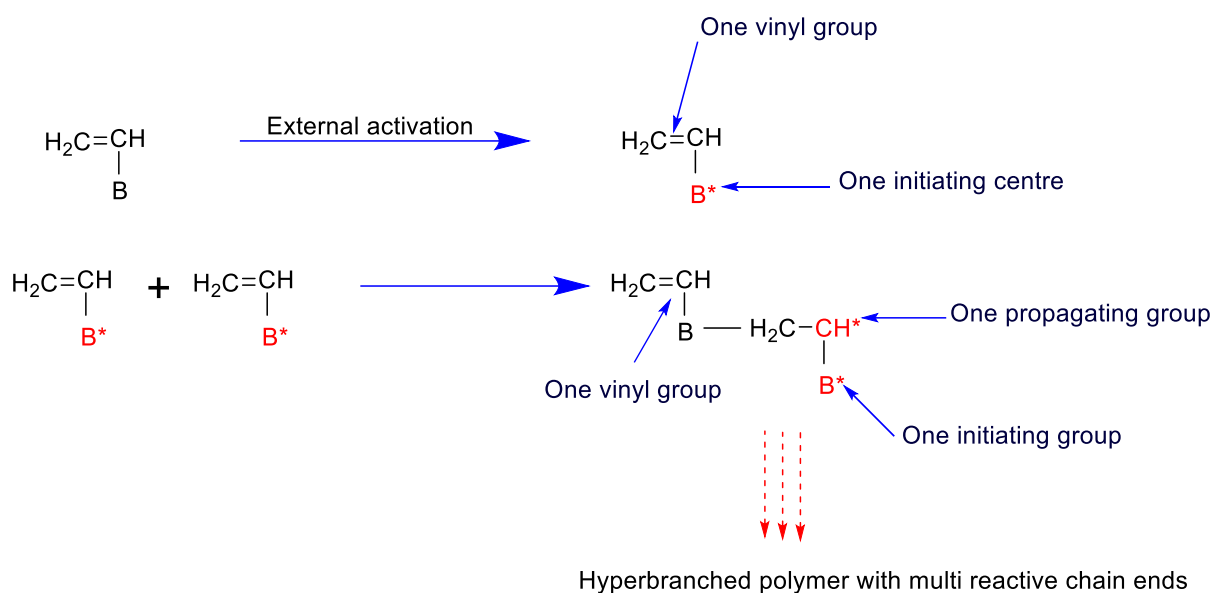
Branched polymers have been prepared through a variety of synthetic procedures; for example, step growth polymerisation through polycondensation with AB_2 ⁴⁷, or with AB_n monomers⁴⁸, self-condensing vinyl polymerisation (SCVP)⁴⁹, ring opening polymerisation⁵⁰⁻⁵¹ and via the Strathclyde route through conventional free radical aqueous emulsion polymerisation⁵²⁻⁵³, as explained below.

Step growth polymerisation is used for a variety of synthesised hyperbranched polymers via polycondensation of the AB_n monomer. Ishida *et al.* reported the synthesis of three hyperbranched aromatic polyamides with AB_2 , AB_4 and AB_8 monomer types. Characterisation confirms that the degree of branching (DB) increased with increasing functionality, from 0.32 for AB_2 , 0.72 for AB_4 and 0.84 for AB_8 ⁵⁴. Generally, the synthesis of branched polymers through step growth polymerisation is limited due to a lack control of polymer size and structure, as well as obtaining broad molecular weight distributions with low molecular weights.

Ring opening polymerisation was used to synthesise hyperbranched polymers in 1992 by Suzuki⁵¹. The polymer terminal functions as a reactive centre, with cyclic monomers further joining to create a larger polymer chain via ionic propagation. Every added monomer step creates an additional reactive centre. This technique is considered in the generation of hyperbranched polymers such as polyethers, polyamines and polyesters^{5, 50}.

The Strathclyde methodology was discovered by Sherrington *et al.* in 2000 as a new route to the synthesis of branched vinyl polymers by employing conventional free radical polymerisation⁵². The method includes copolymerisation of a vinyl comonomer with a bifunctional or multifunctional comonomer in the presence of a free radical transfer agent or catalytic chain transfer species to avoid cross-linking and gelation. This method was carried out in 2009 by Chisholm *et al.* who utilised the copolymerisation of methyl methacrylate (MMA) and ethyl acrylate (EA) with ethylene glycol diacrylate (EGDA) as the branching agent (bifunctional monomer) via a free radical, solvent-free suspension polymerisation using AIBN as a radical initiator and CTA to avoid gelation and cross-linking, as well as to produce branched polymers. It was found that the branched copolymer can be synthesised successfully in aqueous suspension with low viscosity compared to its linear analogue P(MMA-*co*-EA)⁵³. Recently, in 2017, Huang *et al.* effectively synthesised branched poly(styrene) beads with high purities using the Strathclyde procedure⁵⁵. This approach has been proven to be versatile, cheap and scalable as a means to obtaining branched vinyl polymers. However, gel products are often observed along with the target branched soluble polymer and many data sets published in the literature indicate the presence of linear fractions or very lightly branched material.

This current project was carried out using SCVP as one of the most important techniques due to the use of available vinyl monomers that can be polymerised by radical chemistry²⁷. HBP synthesis via SCVP was first identified by Fréchet *et al.* in 1995¹⁹. This technique uses a monomer requiring a general structure of $A=C-B$, where B is an initiating species for the polymerisation of the vinyl group. Activation of B to produce B^* can promote the addition of a different monomer to the vinyl group, which then produces a dimer with two active sites, C^* (propagating group) and B^* (initiating group), and one vinyl group, $A=C$ ⁵⁶. Both B^* and C^* can accordingly react with vinyl groups of other monomers in the same manner to create a branched structure. A general mechanism for SCVP is shown in Scheme 2.4.



Scheme 2.4- The mechanism of self-condensing vinyl polymerisation (SCVP)²⁷

The SCVP method has been successfully applied since its discovery in different polymerisation techniques, such as cationic polymerisation⁵⁷, anionic polymerisation⁵⁸ and photo-mediated radical polymerisation⁵⁹. Moreover, ATRP polymerisation⁶⁰⁻⁶¹, NMP polymerisation⁶² and RAFT polymerisation⁶³ have been conducted, as they are classified as reversible deactivated radical polymerisation methods.

Among these techniques, SCVP can be carried out using RAFT polymerisation as it offers compatibility with different monomer functionalities and solvents and can operate under mild conditions. In 2003, Yang *et al.*⁶⁴ reported on initial work on RAFT-facilitated SCVP and correspondingly provided information on the synthesis of branched polymers through incorporation of a polymerisable dithioester chain transfer agent in the polymerisation of styrene. However, a complication was found with this method, namely that the branching agent used resulted in the dithioester group being incorporated into the main polymer chain, as shown below in Figure 2.3.a. However, Carter *et al.*¹³ successfully identified the problem and altered the process of polymerisation of *N*-isopropylacrylamide by using different branching monomers as chain transfer agents, as seen in Figure 2.3.b.c, which caused the dithioester group to be placed at the chain ends where the chain was not easily degraded.

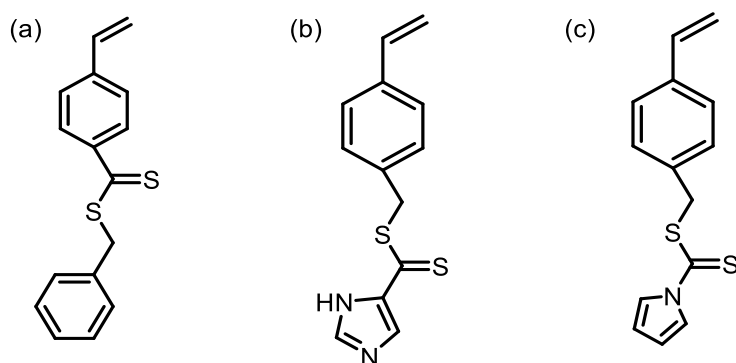


Figure 2.3- The RAFT branching monomer: (a) synthesised by Yang et al., and (b and c) synthesised by Carter et al binding the dithioester as the chain's terminal group ¹⁹

The new method devised by Carter *et al* was a breakthrough in the production of highly branched polymers, which also led Rimmer *et al.* ¹⁴ to synthesise an HB block copolymer, namely HB poly(*N*-isopropyl acrylamide-block-glycerol monomethacrylate). However, the formation of a poly(glycerol monomethacrylate) (PGMA) homopolymer from the initiation of the second monomer is unavoidable for all block copolymer syntheses that employ RAFT polymerisation. Nonetheless, the removal of homopolymers from the branched polymers was later established not to be too difficult due to branched copolymers produced by RAFT SCVP having high molecular weights, whereas the homopolymers do not. In 2014, Roy and De synthesised amino acid HBPs via SCVP/RAFT polymerisation with *tert*-butyl carbamate (Boc)-L-valine acryloyloxyethyl ester (Boc-Val-HEA) as the monomer and S-(4-vinyl)benzyl S'-butylthiocarbonate (VBBT) as the chain transfer agent, with different degrees of branching, functionalities and molecular weights. The Boc groups were deprotected by adding trifluoroacetic acid (TFA), leading to cationic surface charges being obtained. The chain of these polymers can be extended with 2-(2-methoxyethoxy) ethyl methacrylate (MEO₂MA) and poly(ethylene glycol methacrylate) (PEGMA) to obtain star polymers ⁶⁵. SCVP-RAFT offers a cost-effective route to branched polymers that requires only the relatively simple and certainly cost-effective synthesis of a functional dithionate ester as does the "Strathclyde" variant in which the branching structure is separated from CTA.

The intrinsic viscosity (η) of the polymer solution is regarded as a highly important characteristic in polymers and is estimated through the solvent molecules' and polymer chain interactions. In particular, it is described as the ratio of the specific viscosity of a given solution to the solute's concentration. In any specific molecular weight, a higher intrinsic viscosity can be found for a large diffuse molecule rather than a small and compact one. Branched polymers in solution reach a maximum intrinsic viscosity as a function of molecular weight and when

the shape of the polymer becomes compact and globular. However, linear polymers in solution show a linear viscosity increase up to a critical molar mass where a significant increase in viscosity is then observed because of chain interaction and entanglement, as seen in Figure 2.4. In branched polymers, the effect of chain interaction and entanglement depends on branch unit, where longer branches could increase interactions between molecules and hence increase the associated viscosity. In addition, with controlling the branch length, branched polymers can be used to help decrease the viscosity of the system⁶⁶⁻⁶⁷.

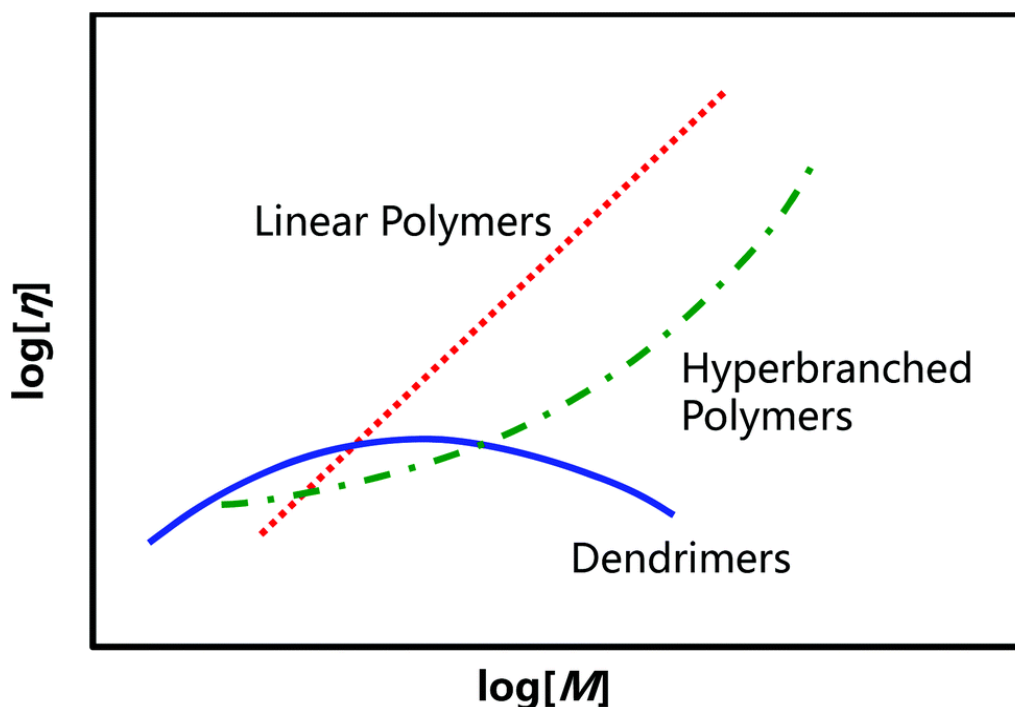


Figure 2.4- Illustration of the differences viscosity of different polymer architectures (image copied without modification⁶⁸)

The current method for understanding the intrinsic viscosity is by using size-exclusion chromatography (SEC), also known as gel permeation chromatography (GPC). The polymer sample is dissolved in a suitable solvent (mobile phase) and injected into a column packed with porous beads, commonly polystyrene (PS). As the solution travels to the column, large molecules cannot enter through the pores because of their size, hence they travel through the column quickly and their retention time is short. Smaller molecules enter more of the pores and so their retention time in the column is longer, such that polymer separation consequently occurs according to molecular size⁶⁹. Commonly, conventional SEC with a single concentration detector such as refractive index (RI) is used for polymer analysis. The elution time of the polymer sample is related to its molecular weight by calibrating the column with narrow polymer standards of a known molecular weight. However, this method of analysis

does not yield a universal curve for all polymer samples, leading to limitations in the use of conventional SEC analysis ⁷⁰. The column separates polymers based on the size or hydrodynamic volume of the molecules rather than molecular weight. Consequently, the accuracy of molecular weight thus determined requires ideal narrow standards that are not chemically different to the polymer under analysis to create appropriate calibration curves, but clearly this is impractical because of the low variety and numbers of commercially obtainable polymer standards. An additional issue is seen during nonlinear polymer analysis; once more, this is as a result of basing separation on hydrodynamic volume. Underestimation of molecular weight can occur while analysing nonlinear polymers using conventional SEC, with a decrease in hydrodynamic volume being seen for branched polymers in comparison to their linear analogues of identical molar mass (Figure 2.5) ⁷¹⁻⁷².

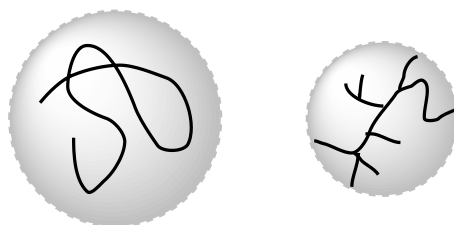


Figure 2.5- Differences in hydrodynamic volume between linear and branched polymers in solution

Increments in this branching level lead to increased inconsistency due to reduction in hydrodynamic volume, which later increases its prominence. An additional aspect to take into consideration is the sample being heterogeneous, not simply in terms of the weight and architecture of the molecule but also its composition, for example its microstructure, copolymers and tacticity, with all these factors having the capacity to influence elution time. SEC can provide absolute molecular weight data by using molecular weight dependent detectors such as a viscometer and multi-angle light scattering (MALS)^{70-71, 73} in combination with a concentration detector. The most modern SEC technique is a universal calibration which combines refractive index (RI) and viscometer detectors, and is based on the theory that polymer molecules are separated depending on hydrodynamic volume (V_h), which is proportional to the product of molecular weight (M) and intrinsic viscosity ($[\eta]$), as seen in equation 2.1:

$$V_h = K \times M \times [\eta] \quad (2.1)$$

$[\eta]$ is intrinsic viscosity, M is the molecular weight, V_h is hydrodynamic volume, and K is a constant that is independent of polymer structure.

Due to the relationship between hydrodynamic volume and intrinsic viscosity and the size of the molecules in the sample solution, the generation of a calibration curve for a set of standards plotting $\log [\eta].M$ against elution volume will be equivalent to plotting $\log V_h$ against elution volume. Hence, the same calibration curve will be generated regardless of the standards used, as per Figure 2.6.

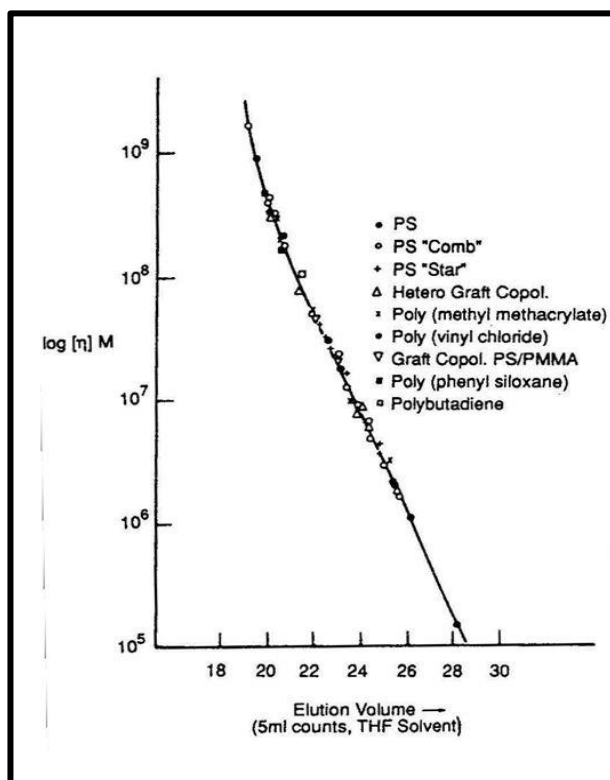


Figure 2.6- Example of a universal calibration of SEC (image copied without modification ⁷⁰)

A viscometer detector was employed to determine the intrinsic viscosity, $[\eta]$, for the particular molecular weight distributions of the polymer samples. These values allow the determination of absolute molecular weight, and the Mark-Houwink (α and $\log K$) ^{72, 74} parameters describe the relationship between intrinsic viscosity and molecular weight, as seen in equation 2.2:

$$[\eta] = KM^\alpha \quad (2.2)$$

where $[\eta]$ is intrinsic viscosity, M is the molecular weight and α with K is the Mark-Houwink constant for the polymer-solvent system.

Rewriting this equation in logarithmic form will give a linear relationship between $\log M$ and $\log [\eta]$ with an intercept of $\log K$ and a gradient of α .

$$\log[\eta] = \log K + \alpha \log M \quad (2.3)$$

This equation is useful for giving the value of α , which can provide information about the topological structure of polymers in solution. The α value can be between 0.2 and 0.5 for branched polymers, and 0.5 to 1 for linear polymers with a random coil structure in a good solvent^{68, 75-76}.

Although rarely reported it is known that α often takes relatively high values between (0.5-0.6) for polymers produced by the ‘‘Strathclyde’’ method in synthesis hyperbranched copolymers of poly(propargyl acrylate-*co*-acrylic acid-*co*-divinylbenzene) P(PA-*co*-AA-*co*-DVB)⁷⁷ compared to the SCVP-RAFT technique by Carter *et al* used in synthesis highly branched poly(*n*-isopropylacrylamide) (HB-PNIPAM), the α value was between (0.2-0.4)¹⁵.

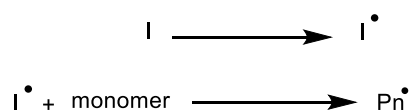
2.1.4 RAFT polymerisation

RAFT polymerisation is the most important RDRP techniques to proceed via the DT mechanism. It is distinct from other RDRP techniques in a number of ways. First, it is more tolerant of functional groups in monomers, solvents and initiators. Second, it offers a different class of chain transfer agent (CTA), which is based on a dithioester compound⁷⁸. Third, in RAFT polymerisation, the chain growth is controlled by a reversible chain transfer mechanism rather than capping. The processing of RAFT polymerisation is similar to conventional radical polymerisation, as they both have radical initiators, solvents, monomers and similar reaction conditions. The only difference is the presence of the chain transfer agent in RAFT polymerisation.

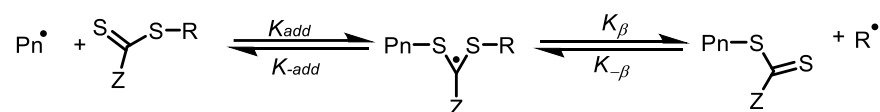
The full mechanism of RAFT polymerisation is based on a sequence of addition fragmentation equilibria, as seen in Scheme 2.5. In the first stage, a conventional free radical initiator, such as benzyl peroxide (BPO), or an azo compound, such as azobisisobutyronitrile (AIBN), initiates polymerisation. Polymer radicals, \mathbf{P}_n^\bullet , are formed through the thermal decomposition and subsequent reaction of the initiator with the monomers. These macro radicals react with the CTA, forming radical adducts. These adduct fragments produce dormant chains, which are capped by a dithioester (R) group and an additional species, \mathbf{R}^\bullet . The newly formed radical species is capable of initiating further polymerisation which occurs in the

reinitiating step, creating another propagating radical polymer chain, P_m^\bullet . In the early stage of polymerisation when all R groups have fragmented and initiated, the reversible chain transfer stage of the mechanism is replaced with the chain equilibration (main equilibrium). The important step in RAFT polymerisation is that the equilibrium between active (P_n^\bullet and P_m^\bullet) and dormant polymer chains occurs quickly at a high rate of addition (K_{add}) to ensure there is an equal probability for all chains to grow with minimal termination, hence providing and producing a polymer with a narrow molecular weight distribution. Termination in RAFT cannot be completely eliminated as it can for other RDRP techniques. Therefore, some polymer chains retain the thiocarbonylthio end group to be used post-polymerisation, when the polymerisation has completed.

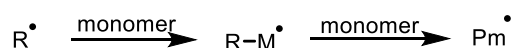
Initiation & radical formation



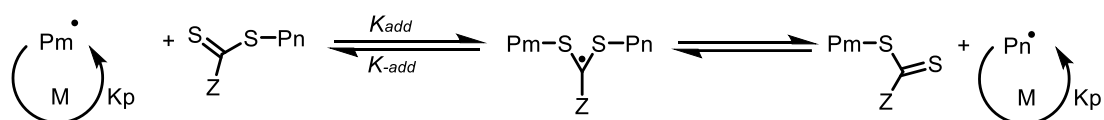
Reversible chain transfer



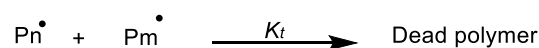
Reinitiation



Chain equilibration



Termination



Scheme 2.5- Mechanism of RAFT polymerisation (I = initiator, M = monomer, R = radical) that can initiate polymerisation (P_n and P_m = polymer chains) ^{27, 79}

Controlling polymerisation requires the appropriate selection of chain transfer agent (CTA), as shown in Figure 2.7. The three classes of CTAs are all thiocarbonylthio species, with varying substituent groups next to the C=S functionality. Variations include dithioobenzoates, trithiocarbonates and dithiocarbamates ^{36, 78}.

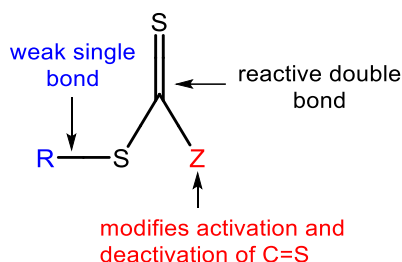


Figure 2.7- General RAFT agent structure

The choice of Z and R groups in the CTA are thought to be important to the success of the RAFT process with respect to selectivity for monomers and polymerisation conditions. The selection of the Z group is vital to the activation of the C=S double bond towards radical addition. It must stabilise the intermediate radical adduct that forms the propagating radical. Z is either an alkyl or aryl group. It is vital that R offers a satisfactory, or preferably good leaving group so that a stable radical can be formed to allow the polymerisation to be reinitiated. The optimum choice of CTA is dependent on the class of monomer being polymerised. For instance, for the polymerisation of methacrylates the benzyl dithiobenzoate would be useful⁸⁰. Likewise, acrylate and styrene monomers often use tertiary cyanoalkyl trithiocarbonates in RAFT polymerisation. The main categories of RAFT agents are shown in Table 2.1 below.

Table 2.1- The three main classes of RAFT chain transfer agent⁸¹

Name of RAFT agent	Architectures	Properties
Dithiobenzoates		-Very high transfer constants -Prone to hydrolysis -May cause retardation in high concentration
Trithiocarbonates		-High transfer constant -More hydrolytically stable than dithiobenzoates -Cause less retardation
Dithiocarbamates		-Activity determined by N substituted -Effective with electron-rich monomers

RAFT can be performed under a variety of reaction conditions, such as bulk, in either organic or aqueous solution, and suspension. It is particularly valuable when there is a large variety of monomers, including those with high functionality. Moreover, it is also tolerant of functionality in the dithio compound and the initiator. This permits the synthesis of polymers with side chain or end group functionality without the need for deprotection. The main disadvantage of RAFT polymerisation is that a limited number of RAFT agents are available commercially, so it is almost always necessary to synthesise them using different, and generally quite complex, synthetic and purification procedures. Moreover, the RAFT agents can be unstable over long time periods, are highly coloured and can have a strong smell due to the decomposition of the dithioester to yield small sulphur compounds. The presence of sulphur at the polymer chain ends might be undesirable for some applications; however, this can be eliminated with further physical and chemical purifications. Furthermore, RAFT agent typically has thiocarbonylthio groups (S=C-S) with substituents of Z and R that impact the polymerisation kinetics and the degree of control. Therefore, there is no one RAFT agent that can be effective for all monomer classes. For example, trithiocarbonate is useful in polymerisations of styrene, acrylate and acrylamide monomers, dithiobenzoate is useful in polymerisation methacrylate and methacrylamide monomers and dithiocarbamate is useful in polymerisation of vinyl ester and vinyl amide monomers.

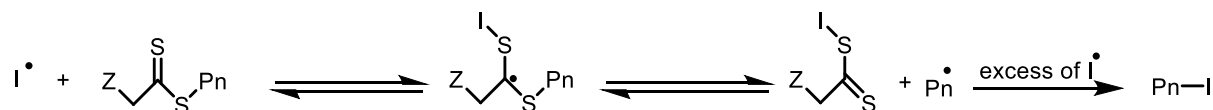
2.1.5 End group modification via RAFT polymerisation

The location of polymer obtained at the end of RAFT polymerisation is between the R (α) group and the Z (ω) group, which in this work is a thiocarbonylthio. In RAFT processing, propagating chains are initiated via R species and are thus covalently bonded to the R/ α group through a C-C bond, while the Z/ ω group is linked to polymer by the thiocarbonylthio, as shown in Figure 2.8. Therefore, the polymer is linked and attached directly to the R group, but not directly to the Z group. The introduction of thiocarbonylthio molecules gives colour to polymers, and indeed some odour due to abstraction of volatile sulphur. Thus, in some cases the release or removal of thiocarbonylthio is desirable, such as in optoelectronic and biomedical applications or transforming the Z/ ω group to a desirable functional group at the end of the polymer chains⁸²⁻⁸⁵.



Figure 2.8- The location of the polymer in RAFT polymerisation, showing the α and ω ends

To completely remove the Z (ω) group, there are several methods available to introduce functionality to the thiocarbonyl end of the polymer post-polymerisation, such as thermal elimination, reaction with a nucleophilic reagent, hetero Diels-Alder and radical-induced reduction or oxidation^{78, 86}. One post-polymerisation technique used in the present work is the transformation of the thiocarbonylthio functionality to a carboxylic acid via radical-coupling. The carboxylic end group functionality can then be used to attach and introduce a variety of primary alkyl amine end groups. Perrier *et al.*⁸⁷ described the procedure which allows the complete removal of the dithio functional group from the polymer chain ends obtained from RAFT polymerisation using an excess of AIBN or different diazo-initiators and which introduces chain-end functionalities to the polymers in addition to allowing for the recovery of the transfer agent. In the processes of radical-induced end group removal, the thiocarbonylthio group can be removed from the polymer chain by free radical initiators via radical cross-coupling. However, although this is a useful method it does suffer from a need to use large concentrations of the radical producing compound and the production of large amounts of waste. Radical species react with the C=S double bond in the polymer chain to form a radical intermediate. The intermediate can either fragment back to the original attacking radical or alternatively free the leaving group. When an excess of the radical is present, the equilibrium favours the formation of the leaving group radical, and thereby allows the radical group derived from the initiator to cap the chain ends as shown in Scheme 2.6.



Scheme 2.6- Mechanism of radical-induced removal thiocarbonylthio via radical cross-coupling from RAFT polymerisation⁸⁸

This novel technique is particularly significant since it achieves three important objectives:

- a) It removed thiocarbonythio (dithio) end groups completely,
- b) It can be used to incorporate a wide range of functionalities onto the HB polymer,
- c) It is capable of completely extracting the chain transfer agent after the reaction.

It has been established that various types of initiators with different functional groups can be utilised to impart a broad range of beneficial functionalities to the HBPs. Modern applications of the discovered functionalities currently form an important area of study in polymer science. Meanwhile, the most frequently prepared and used functionally changed polymers are those with the addition of carboxylic acid terminal ends, using AIBN or ACVA as initiators. Carboxylic acids provide wide-ranging functional potential compared to dithioester ends. An illustration is the attachment of a charged peptide sequence, RGD (arginine-glycine-aspartic acid), to the acid chain ends of highly branched poly(*N*-isopropylacrylamide) P(NIPAM)¹⁵, allowing the formation of stable sub-micron stimulus responsive particles above the critical solution temperature due to the additional stability attained from the polarity of the chain ends for achieving cell adhesion. Another example is the use of HB-P(NIPAM) with a cell-adhesive peptide, GRGDS (glycine-arginine-glycine-aspartic acid serine), at below the critical solution temperature of the polymer to detach or release human cells from substrates with free animal products, such as trypsin, and without the need to centrifuge to collect and transfer cells⁸⁹

2.2 INTRODUCTION TO CELL ADHESION

2.2.1 Biomaterials and biocompatibility

Biomaterials are defined as materials which are used in the body to repair, augment or replace any function of failing tissues or organs^{2, 90-92} as medical devices or as tissue-engineered scaffolds. Recently, the variability and functionality of biomaterials have rapidly progressed as a result of advancements in biology, chemistry, medicine, tissue engineering and materials. The materials used in medical devices can be characterised as metals, ceramics, composite glasses and polymers⁹⁰. In the biomedical field, synthetic biodegradable and non-biodegradable polymers, as well as natural polymers, are widely used as biomaterials in many applications including substrates for *in vitro* cell culture and scaffolds for *in vivo* tissue engineering.

Natural polymers can be classified as the first biodegradable materials applied in the clinical environment⁹³. The bioactive properties of natural biomaterials leads to better interaction of the cells and enhanced cell performance. These are classified as proteins such as silk, collagen, gelatine, fibrinogen, elastin, keratin, actin, and myosin, and polysaccharides such as cellulose, amylose, dextran, chitin, and glycosaminoglycans, and polynucleotides such as DNA and RNA⁹⁴.

Synthetic polymers can facilitate the repair of the structure or function of damaged or diseased tissues and they are particularly useful in biomedical applications due to their various useful features, for instance low density, porosity, mechanical and physio-chemical properties, chemical stability, large-scale producibility with a long shelf time, and biodegradability for some polymers⁹⁵. These synthetic materials have the potential to be a valuable tool in biomedical research as replacements for natural materials as they can be produced under controlled conditions and they represent the largest functional groups depending on specific application.

Several types of polymeric biomaterials have been used in different biomedical applications to solve particular problems, such as resisting protein adsorption or controlling biodegradation⁹⁴. These include polyurethane⁹⁶, poly(lactic glycol acid) (PLGA)⁹⁷ and poly(ethylene glycol) (PEG)⁹⁸, among others. Thus, polymer material applications are wide ranging, including in devices for tissue replacement and regeneration, in addition to use as surface coating applications in cell cultures⁹⁹.

The required properties of polymeric biomaterials or other biomaterials are biocompatibility, sterilisability, adequate mechanical and physical properties and manufacturability¹⁰⁰. It is vital for biomaterials that interact directly with an extracellular environment to have appropriate biocompatibility without damaging the biomolecules or cells, for instance, organisms. The primary assessment required for novel biomaterials in a biological system is biocompatibility testing. Several synthetic polymers, such as poly(lactic acid) and poly(glycolic acid) and their copolymers have been found to be biocompatible with the human body¹⁰¹. Biocompatibility has been defined as “the ability of a material to perform with an appropriate host response in a specific application”^{2, 90, 102}. This description was further expanded by Wintermantel and Mayer, who focused on the distinction between the surface and structural compatibility of a device. The surface compatibility indicates how appropriate the chemical, physical and biological aspects of an implant surface are to the host tissues. Structural compatibility refers to the mechanical properties of the host tissues, for example, elastic modulus. It has been proposed that when both surface and structural compatibility are attained, the optimal interaction between the biomaterial and host occurs².

To evaluate the biocompatibility of biomaterials, numerous *in vitro* and *in vivo* measures have been devised and performed over the previous six decades. To be operational in patients, biomaterials must meet three fundamental aspects of biocompatibility, the most significant of which is that the foreign material should not induce any allergic reactions, carcinogenic effects, toxicity or irritation in the host, and this is termed biochemical compatibility. Following from this, biomaterials must have an adhesion that is suited to the particular application of the material and, therefore, should be specialised for the types of cells or tissues involved. This indicates that excellent adhesive contact between the implant and surrounding tissues must occur so that the biomaterial performs efficiently. Finally, biomaterials should have comparable biomechanical characteristics to the exchanged organ and the surrounding tissues¹.

To formulate new biomaterials, cell adhesion, proliferation and biocompatibility must be improved¹⁰³. Numerous synthetic polymers are viewed as being non-toxic and biocompatible, such as poly(acrylic acid), poly(*N*-isopropylacrylamide), polyacrylamide and poly(hydroxyethyl methacrylate). Early researchers believed that the modification of biomaterial surfaces with adhesive peptides such as RGD or GFOGER would be sufficient to promote cell adhesion and proliferation due to the properties that make them suitable for

medical applications.¹⁰⁴⁻¹⁰⁷ However, the modification of polymers with peptide sequences is an expensive and time-consuming process, and applying alkyl amines to materials is still an emerging technique. Rimmer *et al.* created hydrogel materials with different functional amine groups to enhance the adhesion of epithelial and stromal cells¹¹. Similarly, polymers with a carboxylic acid functional group are considered to have a degree of biocompatibility, which can be used to promote cell attachment and as an *in vitro* wound-bed model, such as where MacNeil *et al.* observed that carboxylic acid end functionality has a degree of biocompatibility, with 3% acid in the polymers enhancing the attachment of keratinocytes and osteoblast-like cells^{9-10, 108}.

In the present study, the characteristics of the biocompatibility of novel synthetic polymers, with various functional groups, were investigated to explore and examine whether these materials promote and affect cell adhesion. Three major cell assays were used to evaluate the biocompatibility of the novel materials: cell viability, cell number determination and cell contact toxicity. Together, a picture emerged by these assays that provided information as to whether the material leaches toxic chemicals, if a material itself is toxic to cells, and if cells are able to adhere to, and proliferate upon, the surface of the material.

2.2.2 Protein adsorption and cell adhesion on biomaterial surfaces

The latest advances in cell therapy and modern medical practice use the adhesion of human cells to polymer substrates, for example poly(methacrylate) hydrogels, as a scaffold owing to its good cell adhesion properties on fibroblast cells¹⁰⁹, as well as poly(ethylenimine) and poly(propylenimine) as the substrates for neuronal cells¹¹⁰. *In vitro* cell culture, often termed “tissue culture”, is utilised as a routine tool to culture cells outside the *in vivo* environment, when using eukaryotic cells. Outside their natural environment, cells can only survive within specialised media, which includes antibiotics, growth factors, glucose, vitamins, etc.

When implanting these devices, a complex layer of the adsorbed proteins is formed at the material surface due to the exposure of this material surface to the various proteins available in interstitial fluid, blood and damaged extracellular matrix. Likewise, cells in culture which are plated over the polymer’s surface are also affected by proteins adsorbed at the material surface¹¹¹. The adhesion of cells to material substrates is a complex process, whose initial step involves protein adsorption to a surface. Adsorption of proteins in the serum or protein

containing the media to the surface starts prior to the approach of the cells to the surface. The ability of a protein not only to adsorb but to do so in an appropriate manner will determine whether cells are able to attach or otherwise.

The complex processing of protein adsorption onto a material's surfaces can occur within milliseconds or take minutes if the surface is conducive to protein adsorption. However, fluid and swollen interfaces (hydrogels) are generally resistant to protein adsorption and these interfaces are often regarded as non-biofouling. Thus, for solid non-swollen surfaces, by the time cells can reach the surface they recognize not the material but the adsorbed protein layer, and this might be led to occur cell adhesion with little control. For these generally hydrophobic interfaces the influence of cell adhesion on biomaterial surfaces includes the density of protein adsorption. Those proteins that have at higher serum concentration will occupy the surface at higher concentration at equilibrium, but it has been suggested that low molar mass proteins arrive at a surface before larger biomolecules. Hence, the composition and density of the biomolecules on the surface may change over time due to competitive protein adsorption and rearrangement between different proteins in a phenomenon known as the "Vroman effect". The Vroman effect is defined as: "In a protein solution sample, the low molecular weight proteins reach first and presented by relatively high molecular weight proteins which arrive later"¹¹²⁻¹¹³. The Vroman effect ignores the effects of surface induced denaturation but it has proved a useful concept in blood contacting applications. However, the effect is associated with high concentrations of protein as found in plasma (e.g. competition between albumin and fibrinogen and later other larger proteins) and there is no substantiated evidence to suggest that the much lower concentrations of proteins encountered during the ECM interactions with cells and synthetic scaffolds would be subject to effects associated with size dependent diffusion beyond the work of Copper *et al*¹¹⁴. Indeed, the effects of concentration are often hardly considered in the literature that cites the Vroman effect. Also, as far as the author is aware there is no confirmative evidence to suggest that the Vroman effect is significant when water swollen interfaces are considered even at high protein concentrations. An example of the difficulties is shown in the work of Smith and Sefton on poly(vinyl alcohol) interfaces where the Vroman effect was discussed¹¹⁵. However, in this rare example of a mention of the Vroman effect on swollen interfaces the authors had to conclude that: "These studies highlight the complexity of the interaction between plasma proteins and polymer surfaces (particularly hydrogel surfaces) and the difficulty of obtaining a clear picture of what happens when a single protein interacts with a polymer in the presence of other proteins."

Similarly, reactive surfaces involving biochemical reactions at the interface are unlikely to be influenced by the Vroman effect other than to say that a reactive surface will preferentially become coated with proteins that react with it, but faster diffusing proteins may coat the surface at earlier time points.

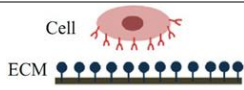
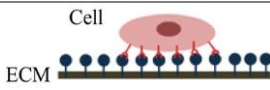
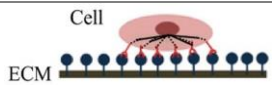

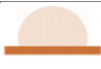

One proposal on the way in which cells adhere to biomaterials is by binding to surface proteins such as the vitronectin, laminin, collagen and fibronectin of the extracellular matrix (ECM) via specific receptors. There are four cell adhesion molecules (CAMs) that are responsible for cell adhesion: (i) the immunoglobulin superfamily (IgSF CAMs) members, which play an important role in the immune system in animals, including immunoglobulins, cell surface antigen receptors and antigen presentation in lymphocytes; (ii) cadherins are calcium-dependent adhesion molecules ensuring cell to cell adhesion in tissue; (iii) selectins, which are able to bind to sugar moieties or sugar polymers; and. (iv) integrins, which are transmembrane proteins that bind and respond cells to the ECM. Integrins not only anchor cells, supporting cell spread and migration, but also trigger signals that regulate survival, proliferation, and differentiation ¹¹⁶. Many important adhesive proteins such as fibronectin, laminin, vitronectin, fibrinogen, and collagen involve an Arg-Gly-Asp (RGD) sequence, which is the key to various integrins and allows the cell to adhere to proteins. This interaction of integrins and surface-adsorbed adhesion proteins is primarily responsible for the ability of cells to adhere to the surface of a biomaterial without adhering to the surface via integrin would lead to cell death (apoptosis) ¹¹⁷⁻¹¹⁸.

Cell adhesion is the first step in cell-polymer interactions, of which there are three types. First, a non-adhesive interaction between cell and the surface. Second, a passive interaction between cells and the surface, which means that the cells can interact but detach easily when small amounts of damage occur. Third, active adhesion between cells and surface, which means the interactions are strong and the cells spread well ¹¹⁹. Among these three kinds of cell-polymer interactions, the polymer surface can be categorised as an adhesive or non-adhesive surface for controlling cell behaviour.

The process of cell adhesion *in vitro* can be classified into three phases, as seen in Table 2.2. In the initial stage, the cell body becomes attached to its substrate. During this stage, the cell body flattens, and spreads and focal adhesions form between the cell and substrate with organisation of the actin cytoskeleton. It appears that the spreading of the cell is accompanied by the organisation of actin into microfilament bundles. As the time during which the cell

adheres to a substrate or to another cell lengthens, the adhesion becomes stronger. The initial adhesive interaction between the cell and substrate is driven by a specific adhesion mediated by integrin which begins when single pairs of receptors and ligands bind. The number of receptor-ligand bonds increases quickly, and this increases the total adhesion strength. After the initial attachment has taken place, the flattening (decrease in cell height) and spreading of cells on the substrate continues, increasing the contact area and constituting Phase I. The next stage (Phase II) is for the cell to spread beyond the unspread spherical cell's projected area. Continuing adhesion combines with the reorganisation of the actin skeleton and its distribution around the edge of the cell's body to initiate the spreading process. In Phase III, expansion causes cells to reach their maximum area of spread, and adhesion becomes stronger ¹²⁰.

Table 2.2- The processing of cell adhesion *in vitro* ¹²⁰

Cell Adhesion Phases	Phase I	Phase II	Phase III
Schematic diagram of cell adhesion			
Schematic diagram of the transformation of cell shape			
Cell adhesion intervention	Electrostatic interaction	Integrin bonding	Focal adhesion
Adhesion stages	Sedimentation	Cell attachment	Cell spreading and stable adhesion

The efficiency of adhesion and the spread of the cells to various polymeric surfaces depends significantly on the physicochemical surface properties of the biomaterial surface, including surface wettability, surface charge, chemistry, roughness and stiffness ¹²¹⁻¹²², as discussed below. Furthermore, the cell type preference on surface properties is important since diverse cell types may respond to surface properties in various ways.

2.2.3 Properties of material surface on cells

2.2.3.1 Surface wettability (hydrophobic / hydrophilic surface)

Surface chemistry wettability is the most crucial parameter for the polymer in terms of the amount, and the conformational changes, of adsorbed proteins¹²³⁻¹²⁵. The surface wettability can be examined by measuring the contact angle within the water spread of a droplet on the surface. Surface materials with higher contact angles are hydrophobic, while lower contact angles with the surface material are hydrophilic. An abundance of studies have examined the problems relating to the consequences of enhancing the hydrophilic or hydrophobic properties of polymers, specifically cell adhesion development and the subsequent increase in the biocompatibility of the materials¹²⁶.

Researchers have shown that a high rate of cell adhesion to polymeric surface can occur on a surface of moderate water wettability¹²⁵. Surfaces of high or low water wettability discouraged cell adhesion. Polystyrene (PS) is one example of a hydrophobic surface which has extensive applications in manufacturing petri dishes and cell culture plates. Many cells are unable to proliferate and adhere to a PS surface due to its hydrophobicity. Therefore, high-energy radiation treatments are used to introduce moderate surfaces for manufacture tissue culture plates via acid treatment and exposure to high-energy ionising radiation in order to decrease PS's contact angle and increase cell adhesion¹²⁷. On the other hand, the bioactivity of a hydrophilic material such as poly(ethylene glycol) PEG is low. The amount of protein that is adsorbed onto the surface is considerably reduced with the hydrophilicity of PEG. Consequently, promotion of further cell adhesion is unfeasible¹²⁸. Increasing cell adhesion and increasing the surface hydrophobicity can be accomplished through mixing PEG with hydrophobic materials¹²⁹.

PEG has been widely used as an antifouling material for biomedical applications, and its hydrogel has been approved by the Food and Drug Administration (FDA) for oral and topical applications¹³⁰. There are many reason for this property such as hydrophilicity, steric hindrance effects, large excluded volume, high mobility, graft density and molecular weight (chain length)¹³¹. It is able to form hydration layers with water, where increasing membrane surface hydrophilicity could effectively inhibit membrane fouling. Both in theory and experimentally, the molecular weight and surface density of PEG would be affected by protein adsorption when adding layers of PEG that provide an entropic barrier to protein adsorption¹³². Therefore, PEG has been used to modify surfaces to enhance antifouling properties¹³³.

There are numerous methods that have been employed in recent years to introduce hydrophilic groups into hydrophobic synthetic biomaterials such as plasma treatment in ammonia or sulphur dioxide, irradiation, photo- or plasma-induced grafting of hydrophilic polymers, ion implantation treatment, and others¹³⁴. One example of introducing a hydrophilic group onto a hydrophobic polymer to improve biocompatibility is the work done on poly-L-lactic acid (PLLA), which has been approved by the FDA for clinical applications but not for cell adhesion and proliferation. The wettability of PLLA and its suitability for the enhancement of cell adhesion via PLLA surface modification and introduction of groups such as OH, COOH and CONH₂ has been demonstrated by Ma *et al.* The applied methods include photoinduced grafting copolymerisation of hydroxymethyl methacrylate (HEMA), methacrylic acid (MMA) and acrylamide (AAM). According to the obtained results, there was considerable improvement in the chondrocyte cell cytocompatibility in the PLLA membrane with the surface amide and hydroxyl groups. However, the carboxylic acid with the original PLLA membrane had worse cytocompatibility¹³⁴⁻¹³⁵.

2.2.3.2 Surface charge

Charge plays a central role in protein adsorption and cell adhesion due to electrostatic interaction between cell membrane and surface materials^{122, 136}. The nature of the chemical surface is capable of greater interaction between surface and protein through electrostatic interactions. Experimental studies have shown that electrostatic forces play a vital role in the process of protein adsorption. It is known that proteins are divided into acidic proteins whose pH is less than 7, and basic proteins whose pH is greater than 7. At pH 7.4, it is equivalent to physiological environment and acidic proteins carry a negative charge and basic proteins carry a positive charge¹³⁷. Zhu *et al.* demonstrated that hydroxyapatite (HA), biphasic calcium phosphate (BCP) and beta tricalcium phosphate (beta-TCP) ceramic particles have negative charges, and preferred to adsorb more basic protein lysozyme (LSZ) than acidic protein bovine serum albumin (BSA) in pH 7.4 phosphate-buffered saline (PBS) solution¹³⁸.

Many researchers have showed that the increase in cell adhesion and biocompatibility often occurs through positive or negative charges at the material surface^{139, 140}; for example, 2-hydroxyethylmethacrylate (HEMA) hydrogel, with its positive charge-promoted cell attachment and spreading of osteoblast and fibroblast cells as compared to natural or negative charges¹⁴¹. Other studies by Yaszemski's group observed that the oligo(poly(ethylene glycol)fumarate) (OPF) hydrogel with its negative charge increased cell attachment and

differentiation of chondrocyte compared with the hydrogel modified using positive or natural charges ¹⁴².

In addition, surface charges are able to modify cell performance within the chemical functionalities, such as through the amine, carboxylic, hydroxyl, carbonyl and aromatic groups of the polymer materials, on the protein molecules in order to control protein adsorption. Chen *et al.* synthesised a series of hydroxyapatites (HA) with amine, carboxylic and methyl groups and observed that the positively charged groups had better biocompatibility with the mouse osteoblast (MC3T3-E1) cell line ¹⁴³. Lee *et al.* also prepared polyethylene (PE) with different chargeable functional groups (carboxylic, hydroxyl, amide and amine) by corona discharge treatment followed by graft copolymerization and a substitution reaction to investigate the effect on cell behaviour. The results showed that Chinese hamster ovary (CHO) cells adhered and grew on grafted surfaces more than a control due to the increased wettability afforded by hydrophilic functional groups. In amine group-grafted PE, which has a positive charge, excellent cell adhesion, spreading and growth was observed. However, poor growth for surfaces grafted with carboxylic groups was observed owing to its negative charge. Furthermore, surfaces grafted with natural amide or hydroxyl groups showed a similar amount of cell adhesion, while the spreading of cells was better with hydroxyl groups than with amides ¹⁴⁴. In the end, it can be said that although the work of the molecular mechanism on modified surface charges is unclear and not well understood, these studies confirm that surface charge plays a vital role in tissue engineering and cell biology applications ¹²⁶.

2.2.3.3 Surface topography and roughness

Surface roughness or topography is another important factor influencing cell adhesion and protein adsorption. Cells in the physiological environment are supposed to be able to deal with various types of surfaces with different levels of smoothness and roughness. Surface roughness can be divided into macro-roughness (100 μm - mm), micro-roughness (100 nm - 100 μm), and nano-roughness (less than 100 nm), each with its specific influence depending on the scale of the irregularities of the material surface ¹⁴⁵.

Several researchers have studied the attachment of cells with surface roughness at the micron level. For example, the behaviour of MG63 osteoblast-like cells on polycarbonate (PC) surfaces with different microrough sizes ranging from 0.2 μm to 8.0 μm has been studied by Lee *et al.* Their results showed that the cell adhesion and proliferation were preferred on

smooth surfaces but cell differentiation with higher osteocalcin expression and ALP-specific activity was apparent in rougher surfaces¹⁴⁶. Huang *et al.* observed the osteoblast-like U-2 OS cells cultured on ground titanium (Ti) surface with a surface roughness of 0.05-1.20 μm . It seems that the best cell adhesion occurred with an R_a of 0.15 μm compared with smoother surfaces (0.05-0.07 μm) or rougher surfaces (0.33-1.20 μm)¹⁴⁷. Furthermore, other studies have been carried out for cell adhesion, spreading and differentiation on surface roughnesses at the nanometre scale. Bartolo *et al.* examined the behaviour of neuronal cells cultured on different roughness surfaces (6.26- 200 nm), where the neurons were found to be increased on moderately rough surfaces (6.26- 49.38 nm) in comparison with very rough surfaces¹⁴⁸. Chung *et al.* used human vein endothelial cells to study different biomaterial surface roughness (10-102 nm) and discovered that the increasing surface roughness enhanced cell adhesion¹⁴⁹. All these studies suggest that the roughness or topography of surface materials respond differently depending on the cell type and size. This is not surprising since cell attachment is a complex process and not fully understood.

2.2.3.4 Surface stiffness

Cell development is also affected by the elastic modulus, or the stiffness of the surface, as another significant surface mechanical property¹⁵⁰⁻¹⁵³. However, the influence of mechanical properties varies with cell type and the nature of the adhesion receptors (integrins) that bind the cells to their substrates¹⁵⁴. In most of these studies, the surface with a higher proportion of stiffness or larger elastic modulus is disposed to be more beneficial for the proliferation, differentiation and spreading of the cells. For example, Khatiwala *et al.* demonstrated that the differentiation of MC3T3-E1 pre-osteoblastic cells cultured on poly(ethylene glycol) (PEG) prefer a stiffer substrate (423.9 kPa) for growing cells and found a high level of alkaline phosphate (ALP) activity in comparison to soft hydrogel (13.7 kPa)¹⁵⁵. Additionally, polyacrylamide hydrogels were synthesised with different elastic moduli to investigate the correlation of cell adhesion and spreading of native mesenchymal stem cells (MSCs) and the stiffness or softness of the substrate by Engler *et al.* The results showed that the human MSCs spread more on a stiffer substrate¹⁵⁶. Also, smooth muscle cells were revealed to spread and organise their cytoskeleton on stiff gels to a greater degree than on soft gels¹⁵⁷. In contrast, mouse spinal cord primary neuronal cells were cultured on a polyacrylamide gel and were shown to grow better on a soft substrate¹⁵⁸. Therefore, the response of the elastic modulus varies with different tissue types and organs, for instance bone is much stiffer than other tissues, so the osteoblast cells need a stiff substrate for cell adhesion

¹⁵⁹. To summarise, it is crucial to thoroughly study the mechanical, physical and chemical properties of new materials to determine whether the surface or substrate is appropriate for cell growth. The differential reactions of the cells, even when the types of surfaces are indistinguishable, make the procedures involved particularly challenging.

2.2.4 Epithelial and fibroblast cells

The human body is a collection of four types of tissues: connective, muscle, nervous and epithelial. The epithelium is one of four major tissue types in the human body and it lines most major organs (skin, kidneys, lungs, etc.). Generally, the epithelium consists of an organised single or multiple layer of epithelial cells resting over a basement membrane. The main function of epithelial tissues is to form a protective barrier between the organism and the environment in order to regulate the permeability, transportation and secretions of ions or molecules between body compartments ¹⁶⁰.

Epithelia are exposed to environmental damage due to their function as a protective barrier. Therefore, epithelium substitutes are broadly desirable for different organs, such as skin and the respiratory tract, to repair the various types of damage caused by trauma. Furthermore, many diseases such as cancer, polycystic kidney disease (PKD) and corneal disease ¹⁶¹ are triggered by damage to the epithelium's structure, which leads to tissue malfunction.

An additional important tissue is connective tissue, which is the most widespread and abundant tissue in the human body. The leading function of connective tissue is to support, connect and anchor different parts of the body. All connective tissues consist of cells supported with an extracellular matrix, and the most common connective tissue cells are fibroblasts, adipocytes and mast cells. The connective tissue extracellular matrix is composed of fibres (collagen and elastic fibres) and a ground substance ¹⁶². Fibroblasts are adherent and spindle-shaped cells, as formed in the tissues and organs of the body, associated with extracellular matrix molecules. The main function of fibroblasts is the production of the ECM component of tissues or organs such as collagen type I. Similarly, the matrix proteins are involved in wound healing and epithelial repair ¹⁶³⁻¹⁶⁵.

This study was assessed through the use of three key varieties of cells: human renal epithelial cells (HREpCs), human lung adenocarcinoma epithelial cell line (A549) and human

dermal fibroblast cells (HDFCs). Cancer cell lines have been selected as they are widely used in biological research due to be a convenient, inexpensive and accessible alternative to primary human epithelial cells. The main advantages of cell lines include the availability and accessibility of a large number of cells, the ability to replicate experiments over multiple passages, the ability to alter or manipulate genetic or phenotypic features of cell lines and the capability to examine effects over multiple generations¹⁶⁶. However, despite all the benefits of using cell lines, one must be careful when replacing primary cells with a cell line. Cell lines should be able to maintain the features of the functions of primary cells. This might be difficult to control as the functions of primary cell are frequently little understood. The number of passages of cell lines can cause a variation of phenotype or genotype over a period of time¹⁶⁷. Moreover, the major disadvantage of cell lines is contamination with other cell lines and mycoplasma. In the 1970s, Walter Nelson-Rees *et al.* showed that the number of cell lines used in the world and distributed within cell banks were contaminated with HeLa cells¹⁶⁸, and this is still a problem today^{167, 169}. When the contamination of cells occurs, a very rapid proliferation cell lines are introduced. It is known that the HeLa cell contamination causes a number of problems. Furthermore, other undetected mycoplasma contamination in cell cultures has been present for long time and can cause extensive modifications in gene expression and cell behaviour. Depending on reports submitted by cell banks, 15–35% of cell lines were estimated to be contaminated with mycoplasma¹⁷⁰⁻¹⁷¹. Therefore, the main findings from cell lines experiments should always be confirmed by comparing with primary cells.

In the other hand, primary cells are superior to cell lines as they are differently differentiated and are not immortalised. In standard culture settings, primary cells acquired directly from a particular species (human or animal tissues) can only be preserved in their differentiated state for a fairly short amount of time (days to weeks). The drawbacks of primary cell cultures is that they have a limited lifespan, are expensive and, although the maintenance of culture properties have been enhanced by various culture conditions and culture media additives such as growth factors and extracellular matrix components, cell-specific functions typically degrade rapidly, thus primary cell cultures are more difficult to use than cell line for experimentation¹⁷².

Fibroblast and epithelial cells are frequently found growing together in body tissue, though they perform different biological roles and display different phenotypes. The differences in the proteins in the plasma membrane are responsible for the interactions of each

cell type. Further, the structures and compositions of the extracellular matrices (ECMs) are different depending on their locations within tissues or organs. Organs rich in parenchymal cells, such as the kidney, have little ECM. However, organs or tissues that have primarily structural functions such as tendons and ligaments have large amounts of ECM relative to their cellular component. For example, the form of the ECM which exists subjacent to structures considered rich in epithelial cells, like the skin epidermis and small intestine mucosa, predominantly have site-specific glycosaminoglycans and type I collagen, as well as numerous growth factors. On the contrary, the ECM type, which is located immediately below epithelial cells like the urinary bladder's urothelial cells, the blood vessels' endothelial cells, as well as the liver's hepatocytes which are comprised of diverse protein collections such as collagen type IV, laminin and entactin¹⁷³. Therefore, fibroblast cells can be distinguished from epithelia and other cell proteins and may adhere differently to equivalent material because of the differences in protein expression and ECM development. All extracellular matrix operate as a store for small signalling molecules that control cell movement, inflammation and angiogenesis. Furthermore, ECM is a scaffold, and it offers structural support and sites for cell attachment¹⁷³. The epithelial sheet has two faces: one is the apical surface, which is free and exposed to the air; the other is the basal surface that rests on additional tissues (usually connective tissue). The basal surface of the epithelium is supported by a thin, tough sheet of extracellular matrix (ECM), called the basal lamina, as per Figure 2.9. The epithelial function differs chemically between the apical and basal surfaces. This relates to tissue polarity, which is responsible for the interaction between the ECM and other cells. In epithelial cells, there are different membrane proteins; one set is on the apical surface to absorb the nutrients from the gut, and the other set is on the basal and lateral surface to transport solutes out of the epithelial cells into the tissues and bloodstream. This distribution of membrane proteins is preserved by a carrier formed along the line called a "tight junction". This junction prevents the transportation of proteins between the apical and basal surfaces¹⁶⁴.

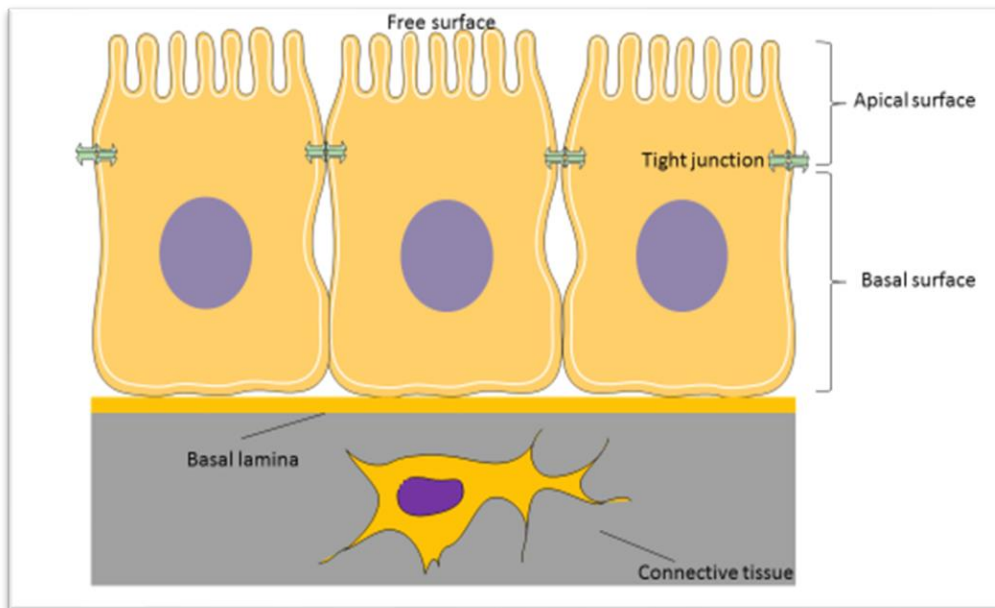


Figure 2.9- The organisation of an epithelial sheet (this figure was adapted from reference ¹⁶⁴ and produced using the Servier Medical Art software)

3 CHAPTER THREE: POLY(N-BUTYL METHACRYLATE) OF VARYING ARCHITECTURE AS A PROTOTYPICAL SYSTEM FOR PROMOTING EPITHELIALISATION

3.1 INTRODUCTION

The long-term aim (beyond the timescale of this thesis) of this work would be to produce a coating system that promotes epithelisation of biomaterials as a strategy to improve biocompatibility. The main goal of this work is to extend the work, to functional coatings, on hydrogels functionalized with primary amine groups as selective substrates for the development of epithelia. Poly(butyl methacrylate) (PBMA) was chosen as a prototypical vehicle and film forming material; similar methacrylic polymers are well-used in the general surface coatings industry already.

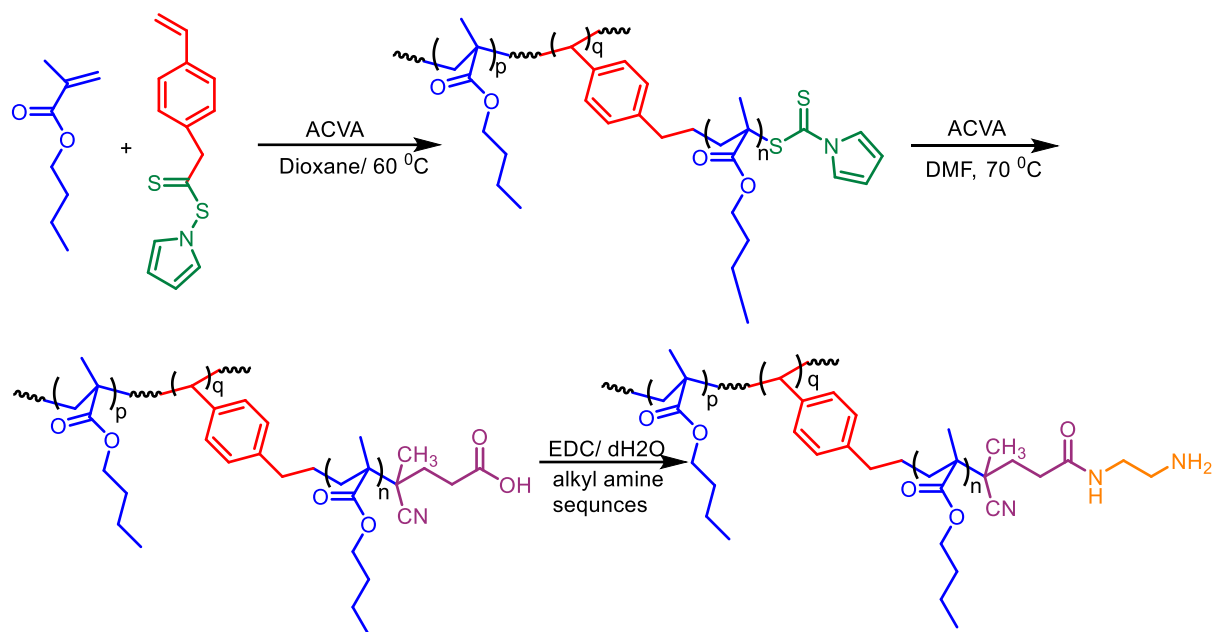
Although, the precise mechanism of the enhanced adhesion and proliferation of epithelial cells on surfaces with primary amine functionality is not yet elucidated presentation of these groups will be an important aspect. Clearly, the area is complex with aspects of protein adsorption and topography also playing a role but in this work the focus will be on presentation of the primary amine functionality via polymer architecture.

The work involves the synthesis of poly(butyl methacrylate) with different architectures (linear and highly branched) of poly *n*-butyl methacrylate with different functional groups using conventional free radical polymerisation and RAFT polymerisation in order to study how cells respond to different PBMA surfaces *in vitro*. Different methods can be used to study various aspects of cell behaviour¹¹. One strategy is the incorporation of an adhesive peptide sequence to the surface of biomaterials for the improvement of cell adhesive properties. A review of peptides has been provided by Le Baron *et al.*¹⁷⁴ and by members of the Rimmer group in relation to improving cell adhesion^{105, 109, 175}. Other modified chemical surfaces created with a surface charge (positive or negative) have been studied to improve cell adhesion to biomaterials. The most common functional groups that have been explored in relation to cell adhesion and proliferation on chemical substrates are carboxyl COOH, amine NH₂, hydroxyl OH and methyl CH₃ groups¹⁷⁶, as shown by many examples in chapter 2 section 2.2.3 (Surface charged). Additionally, polymer architectures not only influence chemical and physical properties, but also the various aspects of biocompatibility when cells or tissues interact with biomaterials. Thus, optimizing polymer architectures would be a useful strategy to improve

biomaterials for bio-applications. For example, Zeng *et al.* cultured the human cervical cancer cell line (HeLa) and human recessive dystrophic epidermolysis bullosa keratinocyte (RDEBK) cells on a series of linear and hyperbranched poly(5-amino-1-pentanol-*co*-1,4-butanediol diacrylate). They observed that the higher gene transfection efficiency of Luciferase DNA was improved on hyperbranched, rather than linear, polymers¹⁷⁷. In another study, linear and hyperbranched polyglycidol (PGs) were prepared to study the cytotoxicity of the human umbilical vein endothelial cells (HUVEC) and L-929 fibroblast cell line *in vitro*. The results showed that both PG polymer architectures are highly biocompatible in *in vitro* and *in vivo* assays¹⁷⁸.

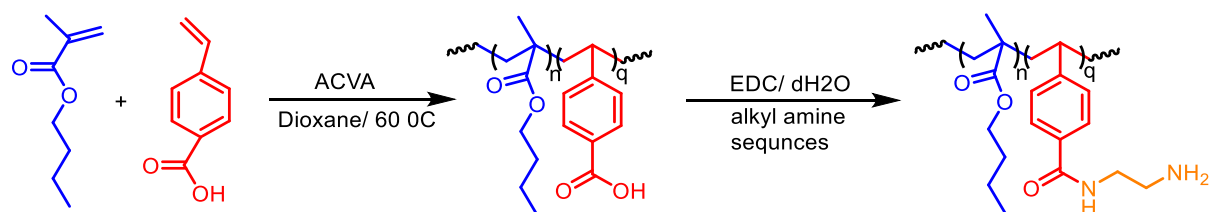
Several studies have demonstrated that amine or acid functionality¹⁷⁹⁻¹⁸² can affect the cell adhesion of different cell types. In previous work, Cox-Nowac *et al.* showed that the oligomer P(BMA-2COOH) provided a good substrate for fibroblast and epithelial cells; otherwise, the oligomer P(BMA-2NH₂) supported epithelial cells only¹⁸³. From these results, the suggestion is one of synthesising a more complex polymer architecture based on *n*-butyl methacrylate as a hydrophobic material to produce coating materials for use in medical devices.

Therefore, highly branched poly(*n*-butyl methacrylate)s were synthesised using reversible addition fragmentation chain transfer (RAFT) polymerisation in dioxane and 4-vinyl-pyrrole carbodithioate as the chain transfer agent (CTA) in a different molar monomer:CTA ratio to produce polymers with a pyrrole carbodithioate end groups, which can be modified to add a useful functional group. The pyrrole carbodithioate end group was converted to acid functionality through reaction with excess ACVA initiator. These acid functionalities were then reacted with diamine to produce functional biomaterials that could promote cell adhesion, as shown in Scheme 3.1.



Scheme 3.1- General scheme of synthesis of highly branched poly(butyl methacrylate) with pyrrole, acid and amine functionalities

Linear analogue polymers of PBMA were synthesised in a three-molar monomer:4-vinyl benzoic acid ratio by conventional free radical polymerisation. These linear polymers with acid functionality were then reacted with diamine to produce amine functional polymers, as seen in Scheme 3.2.



Scheme 3.2- General scheme of synthesis of linear poly(butyl methacrylate) with acid and amine functionalities

The three different molar ratios of the polymers were synthesised due to analysing the chemical properties and choosing the best in terms of viscosity, molecular weight and polymer conversion to study cell biology. All of the synthesised polymers were analysed with different characterisation techniques such as NMR, SEC, elemental analysis and FTIR to confirm the success of the polymerisation method. As the aim of this work was to synthesise polymer coatings to improve cell adhesion and obtain target polymers using reproducible methodology further studies on, for example, polymer kinetics were regarded as useful but out of scope of the aim of this work.

Primary alkyl amines with a chain length of between 2 and 6 carbons were chosen to functionalise the polymers. This was due to the ease of the amination reaction at the carboxylic groups^{11-12, 184-185} and because of chemical similarity to the amino acid lysine. Lysine, the eighth most abundant amino acid, is present in all proteins. It is a positively charged amphiphile, and is involved in a salt bridge with negatively charged amino acids such as aspartate, which has a stabilising effect on protein structure¹⁸⁶⁻¹⁸⁷. In addition, the action of lysyl oxidase on lysine in the extracellular matrix forms the derivative allysine, as per Figure 3.1, which is then used in the synthesis and crosslinking of collagen and elastin¹⁸⁸⁻¹⁹⁰.

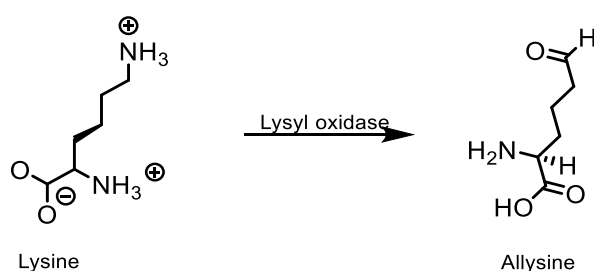


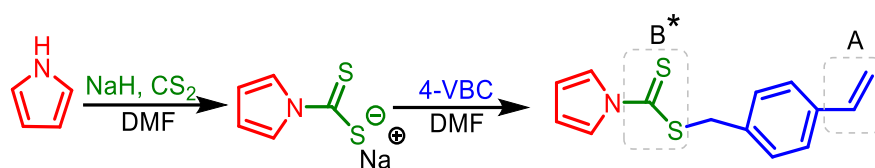
Figure 3.1- The conversion of lysine to allysine via lysyl oxidase in the ECM

The hypothesis of this work is that an amine functional polymer would promote the action of lysyl oxidase by mimicking lysine and would encourage the formation of crosslinks in the extracellular matrix.

3.2 RESULTS AND DISCUSSION

3.2.1 Chain transfer agent of 4-vinylbenzyl-pyrrole carbodithioate

The goal of this work was to investigate the use of RAFT SCVP for the synthesis of highly branched poly(*n*-butyl methacrylate). Therefore, the first step of this work was to synthesise the RAFT agent 4-vinylbenzyl-pyrrole carbodithioate (4-VBPC) as the chain transfer agent (CTA) shown in Scheme 3.3. This protocol was first established by Carter *et al.*¹³ and proceeded as expected with a 30.7% yield. It was synthesised by base mediated nucleophilic addition of pyrrole to carbon disulphide, followed by nucleophilic addition with vinyl benzyl chloride.



Scheme 3.3- Synthesis of the chain transfer agent 4-vinylbenzyl-pyrrole carbodithioate

4-VBPC is a typical AB^{*}-type inimer for SCVP, for which B^{*} is a carbodithioate functionality for the RAFT polymerisation of the vinyl group A and other comonomers. Hence, 4-VBPC can be used to control polymerisation by the RAFT process and allow for the simultaneous formation of branching points throughout the A group.

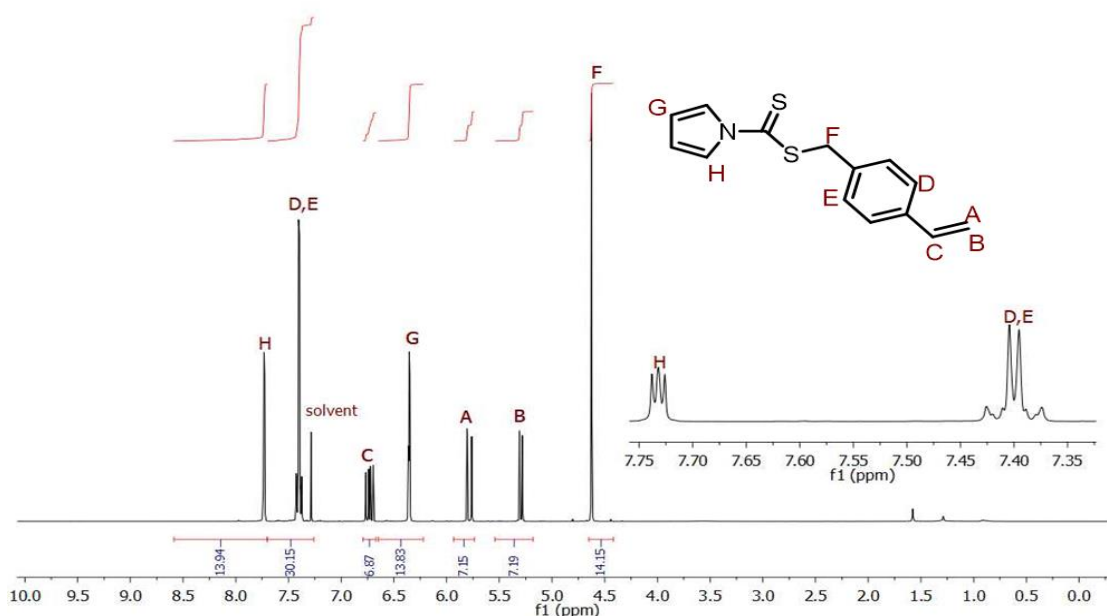


Figure 3.2- Proton NMR of 4-vinylbenzyl-pyrrole carbodithioate in chloroform-d solvent

$^1\text{H-NMR}$ characterisation in Figure 3.2 showed all the expected peaks and helped assess the purity of the chain transfer agent because the presence of impurities would affect the efficiency of the polymerisation. The proton of the vinyl group was observed at 5.3 -5.8 ppm, and the multiple signals of the hydrocarbon protons were observed at 6.8 ppm. The styryl signals are seen at 7.4 ppm, while the signals at 6.4 ppm and 7.7 ppm can be assigned to pyrrole protons. Additionally, the resonance at 4.6 ppm is associated with $-\text{S-CH}_2\text{-Ar}$. This demonstrated the purity of the compound as no additional peaks appeared in the $^{13}\text{C-NMR}$ spectrum. The carbon signal of carbodithioate was seen at 199 ppm and the other carbon signals can be clearly classified, as seen in Figure 3.3.

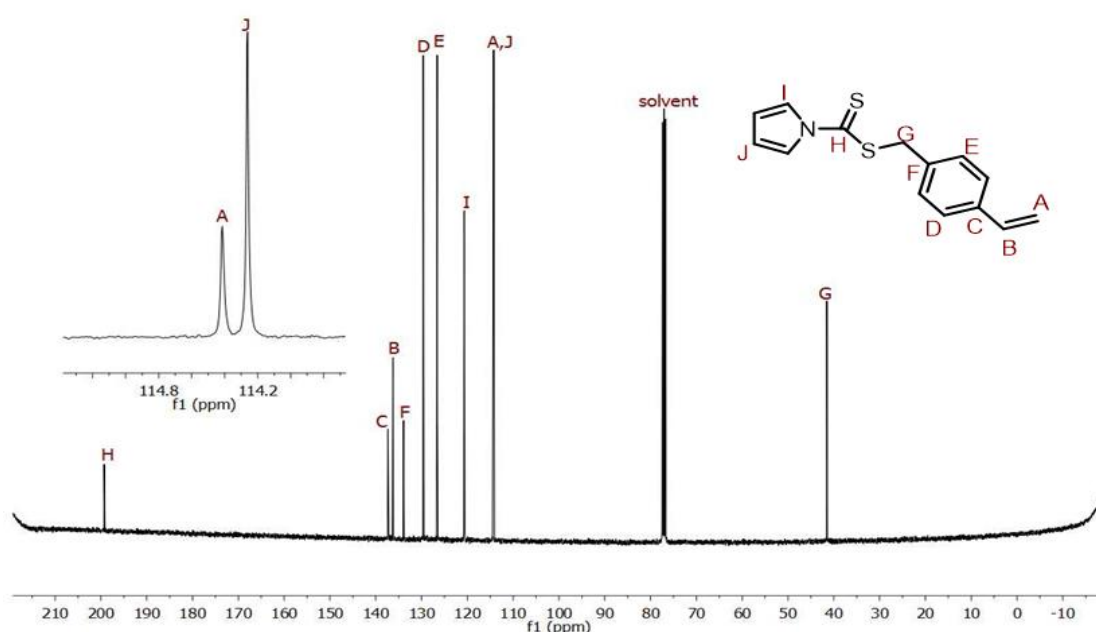


Figure 3.3- $^{13}\text{C-NMR}$ spectrum of 4-vinylbenzyl-pyrrole carbodithioate in chloroform-d solvent

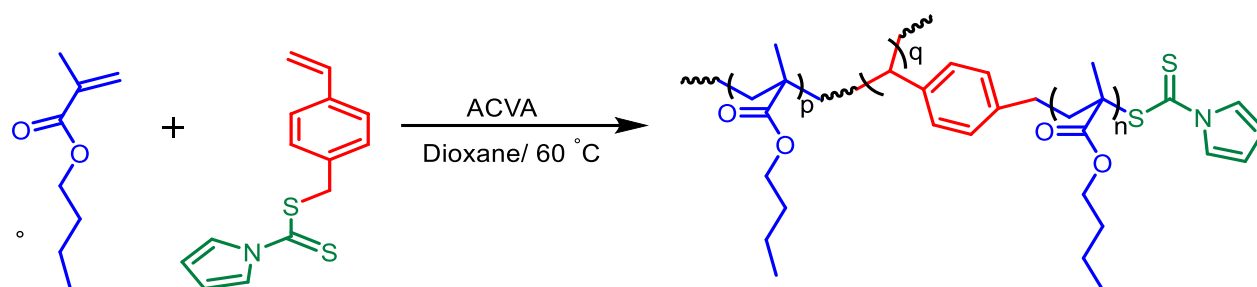
Another assignment was carried out to demonstrate that the chain transfer agent had a suitable degree of purity was elemental analysis, which demonstrated that the actual composition of the compound was close to the calculated theoretical content, as reported in Table 3.1.

Table 3.1- Elemental analysis for the chain transfer agent of theoretical and actual compounds

Compounds	Carbon (C)	Hydrogen (H)	Nitrogen (N)	Sulphur (S)
Theoretical %	65.65	5.88	5.10	24.70
Actual %	65.25	5.11	5.41	24.20

3.2.2 Highly branched poly(*n*-butyl methacrylate) with pyrrole end group

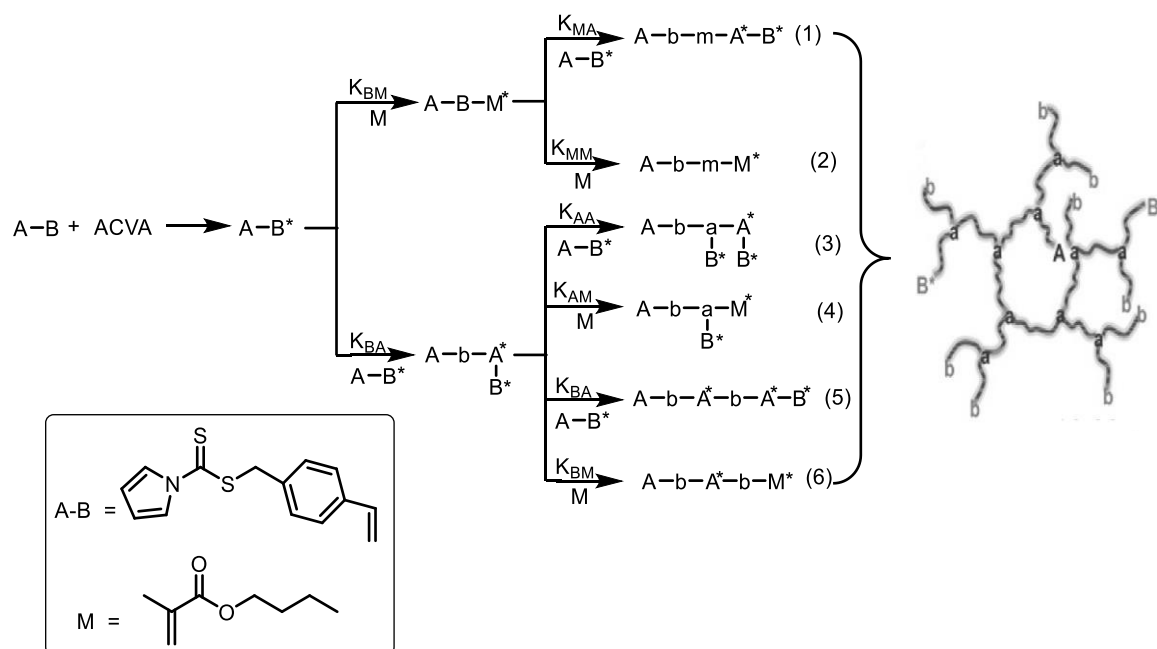
Highly branched poly(butyl methacrylate) was produced in three molar ratios of BMA as monomer:4-VBPC as the chain transfer agent (CTA) and 4-4'-azobis(4-cyanovaleric acid) (ACVA) as the free radical initiator. The general scheme for the preparation of HB-PBMA is shown below in Scheme 3.4 and further detail as to the description of the method is provided in the experimental chapter.



Scheme 3.4- RAFT polymerisation of *n*-butyl methacrylate with a pyrrole end using ACVA as the initiator and dioxane as the solvent

Copolymerisation of 4-VBPC with BMA was achieved using a freeze-pump-thaw technique with a dioxane solvent at 60 °C in three different volumes. As the amount of BMA monomer in the reaction was increased, the amount of solvent was decreased to keep the volume of liquid in the ampoule the same. Due to this, PBMA in varying molar ratios was applied to different reaction times in a water bath during the polymerisation process to avoid crosslinks and gelation of polymers in the ampoule.

The RAFT copolymerisation of the monomer and chain transfer monomer follow the typical mechanism of a SCVP¹⁹¹ as illustrated in Scheme 3.5. The ACVA free radical initiator provided radicals, through thermal decomposition, which react with the dithiocarbonate group of to form A-B*. Then, A-B* attaches to the double bond of CTA (A-B) and BMA (M) at rate constants K_{BM} and K_{BA} to form species A-B-M* and A-b-A*-B*, respectively. Afterward, A-B-M* couples with the monomer (M), forming species 1 and 2 at rate constants K_{MA} and K_{MM} , respectively, and A-b-A*-B* couples to A-B*, forming species 3, 4, 5 and 6 with rate constants K_{AA} , K_{AM} , K_{BA} and K_{BM} , respectively. In an ideal copolymerisation of BMA as the monomer and 4-VBPC as the chain transfer agent, the highly branched macromolecules are built from linear chains by these reactions.



Scheme 3.5- Reaction mechanism for the synthesis of highly branched polymers via RAFT-SCVP copolymerisation ¹⁹²⁻¹⁹³

Where M: BMA monomer, A: vinyl group of 4-VBPC, B: dithiocarbonate function of 4-VBPC, a: reacted A, b: reacted B, m: reacted M, *: radical site generated via fragmentation of dithiocarbonate group.

The incorporation of the chain transfer agent into PBMA was assessed using ¹H-NMR spectroscopy in deuterated chloroform, as shown in Figure 3.4. The presence of styryl as a branching point in the polymer was observed at 6.9 ppm and 7.4 ppm as broad signals. The pyrrole groups sit at the chain ends and the signals derived from the CH of pyrrole were observed at 6.3 ppm and 7.7 ppm. The spectra of BMA-1 showed small signals at 5.1 ppm and 5.5 ppm attributed to the vinyl proton (CH₂=CH-) of the unreacted vinyl group. However, all the CTA had been incorporated into the BMA-2 and BMA-3 polymers, since no unreacted vinyl CH₂= groups were observed in the appropriate region. This indicates that all molecules of the CTA have undergone transfer and reinitiate.

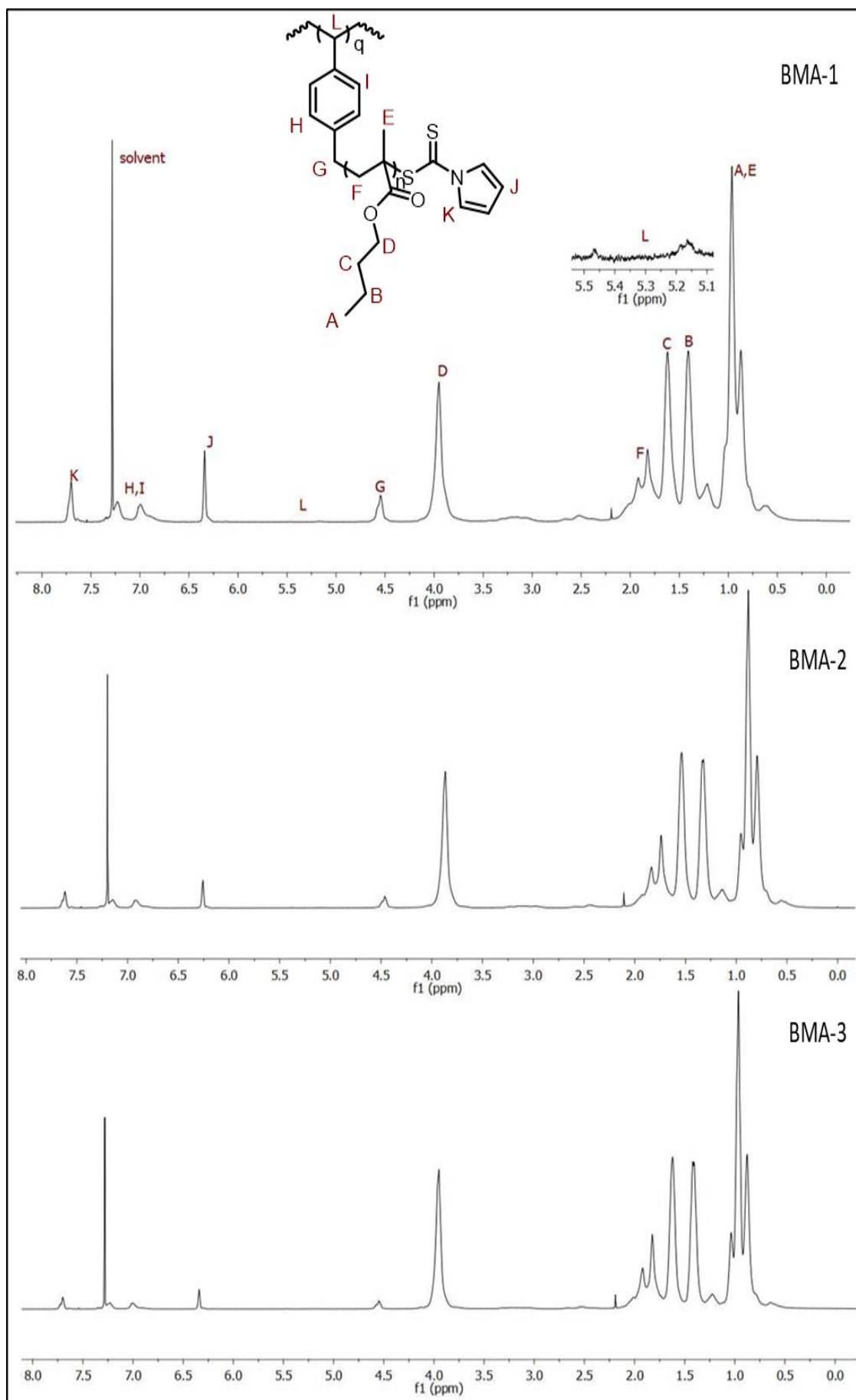


Figure 3.4- ¹H-NMR spectra of highly branched poly(butyl methacrylate)

Moreover, analysis of the ^{13}C -NMR spectrum of this material confirmed the formation of highly branched polymers in Appendix 3.1. Many carbon signals appeared in the regions of the methylene carbons between 14 to 50 ppm. The styryl and pyrrole peaks were observed at about 112 and 120 ppm, respectively. Further, the carbon of C=O observed at 190 ppm, whereas the carbon peak at 65 ppm corresponds to the CH_2 close to the oxygen atom in butyl methacrylate.

The results calculated based on ^1H -NMR spectra for the different molar ratios are seen in Table 3.2. The polymer composition and monomer feed are determined by comparing the integration of the proton signal from BMA, labelled “D”, with the proton signal of the CTA, labelled “H”, “I”, “K” and “J”. The molar ratios of this copolymerisation were calculated to be 6.9 for BMA-1, 15.4 for BMA-2 and 26 for BMA-3, which is quite similar to the feed ratios. These results indicated that high conversions of BMA and CTA had occurred, as seen in the monomer conversions which were above 90% for all of the different molar ratios, promising a high resultant molecular weight. The integration spectra for all the polymers are shown in Appendix 3.2, Appendix 3.3 and Appendix 3.4 depending on molar ratio, respectively, where errors in the integration measurement of the NMR intensities were estimated to be about $\pm 5\%$.

Table 3.2- Result of SCVP RAFT polymerisation reaction of BMA in the presence of CTA determined by ^1H -NMR spectroscopy

HB-PBMA:pyrrole	Feed ratio ^a	(v)	(\acute{u})	Conversion ^b %	Pyrrole ^c %	Benzyl ^c %	BMA ^c %	D_{br} ^d	RB ^e
BMA-1	8:1	0.125	0.145	94	11.6	10.9	77.5	0.22	4
BMA-2	16:1	0.062	0.065	97	6.2	5.3	88.5	0.11	9
BMA-3	24:1	0.041	0.037	98	3.7	3.3	93	0.07	14

^a Initial molar ratio of [monomer/CTA]. v = Mole fraction of CTA in the BMA feed, \acute{u} = Mole fraction of CTA in the polymer. ^b Percentage conversions determined by ^1H -NMR. ^c Percentage of terminal, dendritic and linear units in polymers determined by ^1H -NMR. ^d Degree of branching calculated from equation 3.2.1. ^e Repeating unit per branch (RB) = $1/D_{br}$.

One advantage of SCVP is its ability to determine the degree of branching (D_{br}) of HBPs, the values of (D_{br}) were produced by the proton integrations of the pyrrole group as the terminal unit, labelled “J” and “K”, and the styryl group as a branched unit, labelled “H” and “I”, and the proton integration of the ethyl group, labelled “D”, derived from BMA as a linear unit using the following equation:

$$\text{Degree of branching } (D_{br}) = \frac{D+T}{D+T+L} \quad (3.1)$$

Where D is dendritic or branched unit, T is the terminal unit and L is the linear unit.

As expected, the increase in the amount of pyrrole in the polymer resulted from a decrease in the monomer concentration and increased CTA in the reaction. In addition, the quantities of D_{br} were used to describe the branched features of highly branched polymers. High degrees of branching indicated that their architecture was similar to that of dendritic polymers, while a low degree of branching would indicate that their architecture was close to that of linear polymers. The degree of branching was determined to lie between 0.22 and 0.07, as seen in Table 3.2. D_{br} was increased with the amount of CTA increasing due to the 4-VBPC as the chain transfer agent, with it being able to regulate chain length and branching; thus, the greater the amount of CTA present, the shorter the chains produced. Furthermore, a high degree of branching means that the polymers had a lower viscosity¹⁹⁴. In addition, the number of repeat units per branch (RB) was obtained, which showed that the more CTA present the shorter the chains produced, i.e., fewer repeat units per branch and therefore the greater the value of D_{br} .

Solid-state FTIR was used to obtain more information about the success of the inclusion of the RAFT agent into PBMA. Figure 3.5 below demonstrates the strong C=O and C–O intensities of the ester group in HB-PBMA, clearly visible at 1720 and 1140 cm^{-1} , respectively. The stretch at 1050 cm^{-1} is related to the C=S thiocarbonyl bond, whilst the C–N stretch was observed at 1300 cm^{-1} . The stretch seen at 2950 cm^{-1} is due to C–H bonds, and the variable absorbance at 1380 cm^{-1} can be attributed to the bending of CH in polymers. The weak aromatic stretch that was expected at around 1600 cm^{-1} cannot be seen due to the concurrent C=O signal, but a C=C stretch in ring signal can be observed at 1460 cm^{-1} that confirms the RAFT agent was incorporated successfully.

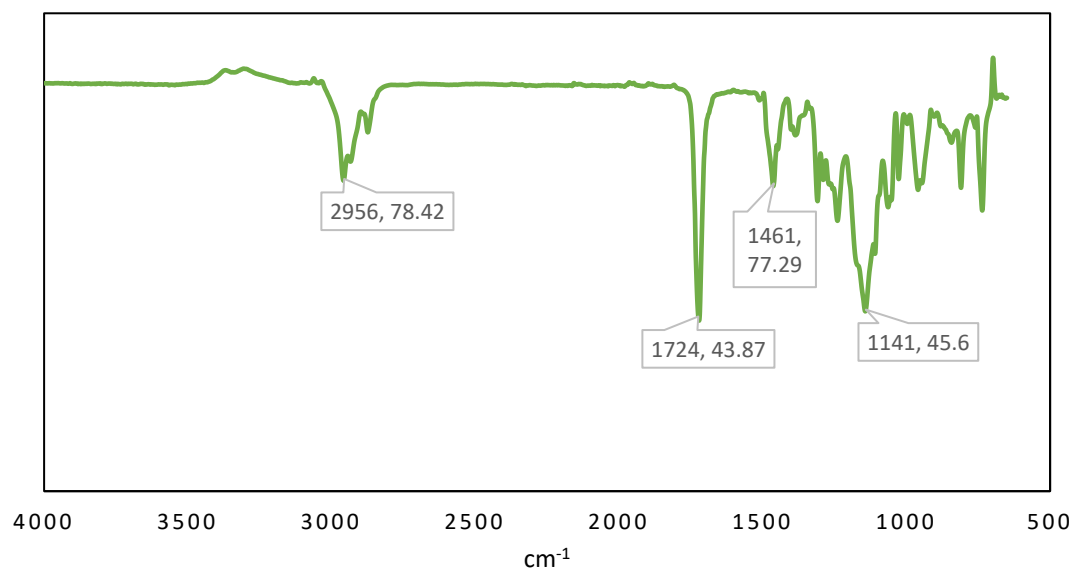


Figure 3.5- FT-IR of highly branched poly(butyl methacrylate) HB-PBMA-2

Figure 3.6 shows the results of SEC analysis using THF as the eluent and polystyrene as the standard calibration via RI detector. The molecular weight of polymers ranged from 25,000 to 78,000 $\text{g}\cdot\text{mol}^{-1}$, depending on the ratio of monomer to chain transfer agent used (i.e. the feed ratio increased from 8:1 to 24:1), as expected for highly branched copolymerisation reactions with high conversion of monomer, in agreement with previous reports^{49, 195-196}. The MW distributions was broad with a slight shoulder, as would be expected for polymers produced through SCVP RAFT polymerisation. This observation is in agreement with the prediction of Han *et al.* He demonstrated that the RAFT-based hyperbranched synthesis lead to produced high molecular weights and broad dispersity¹⁹³.

HB-PBMA	M_n ($\text{g}\cdot\text{mol}^{-1}$)	M_w ($\text{g}\cdot\text{mol}^{-1}$)	M_z ($\text{g}\cdot\text{mol}^{-1}$)	\mathcal{D}
PBMA-1	10376	25345	48419	2.4
PBMA-2	15477	51459	143871	3.3
PBMA-3	22195	78613	231643	3.5

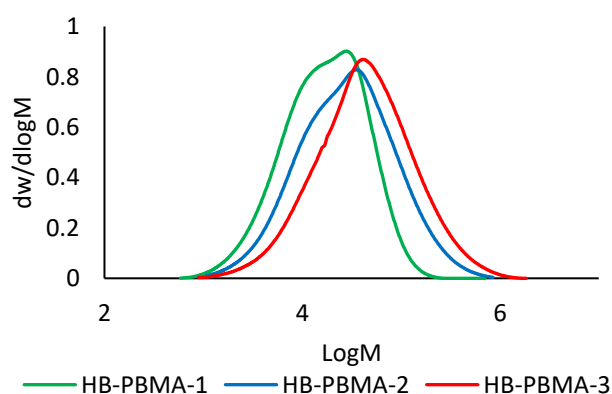
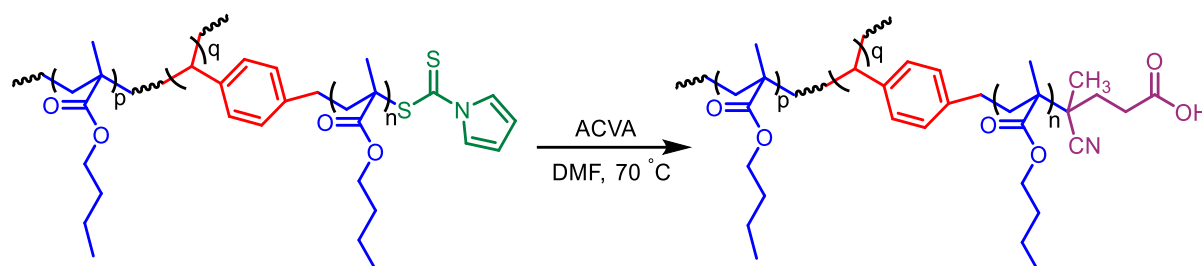


Figure 3.6- SEC results of HB-PBMA with pyrrole functionalities

(left) number averaged molecular weight (M_n), weight averaged molecular weight (M_w), z-averaged molecular weight (M_z), and dispersity index (\mathcal{D}). (right) SEC traces of molar mass distribution.

3.2.3 Functionalised highly branched poly(butyl methacrylate) with an acid end group

Highly branched polymers were reacted with excess ACVA to convert the pyrrole end groups to more useful carboxylic acid functional end groups, as shown in Scheme 3.6.



Scheme 3.6- Functionalisation of HB-PBMA with acid end group using an excess of ACVA

This method has been used by the Rimmer group to synthesise highly hyperbranched PNIPAM with acid functionalisation⁸⁹. The three different molar ratios of BMA:CTA were reacted as per the protocol used for PNIPAM, which involved using excess ACVA (about 20 equivalents relative to number of pyrrole chain end groups) and dry DMF as the solvent. These polymers were subjected to characterisation by proton and carbon NMR, FTIR and SEC after extensive purification in order to support pyrrole carbodithioate end groups being converted to acid groups.

The ¹H-NMR spectrum in Figure 3.7 shows that a new peak at 10 ppm demonstrating the success of this reaction due to the presence of the OH of a carboxylic acid. The peaks of the pyrrole group were removed, indicating the loss of pyrrole groups from the structure and the incorporation of the acid group. Another peak showed the successful introduction of ACVA onto the polymer chain ends at 2.6 ppm due to the CH₂ from the ACVA initiator.

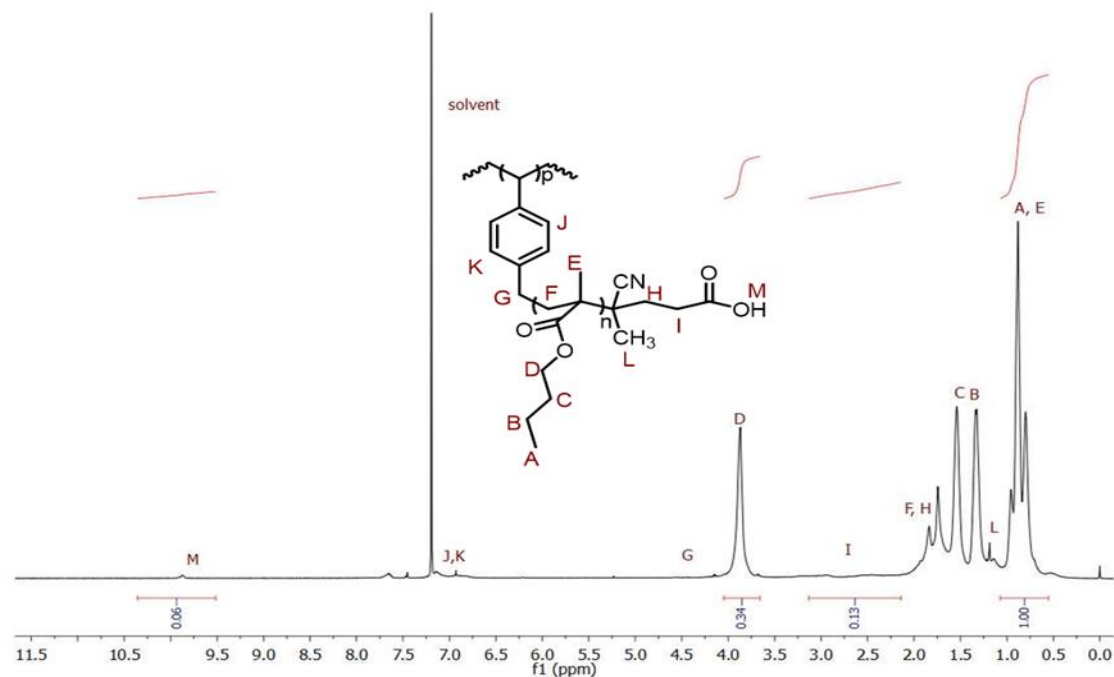


Figure 3.7- ¹H-NMR spectrum of highly branched with carboxylic end group (HB-PBMA:COOH-2)

The FTIR spectrum was used to give more information on the success of adding acid functionality to the pyrrole end group. Error! Reference source not found. shows the differences in absorbance bands for HB-PBMA before and after functionalisation. The spectra for each of the polymers shows that strong C=O and C-O absorptions are clearly visible at the expected frequency for the ester group. In the functionalised materials, a large broad OH stretch was apparent at about 3370 cm⁻¹. There are two C=O in the acid-ended material, one at 1720 cm⁻¹ related to carbonyl in ester group, and the second one at 1640 cm⁻¹ for carbonyl in carboxylic acid. This spectrum confirms the success of functionalising the material with an end acid group.

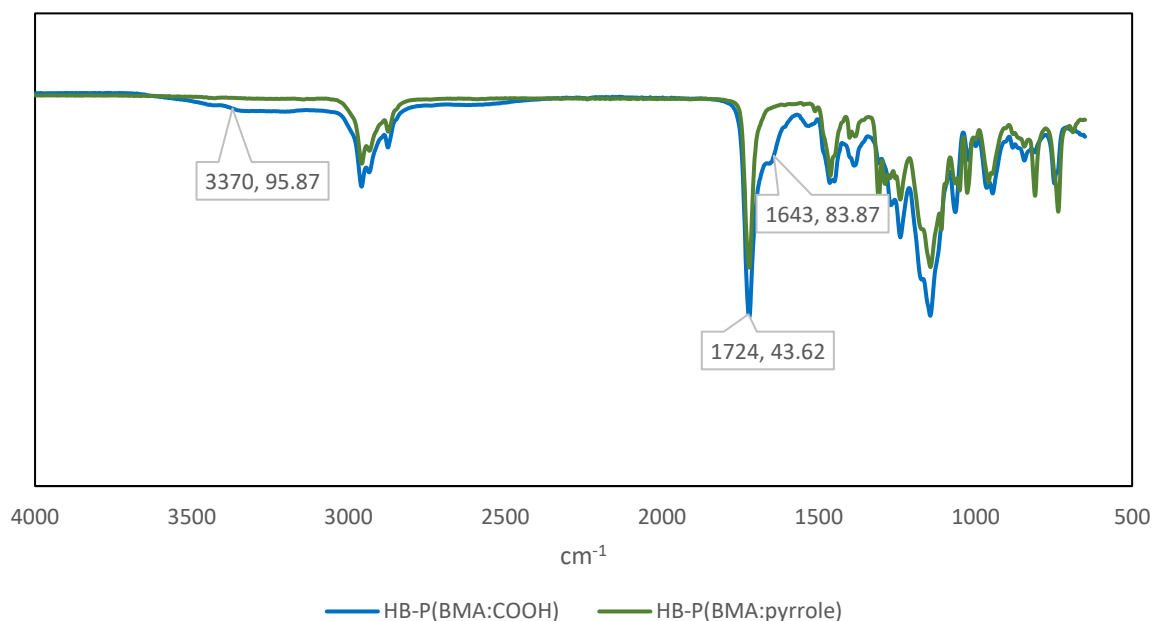


Figure 3.8- FTIR spectra showing the differences between HB-PBMA-2 before and after functionalisation

SEC data were obtained for these materials in THF, as shown below in Table 3.3. It would be expected that the molecular weight distribution of polymers with a pyrrole end group and polymers with a carboxylic acid end group would essentially be the same because the only difference between the two materials is the end group. However, this was not observed.

Table 3.3- SEC results for highly branched polymers before and after functionalities

HB-PBMA	M_n	M_w	M_z	\mathcal{D}
PBMA-1	10376	25345	48419	2.4
PBMA:COOH-1	6543	9076	12004	1.4
PBMA-2	15477	51459	143871	3.3
PBMA:COOH-2	14647	28457	48836	1.9
PBMA-3	22195	78613	231643	3.5
PBMA:COOH-3	20317	51664	122096	2.5

Number averaged molecular weight (M_n), weight averaged molecular weight (M_w), z-averaged molecular weight (M_z), and dispersity index (\mathcal{D}).

According to these data, the polymers experienced a reduction in molar mass, which was expected as a result of undergoing the acid functionalisation, for which there was an associated decrease in dispersity. This was unexpected as the chains should be stable in solution at the

reaction temperature; the C-S bond is the weakest link in the structure, but during the functionalisation this is being broken. A possible explanation is that the solvency of the polymer in THF changed after the acid functionalisation; the acid-ended polymer is less soluble in THF than the pyrrole functional polymer, as the data indicated. This produces a low hydrodynamic volume and hence the apparent molar mass distribution is altered. However, the narrowness of the distribution also suggests that adsorption plays a more important role in these acid-ended polymers. Molecules with charge can adsorb into the SEC column, which changes their retention time; since they take longer to elute they appear to have a lower molar mass, which would explain the above observations. Figure 3.9 below shows the polymer distribution before and after functionalisation. The narrowing of the distribution can be clearly seen, and the peak has shifted to lower molecular weight. In this context the GPC data of these COOH polymers do not reflect the molar mass distributions. However, the data do indicate a structural change that is reflected in the chromatographic behaviour of the polymers.

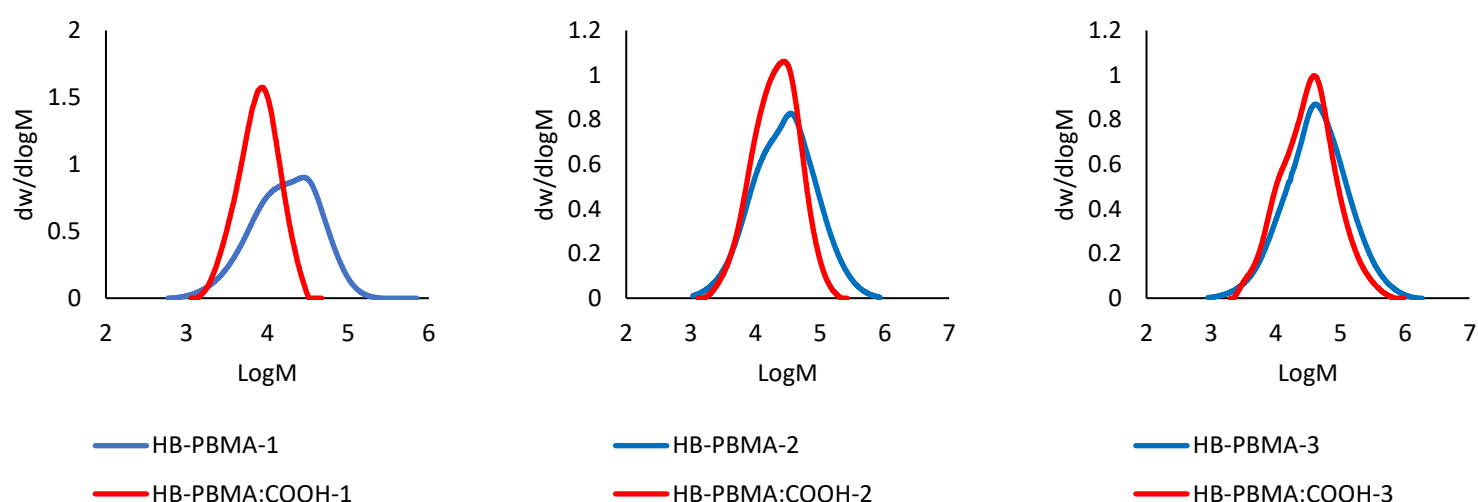


Figure 3.9- Molar mass distribution of highly branched polymers before and after functionalities

The last analytical technique used was elemental analysis, which was carried out in order to determine the success of the functionalisation reactions. If the percentage of S detected in the polymer is zero, and all pyrrole chain ends have been converted to carboxylic acid groups, so the functionalisation of the polymers can be described as having been 100% successful. The results obtained are shown in Table 3.4.

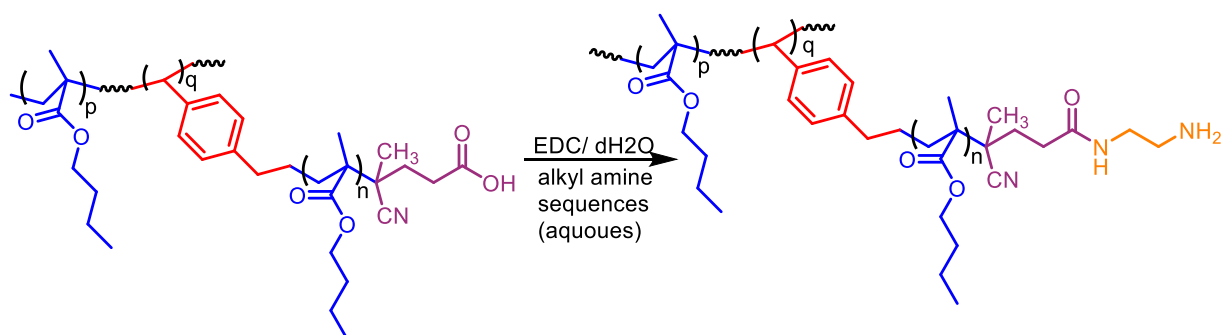
Table 3.4- Summary of theoretical and actual elemental analysis for poly(butyl methacrylate) with pyrrole and acid end groups

HB-PBMA	End group	Theoretical Elemental Analysis %				Actual Elemental Analysis %			
		C	H	N	S	C	H	N	S
BMA-1	Pyrrole end	67.8	8.9	1	4.6	66.8	8.9	1.3	5.0
	Acid end	64.9	9.4	1.1	0	65.3	9	1.7	1.1
BMA-2	Pyrrole end	67.3	9.3	0.6	2.6	67	9.1	0.6	3.6
	Acid end	66.2	9.6	0.6	0	67	9.2	0.8	0
BMA-3	Pyrrole end	67.4	9.5	0.4	1.8	67.1	9.4	0.5	2.1
	Acid end	66.7	9.6	0.4	0	66.6	9.3	0.8	1.6

The results from the elemental analysis for the pyrrole end group polymers proved to be close to the predicted values. This implies pure products and indicates that the initial polymerisations proceeded as expected. For the carboxylic acid end group polymers, the percentage of sulphur decreased, indicating the loss of pyrrole carbodithioate groups from the structure. However, there was still sulphur in BMA-1 and BMA-3 and there had been a decrease to 78% and 24% sulphur content after functionalisation, but in BMA-2 the sulphur content was zero, which proved that all pyrrole carbodithioate groups had been converted to carboxylic acid end groups. Another aspect of the elemental analysis was that the nitrogen content increased after functionalisation when it should have remained the same. This is may be due to unreacted ACVA remaining trapped in the polymers, as ACVA has a relatively high nitrogen content.

3.2.4 Diamine addition to HB-PBMA with acid end group

The main purpose of the synthesis of highly branched BMA polymers was to convert the acid end groups to amine functional polymers. The HB-PBMA:COOH-2, with a molar ratio of 16:1, was selected for the incorporation of a primary alkyl diamine due to its high conversion compared to HB-PBMA:COOH-1 and high solubility compared to HB-PBMA:COOH-3. The amidation of the polymers occurs through the formation of an amide linker between COOH in highly branched polymers and NH₂ on the primary alkyl amine in an aqueous system. An amidation reaction was carried out using sodium dodecyl sulphate (SDS) as an emulsifier stabiliser and 1-ethyl-3-(3dimethylaminopropyl)carbodiimide (EDC) as a coupling agent. The reaction process is shown below in Error! Reference source not found..

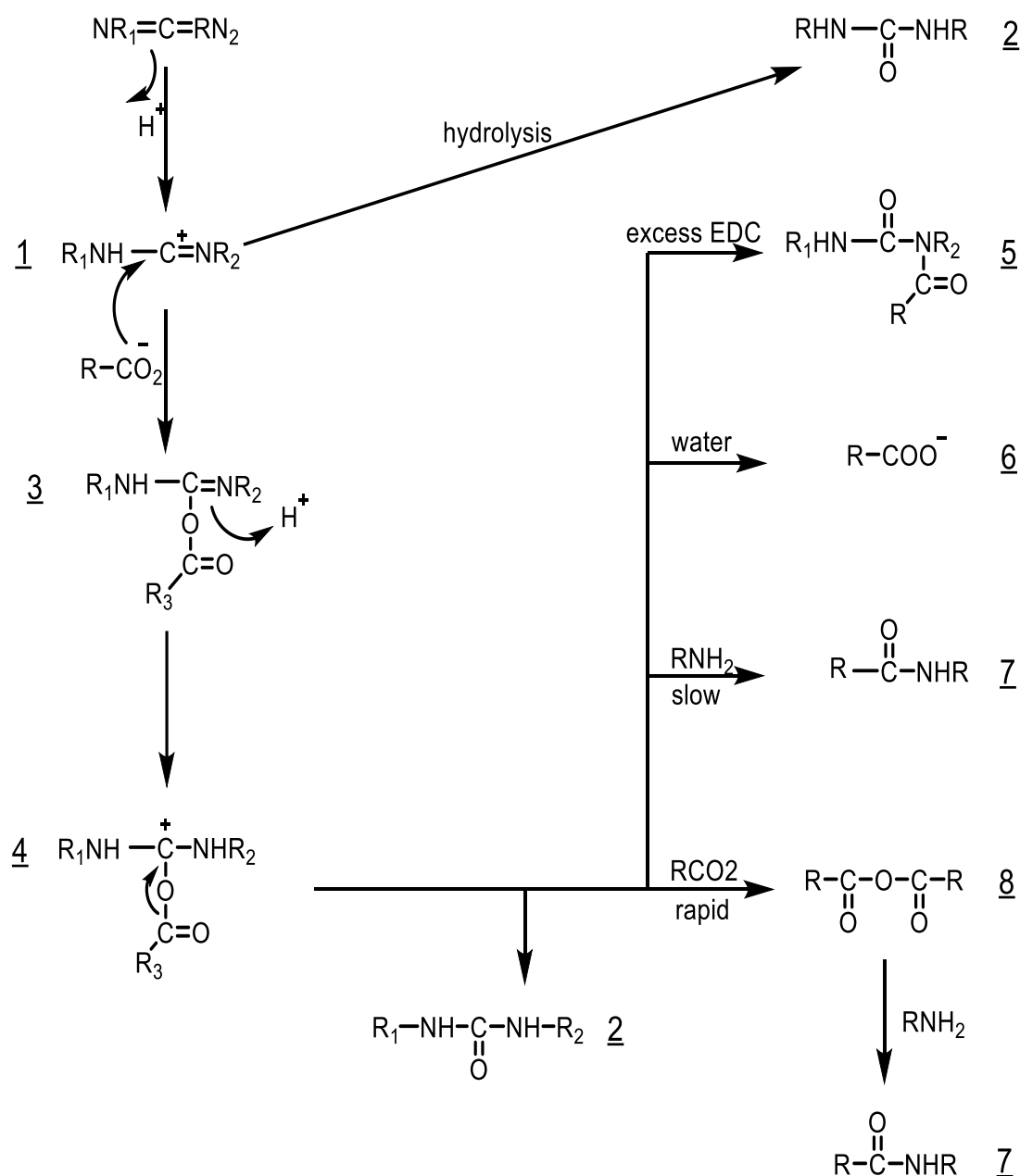


Scheme 3.7- Amination of highly branched poly(*n*-butyl methacrylate)

This method has been used by the Rimmer group for the synthesis of the oligomer butyl methacrylate with amine functionality¹⁶. The HB-PBMA:COOH end was dissolved in DCM and SDS was added as an anionic surfactant with vigorous stirring. The EDC and an excess of a primary amine (1,2-diaminoethane, 1,3-diaminopropane, 1,4-diaminobutane and 1,6-diaminohexane) were added to the reaction mix after evaporating the solvent to form an amide linker with amine functionality (further details of this method in the experimental section).

Carbodiimide compounds have a role as dehydrating agents, which activate carboxylic acids for the formation of an amide or ester, though they can also produce undesirable by-products. The mechanism of amide formation in aqueous solution is via an EDC coupling agent, as shown in Error! Reference source not found., which was first demonstrated by Nakajima and Ikadan¹⁸⁵. First, EDC and the carboxylic acid react to form a carbocation derivative of carbodiimide **1**, where this product will be hydrolysed into the corresponding urea derivative **2**. Carbocation **1** could react with an ionised carboxyl group to form **3**, which is *O*-

acylisourea. **3** will be changed into a carbocation **4**, followed by an attack of various bases in the aqueous media. If the nucleophile is absent, **4** will transfer into urea derivative **2**, but the presence of an ionised carboxyl group as a nucleophilic species and a strong base that is capable of forming the carbocation derivative of *O*-acylisourea **4** to produce **8** (carboxylic anhydrous), which quickly forms amide **7** when amine is present in the cyclisable group. However, in the case of a non-cyclisable carboxyl group, **4** will react with the amine to form **7** (amide), or react with water to produce **6** (carboxylate). Additionally, **4** could react with an excess of carbodiimide to yield *N*-acylurea **5**.



Scheme 3.8- Mechanism of amide formation between carboxylic acid and amine with EDC as a coupling agent in an aqueous system

The hydrophobic part of BMA is not easily soluble in aqueous solution and amide formation needs to replace a carboxylic acid in aqueous reaction, therefore, the anionic surfactant was used as an emulsifier stabiliser. The surfactant or (surface active agent) has an amphiphilic character, as it contains hydrophobic and hydrophilic parts. Due to amphiphilic nature, the hydrophilic (polar) group interacts with the water whereas the hydrophobic (non-polar) group will migrate above the interface¹⁹⁷⁻¹⁹⁸. This amphiphilic nature allows these compounds to stabilise hydrophobic molecules in aqueous media. The use of carbodiimide as a coupling agent provides for amide formation between a carboxylic acid and an amino group at the chain ends. A favourable pH range (3.5–4.5) is needed for the formation of carboxyl anhydride rather than allowing hydrolysis in the first step of the reaction, followed by the addition of an amine. The role of anionic surfactant

After aminating the highly branched polymers with different alkyl amines, they were analysed using different characterisation techniques, for example NMR, FTIR, elemental analysis. ¹H-NMR was used to confirm that the inclusion of alkyl amines with HB-PBMA had proceeded successfully. Error! Reference source not found. shows the ¹H-NMR spectra of branched polymers functionalised with different diamines. The new peaks of the aminated polymers appear at 1.7 ppm as single broad peak of -CH₂NH₂, and for -NH-CH₂ at 5.3 ppm. In addition, the resonance at 2.8-3.4 ppm ppm is associated with -NH-CH₂- and -CH₂NH₂, as well as the -CH₂-(CH₂)₂-CH₂ alkyl spacer at 1.1 ppm.

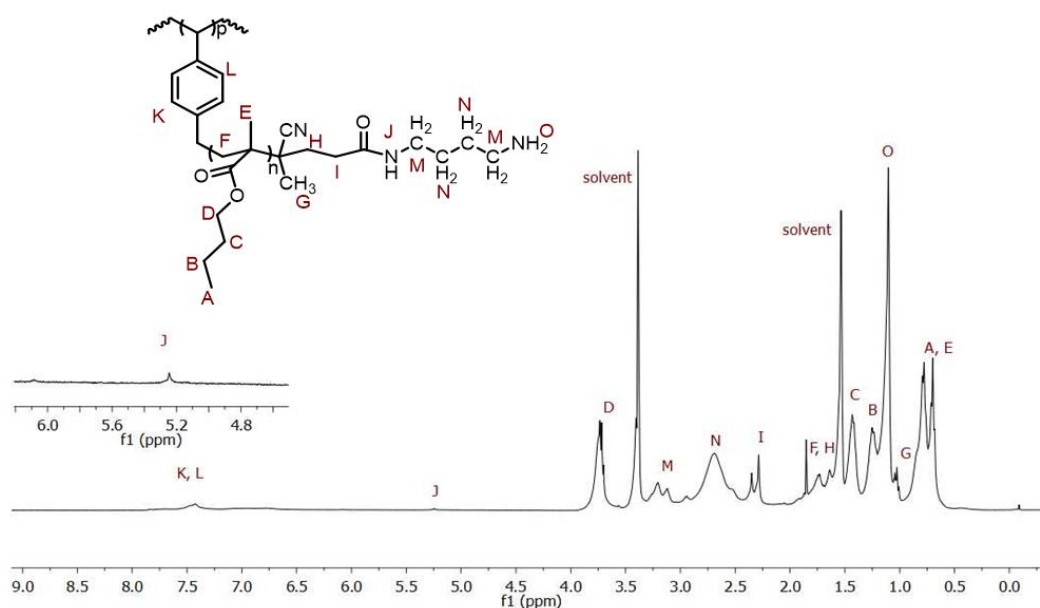


Figure 3.10- ¹H-NMR spectra of aminated HB- PBMA:1,4-DAB

The amount of recovered aminated HBPs were insufficient to perform all the appropriate characterisation and cell biology work. Therefore, FTIR was used to confirm the amine functionality and that the amide linker had appeared after the amination reaction. Figure 3.11 shows that the aminated highly branched polymers have a broad absorbance band at about 3400 cm^{-1} related to an NH stretch. There are two C=O bands in the aminated ended material, one at $\sim 1640\text{ cm}^{-1}$ related to amide formation, and the second at 1727 cm^{-1} due to an ester carbonyl group. This confirms the successful reaction of excess diamine and EDC to form HB-PBMA with acid end functionality.

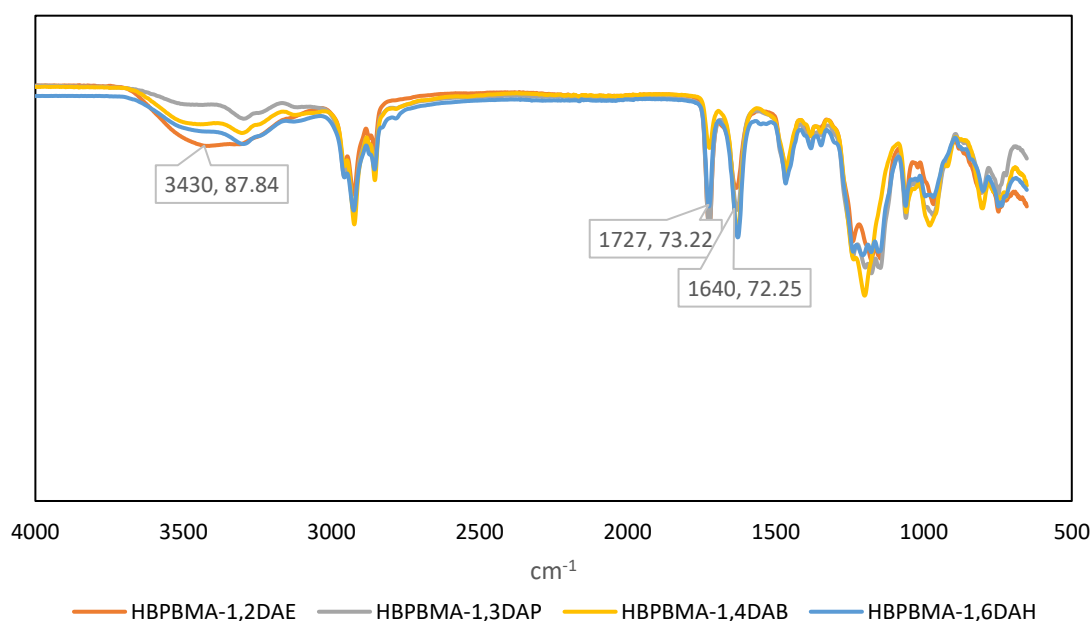


Figure 3.11- FTIR spectra of acidic HB-PBMA-2 after amination with primary alkyl amine

Elemental analysis was used to determine the percentage of nitrogen present in the polymers with amine functionality and nitrogen was shown to be much reduced in polymers with a carboxylic end. as a performance in supporting cells *in vitro*.

Table 3.5 shows that the quantity of nitrogen observed in aminated polymers compared to acidic polymers. However, the percentage of nitrogen found in the aminated polymers was more than is accepted theoretically, especially for polymers with 1,2-DAE and 1,3-DAP. Despite this problem, a new protocol of incorporating amine functionality into branched polymers or just decreasing the amount of alkyl amine in the reaction could represent a possible avenue of future investigation. Overall, in this work the desired aminated highly branched

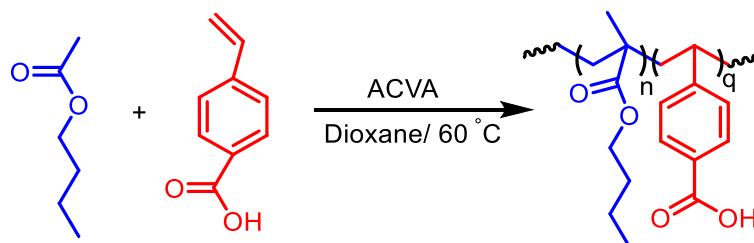
poly(butyl methacrylate)s were successfully synthesised through an aqueous reaction to show their effect as a performance in supporting cells *in vitro*.

Table 3.5- The theoretical and actual CHN elements before and after amination reaction

HB-PBMA	Theoretical Elemental analysis %			Actual Elemental analysis %		
	C	H	N	C	H	N
BMA:COOH-2	66.2	9.6	0.6	67	9.2	0.8
BMA:1,2-DAE	66.4	9.7	1.2	64.7	9.4	3.1
BMA:1,3-DAP	66.5	9.7	1.2	65.7	9.7	4.5
BMA:1,4-DAB	66.6	9.7	1.1	65.3	9.3	2.9
BMA:1,6-DAH	66.8	9.8	1.1	65.91	9.7	2.4

3.2.5 Linear analogue poly(n-butyl methacrylate) with acid ends

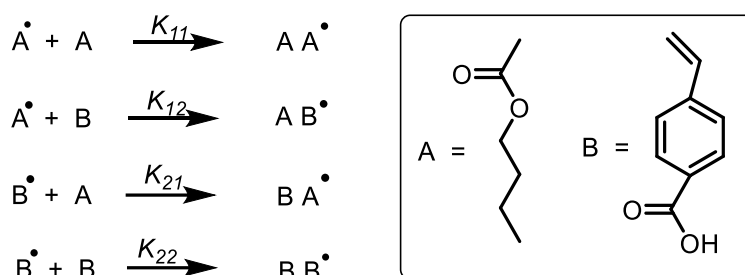
A linear analogue copolymer of butyl methacrylate and 4-vinylbenzoic acid (4-VBA) was prepared to enable a comparison between the properties of highly branched and linear polymer architectures, as shown in the general Scheme 3.9. Further details of this method are described in the experimental section.



Scheme 3.9- Free radical polymerisation of linear analogue P(BMA-co-4-VBA)

4-VBA was used since it contains both a styryl unit and a carboxylic acid functional group, giving an approximation of the structural and chemical properties of HB-PBMA with acid ends. This copolymer was prepared using conventional free radical polymerisation, in the same three molar ratios as the RAFT polymerisation of HB-PBMA polymers; thus, the same number of functional groups will be within the polymer structure to allow for optimum comparison. Conventional radical polymerisation run to high monomer conversion was used in order to produce broadly disperse molar mass distributions that were similar to those produced by SCVP-RAFT. As in homopolymerisation, free radical copolymerisation proceeds via the same initiation, propagation and termination mechanism described in Chapter 2

(Scheme 2.1). However, in copolymerisation, due to the presence of two monomers, A and B, the propagation step consists of at least four different reactions, as seen in Scheme 3.10.



Scheme 3.10- Possible propagation step sequences in free radical copolymerisation of P(BMA-co-4-VBA)

To describe copolymer composition, Mayo and Lewis presented reactivity ratios for each monomer¹⁹⁹ as given in the following equation:

$$r_1 = \frac{k_{11}}{k_{12}}, r_2 = \frac{K_{22}}{K_{21}} \quad (3.2)$$

Understanding the reactivity ratio is valuable to the determination of the copolymerisation behaviour of the comonomers. The Fineman-Ross and Kelen-Tudos and nonlinear squares methods can be used, however, these methods require a low conversion (< 10) of the monomer in the copolymerisation to minimise the drift in the copolymer composition with conversion²⁰⁰. From known parameters the Q-e scheme of Alfrey and Price²⁰¹⁻²⁰² can be used in order to estimate the reactivity ratio of BMA with 4-VBA. The Q-e scheme is a semi-quantitative approach to determining the monomer reactivity ratios of a comonomer pair, as shown in the following equations:

$$r_1 = \left(\frac{Q_1}{Q_2}\right) \exp[-e_1(e_1 - e_2)] \quad (3.3)$$

$$r_2 = \left(\frac{Q_2}{Q_1}\right) \exp[-e_2(e_2 - e_1)] \quad (3.4)$$

Where r_1 and r_2 are reactivity ratio of n-BMA and 4-VBA, respectively, Q_1 and Q_2 are the reactivity of each monomer obtained from the literature²⁰², and e_1 and e_2 are the polarities of each monomer, also obtained from the literature²⁰².

In this study, the prediction of reactivity ratio of the copolymerisation of BMA and 4-VBA was determined via the Q-e scheme, as shown in Table 3.6, using equations 3.3 and 3.4.

Table 3.6- Predication of reactivity ratio of p(BMA-co-VBA)

Monomer	Q	e	r
n-BMA	0.82	0.28	0.19
4-VBA	5.17	1.08	2.65

The relative reactivity ratios of n-BMA and 4-VBA were 0.19 and 2.65, respectively, indicating that the sequence distribution of the product copolymer had somewhat larger reactivity with 4-VBA, and hence the more reactive monomer was incorporated faster during the reaction. However, these linear polymerisations were run to high conversion and the reactivity ratios simply predict increased dispersity in composition as conversion progresses, as well as size. Similarly, the SCVP-RAFT polymerisations are complicated by the RAFT branching process and further analysis would require numerical simulation techniques as well as knowledge of the rates of transfer and reinitiation. This is beyond the scope of the current work.

The $^1\text{H-NMR}$ spectra were to some extent very similar to those of the HB-PBMA with acid ends, as seen in Figure 3.12. In the upfield region of the spectra, all peaks due to the BMA segments of the polymer appeared with the same or very similar shift values for both polymers. Both showed a very broad low intensity peak resulting from the carboxylic acid proton, although this appeared at a higher shift for P(BMA-co-VBA) due to the proximity of the acid group to the aromatic ring in this structure. The carboxylic acid peak decreased in intensity as the mole fraction of 4-vinyl benzoic acid in the feed decreased, which is the expected trend. The only significant differences between the spectra of the two polymers occurred in the aromatic region and arose due to the major differences in structure between the branched polymer and the linear analogue. P(BMA-co-4-VBA) has only two different aromatic proton environments in the benzyl group, whereas HB-PBMA with its acid ends and containing pyrrole groups within its structure, provided additional environments to those in the styryl group.

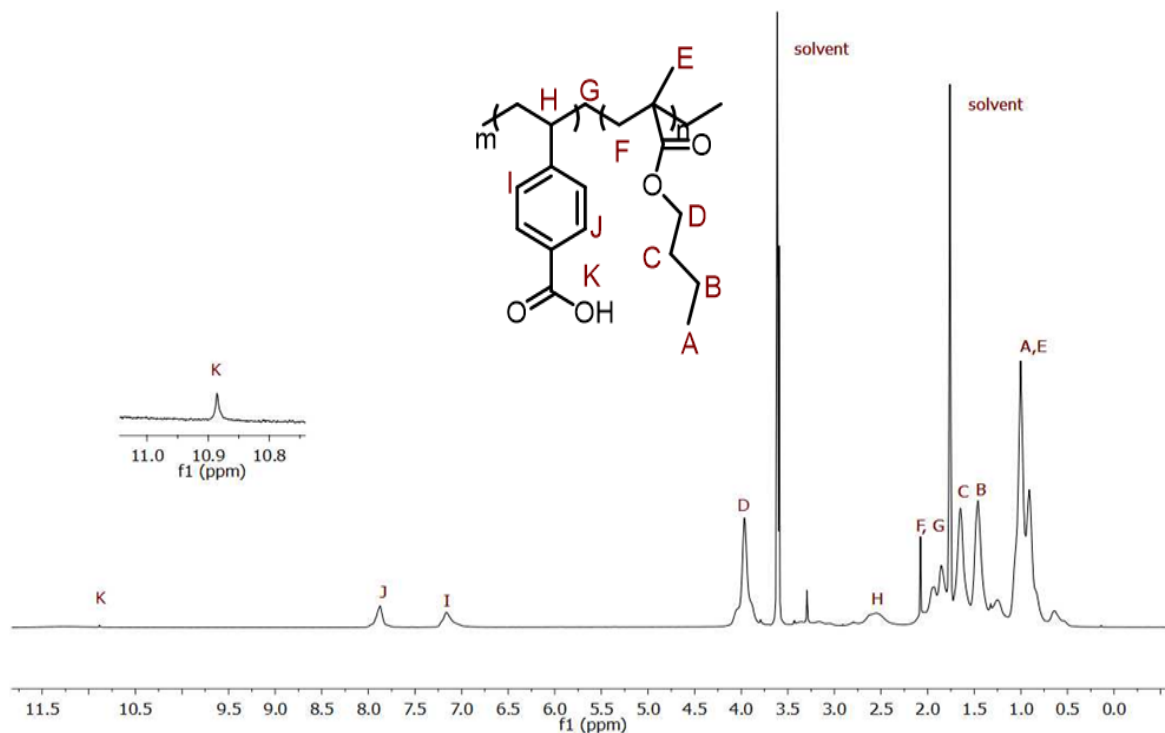


Figure 3.12- ^1H -NMR spectra of analogue linear poly(butyl methacrylate-co-vinyl benzoic acid)

Moreover, ^{13}C -NMR was conducted to see whether P(BMA-co-VBA) had been synthesised successfully via copolymerisation (see in Appendix 3.5). All carbon peaks found in the highly branched polymer have similar shifts to those in the linear polymer. The carbon signals of methylene appeared between 13 to 30 ppm, and the resonances of the benzyl peaks were observed at 117 and 128 ppm, whereas the C=O was at 197 ppm.

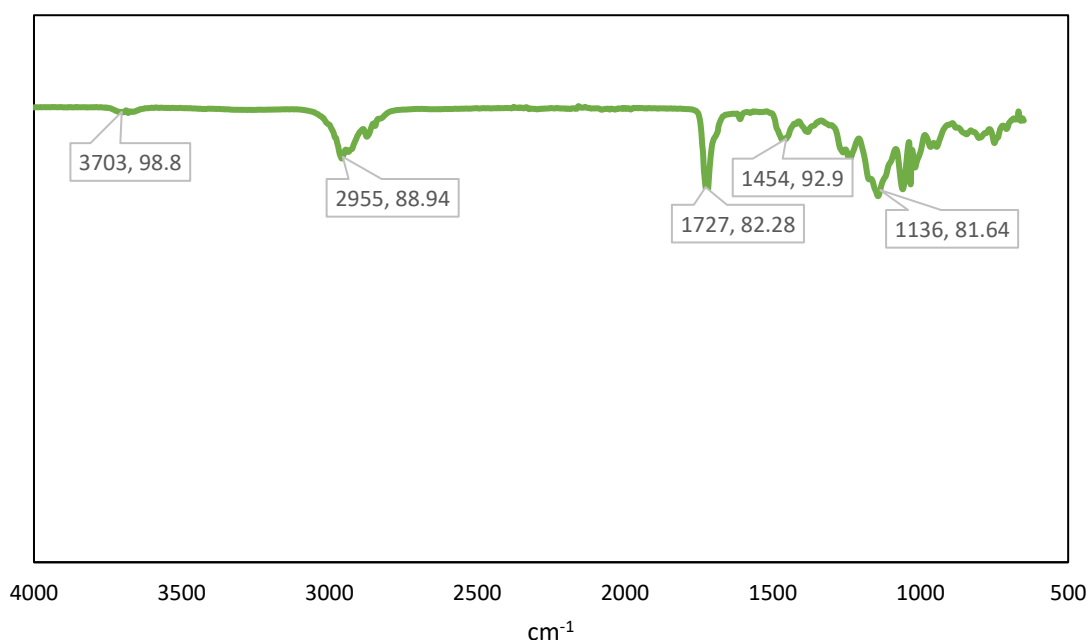
The results calculated based on ^1H -NMR spectra for the different molar ratio can be seen in Table 3.7. The polymer composition and monomer feed are determined by comparing the integration of the proton signal of BMA, labelled “D”, with the proton signals of 4-VBA, labelled “I and J”. The molar ratio of this copolymerisation was calculated to be 5 for BMA-1, 7 for BMA-2 and 9 for BMA-3, which is not similar to the feed ratios. This might be because of a high reactivity ratio of 4-VBA and the it was consumed faster than the BMA monomer.

Table 3.7- Result of copolymerisation reaction of BMA and 4-VBA determined by ¹H-NMR spectroscopy

L-P(BMA-co-4-VBA)	Feed ratio ^a	(v)	(\hat{v})	BMA ^b %	Benzyl ^b %
BMA-1	8:1	0.125	0.22	82	18
BMA-2	16:1	0.062	0.16	86	14
BMA-3	24:1	0.041	0.12	89	10

^a Initial molar ratio of [BMA:4-VBA]. v= Mole fraction of 4-VBA in reaction mixture, \hat{v} = Mole fraction of 4-VBA in copolymers, ^b percentage of BMA and 4-VBA in copolymer composition.

FTIR was used, to ascertain whether P(BMA-co-VBA) had been synthesised successfully. Error! Reference source not found. shows the C=O and C-O bands of the ester group in butyl methacrylate at approximately 1720 and 1130 cm⁻¹, respectively. The stretch seen at about 2950 cm⁻¹ relates to C-H bonds. The C-C stretch in the aromatic ring appeared at 1600 cm⁻¹ and the C=C stretch at 1450 cm⁻¹. The O-H bend of carboxylic acid can be observed at 940 cm⁻¹, while the O-H stretch can be seen at 3700 cm⁻¹. The weak C=O stretch of carboxylic acid cannot be seen, which was expected to occur around 1690 cm⁻¹ due to concurrence with the C=O signal of the ester group.

**Figure 3.13- FTIR spectra of linear P(BMA-co-vinyl benzoic acid) P(BMA)-2**

As shown in Figure 3.14, the molecular weight of the linear analogues increased as the amount of BMA in the reaction was increased from 8:1 to 24:1. This might be due to higher monomer concentration favouring chain extension, and hence an increase in molecular weight. The molecular weight of the linear polymers was higher than the molecular weight of the highly branched polymers in the same ratio. This is evidence that the inclusion of the chain transfer agent in the RAFT branching polymerisation controls molecular weight. The linear materials have a broad distribution and dispersity, which was broader but similar to the dispersities of HB-PBMAs. The molar mass distributions of the linear materials were all unimodal, which suggests that the bimodal distributions observed for the branched materials were a consequence of the branch-producing transfers occurring during polymerisation.

LIN P(BMA)	M_n	M_w	M_z	\mathcal{D}
PBMA-1	31898	168309	697018	5.2
PBMA-2	60949	295167	840100	4.8
PBMA-3	102958	462145	1889434	4.5

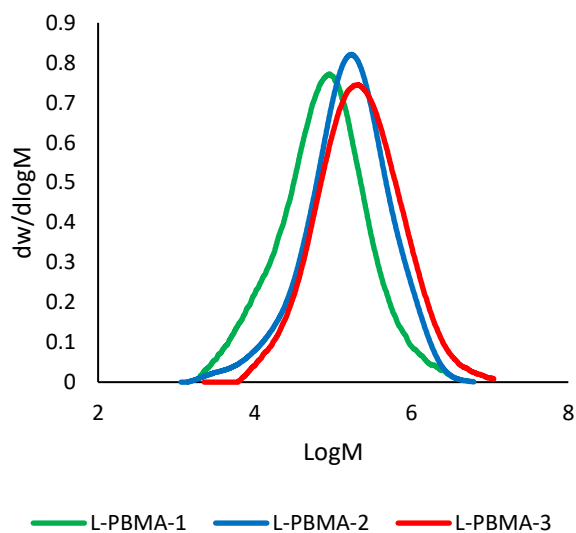
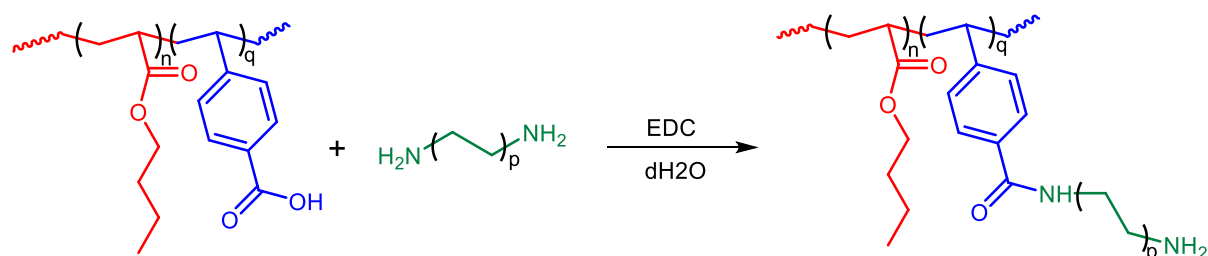


Figure 3.14- SEC results of L-P(BMA-co-VBA)

(left) number averaged molecular weight (M_n), weight averaged molecular weight (M_w), z-averaged molecular weight (M_z), and dispersity index (\mathcal{D}). (right) SEC traces of molar mass distribution.

3.2.6 Coupling of linear butyl methacrylate copolymers to diamine

The L-PBMA-2 (16:1) polymer was reacted with four different diamine products (1,2-diaminoethane, 1,3-diaminopropane, 1,4-diaminobutane and 1,6-diaminohexane) using EDC as a coupling agent for the formation of an amide end group instead of a carboxylic end group, as shown in Scheme 3.11 below.



Scheme 3.11- Amination of linear butyl methacrylate with acid end group using different diamines

FTIR was used to confirm that the amino functional group had been inserted successfully into linear PBMA, as shown in Figure 3.15 below. There are two C=O groups in the aminated ended material, one at $\sim 1626\text{ cm}^{-1}$ and other at 1725 cm^{-1} . In adding diamines to a copolymer of butyl methacrylate and 4-vinyl benzoic acid, there is a band at 3280 cm^{-1} due to the concurrent NH signal. This confirms the successful reaction of diamine L-P(BMA-co-VBA).

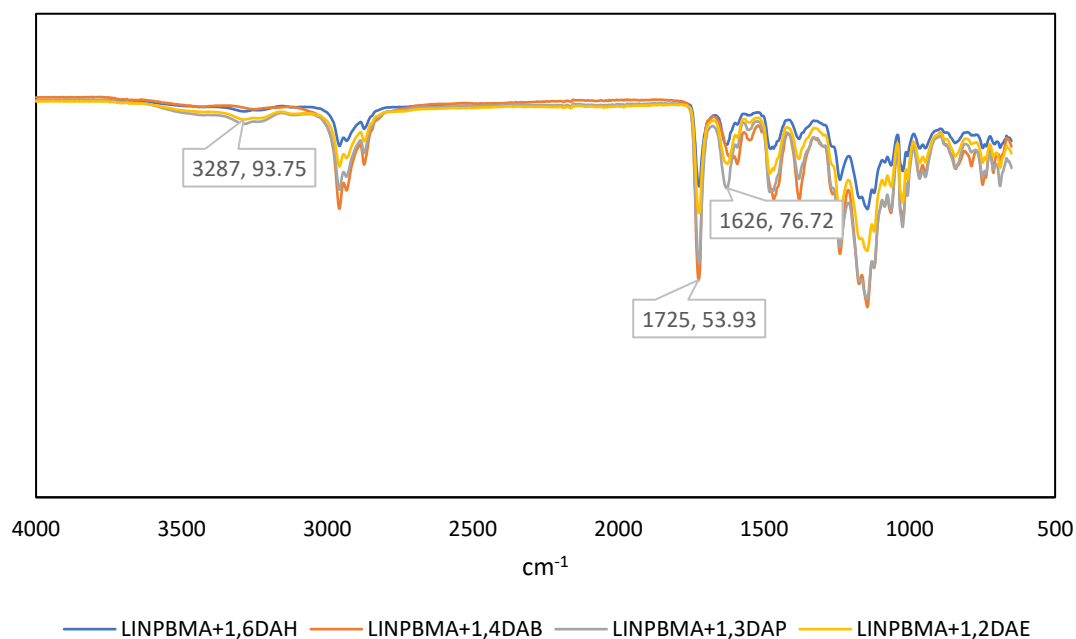


Figure 3.15- Solid FTIR of aminated linear poly(butyl methacrylate) P(BMA)-2

Elemental analysis was used to confirm the inclusion of the nitrogen compound into the acidic linear polymers, as seen in Table 3.8. The results showed that the acid ends of L-PBMA were converted to amine functionalities by finding the percentage of nitrogen compounds in the aminated polymers. However, the nitrogen found in aminated polymers was more than expected on theoretical grounds. This is likely due to the higher diamine concentrations that were added in the reaction. Therefore, the formation of a film of aminated polymers was considered to be sufficient to study cell adhesion *in vitro* in this work.

Table 3.8- Elemental analysis of linear P(BMA) before and after amination with different primary alkyl amine

LIN P(BMA)	Theoretical Elemental analysis %			Actual Elemental analysis %		
	C	H	N	C	H	N
BMA-COOH	67.4	9.5	0	66.9	9.2	0
BMA-1,2-DAE	67.3	9.6	1.1	65.9	9.3	2.8
BMA-1,3-DAP	67.4	9.6	1.1	65.7	9.4	2.4
BMA-1,4-DAB	67.5	9.6	1.1	66.9	9.8	1.8
BMA-1,6-DAH	67.7	9.7	1.1	67.2	9.5	2.1

3.2.7 Diffusion ordered NMR spectroscopy

The SEC derived molar mass data of the branched polymers obtained in THF appear to be subject to adsorption. An alternative that can give the size of the polymers without the use of chromatography is to use NMR spectroscopy. The diffusion ordered NMR spectroscopy (DOSY) technique is designed for the characterisation of macromolecules and intermolecular interactions in a mixture. Correlation of the data to provide molar mass distributions can be achieved but the technique can also provide hydrodynamic volumes. In comparing linear and branched polymers hydrodynamic volume maybe a more useful parameter than molar mass. The method is based on a pulsed-field gradient using a special pulse sequence to obtain NMR data that allows for the determination of the diffusion coefficients of different species²⁰³⁻²⁰⁴. Two-dimensional spectra are obtained which correlate the observed diffusion coefficients of each component with their corresponding chemical shifts²⁰³⁻²⁰⁵. DOSY has been widely used to determine the size of polymers. Le *et al.* have reported that DOSY can be applied to the study or determination of the molecular weight of polystyrene, which is prepared via different procedures such as reversible addition-fragmentation chain transfer (RAFT), atom transfer radical polymerisation (ATRP) and ring-opening metathesis polymerisation (ROMP), and can obtain a result that closely correlates with the results of SEC measurements²⁰⁶. Recently, NMR DOSY has been used to determine the selection of polymerisation methods that essentially eliminate side reactions. In 2016, Cherifi *et al.* were the first to demonstrate that the nitroxide-mediated polymerisation of poly(methyl methacrylate) with styrene could proceed successfully by studying polymerisation mechanisms in terms of the side reactions with DOSY NMR²⁰⁵. In addition, DOSY NMR has been used to determine the intrinsic viscosity and size of materials²⁰⁷. Swift *et al.* reported that the hydrodynamic radius and the intrinsic viscosity of branched and linear poly(*N*-isopropylacrylamide) could be determined via DOSY spectroscopy²⁰⁸.

The principle of the DOSY technique is that molecules or ions are measured in solution at one constant motion according to their diffusion constant (D). Assuming that the polymer chain acts as a non-draining sphere in which solvent diffuses with the polymer chain, the diffusion constant can have related to hydrodynamic radius, R_H , through the Stokes-Einstein equation:

$$D = \frac{k_B T}{6\pi\eta R_H} \quad (3.5)$$

Where K_B is the Boltzmann constant, T is the absolute temperature in Kelvin, η is the viscosity of the solution and R_H is the hydrodynamic radius of the sample.

Linear and highly branched poly(butyl methacrylate)s of known molar mass, as provided by size exclusion chromatography (SEC), were analysed by DOSY NMR. Providing the appropriate reference diffusion value of the deuterated solvent is important to the determination of the hydrodynamic radius or hydrodynamic volume distribution of the polymer by the rearrangement of the Einstein equation:

$$R_H = \frac{K_B T}{6\pi\eta D} \quad (3.6)$$

By knowing the molar mass of the polymer sample, the hydrodynamic volume distribution can be transformed to the distribution of the intrinsic viscosity using the Fox-Flory equation:

$$[\eta] = \frac{2.5NV_H}{M} \quad (3.7)$$

Where V_H is the hydrodynamic volume distribution, N is Avogadro's number and M is the molar mass of the polymer.

The hydrodynamic volume can be calculated as follows:

$$V_H = \frac{4}{3}\pi R_H^3 \quad (3.8)$$

DOSY NMR was used to determine the V_H of highly branched PBMA with pyrrole or carboxylic acid end groups and linear PBMA with a carboxylic acid functionality at 25 °C. Unfortunately, insufficient quantities of the aminated polymers were available. The software used for processing DOSY data was TopSpin 3.2.

The DOSY in the 2D spectrum shows NMR chemical shift on the horizontal axis, and the vertical axis has the logarithm of the diffusion coefficient (log D) of the polymer mixture. Error! Reference source not found. shows example of some polymers spectra. Further, the logarithm diffusion coefficient distributions of all polymers and deuterated solvents were also determined via DOSY analysis and are shown in Appendix 3.9 and tabulate in Table 3.9.

Examples of the $^1\text{H-NMR}$ DOSY spectra are shown in Figure 3.16. The highly branched pyrrole terminated polymer showed the presence of the pyrrole and benzyl units. However, after functionalising this polymer, by the addition of ACVA, a carboxylic acid functional group formed on the polymer, this was indicated by the appearance of a new region of signals in the DOSY spectra and disappearance of two signals that correspond to pyrrole functionality, confirming the successful functionalisation of this polymer with the carboxylic acid.

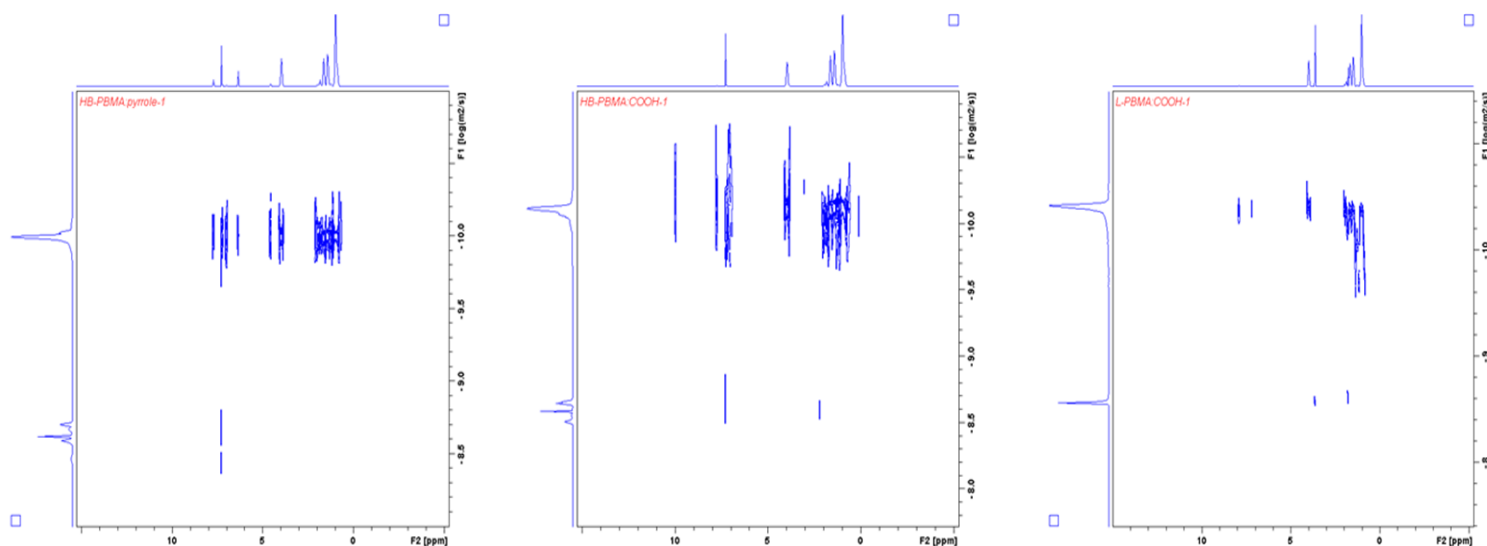


Figure 3.16- Examples of 2D DOSY spectra of (left) HB-PBMA:pyrrole, (middle) HB-PBMA:COOH and (right) L-PBMA:COOH

The logarithms of the diffusion coefficients were converted to self-diffusion coefficient (D) distributions for all polymers and deuterated solvents, as shown in Figure 3.17- Diffusion coefficient distributions obtained from DOSY analysis

Table 3.9. From these data, the diffusion coefficient of deuterated chloroform and THF were almost identical at 275 K for highly branched and linear polymers. This confirms that the solutions had diluted the polymers sufficiently with no retarding effects on the solvent diffusion. Further, the self-diffusion coefficients were higher in highly branched rather than linear copolymers.

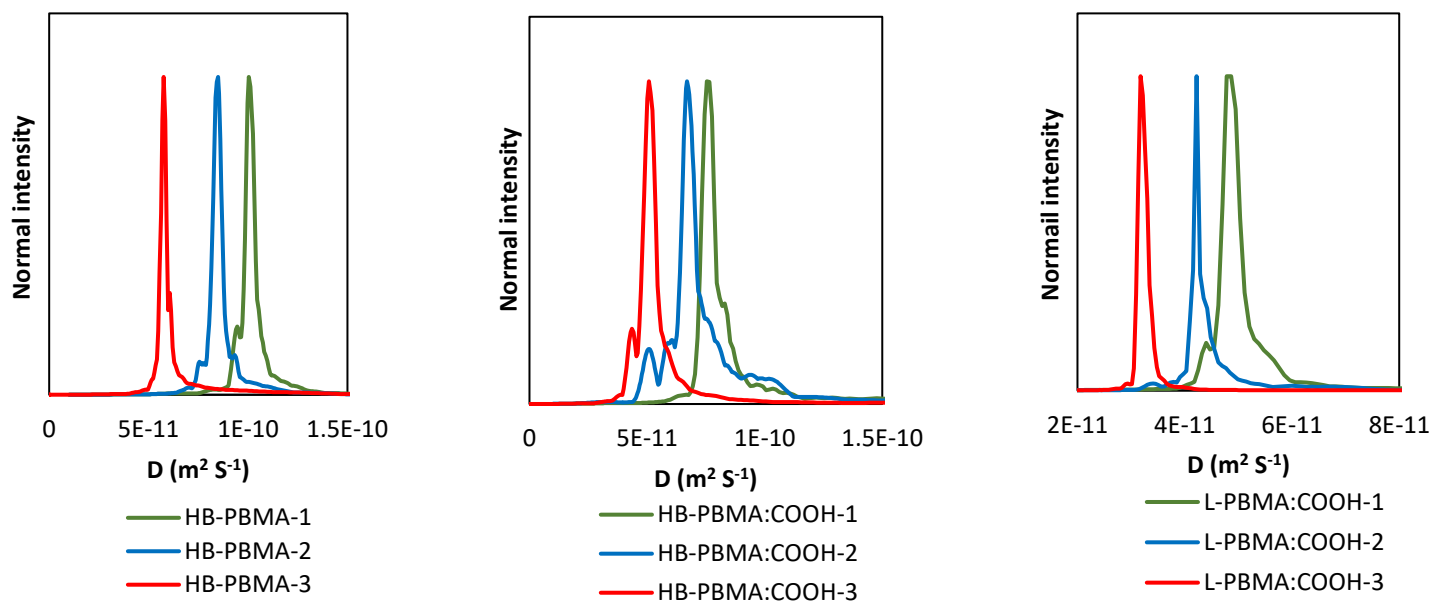


Figure 3.17- Diffusion coefficient distributions obtained from DOSY analysis

Table 3.9- The values of the logarithms of self-diffusion coefficients of all polymers

polymers	$-\log D (S)$	$-\log D (P)$	$D (S)$	$D (P)$
		(m^2/S)	$(m^2 S^{-1} \times 10^{-9})$	$(m^2 S^{-1} \times 10^{-11})$
HB-PBMA-1	8.63 ± 0.005	9.99 ± 0.005	$2.4 \pm 3.09 \times 10^{-11}$	$1.005 \times 10^{-10} \pm 1.38 \times 10^{-12}$
HB-PBMA:COOH-1	8.61 ± 0.02	10.09 ± 0.02	$2.4 \pm 1.3 \times 10^{-11}$	$7.55 \pm 2.7 \times 10^{-12}$
HB PBMA-2	8.60 ± 0.02	10.08 ± 0.01	$2.5 \pm 6.5 \times 10^{-11}$	$8.43 \pm 1.9 \times 10^{-12}$
HB-PBMA:COOH-2	8.60 ± 0.01	10.18 ± 0.01	$2.4 \pm 5.5 \times 10^{-11}$	$6.7 \pm 2.7 \times 10^{-12}$
HB-PBMA-3	8.60 ± 0.005	10.24 ± 0.005	$2.5 \pm 6.5 \times 10^{-11}$	$5.77 \pm 7.7 \times 10^{-13}$
HB-PBMA:COOH-3	8.60 ± 0.01	10.30 ± 0.005	$2.4 \pm 5.1 \times 10^{-11}$	$5.07 \pm 6.1 \times 10^{-13}$
L-PBMA:COOH-1	8.56 ± 0.005	10.32 ± 0.005	$2.79 \pm 3.4 \times 10^{-11}$	$4.86 \pm 6.3 \times 10^{-13}$
L-PBMA:COOH-2	8.56 ± 0.009	10.37 ± 0.008	$2.75 \pm 5.4 \times 10^{-11}$	$4.26 \pm 8.3 \times 10^{-13}$
L-PBMA:COOH-3	8.56 ± 0.009	10.49 ± 0.005	$2.75 \pm 5.8 \times 10^{-11}$	$3.18 \pm 4.3 \times 10^{-13}$

Results were repeated three times and their average taken, where (S) is diffusion of solvent and (P) is diffusion of polymer.

After determining the diffusion coefficients for each polymer from DOSY analysis, the Stokes-Einstein equation, along with the Boltzmann constant and the known solvent viscosities at 275 K of $0.00053 \text{ kg}\cdot\text{m}^{-1}\cdot\text{s}^{-1}$ for CDCl_3 and $0.00045 \text{ kg}\cdot\text{m}^{-1}\cdot\text{s}^{-1}$ for $\text{C}_4\text{D}_8\text{O}$ were used to evaluate the hydrodynamic radius of the polymers, as seen in Figure 3.18 and tabulated in Table 3.10.

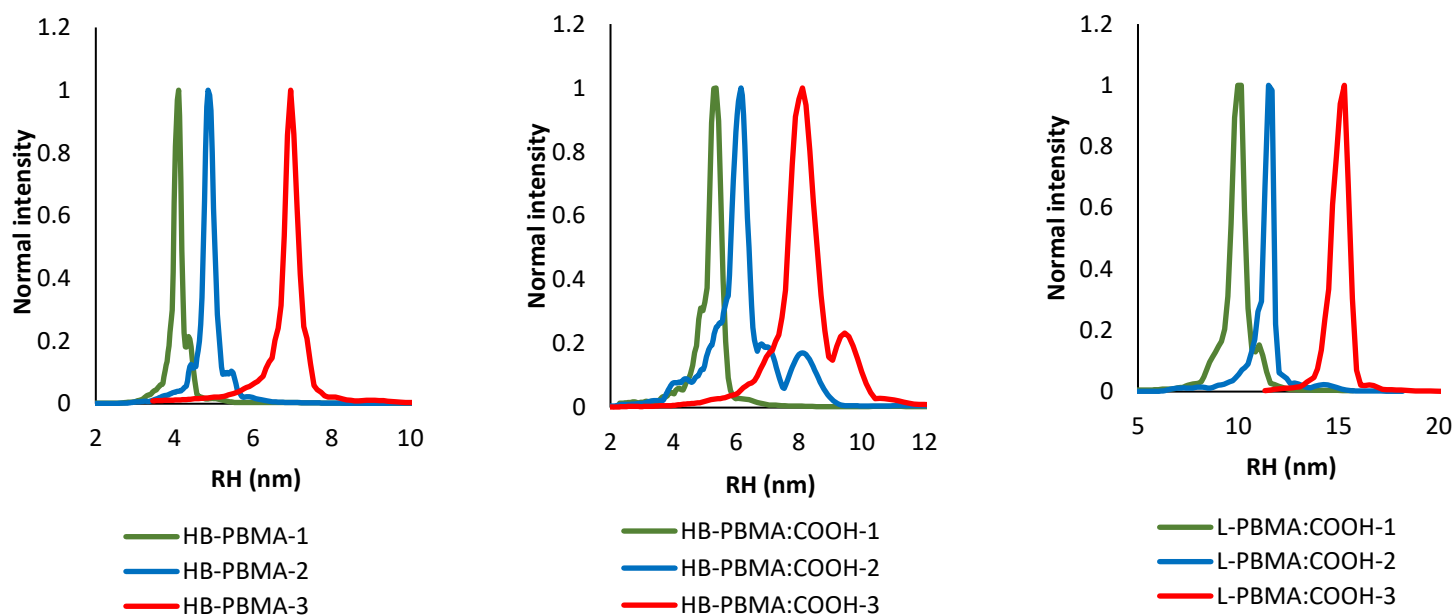


Figure 3.18- ^1H -NMR DOSY analysis of R_H distribution (left) HB-PBMA:pyrrole, (middle) HB-PBMA:COOH and (right) L-PBMA:COOH

From Table 3.10, the hydrodynamic radius distribution of linear and highly branched polymers was seen to increase with increasing molar mass, following the reduction of vinyl benzoic acid in linear copolymers and its chain transfer agent in highly branched copolymers to monomers in the reaction feed. Further, it was observed that the highly branched polymers have a shoulder in the distribution peaks. This shoulder is reminiscent of the bimodal features in the molar mass distributions obtained from SEC analysis.

Table 3.10- Hydrodynamic radius (R_H) and intrinsic viscosity (IV) calculated using DOSY, M_n calculated from SEC

polymers	M_n (kg.mol ⁻¹)	V_H (m ³)	R_H (nm)	IV (dl.g ⁻¹)
	SEC			
HB-PBMA-1	10376	0.04	4.06	0.42
HB-PBMA:COOH-1	6543	0.12	5.02	1.22
HB-PBMA-2	15477	0.05	4.86	0.47
HB-PBMA:COOH-2	14647	0.10	5.95	0.91
HB-PBMA-3	22195	0.09	6.88	0.92
HB-PBMA:COOH-3	20317	0.16	8.01	1.6
L-PBMA:COOH-1	31898	0.14	9.81	1.5
L-PBMA:COOH-2	60949	0.18	11.2	1.8
L-PBMA:COOH-3	102958	0.20	15	2.07

Finally, by obtaining the hydrodynamic radius of each polymer and by determining the number average molecular weight from SEC, it was possible to estimate and evaluate intrinsic viscosity (η) using Equation 3.7 and 3.8. The viscosity increased in linear polymers followed by HB with carboxylic acid terminated polymers, and then HB with pyrrole end polymers. The data confirmed the issues in the THF SEC data. The R_H values after functionalising the branched polymers with carboxylic acid were increased. However, SEC in THF indicated that the molar masses were decreased. This contradiction (i.e. increased R_H should be reflected in increased molar mass even if the data were not absolute) shows that the SEC data obtained in THF were subject to adsorption. These interactions change the elution times of the polymers, ultimately altering the extracted molecular weight distribution²⁰⁹.

3.3 CONCLUSION

In this chapter, 4-vinylbenzyl pyrrole carbodithioate was prepared, the analysis of which showed that it can be successfully used as a chain transfer agent in the formation of highly branched polymers. Three polymers were synthesised with different CTA:BMA molar ratios via SCVP RAFT polymerisation. A higher conversion of monomers to polymers was obtained, and evidence of branching was observed from the NMR spectra. All of these polymers were reacted with excess ACVA to remove pyrrole carbodithioate and to replace it with a carboxylic acid end functional group. The aminated highly branched polymers were synthesised in aqueous solution using different alkyl diamines to obtain the desired polymers for the cell culture.

In order to compare the different architectures that can have an effect on cells, the linear analogues of poly(butyl methacrylate) with acid ends were successfully prepared, also in three BMA:VBA molar ratios by free radical polymerisation. Additionally, as with the highly branched polymers, these polymers were reacted with diamine to produce a species with amine functionality for the cell culture study in order to mimic branched functionality.

^1H - and ^{13}C -NMR spectroscopy, elemental analysis and FTIR, were conducted to provide valuable data to allow for further polymer characterisation. The molar mass and molecular weight distribution of the polymers were measured to the elution volume of the polymer sample to the THF solvent by SEC using RI detector, the main findings of which were that the molar mass was higher in linear copolymers compared to branched copolymers. This constitutes evidence that the inclusion of the chain transfer agent in the RAFT branching polymerisation controls molecular weight.

Finally, NMR DOSY was used for the first time as an efficient tool due to its ability to separate different chemical species, confirming their successful synthesis during the appropriate reaction, and also to evaluate polymer size, hydrodynamic radius and intrinsic viscosity. The results provided the higher hydrodynamic radius and viscosity in linear polymers compared to highly branched polymers.

3.4 EXPERIMENTAL

3.4.1 Synthesis of RAFT agent of 4-vinylbenzyl-pyrrolocarbodithioate

Materials:

Pyrrole (99 %, Aldrich), sodium hydride (60 % in mineral oil dispersion, Aldrich), carbon disulphide (99+ %, Aldrich), 4-vinylbenzyl chloride (90 %, Aldrich), diethyl ether (Fischer), hexane (Fischer) were used as received, and dimethyl formamide (DMF) was used from a Grubb's dry solvent system under anhydrous magnesium sulphate (99.5 %, Aldrich). Pyrrole was distilled over calcium hydride (99 %, Aldrich) under reduced pressure at 75 °C to obtain a colourless liquid.

Method:

A 250 ml three-neck round-bottom flask was equipped with a condenser, bubbler, a pressure equalising funnel, a suba seal and a magnetic stirrer bar. The apparatus was flame-dried and purged with nitrogen to remove any moisture. Sodium hydride (2.98 g) (N.B. in mineral oil dispersion) was added to the flask followed by DMF (80 ml) to form a suspension. Pyrrole (5.00 g) was added to the pressure-equalising funnel with DMF (10 ml) and added dropwise at room temperature to the rapidly stirred suspension of sodium hydride over a period of 30 minutes (a yellow foam was produced). This solution was stirred at room temperature for 30–40 minutes and was cooled to 0 °C using an ice bath. Carbon disulphide (5.68 g) was added to the pressure-equalising funnel with DMF (10 ml) and added dropwise over a period of 10 minutes to produce a dark red solution. This solution was stirred at room temperature for 30 minutes and then cooled to 0 °C. 4-vinylbenzyl chloride (11.37 g) was added to the pressure-equalising funnel with DMF (10 ml) dropwise over a period of 20 minutes. The solution was stirred for a further 16 hours at room temperature. The solution was transferred to a 1 litre separating funnel followed by diethyl ether (80 ml) and distilled water (80 ml). The organic layer was recovered and then the aqueous layer was extracted with diethyl ether (3 x 160 ml). The extracts were combined and dried over magnesium sulphate before filtration and removal of the solvent by rotary evaporation to give brown oil.

The oil was purified by flash chromatography (6 cm diameter column) using 100% hexane or petroleum ether as the eluent (N.B. the column took 7–8 hours for completion). The desired product had an R_f value of 0.180 in pure hexane. The solvent was removed by rotary evaporation to give a bright yellow oil. The product was stored at 18 °C under N₂.

NMR spectroscopy result:

¹H-NMR (400MHz, CDCl₃): δ/ppm 7.28 (solvent), 4.62 (s, 2H), 5.2-5.3 (d, 1H, =CH₂ vinyl, *J* = 12 Hz), 5.7-5.8 (d, 1H, =CH₂, *J* = 16 Hz), 6.34 (t, 2H, =CH Pyrrole, *J* = 4 Hz), 6.69-6.76 (dd, 1H, =CH, *J* = 12 Hz), 7.40 (m, 4H, C₆H₄, aryl), 7.73 (t, 2H, N-CH= Pyrrole, *J* = 4 Hz).

¹³C-NMR (400MHz, CDCl₃): δ/ppm 77.28 (solvent), 41.56 (1C, -C(=S)-S-CH₂-), 114.16 (1C, CH=CH₂, pyrrole), 114.49 (2C, aryl), 120.35 (2C, N-(CH)₂, pyrrole), 126.57 (2C, CH, aryl), 129.63 (1C, CH-CH₂-S, aryl), 133.84 (1C, -CH=CH₂), 136.29 (1C, CH₂C-), 137.21 (2C, C-C=CH₂), 191.85 (1C, -C=S-S-CH₂-).

3.4.2 RAFT polymerisation of *n*-butyl methacrylate using 4-vinylbenzyl pyrrolecarbodithioate as the chain transfer agent**Materials:**

The monomer of *n*-butyl methacrylate (*n*-BMA, Aldrich, 99%) was distilled in vacuum before use to remove inhibitor and then cooled under refrigeration. The initiators 4,4-azobis 4-cyanovaleric acid (ACVA, Aldrich, 98%), 4-vinylbenzyl pyrrole-carbodithioate (4-VBC, produced as previously described), 1,4-dioxane (anhydrous, 99.8%, Sigma-Aldrich), and methanol (Fisher) were used as received.

Method:

4-VBPC, BMA, dioxane and ACVA were mixed until the solid initiator had dissolved. The resulting solution was added to a 50 ml ampoule, which was evacuated under high vacuum using the freeze-thaw technique. The ampoule was then flame sealed and the final pressure in the ampoule was approximately 3×10^{-3} mbar. Polymerisation was conducted in a water bath at 60 °C for up to 18 hours. The ampoule was opened by cracking and the polymer diluted with the addition of dioxane. This solution was added dropwise into rapidly stirred methanol to give a very fine dispersion of polymer particles. The polymer was placed in a watchglass and dried *in vacuo* to produce a bright yellow solid.

Table 3.11- Summary of reagent quantities used in RAFT polymerisation of *n*-butyl methacrylate

Ampoule	Molar ratio	<i>n</i> -BMA added/ ml (moles)	CTA added/ g (moles)	ACVA added/ g (moles)	Dioxane added/ ml	Mass (g)	Yield (%)
1	8:1	5 (0.03)	1 (0.004)	1.29 (0.004)	20	3.40	68
2	16:1	10 (0.06)	1 (0.004)	1.29 (0,004)	20	8	80
3	24:1	15 (0.09)	1 (0.004)	1.29 (0.004)	15	10.60	70.6

NMR spectroscopy result:

¹H-NMR (400 MHz, CDCl₃): δ/ppm 7.28 (solvent), 0.89 (3H, -CH₃), 0.96 (3H, -(CH₂)₃CH₃), 1.42 (2H, CH₂CH₃), 1.62 (2H, CH₂CH₂O-), 1.82 (2H, CH₂C(CH₃)(C(=O)O(CH₂)₃CH₃-), 3.95 (2H, CH₂OC=OCCH₃-), 4.55 (2H, -CHAr-), 6.33 (2H, pyrrole), 7.00 (2H, Ar), 7.23 (2H, Ar), 7.7 (2H, pyrrole).

¹³C-NMR (400 MHz, CDCl₃): δ/ppm 77.07 (solvent), 13.84 (1C, -(CH₂)₃ CH₃), 16.2 (1C, -CH₃) 19.7 (1C, -CH₂CH₃), 30.19 (1C, -CH₂CH₂CH₃), 64.50 (1C, -OCH₂(CH₂)₂CH₃), 114.21 (2C, Ar), 120.3 (2C, Ar), 178 (1C, C=O).

3.4.3 Conversion of the pyrrole-carbodithioate end group to carboxylic acid in HB P(BMA)**Materials:**

Acetone (HPLC grade, Fisher), ethanol (absolute, Fisher), methanol (HPLC grade, Fisher), ultrapure water (18.8Ω, MilliQ systems), HB P(BMA) synthesised as previously described and ACVA were used as received. Dimethyl formamide (DMF) was obtained from the Grubb's dry solvent system.

Method:

A 250 ml three-neck round-bottomed flask was equipped with a condenser, inlet nitrogen and bubbler and a magnetic stirrer bar. The apparatus was flame dried and purged with nitrogen to remove any moisture. A known amount of highly branched P(BMA) polymer was added to the flask, followed by DMF to dissolve the polymer. The reaction mixture was stirred for 30 minutes at 70 °C using an oil bath. Then, 20 equivalents of ACVA, dissolved in a minimal quantity of DMF, were added to the flask. The solution was subjected to continuous stirring at 70 °C for 24 hours. After this time, another 20 equivalents of ACVA were added to the reaction,

followed by a third addition of 20 equivalents of ACVA after a further 24 hours. After three days, the reaction was cooled to room temperature. The majority of the DMF solvent was removed under nitrogen, and then the reaction mixture was ultra-filtered through a 3000 MWCO cellulose membrane after dissolving in a 10% ethanol/acetone solvent mixture. The ultra-filtrated product was placed in a rotary evaporator to remove the remaining solvent.

NMR spectroscopy result:

¹H-NMR (400 MHz, CDCl₃): δ/ppm 7.28 (solvent), 0.92 (3H, -CH₃), 1.003 (3H, -(CH₂)₃CH₃), 1.3 (3H, CNCH₃), 1.46 (2H, CH₂CH₃), 1.656 (2H, CH₂CH₂O-), 1.86 (2H, CH₂C(CH₃)(C(=O)O(CH₂)₃CH₃-), 2.52 (2H, CH₂COOH), 3.96 (2H, -CH₂O-C=O-), 4.55 (2H, -CHAr-), 7.2-7.8 (4H, Ar), 9.9 (1H, COOH).

¹³C-NMR (400 MHz, CDCl₃): δ/ppm 77.07 (solvent), 13.13 (1C, -(CH₂)₃CH₃), 19.05 (1C, -CH₂CH₃), 30.47 (1C, -CH₂CH₂CH₃), 44.89 (1C, -C(CH₃)C=O-O(CH₂)₃CH₃), 64.5 (1C, -OCH₂(CH₂)₂CH₃).

3.4.4 Highly branched poly (*n*-butyl methacrylate) with amine ends

Materials:

Highly branched poly(butyl methacrylate) with acid, 1,2-diaminoethane (99%, Aldrich), 1,3-diaminopropane (99%, Aldrich) 1,4-diaminobutane (99%, Aldrich), 1,6-diaminohexane (99%, Aldrich), 1-(3-dimethyl-aminopropyl)-3-ethylcarbodiimide hydrochloride (Alfa Aesar), sodium dodecyl sulphate (SDS, Alfa Aesar) were used as received. MES buffer at pH 4.19 was used throughout.

Method:

Polymer solution was formed by dissolving 0.5 g polymer in 10 mL dichloromethane (DCM). To this, 0.25 g SDS was solvated in 10 ml buffer with high agitation. The DCM was then removed using nitrogen under high agitation. The resultant polymer in water solution was added to a three-neck round bottom flask equipped with a condenser and magnetic stirrer bar. At the same time, 1-(3-dimethyl-aminopropyl)-3-ethylcarbodiimide hydrochloride (EDC) was weighed out and dissolved in 30 ml of MES buffer. The stirring polymer solution was then submerged in an ice bath and the aqueous solution of EDC was slowly added. The appropriate diamine was then slowly added to the stirring mixture over a period of at least an hour.

Substantial effervescence was observed at this stage. The reaction was left to warm to room temperature and stirring continued for a further 24 hours. The quantities used for each reaction are shown in Table 3.12.

Table 3.12- Summary of reagents used in the coupling of highly branched PBMA to diamine

Diamine	Amount used/ g (moles)	EDC/ g (moles)	Mass (g)	Yield (%)
1,2-diaminethnae	1.52 (0.02)	1.17 (0.006)	0.26	52
1,3-diaminopropane	2.89 (0.03)	1.23 (0.006)	0.24	48
1,4-diaminobutane	4.97 (0.05)	1.49 (0.007)	0.19	38
1,6-diaminohexane	8.58 (0.07)	1.63 (0.008)	0.21	42

1,6-diaminohexane is a solid, an aqueous solution of which was prepared in 90 ml of water, which was then added to the reaction mixture.

Purification of animated polymers:

The stable emulsions were placed into dialysis visking tubing which was then placed into distilled water for 2 weeks, with daily changes of water taking place.

NMR spectroscopy result:

¹H-NMR (400 MHz, THF): δ/ppm 1.76 & 3.61 (solvent), 0.92 (3H, -CH₃), 0.98 (3H, -(CH₂)₃CH₃), 1.03 (3H, CNCH₃), 1.12 (2H, NH₂), 1.25 (2H, CH₂CH₃), 1.45 (2H, CH₂CH₂O-), 1.8 (2H, CH₂C(CH₃)(C(=O)O(CH₂)₃CH₃-), 2.28-2.38 (2H, CH₂COOH), 2.7 (4H, -NHCH₂(CH₂)₂CH₂), 3.1 (2H, CH₂NH₂), 3.3 (2H, C=ONH-CH₂), 3.75 (2H, -OCH₂(CH₂)₂CH₃), 5.4 (1H, CH₂C=ONH-), 7.7-7.9 (4H, Ar).

¹³C-NMR (400 MHz, THF): δ/ppm 23.8 & 66.6 (solvent), 13.42 (1C, -(CH₂)₃CH₃), 22.4 (1C, -CH₃), 24.9 (1C, CH₂CH₂C=ONH), 25.9 (1C, CH₂CH₂C=ONH) 36.6 (1C, CH₂CH₃), 38.9 (1C, -CH₂CH₂O-), 43.17 (1C, -C(CH₃)C=O-O(CH₂)₃CH₃), 67.1 (1C, OCH₂(CH₂)₂CH₃), 203.6 (1C, C=ONH).

3.4.5 Conventional free radical polymerisation of *n*-butyl methacrylate and 4-vinyl benzoic acid

Materials:

n-butyl methacrylate (*n*-BMA, Aldrich, 99%) was distilled in vacuum before being used to remove inhibitor and then cooled under refrigeration. The initiators 4,4-azobis 4-cyanovaleric acid (ACVA, Aldrich, 98%), 4-vinyl benzoic acid (4-VBA, Sigma Aldrich, 98%), 1,4-dioxane (anhydrous, 99.8%, Sigma-Aldrich), and methanol (Fisher) were used as received.

Method:

4-VBA, BMA, ACVA and dioxane were mixed in the desired ratio until the solid initiator and 4-vinyl benzoic acid had dissolved. The resulting solution was pipetted into a 50 ml ampoule and evacuated under high vacuum using the freeze-thaw technique. The end pressure in the ampoule was approximately 3×10^{-3} mbar. The ampoule was sealed using a gas/oxygen blowtorch and then placed in a water bath at 60°C for up to 11 hours to undergo polymerisation. Products were precipitated by cracking open the ampoule and diluting the polymer with additional solvent. This solution was added dropwise into rapidly stirred methanol to give a fine dispersion of polymer particles. Some polymer aggregated around the stirrer bar, which was removed and dried on a watchglass. The dispersion was centrifuged in 50 ml portions to precipitate the polymer, which was collected from the centrifuge tubes and dried under vacuum to produce a white solid.

Table 3.13- Summary of reagent quantities used in free radical copolymerisation of *n*-butyl methacrylate and 4-vinylbenzoic acid

Ampoule	Molar ratio	<i>n</i> -BMA added/ ml (moles)	4-VBA added/ g (moles)	ACVA added/ g (moles)	Dioxane added/ ml	Mass (g)	Yield (%)
1	8:1	5 (0.03)	0.57 (0.003)	0.05 (0.0001)	20	2.4	30
2	16:1	10 (0.06)	0.58 (0.004)	0.1 (0.0003)	20	6.8	42.5
3	24:1	15 (0.09)	0.58 (0.004)	0.14 (0.0004)	15	4.7	19.5

NMR spectroscopy result:

¹H-NMR (400MHz, THF): δ /ppm 1.76 & 3.61 (solvent), 0.916-1.006 (3H, (CH₂)₃CH₃), 1.312 (3H, -CH₃), 1.462 (2H, CH₂CH₃), 1.655 (2H, CH₂CH₂O-), 1.957 (2H, CH₂C(CH₃)(C(=O)O(CH₂)₃CH₃-), 2.70 (2H, CH₂CH-Ar), 3.96 (2H, -CH₂O-C=O-), 7.17 (2H, Ar), 7.87 (2H, Ar) 11.10 (1H, COOH).

¹³C-NMR (400 MHz, THF): δ /ppm 23.8 & 66.6 (solvent), 12.9 (1C, -(CH₂)₃ CH₃), 19.2 (1C, -CH₂CH₃), 30.4 (1C, -CH₂CH₂CH₃), 64.1 (1C, -OCH₂(CH₂)₂CH₃), 129.3 (4C, -C₆H₄-, Ar).

3.4.6 Linear poly(*n*-butyl methacrylate) with amine functionality**Materials:**

Linear poly(butyl methacrylate), 1,2-diaminoethane (99%, Aldrich), 1,3-diaminopropane (99%, Aldrich) 1,4-diaminobutane (99%, Aldrich), 1,6-diaminohexane (99%, Aldrich), 1-(3-dimethyl-aminopropyl)-3-ethylcarbodiimide hydrochloride (Alfa Aesar), and DOWFAX 2a1 (DOW chemicals) were used as received. Distilled water was used throughout.

Method:

A polymer solution was formed by dissolving 0.5 g of polymer in 10 ml dichloromethane (DCM). To this was added 1 g of DOWFAX 2a1 solvated in 50 ml dH₂O with high agitation. The DCM was then removed using nitrogen under high agitation. The resultant polymer in water solution was added to a three-neck round bottom flask equipped with a condenser and magnetic stirrer bar. At the same time, 1-(3-dimethyl-aminopropyl)-3-ethylcarbodiimide hydrochloride (EDC) was weighed out and dissolved in 30 ml dH₂O. The stirring polymer solution was then submerged into an ice bath and the aqueous solution of EDC was added slowly. The appropriate diamine was then added to the stirring mixture slowly over a period of at least an hour. Substantial effervescence was observed at this stage. The reaction was left to warm to room temperature and stirring continued for a further 24 hours. The quantities used for each reaction are shown in Table 3.14.

Table 3.14- Summary of reagents used in the coupling of linear PBMA to diamine

Diamine	Amount used/ g (moles)	EDC/ g (moles)	Mass (g)	Yield (%)
1,2-diaminethnae	4.651 (0.07)	3.6971 (0.02)	0.31	62
1,3-diaminopropane	5.841 (0.08)	3.7123 (0.02)	0.28	56
1,4-diaminobutane	6.812 (0.07)	3.6991 (0.02)	0.20	40
1,6-diaminohexane	7.941 (0.06)	3.7114 (0.02)	0.23	46

1,6-diaminohexane is a solid, an aqueous solution of which was prepared in 90 ml water which was then added to the reaction mixture.

Purification of animated polymers:

The stable emulsions were placed into dialysis visking tubing and placed into distilled water for 2 weeks, with daily changes of water taking place.

NMR spectroscopy result:

¹H-NMR (400 MHz, THF): δ /ppm 1.76 & 3.61 (solvent), 0.784 (3H, -CH₃), 0.866 (3H, -(CH₂)₃CH₃), 1.19 (2H, NH₂), 1.34 (2H, -(CH₂)₃O-), 1.5 (2H, -(CH₂)₂O-), 1.7 (2H, CH₂), 2.5 (2H, CH₂), 3.2 (2H, -CH₂-NH₂), 3.7 (2H, -C=O-NH-CH₂-), 3.9 (2H, -CH₂O-), 5.13 (1H, -C=O-NH), 7.17 (2H, -CH₂-C₆H₄-), 7.87 (2H, -C₆H₄-COOH).

¹³C-NMR (400 MHz, THF): δ /ppm 23.8 & 66.6 (solvent), 13.4 (1C, -(CH₂)₃ CH₃), 19.3 (1C, -CH₂CH₃), 31.8 (s, 2H, -CH₂CH₂CH₃), 64.1 (1C, -OCH₂(CH₂)₂CH₃-), 43.2 (1C, -CH₂NH₂), 44.6 (1C, -C=ONHCH₂-), 129.3 (4C, -C₆H₄-, Ar)

3.5 INSTRUMENTATION

3.5.1 Freeze-pump-thaw polymerisation

Ampoules were degassed on a high vacuum line equipped with a Pirani gauge.

3.5.2 Nuclear magnetic resonance spectroscopy

NMR spectra were performed at ambient temperature using a Bruker AV-400 at 400 MHz (an average of 64 or 128 scans per spectrum) for proton or carbon and 64 scans for the DOSY experiment. Sample preparation was performed by dissolving 20–40 mg of sample in deuterated chloroform (CDCl_3) or an alternative solvent system, which was filtered and placed in 7 mm NMR tubes. TopSpin 3.2 was used to analyse and process the NMR spectra. For DOSY experiments, polymer samples were dissolved in an appropriate solvent with a 0.5 $\text{mg}\cdot\text{ml}^{-1}$ concentration.

3.5.3 Infrared spectroscopy

Information on the polymer surfaces and functional groups were recorded on a Perkin-Elmer Spectrum 100 FT-IR spectrometer with a universal ATR crystal attachment in the range of 400–4000 cm^{-1} . Spectra were analysed using Perkin-Elmer software.

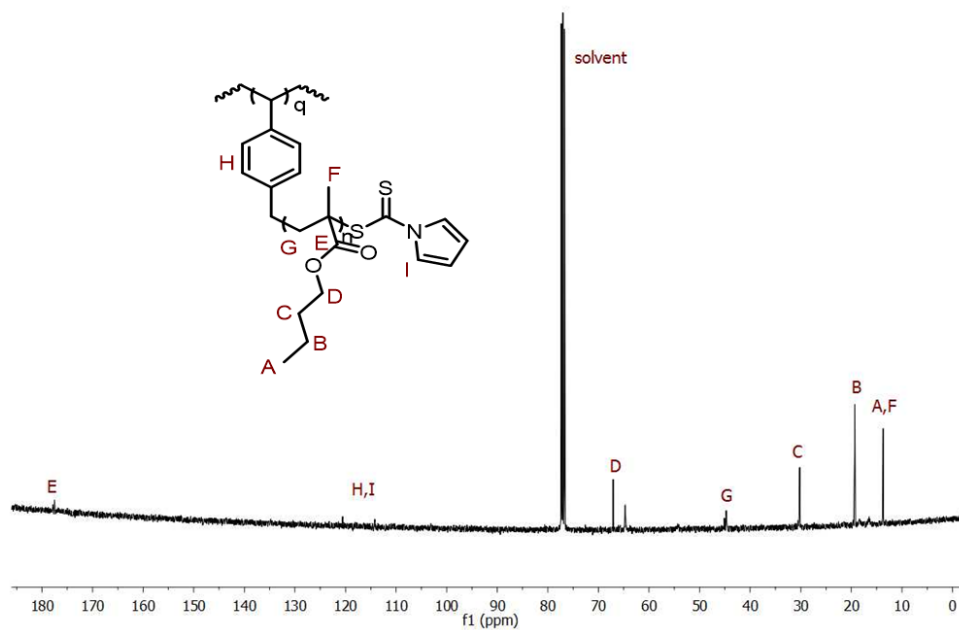
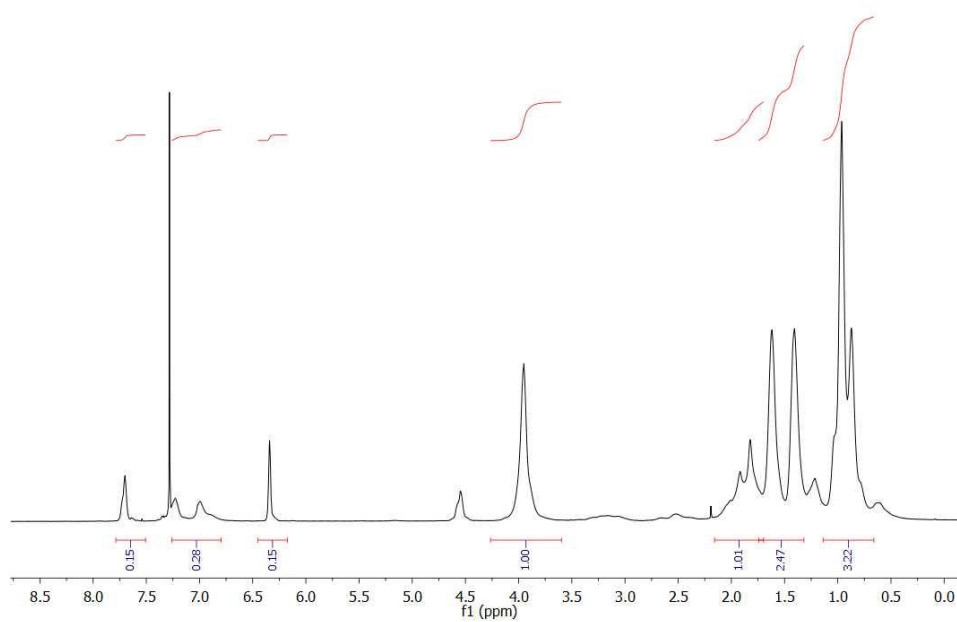
3.5.4 Size exclusion chromatography (SEC)

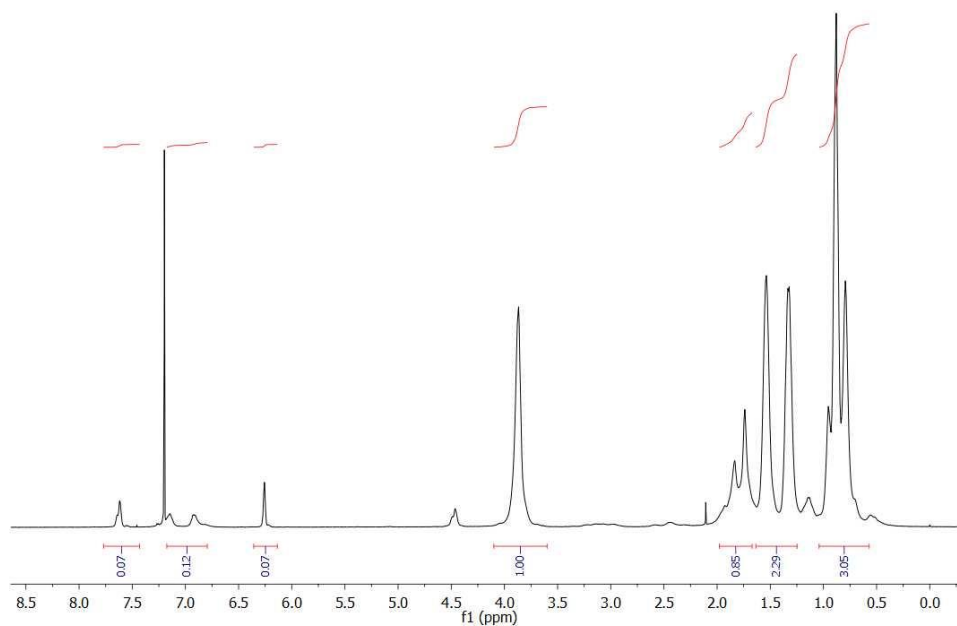
SEC was performed to determine average molar mass and molar mass distributions with polystyrene as a standard using tetrahydrofuran (THF) as the eluent. Samples were prepared at approximately 2 $\text{mg}\cdot\text{ml}^{-1}$ concentration in THF and were injected via a Gilson 234 Auto Injector through two PL Gel Mixed-B and guard columns with a refractive index detector (Agilent 1260 Infinity series). Analysis was performed using an Agilent GPC and Excel software system.

3.5.5 Elemental analysis

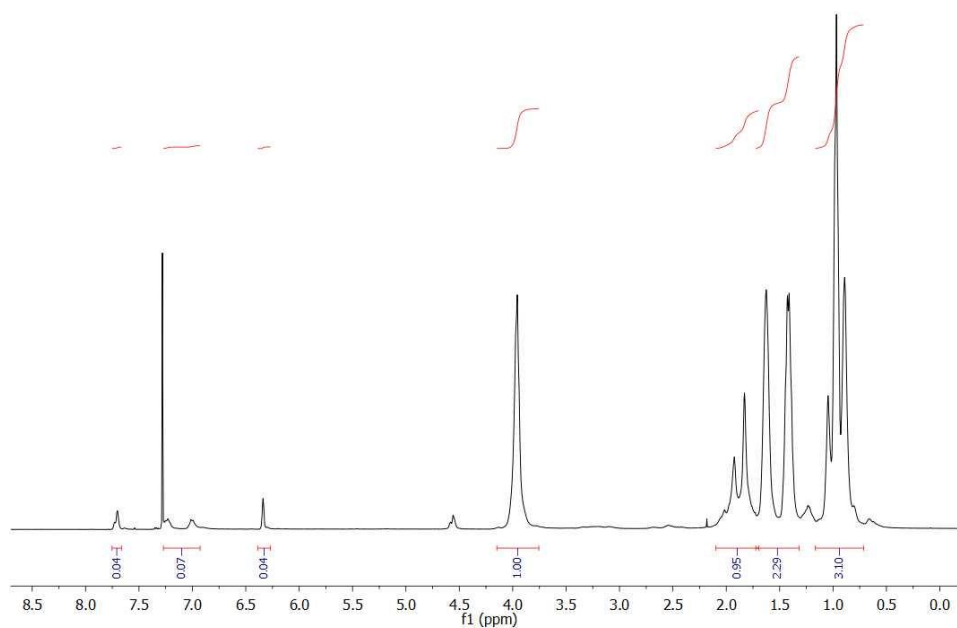
Elemental analysis was performed on a Perkin-Elmer 2400 CHNS Elemental Analysis instrument. 5–10 mg of sample was combusted in the presence of excess oxygen and combustion reagent to form CO_2 and water. The levels of each element were detected using a thermal conductivity detection system.

3.6 APPENDIXES

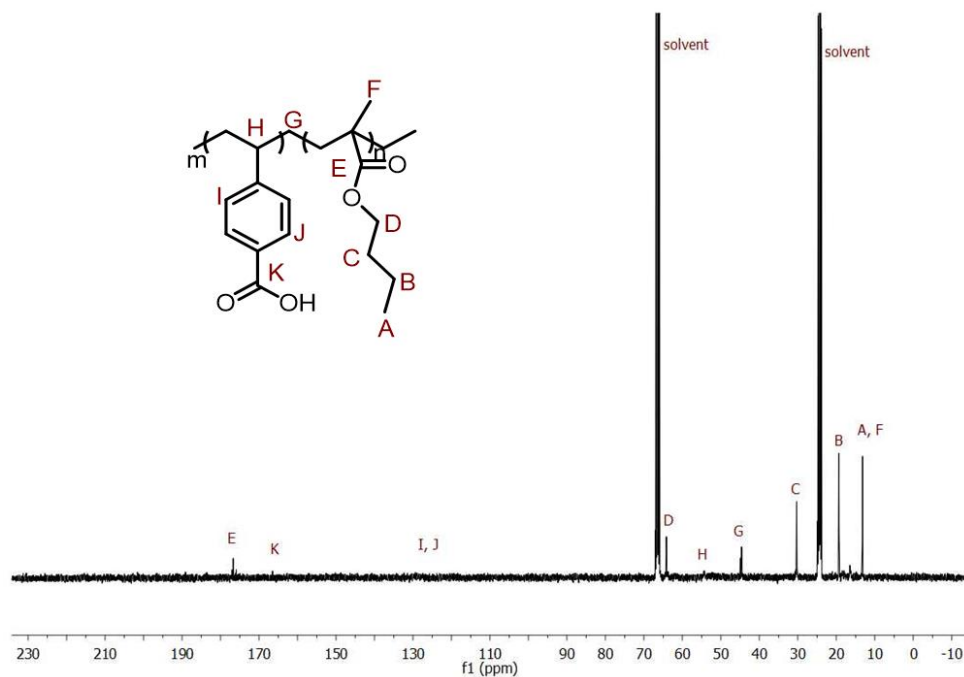
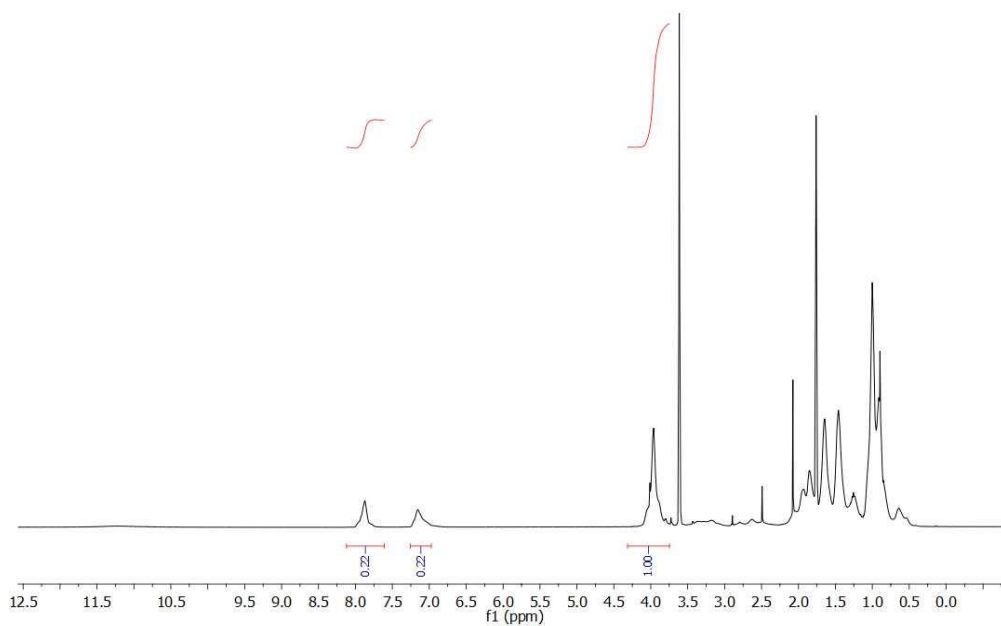
Appendix 3.1- ^{13}C -NMR of highly branched poly(butyl methacrylate)Appendix 3.2- ^1H -NMR for showing the Integration of HB P(BMA)-1

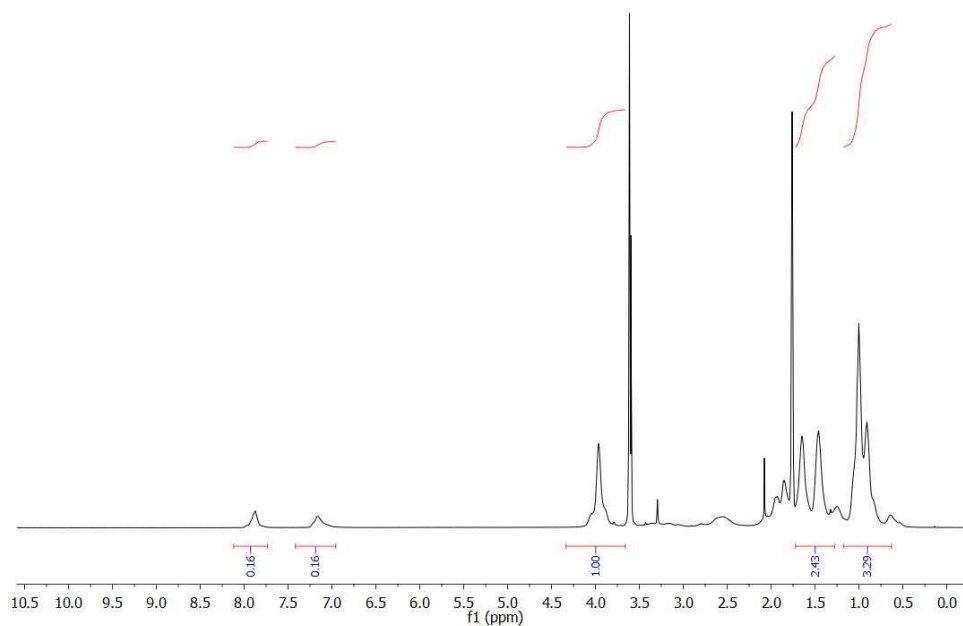


Appendix 3.3- $^1\text{H-NMR}$ for showing the Integration of HB P(BMA)-2

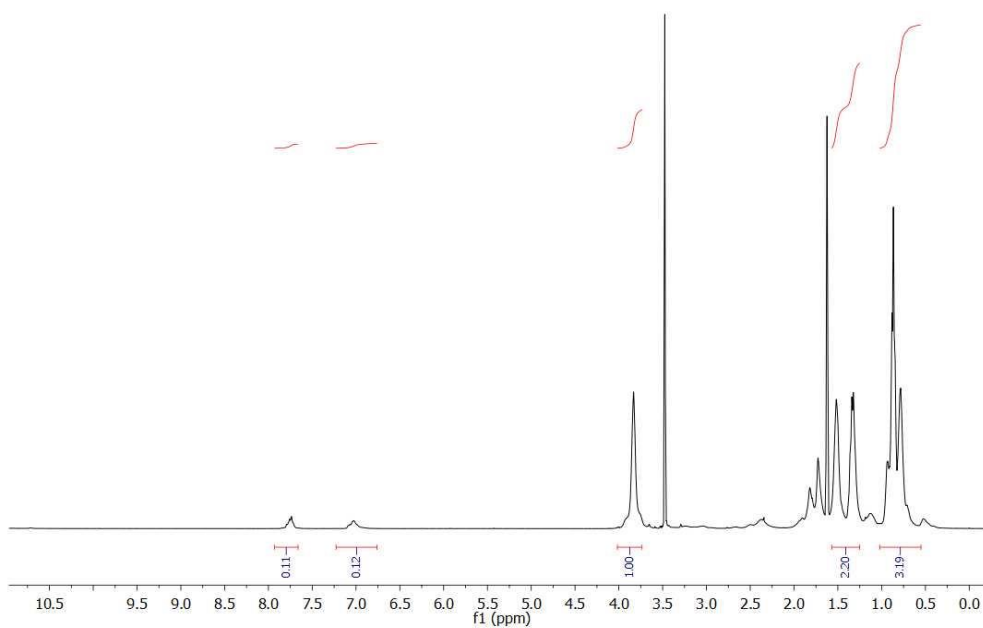


Appendix 3.4- $^1\text{H-NMR}$ for showing the Integration of HB P(BMA)-3

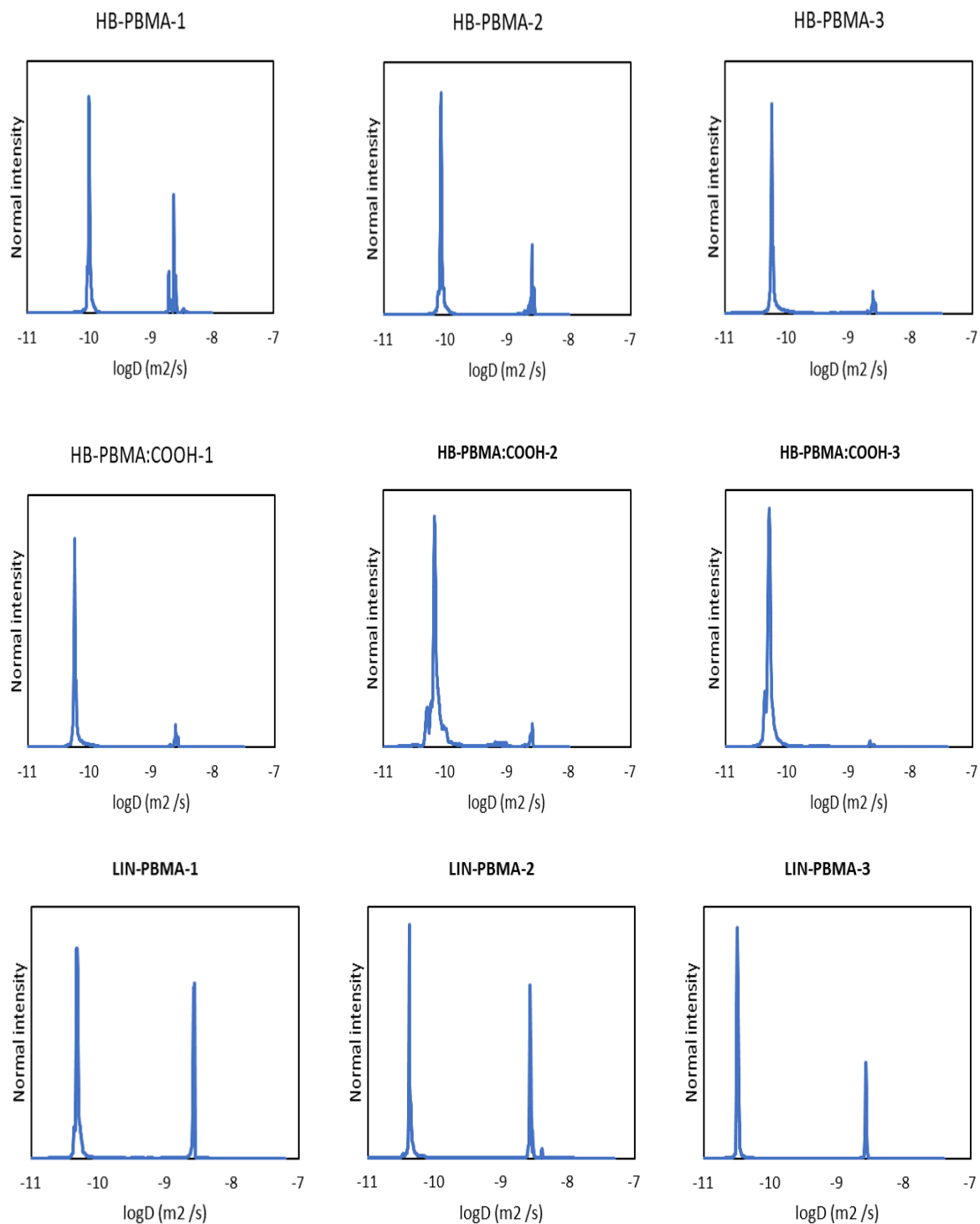
Appendix 3.5- ^{13}C -NMR of linear poly(butyl methacrylate)Appendix 3.6- ^1H -NMR for showing the Integration of LIN P(BMA)-1



Appendix 3.7- $^1\text{H-NMR}$ for showing the Integration of LIN P(BMA)-2



Appendix 3.8- $^1\text{H-NMR}$ for showing the Integration of LIN P(BMA)-3



Appendix 3.9- The logarithm of diffusion coefficient distributions of highly branched and linear polymers obtained from DOSY analysis

4 CHAPTER FOUR: THERMAL, PHYSICAL AND MECHANICAL PROPERTIES OF POLYMERS

4.1 INTRODUCTION

Exploring the interaction of cells with synthetic biomaterials is vital for understanding how material properties affect cell adhesion. The ability of cells to adhere to polymeric surfaces depends not only on their chemical properties but their physical and mechanical properties too. Properties such as functional groups, surface energy and wettability, surface topography and roughness, along with stiffness, can play an essential role in cell adhesion^{121, 210-211}. Understanding the interplay of these parameters is a challenging but important part of designing novel biomaterials for cell therapy and tissue engineering²¹².

The mechanical properties of biomaterials are considered important contributors to the understanding of bio-adhesion (cells adhering to materials). The surface roughness, stiffness and topography parameters would be useful to consider in this regard. A number of studies have shown that a smooth surface is an important feature of biomaterials for growing healthy cells and resisting bacterial adhesion^{122, 213}; other studies in the literature have demonstrated that some cells prefer rough surfaces for the initial cell adhesion^{147, 214-215}. Cell growth and attachment also depends on the elastic modulus or substrate stiffness; the substrate stiffness measures the ability of a material to resist deformation²¹⁶. Most studies have observed that the ideal surface material needs to be stiffer than the cells involved in adhesion^{153, 217-219}. The physical properties of polymers are to a large part influenced by the glass transition temperature (T_g). The T_g of polymers is an important parameter in determining the state of the polymer; glassy or rubbery. The T_g of homo poly(butyl methacrylate) is around 20 °C²²⁰, but this value may show variations depending on polymerisation method, molecular weight, chain mobility and functionality²²¹. An amorphous polymer above T_g behaves as a viscous liquid, whilst below T_g the material can be described as in a hard glassy state²²². Therefore, the mechanical and viscoelastic properties of biomaterials, are sensitive to structure and temperature, respectively²²³. Various papers demonstrate a relation between the T_g and the material's mechanical properties such as toughness, stiffness or roughness²²⁴⁻²²⁶. In general, for homogeneous amorphous systems at constant molar mass, the comparison of linear and branched polymers with similar chemical structures shows that the branched polymers have lower T_g ⁵⁵. However, the T_g and attendant properties are also subject to modification of main chain groups and/or pendant functionality²²⁷⁻²²⁸.

A considerable amount of research has focused on how materials hydrophobicity or hydrophilicity influence cell adhesion and proliferation on biomaterials. This is called surface wettability, and can be measured by water contact angles ²²⁹⁻²³⁰. A number of studies have shown that hydrophilic surfaces enhance cell adhesion more efficiently than hydrophobic ones ²³¹⁻²³⁴. Furthermore, other research studies have reported that a greater amount of cell attachment occurs on hydrophobic surfaces ²³⁵⁻²³⁷ or on intermediate surfaces ²³⁸⁻²⁴⁰. The terms hydrophobic and hydrophilic are relative and are often confused with behaviour that reflects the initial entanglement of the surface energies of the non-modified substrate. None the less the wettability must be studied in order to understand the mechanism of cell attachment to solid surfaces.

Furthermore, the adhesion and growth of cells on polymer surfaces has been related to the polar and dispersion components of surface free energy. Surface free energy is a measure of the increase in energy taken from the bulk of the material and placed at its surface by the type or number of dangling bonds present. The bonds can be divided into primary bonds (ionic, metallic and covalent) for metal, ceramic and oxide materials found in high-energy surfaces, and secondary bonds (van der Waals) for polymers and molecular crystals found in low-energy surfaces ²⁴¹. The influence of the surface free energy components on cell adhesion to solid surfaces has been studied by Birdi. It was found that cell adhesion increased with the increase in polarity of the polystyrene substrate ²⁴². Also, the effect of the surface free energy electron donor and electron acceptor parameters could be considered in different interfacial phenomena, for example, biofouling, phagocytosis and microbial adhesion ²⁴³. Therefore, determining the effect of the electron donor or acceptor properties of a material on cell adhesion could be an important area of research. A study by Bren and colleagues examined the influence of the surface electron donor and electron acceptors parameters with regards to the attachment of osteoblast cells to stainless steel and titanium-vanadium-aluminium alloys. It was found that the electron acceptor (acid component) of the surface energy had a strong correlation with the alkaline phosphatase activity and hence a surface with higher electron acceptor character encouraged osteoblast differentiation ²⁴⁴.

The aim of this study was to analyse the particular polymer surface properties that are most strongly associated with enhanced biological activity of cell adhesion and cell attachment. In this chapter, the investigation of the thermal properties of synthesised PnBMA with different architectures and functionalities, compared to the manufactured homo PnBMA, was carried

out using differential scanning calorimetry (DSC) and thermogravimetric analysis (TGA). The homo PnBMA was purchased from Sigma Aldrich, UK to compare the thermal and wettability properties of the pure PnBMA to HB-PBMA and L-PBMA with different terminal ends, and investigate the effects of different functionalities compared to pure PnBMA. The surface wettability of all polymers was measured by water contact angle (CA). The surface energies of the polymers were also evaluated by contact angles using three different liquid probes. Two approaches were used to determine the polar and dispersion components of the surface free energy; the “dispersion-polar” and “Lifshitz-van der Waals acid-base”. The polymers selected in this study were based on the 16:1 molar ratio according to their synthesis and re-functionalisation with acid or amine. Only one of the diamines was chosen to study the thermal properties for both architectures which is 1,6-DAH, due to the limited amount of available aminated polymers, which was insufficient to perform all the physical and chemical characterisations. However, all aminated functional polymers were analysed by contact angle measurements. Furthermore, the topography and elastic modulus (stiffness) of acidic highly branched and linear PnBMA at different temperatures were evaluated via atomic force microscopy (AFM) in order to compare the differences in mechanical properties of polymeric material surfaces for the study of cell adhesion. Due to insufficient time, the mechanical properties of aminated highly branched or linear polymers were not studied.

4.2 RESULTS AND DISCUSSION

4.2.1 Thermal analysis

The thermal properties of linear and highly branched poly(butyl methacrylate) with different functionality were analysed via thermogravimetric analysis (TGA) and differential scanning calorimetry (DSC) in this research. Thermogravimetric analysis is a simple thermal analysis technique that measures the amount and rate of change in the weight of materials over a wide range of temperatures or time. TGA can characterise materials that exhibit weight loss or gain due to decomposition, oxidation, or dehydration. However, differential scanning calorimetry (DSC) is a valuable tool in polymer science and engineering to measure the heat effects of the phase transitions of polymeric materials. In brief, DSC determines critical information, for example, glass transition state, melt transition state, crystallisation state, and heat capacity and percentage of crystallinity.

4.2.1.1 TGA measurements

The TGA thermogram of pure PnBMA and HB-PBMA with pyrrole, acid or amine functional groups, as well as L-PBMA containing acid or amine functionality, were evaluated at a heating rate of 10 °C from 25 to 500 °C under N₂ gas, as shown in Figure 4.1 and labelled results can be seen in the Appendix.

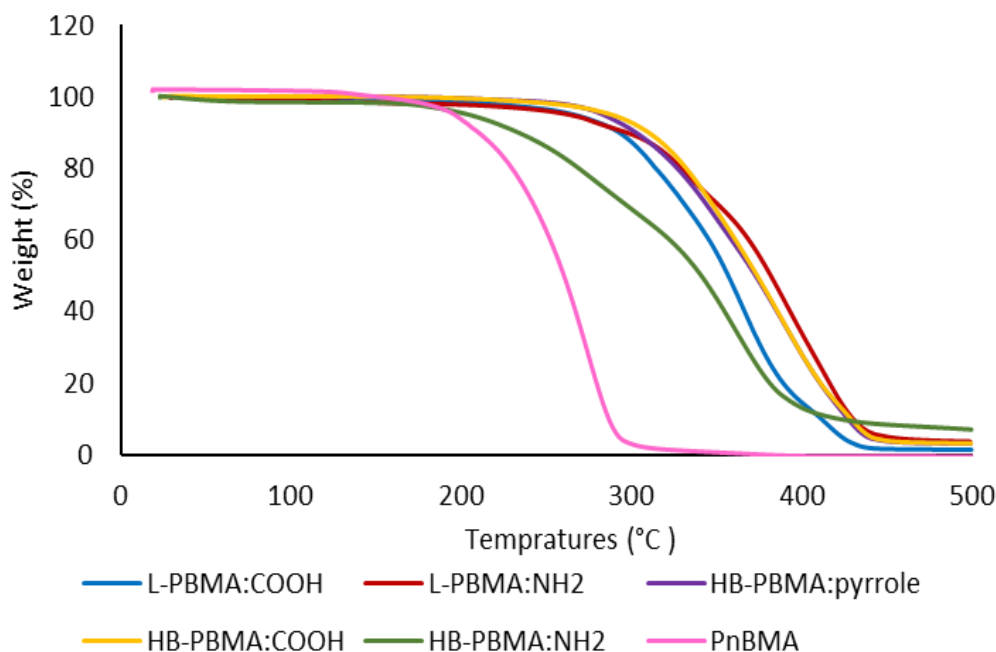
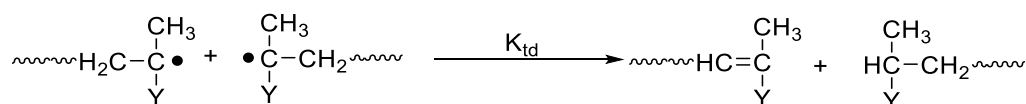
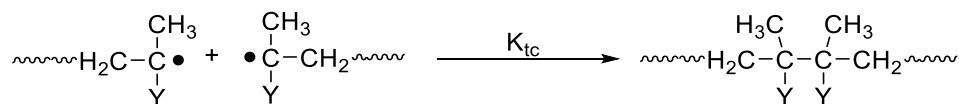


Figure 4.1- TGA graphs of poly(butyl methacrylate)s with varying architectures and functionalities

The start of weight loss to the degraded functional polymers in TG curves vary depending on the functionality and architecture of the polymer. The initial decomposition temperatures measured at 5 % weight loss of HB-PBMA with pyrrole, acid and amine functionalities were 268, 288 and 208 °C, respectively. The degradation of linear polymers began at lower temperatures, which were 247 °C for an acidic functionality and 263 °C for an amine functionality. The difference is probably associated with the different structure of the functional groups. The HB polymers were prepared using RAFT whilst controlling the end groups. Conversely, the linear polymers were prepared using conventional free radical polymerisation. Furthermore, it can be seen that there was a substantial enhancement of thermal stability by both copolymerization and by using the RAFT process to provide the branched polymers, as tabulated in Table 4.1. It is clearly observed that on heating the copolymer samples showed little weight loss until 350 °C. Increasing weight loss was observed above this temperature with a sharp decrease at 450 °C with some residual materials at 500 °C. However, the chain scission of the homopolymer, PBMA, starts at 187 °C with higher degree of loss of material (99 %) at 350 °C and no residual material at 500 °C. The lower thermal stability of PBMA is best rationalized by considering changes in end group structure due to different termination mechanisms. In conventional radical polymerization of BMA²⁴⁵⁻²⁴⁶ termination by disproportionation as shown in Scheme 4.1 plays a major role in termination compared to termination by combination as shown in Scheme 4.2.



Scheme 4.1- Two radicals terminated by a disproportionation in FRP



Scheme 4.2- Two radicals terminated by combination (coupling) in FRP

The termination by disproportionation produces allylic end groups that cleave homolytically at relatively low temperatures²⁴⁷⁻²⁴⁸. This homolytic cleavage leads degradation by the unzipping mechanism to produce monomers^{247, 249}. The RAFT process does not involve termination by disproportionation, so the fraction changed end allylic groups is minimized and the branched polymers have increased thermal stability. The enhanced thermal stability of the

linear copolymers, compared to the homopolymer of BMA, suggests that copolymerization with vinyl benzoic acid also reduces the fraction of terminations that occurred by disproportionation.

Table 4.1- TGA data for the polymers

Polymers	Initial temperature at 5% weight loss (°C)	Weight loss at 350 °C (%)	Weight loss at 450 °C (%)	Residue at 500 °C (%)
PnBMA	187	99	100	0
HB-PBMA:pyrrole	268	39	96	2.8
HB-PBMA:COOH	288	32	96	3.2
HB-PBMA:NH₂	208	48	94	5.2
L-PBMA:COOH	265	44	98	1.4
L-PBMA:NH₂	263	30	95	3.7

In highly branched polymers, the acid and pyrrole end groups exhibited similar thermal and degradation behaviours, but the amine functionality was different as the degradation temperature of the polymer was lower than that for HB samples with 5 % residual material at 500 °C. The data thus indicate an effect of adding amine functionality. However, the same effect is not observed with the linear polymer with 1,6-DAH functionality. Comparing the linear COOH and amine functional polymers the residual material was higher in the aminated polymer than the COOH functional material. The initial decomposition at 5 % weight loss occurred at low temperatures for amine functional polymers of both architectures. The residue yield of the branched materials is higher than the linear materials. The data presented here do not directly affect the main focus of the work and are preliminary, but they do indicate enhanced thermal stability on both copolymerization and/or utilizing the RAFT process.

4.2.1.2 DSC measurements

Considering the glass transition temperature (T_g), all polymer samples were run under a heat/cool/heat cycle since the samples had shown residual polymeric material, as can be seen in Figure 4.2 and labelled results can be seen in the Appendix. The top curve corresponds to the second heating cycle while the bottom curve corresponds to the first. In the first heating cycle, there are slight endothermic peaks at particular temperatures above the T_g of the polymers, which are at 38, 46, 50, 65 and 80 °C for PnBMA, HB-PBMA:pyrrole, HB-PBMA:COOH, L-PBMA:COOH and L-PBMA:NH₂, respectively. This could be related to

incomplete polymerisation of the residual monomers within the polymer which subsequently evaporated in the first cycle²⁵⁰⁻²⁵¹. A similar observation was noted in the study of the glass transition of acrylic resin²⁵¹, and in poly(methyl methacrylate) with barium titanate²⁵⁰ by DSC. The authors reported that the first heating cycle showed an endothermic peak while the second heating cycle showed no endothermic region, only a T_g peak. Moreover, in the case of polymers modified with diamine, wide and distinct endothermic peaks are observed, which can be attributed to the process of moisture vaporisation. This phenomenon is related to the presence of an amino group on the modified polymers that could encourage the adsorption of water²⁵².

The T_g of functional PBMA with linear and branched architectures were compared to PnBMA homopolymer as shown below. It was observed that the T_g was affected by the incorporation functional groups, the end groups of branched or linear PBMA copolymers showed T_g values higher than the T_g of the homopolymer of BMA. This indicates that there is an interaction between the polymer chain and the pyrrole, carboxylic and amine functionalities. These interactions can alter the properties of materials. Briefly, the data showed that the addition of benzyl and COOH to the linear polymers increases the T_g , however, the branched polymers have lower T_g even though they contain rigid benzyl groups. Amine polymers appear to contain water and so they gave very broad transitions. These results showed how the architecture can control T_g with the same chemical functionality.

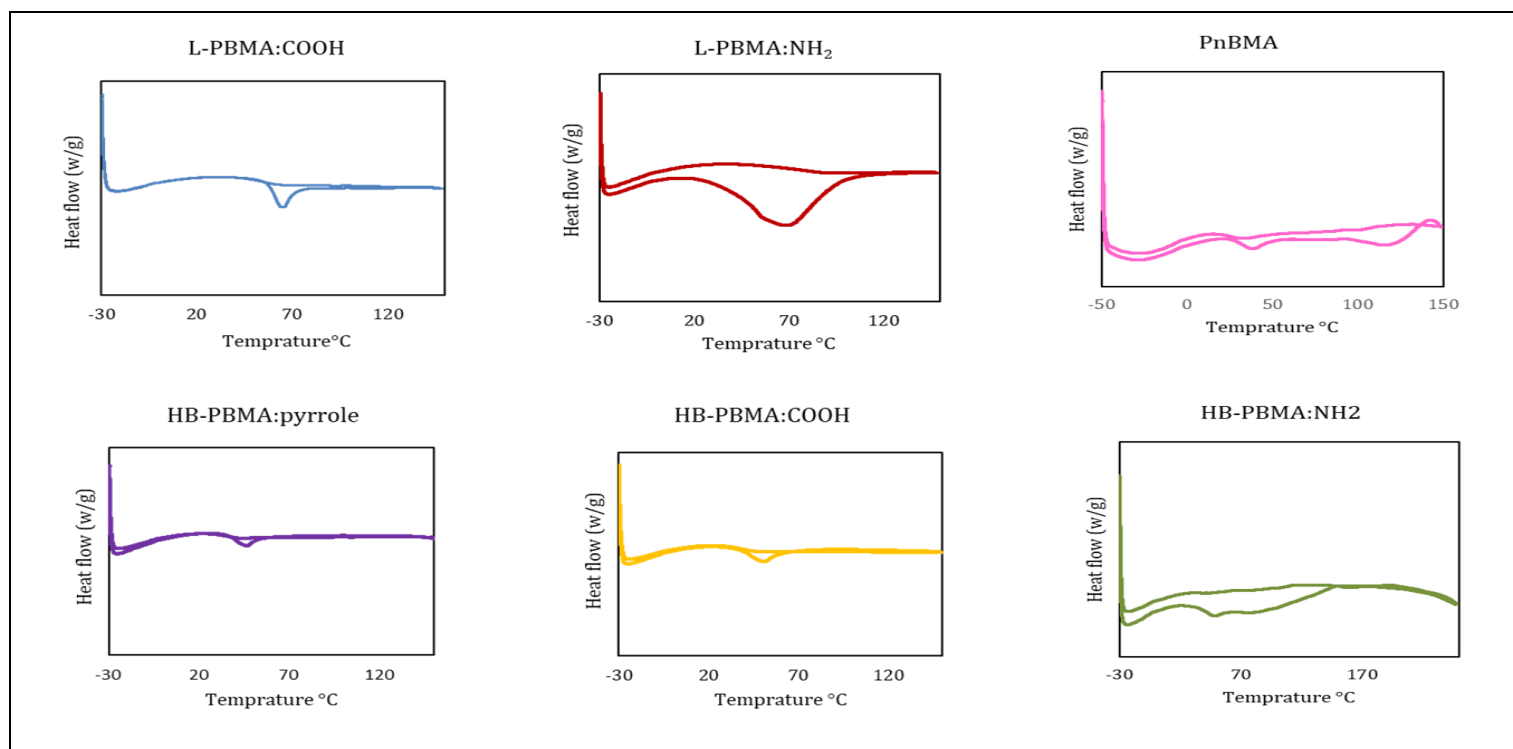


Figure 4.2- DSC thermograms for polymers. The top response for each sample was for the second heating cycle, while the bottom response was for the first heating cycle

The associated glass transitions were determined from the inflection points of DSC on the second heating cycle, as seen in Table 4.2.

Table 4.2- Glass transition temperatures of different polymers

Polymers	L- PBMA:COOH	L- PBMA:NH ₂	HB- PBMA:pyrrole	HB- PBMA:COOH	HB- PBMA:NH ₂	PnBMA
$T_g / ^\circ\text{C}$	55	80	36	39	59	25

It can be seen that the T_g values of the synthesised poly(BMA)s were in the range of 30 to 80 °C, and no melting transition was observed in the DSC traces due to the amorphous nature of these polymers. The glass transition increases from 55 °C to 80 °C in the linear PBMA with acid and amine functionality respectively, and from 36 °C to 39 °C or 59 °C in highly branched PBMA with pyrrole, acid and amine-terminating groups, respectively.

As a comparison between linear and highly branched polymers T_g , the T_g of linear PBMA was higher than that of branched PBMA²⁵³. The branched polymers were characterised by a large proportion of structural units as end groups and the reduction in T_g can be rationalised by considering that these extra end groups require more free volume than equivalent functionalities pendant to linear polymers. Another reason for the higher T_g values in linear

than in branched polymers could be a reflection of the absence of chain entanglement in the solid state in branched materials²⁵⁴. In addition, it was found that the T_g values of PBMA polymers shifted slightly towards higher temperatures with the addition of acid functionality. This increase in the T_g value of acidic PBMA is due to the increased possibility for dipolar polymer/polymer interactions. The same features were observed by Kim in studies on the effects of the chain end group of hyperbranched polyphenylene. The results showed that T_g increases with the increasing polarity of the end groups present²⁵⁵. Amination of the polymers produced more complex thermograms in which it was difficult to identify defined T_g . The diffuse nature of these thermograms were probably the result of water ingress and uneven plasticisation.

4.2.2 Investigating the wettability of polymer surfaces via contact angles

Wettability is another important factor for understanding the physicochemical characterisation of polymer surfaces. The most commonly used method for measuring the wettability of hydrophobic and hydrophilic surfaces is the water contact angle (CA), which measures the angle that is formed when a liquid meets a solid surface²⁵⁶. A hydrophobic surface has a CA of more than 90° , whereas a hydrophilic surface has a CA of less than 90° . In terms of hydrophobicity/hydrophilicity, distilled water was used to analyse the surface wettability via the sessile drop technique. The surfaces were prepared by coating cleaned and sterilised coverslips with all smooth and flat polymers. The data were collected from at least three drops placed in different positions, and the final contact angle was calculated as the average along with the standard deviation. Image processing and data collection of the contact angle values were analysed via the ImageJ software.

The wettability of the HB-PBMA surface with varying architectures and termination with pyrrole, COOH and NH_2 were quantified by sessile contact angles, as seen in Figure 4.3, which illustrates that the droplet images and contact angles of the branched polymer terminated with pyrrole produced a surface with water contact angle (θ) of $84^\circ \pm 0.9$, while the contact angle decreased for HB-PBMA:COOH ($\theta = 77^\circ \pm 1.9$), and further decreased for the polymers with NH_2 functionality ($\theta = 29\text{--}67^\circ$). The increased hydrophilic nature of the amine polymers confirmed the result of the DSC study in which complex thermograms were obtained that could be explained by the ingress of water. The contact angle of the homo PnBMA was also measured ($\theta = 90^\circ \pm 2.3$) to show the effect of adding polar groups into the polymer. These results demonstrated that the influence of carboxylic or amine functional groups was to decrease the

hydrophobicity of PnBMA and resulted in lower contact angles and confirmed that the modification of PnBMA surface had indeed occurred, resulting in a more hydrophilic surface. Given that the animated branched polymer formed a wettable surface of $\theta \sim 67^\circ \pm 2.7$ and $55^\circ \pm 3.2$ on 1,6-DAH and 1,4-DAB, respectively, while the other animated polymer surfaces; which were between $\theta \sim 29\text{--}39^\circ$. This difference could occur from the long carbon chain in diaminohexane (C6) and diamionbutane (C4) that provides a more hydrophobic surface than the other alkyl diamines. Moreover, the decreased water contact angles of 1,3-DAP compared to 1,2-DAE-modified PnBMA surfaces might be related to the quantity of diamine which was added during the reaction, as elemental analysis results showed that the nitrogen content in 1,3-DAP was higher than in 1,2-DAE, at 4.5 % and 3.1 %, respectively but these differences are rather small and were not considered further.

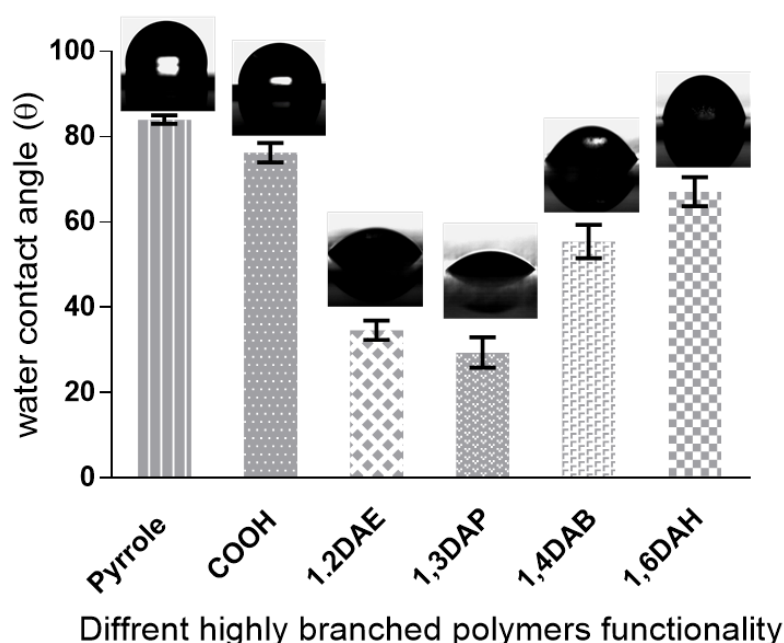


Figure 4.3- Wettability of different polymer surfaces with drop imaging of highly branched polymers by water contact angles using the sessile drop method

Results are the mean \pm SD of three independent experiments

The wettability of a linear analogue copolymer was also measured, and images of the water drops are shown in Figure 4.4. The COOH-terminated linear PBMA surface is quite hydrophobic with contact angles above 80° due to the benzene groups in the polymerisation of 4-vinylbenzoic acid with BMA. Modification of the acidic linear polymer with different alkyl amines to provide amine end functionality decreased the water contact angles, with contact angles of $\theta \sim 70^\circ$ being observed. The main difference in the wettability of the surfaces between

amine-terminated surfaces in the highly branched polymer and the linear polymer was that the HB animated surfaces were more hydrophilic than the animated linear surfaces. This can be attributed to the consideration that in the branched architecture the multitude of end groups require increasing amounts of free volume and they cannot penetrate the coil. The entanglement of chains is much impaired in a branched polymer whereas linear polymers in the bulk state are highly entangled. The entanglement provides a kinetic barrier to migration of polar groups to the surface. On the other hand, polar groups located at chain ends of branched polymers are not subject to this kinetic barrier and the data here clearly shows that the branched architecture provides a means of more effectively functionalising the interface.

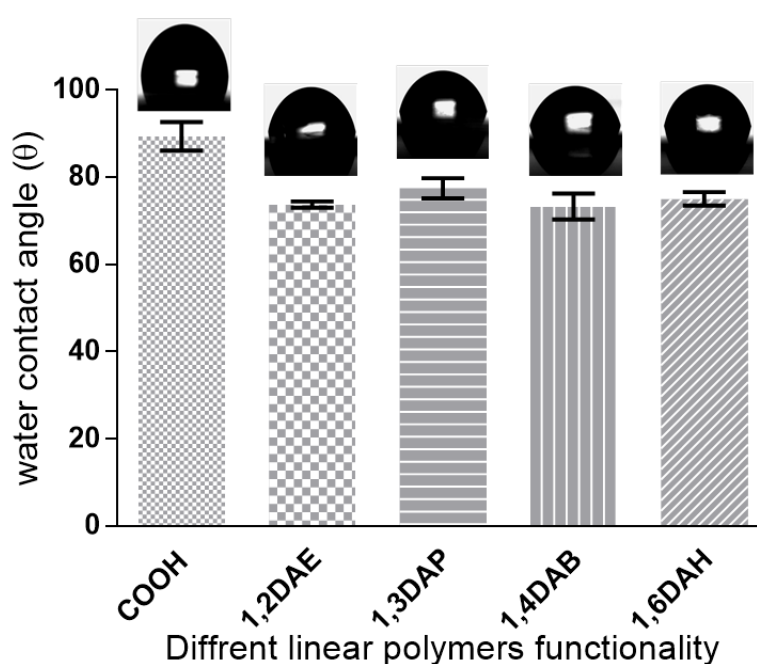


Figure 4.4- Wettability of different polymer surfaces with drop imaging of linear polymers by water contact angles using the sessile drop method

Results are the mean \pm SD of three independent experiments.

The average contact angle measurements of the three different probe liquids on the highly branched and linear polymers and their standard deviations are given in Table 4.3. It can be seen that the contact angle measurements of ultrapure water on the different polymer surfaces returned the largest values compared to the methylene iodide or glycerol probe liquids for most polymer surfaces. This difference is related to the surface tension of the probe liquids. The surface tensions of methylene iodide and glycerol (50.8 mJ/m^2 and 64 mJ/m^2 , respectively) are lower than the surface tension of water (72.8 mJ/m^2). Based on this, the contact angle of methylene iodide on acidic and pyrrole end group polymers should be lower than that on

aminated polymers, the opposite to the cases of water and glycerol, indicating the more hydrophilic nature of the aminated polymers.

Table 4.3- Contact angle measurements on poly(butyl methacrylate)s with different architectures and functionality coated on coverslips as substrates

Polymers	θ water (deg)	θ CH ₂ I ₂ (deg)	θ glycerol (deg)
PnBMA	90.7 ± 2.3	41.5 ± 0.9	75.6 ± 2.3
HB-PBMA:pyrrole	84.02 ± 0.9	43.4 ± 3.5	69.5 ± 3.6
HB-PBMA:COOH	77.59 ± 1.9	42.6 ± 3.2	65.2 ± 2.5
HB-PBMA:1,2-DAE	34.6 ± 1.9	62.5 ± 3.6	32.2 ± 1.7
HB-PBMA:1,3-DAP	29.4 ± 2.9	69.7 ± 2.7	25.3 ± 2.6
HB-PBMA:1,4-DAB	55.4 ± 3.2	49.4 ± 1.1	55.3 ± 1.8
HB-PBMA:1,6-DAH	67.2 ± 2.7	46.7 ± 3.4	57.4 ± 3.3
L-PBMA:COOH	89.2 ± 1.6	43.8 ± 2.9	74.31 ± 2.1
L-PBMA:1,2-DAE	73.6 ± 0.7	51.3 ± 2.7	60.8 ± 2.4
L-PBMA:1,3-DAP	76.4 ± 2.3	50.2 ± 4.1	63.2 ± 1.7
L-PBMA:1,4DAE	73.2 ± 2.9	50.3 ± 3.2	63.1 ± 2.9
L-PBMA:1,6-DAH	74.9 ± 2.8	50.9 ± 2.3	62.8 ± 2.1

Results are the mean values and standard deviation of water, methylene iodide (CH₂I₂) and glycerol contact angles (θ); at least three measurements for each species were taken.

The contact angles measured using water and glycerol as the polar probe liquids show that there are only small differences in contact angles between HB-PBMA:pyrrole and HB-PBMA:COOH, as well as between L-PBMA:COOH and L-PBMA:NH₂. However, compared to the homo PnBMA, these differences are significant in the sense of confirming that the behaviour and properties of acidic and amine functionalised polymers are altered such as to become slightly hydrophilic. The much lower contact angles that were calculated for aminated highly branched polymers is associated to the lack of opportunities for chain entanglements in the branched polymers. The aminated highly branched polymers with 1,2-DAE and 1,3-DAP formed more wettable surfaces than 1,4-DAB and 1,6-DAH. This result is as expected since 1,6-diaminohexane (C6) and 1,4-diaminobutane (C4) contain more hydrophobic spacer groups than the other alkyl diamines.

In the case of methylene iodide as a non-polar probe liquid, it was found that, in contrast to polar liquids, the contact angles are smaller, with the exception of a number of aminated branched polymers having higher contact angles than the polar probes. This means that these polymers have more hydrophilic surfaces and have more polar substrates. Again, the contact angles for all polymer substrates show that the polar probe liquids are more wetting than non-polar liquids, except for aminated branched polymers with 1,2-DAE and 1,3-DAP. This indicates that all polymer substrates have non-polar rather than polar characters, except for some aminated branched polymers, and the data provide a unique way of modifying the surface free energies with rather small changes in the polymer structure. Of major importance is the observation that functionalisation of the linear polymers is not subject to this significant structural effect.

4.2.3 Surface free energy of polymers

A variety of theories have been associated with calculating solid surface energy through contact angle measurements. Examples are Zisman's approach, harmonic mean approach, geometric mean approach, Owen and Wendt (dispersion polar) approach and Lifshitz-van der Waals interaction (acid-base) approach. In this study, two approaches for surface energy calculation were chosen:

4.2.3.1 Theory of dispersion-polar approach

Owen and Wendt (OW) method, also called (dispersion-polar),²⁵⁷⁻²⁵⁹ gives the long-range dispersion γ^d and the short-long polar γ^p (hydrogen bonding) components of surface free energy (SFE), using the following equation:

$$\gamma_L = \gamma_L^p + \gamma_L^d \quad (4.1)$$

$$\gamma_S = \gamma_S^p + \gamma_S^d \quad (4.2)$$

where γ_S, γ_L are the surface tension of the substrate and liquid, respectively. Combining equations 4.1 and 4.2 the total surface tension would be as following:

$$\gamma_{SL} = 2 \left(\sqrt{\gamma_S^d \cdot \gamma_L^d} + \sqrt{\gamma_S^p \cdot \gamma_L^p} \right) \quad (4.3)$$

The Young equation always describes the phenomena of thermodynamic wetting as shown in equation 4.4, as it is a basic method for calculating the SFE from contact angle data:

$$\gamma_L \cos \theta = \gamma_s - \gamma_{SL} \quad (4.4)$$

Combining Equation 4.3 and 4.4 results in the following equation:

$$1 + \cos \theta = 2\sqrt{\gamma_S^d} \left(\frac{\sqrt{\gamma_L^d}}{\gamma_L} \right) + 2\sqrt{\gamma_S^p} \left(\frac{\sqrt{\gamma_L^p}}{\gamma_L} \right) \quad (4.5)$$

Where θ is the measured contact angle, γ_S^d is the dispersive component of the substrate material, γ_S^p is the polar component of the substrate, γ_L^d is the dispersive component of liquid, γ_L^p is the polar component of liquid and γ_L is the surface energy of liquid.

Equation 4.5 can be used to determine the polar and dispersive components of the SFE of a polymer based on the contact angle measurements of two different probes. When the liquids of a known surface tension are used, then the γ_L is known, $\cos \theta$ is determined by the contact angle, and the other parameters γ_S^d and γ_S^p can be calculated. The most important property of the selected probe liquids is that one liquid just has a dispersive component, and the other liquid has both dispersive and polar parts to find γ_S^d and γ_S^p in this method.

4.2.3.2 Theory of acid-base approach

Calculating SFE using the Lifshitz-van der Waals (Van Oss-Chaudhey-Good/ acid-base) (LW-AB) approach²⁶⁰ is based on the concept that the surface tension of a solid surface can be divided into two components; one is the long-range interactions; called Lifshitz-van der Waals component (γ^{LW}) and the other includes the short-range interactions; called the acid-base component (γ^{AB}). The latter can be divided into two parts, acidic (γ^+) and basic (γ^-)²⁶⁰⁻²⁶¹. As a result, the total surface tension of substrate-liquid interface is written as the following equation:

$$\gamma_{total}^{S-L} = \gamma_{SL}^{LW} + \gamma_{SL}^{AB} \quad (4.6)$$

Where γ_{SL}^{LW} is the surface tension components of non-polar interaction and γ_{SL}^{AB} is the surface tension components of polar (acid-base) interaction.

According to Fowkes²⁶², if the dispersion (LW) interaction forces are just between a solid and liquid, the interfacial tension of γ_{SL}^{LW} is addressed by the following equation:

$$\gamma_{SL}^{LW} = \left(\sqrt{\gamma_S^{LW}} - \sqrt{\gamma_L^{LW}} \right)^2 \quad (4.7)$$

Van Oss and colleagues²⁶¹ describe the acid-base (AB) interaction forces as comprising electron acceptor γ^+ (Lewis acid) and electron donor γ^- (Lewis base) components. The interfacial tension of γ_{SL}^{AB} can be written as:

$$\gamma_{SL}^{AB} = 2 (\sqrt{\gamma_S^+} - \sqrt{\gamma_L^+})(\sqrt{\gamma_S^-} - \sqrt{\gamma_L^-}) \quad (4.8)$$

This approach combined the Young equation to evaluate the SFE components of liquid and solid surface according to acid-base approach.

The surface energy components of a polymer solid surface (γ_S^+ , γ_S^- , γ_S^{LW}) were determined by contact angle measurements using three probe liquids, one non-polar (methylene iodide) and two polar (ultrapure water and glycerol), with known surface tension (γ_L^+ , γ_L^- , γ_L^{LW}) parameters. As a dispersion-polar approach, the Young's equation is used for each probe solvent that is able to evaluate the three unknown parameters as given in the below equation:

$$(1 + \cos \theta)\gamma_L = 2 \left(\sqrt{\gamma_S^{LW} \gamma_L^{LW}} \right) + \sqrt{\gamma_S^+ \gamma_L^-} + \sqrt{\gamma_S^- \gamma_L^+} \quad (4.9)$$

where θ is the measured contact angle, γ_L is the surface energy of the liquid, γ_S^{LW} , γ_L^{LW} are the Lifshitz-van der Walls components of the substrate and the liquid, respectively and γ_S^+ , γ_L^- , γ_S^- , γ_L^+ are the electron donor and electron acceptor components of the substrate and liquid, respectively.

According to this approach, equation 4.9 can determine the non-polar (LW) components of the surface energy of a substrate or a liquid through the contact angle measurements of three different probe liquids. If the liquids of a known surface tension are used, the γ_L is known and $\cos \theta$ is determined by the contact angle. The values of γ_L^{LW} , γ_L^+ and γ_L^- for the probe liquids were determined from the literature, and the values of γ_S^{LW} , γ_S^+ and γ_S^- for the various polymeric surfaces could be therefore calculated. The most important property of the selected probe liquids is that one liquid is apolar, and the other two liquids are polar.

The three probe solvent of different polarities with known surface energy components^{260, 263}, including ultrapure water, methylene iodide and glycerol were used in this study as shown in Table 4.4.

Table 4.4- Surface tension properties (mJ/m-2) of the three probe liquids

Liquid	γ_{total}	γ_{LW}	γ_{AB}	γ^+	γ^-
Ultrapure water	72.8	21.8	51	25.5	25.5
Methylene iodide	50.8	50.8	0.0	0.0	0.0
Glycerol	64	34	30	3.92	57.4

4.2.3.3 Calculating SFE by dispersion-polar approach

The presented data in Table 4.5 show the results of the surface free energy of the polymers according to the Owens Wendt (dispersion-polar) approach. Equation 4.5 was used to determine the polar and dispersive components of the surface energy of a polymer based on the contact angle measurements of two different liquids. When the liquids of a known surface tension are used, then the γ_L is known, the $\cos\theta$ is determined by the contact angles, and the other parameters γ_S^d and γ_S^p can be calculated. The most important property of the selected probe liquid is that one liquid just has a dispersive component and the other liquid has both dispersive and polar components to find γ_S^d and γ_S^p from this equation.

Table 4.5- Total surface-free energy (γ_{total}) of P(BMA) polymers, its dispersion (γ_S^d) and polar (γ_S^p) components

Polymers	θ water	θ CH ₂ I ₂	Surface-free energy components (mJ/m ²)		
			γ_S^d	γ_S^p	γ_{total}^{d-p}
PnBMA	90.7±2.3	41.5 ± 0.9	38.85	0.9	39.8
HB-PBMA:pyrrole	84.02 ± 0.9	43.4 ± 3.5	37.9	2.8	40.5
HB-PBMA:COOH	77.59 ± 1.9	42.6 ± 3.2	38.2	4.6	42.9
HB-PBMA:1,2-DAE	34.6 ± 1.9	62.5 ± 3.6	27.15	34.7	61.8
HB-PBMA:1,3-DAP	29.4 ± 2.9	69.7 ± 2.7	23.1	40.9	64
HB-PBMA:1,4-DAB	55.4 ± 3.2	49.4 ± 1.1	34.6	17.2	51.9
HB-PBMA:1,6-DAH	67.2 ± 2.7	46.7 ± 3.4	36.1	9.9	46
L-PBMA:COOH	89.2 ± 1.6	43.8 ± 2.9	37.7	1.4	39
L-PBMA:1,2-DAE	73.6 ± 0.7	51.3 ± 2.7	33.6	7.57	41.13
L-PBMA:1,3-DAP	76.4 ± 2.3	50.2 ± 4.1	34.17	6.13	40.31
L-PBMA:1,4DAE	73.2 ± 2.9	50.3 ± 3.2	34.12	7.58	41.70
L-PBMA:1,6-DAH	74.9 ± 2.8	50.9 ± 2.3	33.8	6.9	40.7

These results were calculated from contact angle data according to the “dispersion-polar” approach.

The surface free energy is the sum of the dispersive and polar components, according to OW approach. The results showed that the polymers presented differences in their polar and dispersive components, and this influenced the total surface energies too. It is clear that the polar components increased after the modification of polymers with amines or acids. In highly branched polymers, the dispersive component of functionalised materials coated glass was found to be between 23 to 37 mJ/m², and the polar component was between 3 to 40 mJ/m². The total SFE ranged from 40 to 64 mJ/m² depending mainly on the polar component of the sample. In linear polymers, the dispersive and polar components of materials were found to be similar, ranging from 33 to 37 mJ/m² and from 1 to 7 mJ/m², respectively.

The overall results from the OW approach showed that the different architectures of the same polymer had a substantial effect on the polarity of substances. For example, the polar component of HB-PBMA:COOH was 4.6 mJ/m², while for the L-PBMA-COOH it was 1.4 mJ/m². The branched material presented higher total surface free energy too, in comparison to the linear. Additionally, the amine functional materials have higher polar components. This means that the alkyl amine encourages the polymer surfaces to be more polar due to the inclusion of NH₂ at the end of the polymer chain.

4.2.3.4 Calculating SFE by Lifshitz-van der Waals (acid-base) approach

The total surface free energy of the various polymers, and its components, calculated according to the Lifshitz-van der Waals acid-base (LW/AB) approach, is shown in Table 4.6. This approach also uses contact angle measurements of three-probe liquids; ultrapure water and glycerol as polar liquids and methylene iodide as a non-polar one. Equation 4.9 was used to determine the Lifshitz-van der Waals/non-polar (γ_{SL}^{LW}) and the acid-base/polar W_{SL}^{AB} components of the total surface free energy. It was also used to calculate the electron acceptor (γ^+) and electron donor (γ^-). The parameters of γ_L^{LW} , γ_L^+ and γ_L^- for the probe liquids were obtained from the literature (see Table 4.4).

Table 4.6- Total surface-free energy (γ_{total}) of poly (n-butyl methacrylate) polymers, its polar (γ_S^{AB}) and non-polar (γ_S^{LW}) components, electron donor (γ_S^-) and electron acceptor (γ_S^+)

Polymers	θ water	θ CH2I2	θ glycerol	Surface-free energy components (mJ/m ²)				
				γ_S^{LW}	γ_S^+	γ_S^-	γ_S^{AB}	γ_{total}^{AB-LW}
PnBMA	90.7 ± 2.3	41.5 ± 0.9	75.6 ± 2.3	38.85	0.02	1.42	0.40	39.2
HB-PBMA:pyrrole	84.02 ± 0.9	43.4 ± 3.5	69.5 ± 3.6	37.9	0.3	3.1	1.8	39.7
HB-PBMA:COOH	77.59 ± 1.9	42.6 ± 3.2	65.2 ± 2.5	38.2	0.4	5.9	2.9	41.2
HB-PBMA:1,2-DAE	34.6 ± 1.9	62.5 ± 3.6	32.2 ± 1.7	27.15	4.8	37.7	26.9	54
HB-PBMA:1,3-DAP	29.4 ± 2.9	69.7 ± 2.7	25.3 ± 2.6	23.1	7.2	40.4	34.2	57.3
HB-PBMA:1,4-DAB	55.4 ± 3.2	49.4 ± 1.1	55.3 ± 1.8	34.6	0.6	25.9	7.9	42.5
HB-PBMA:1,6-DAH	67.2 ± 2.7	46.7 ± 3.4	57.4 ± 3.3	36.1	0.9	12.1	6.7	42.9
L-PBMA:COOH	89.2 ± 1.6	43.8 ± 2.9	74.31 ± 2.1	37.7	0.09	1.9	0.8	38.5
L-PBMA:1,2-DAE	73.6 ± 0.7	51.3 ± 2.7	60.8 ± 2.4	33.56	1.2	7.8	6.2	39.7
L-PBMA:1,3-DAP	76.4 ± 2.3	50.2 ± 4.1	63.2 ± 1.7	34.17	0.7	6.7	4.7	39
L-PBMA:1,4DAE	73.2 ± 2.9	50.3 ± 3.2	63.1 ± 2.9	34.12	0.7	9.3	5.2	39.2
L-PBMA:1,6-DAH	74.9 ± 2.8	50.9 ± 2.3	62.8 ± 2.1	33.8	0.9	7.5	5.3	39.1

These results were determined from contact angle data according to Lifshitz-van der Waals acid-base approach

The surface energy is a sum of polar and apolar components of surface tension, according to (LW/AB) approach. The significant differences between polar and non-polar components are clear; the non-polar (LW) components have just one property addressed by a single van der Waals constant and then the non-polar components of the substrate and liquid interfacial free energy follow the geometric mean combining rule, as two different materials interact by dispersion forces^{259, 264}. However, the polar (AB) components of the substrate and liquid interfacial free energy include two non-additive parameters, which are electron acceptor (γ^+) (Lewis acid) and electron donor (γ^-) (Lewis base) parameters.

The results show that the non-polar (γ_S^{LW}) components are greater than the polar (γ_S^{AB}) components and the electron donor (γ^-) is much greater than the electron acceptor (γ^+) components for most polymer coated glass. The Lewis base component tends to dominate the polar surface energies of polymer surfaces. The values of the electron donor are increased in COOH and NH₂ functionalities, which may suggest that modified polymers present a basic

character and Lewis base properties. Comparing the highly branched and linear polymers, the surface energies in HBPs are between 39-57 mJ/m², whereas in LPs are between 38-39 mJ/m². The alteration of the architecture of the polymers clearly provides a unique way of changing the surface properties of the substrate.

The overall results from the LW/AB approach are in agreement with those obtained with the dispersion-polar approach. The increased functionality at the surface of the branched polymers, due to the decreased possibility of chain entanglements, produces surfaces with SFEs that are greater in branched polymers compared to linear polymers. The dispersive values are similar for both approaches. The polar components of SFE determined by the dispersion-polar method are always higher than the polar components calculated from the LW/AB method. Importantly, the two aminated branched polymers with the shorted spacer groups, which are HB-PBMA:1,2-DAE and HB-PBMA:1,3-DAP, presented the highest polar components and total surface energies. Elemental analysis results showed that the concentration of nitrogen in 1,3-DAP and 1,2-DAE were higher than in the other alkyl diamines. The amount of amine added to the HB-PBMA:1,2-DAE and HB-PBMA:1,3-DAP materials (N content of 3.1 and 4.5 % respectively (see Table 3.5) was slightly higher than to the other polymers (N content of 2.9 and 2.4 for HB-PBMA:1,4-DAB and HB-PBMA:1,6-DAH respectively).

4.2.4 Surface morphology and roughness for polymers

Atomic force microscopy (AFM) is a type of microscopy that is used to scan a surface with a sharp probe, for example, a cantilever, to image and analyse materials properties, and biological substrates. AFM is not only able to image the sample topography but also measure materials mechanical properties after indentations at various temperatures²⁶⁴⁻²⁶⁶. Due to its high-resolution AFM is used to visualise the surface topography and measure the elastic modulus (stiffness) of the polymer surface in this study. The purpose of this study was to compare the various polymers surface topography and roughness that may affect the adhesion of cells to new biomaterials, as discussed in Chapter 2.

The topography of polymers coated on glass coverslips was examined by tapping-mode AFM for scan size of 5x5 μm and the results are presented using two-dimensional (2D) and three-dimensional (3D) images of films that were examined at ambient temperatures. Figure 4.5 displays the highly branched polymer surface imaged compared to linear and pure P(BMA) as seen in Figure 4.6. The corresponding roughness values measured using the Igor Pro

software are shown in Figure 4.7. The three branched polymers with pyrrole, carboxylic acid and amine functionality presented smoother topographies than the pure P(BMA). In the case of linear polymer, as seen in Figure 4.6, the amine functional polymer surface presented significantly rougher topographies than the carboxylic end polymers, although the amine surface had lower water contact angle and more wettable surface than the carboxylic one.

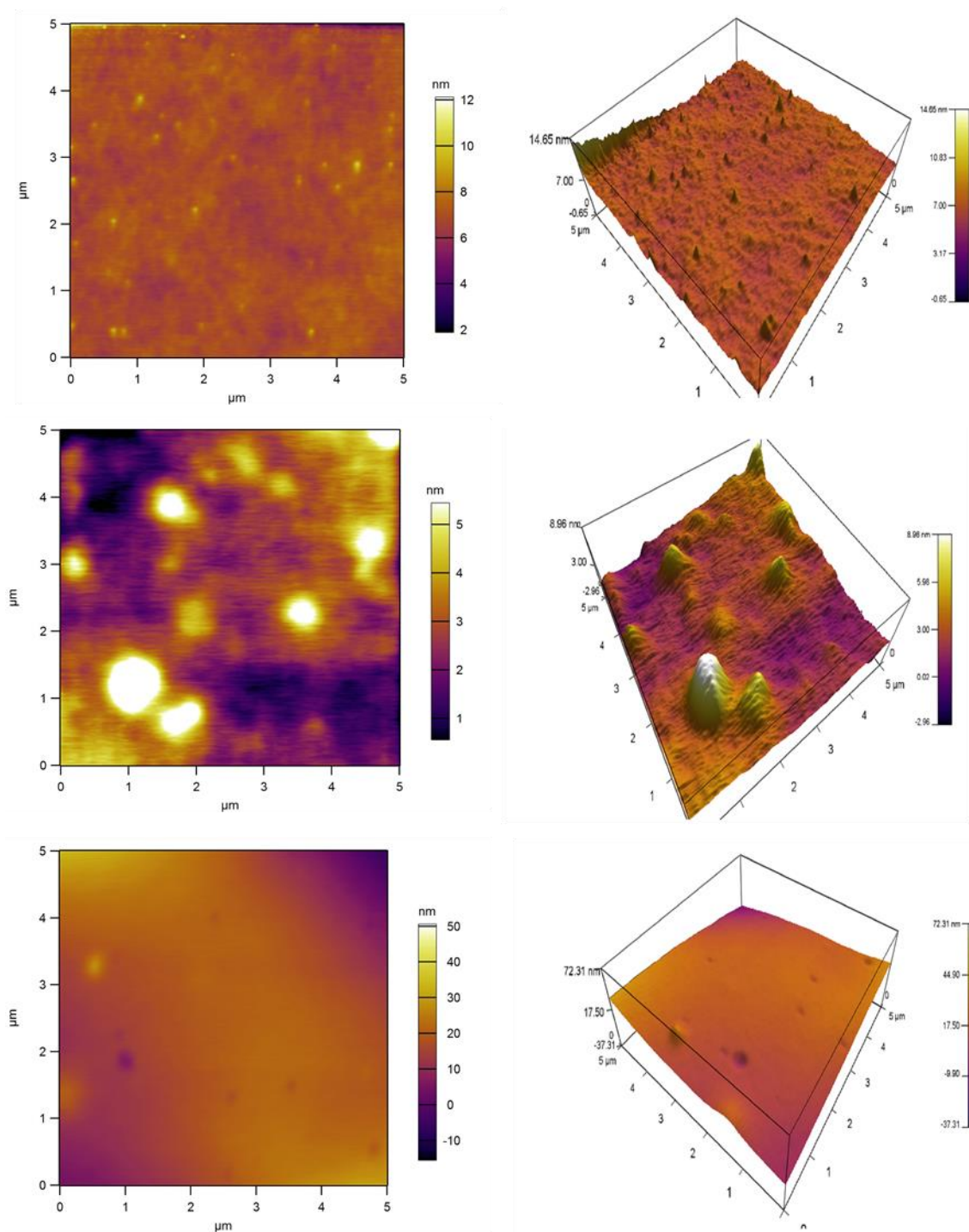


Figure 4.5- AFM height images of (top) HB-PBMA:pyrrole film, (middle) HB-PBMA:COOH film and (bottom) HB-PBMA:1,6DAH film -(scan size 5 μ m x 5 μ m)

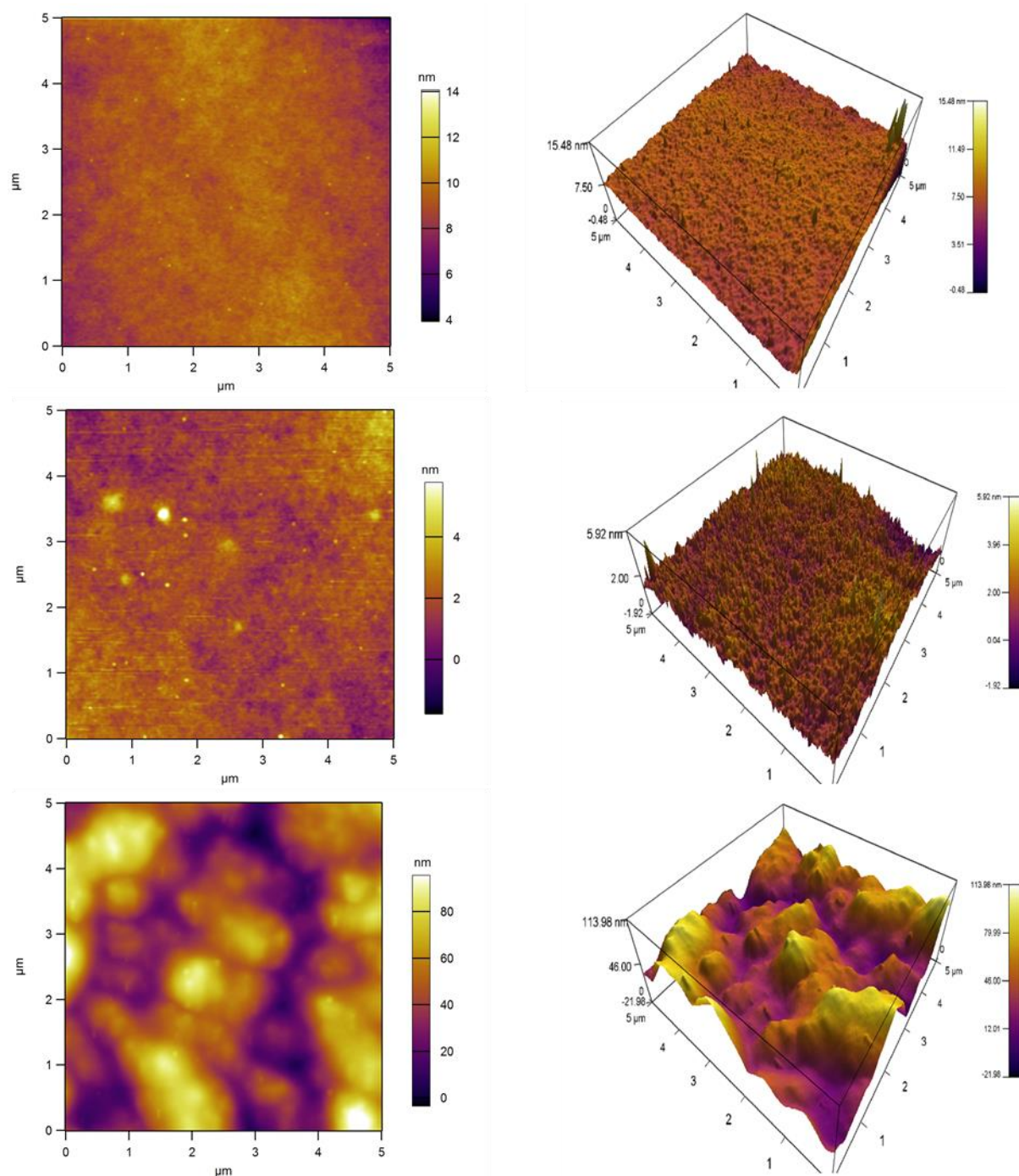


Figure 4.6- AFM height images of (top) pure-PBMA film, (middle) L-PBMA:COOH film and (bottom) L-PBMA:1,6DAH film -(scan size 5 μ m x 5 μ m)

Figure 4.7 shows that the measured average roughness values of the surface of pure P(BMA) was $9.04 \text{ nm} \pm 0.7$ compared to $6.7 \text{ nm} \pm 0.6$, $3.2 \text{ nm} \pm 0.5$ and $3.6 \text{ nm} \pm 0.8$ for branched polymer with pyrrole, carboxylic acid and linear polymer with carboxylic acid, respectively. However, it is surprising that the amine end polymers presented higher roughness values than the other functionalities. The average roughness of amine branched structures was $15.9 \text{ nm} \pm 1.2$ and of amine linear structures $40.8 \text{ nm} \pm 5.07$; although these surfaces showed

lower water contact angles and more wettable surfaces than the other polymers. This observation might be attributed to these materials having a nano-phase separated structure leading to a not tightly packed and uniform surface.

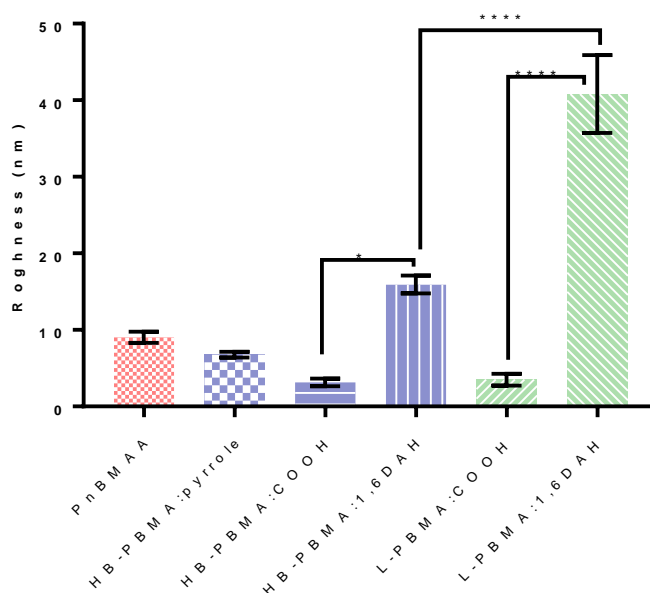


Figure 4.7- The results of roughness values of polymers

Data analysed with one-way analysis of variance (ANOVA) and post-hoc Tukey's analysis. Error bars are the standard error of the mean \pm SEM of three dependent experiments, significance value marked with **** $p < 0.0001$.

4.2.5 Topography and mechanical properties of carboxylic polymers

The morphology of acidic linear and branched PBMA surfaces was examined by tapping-mode AFM for scan size of $5 \times 5 \mu\text{m}$ and the results are presented using two-dimensional (2D) or three-dimensional (3D) images of films that were examined at ambient temperatures, as shown in Figure 4.8.

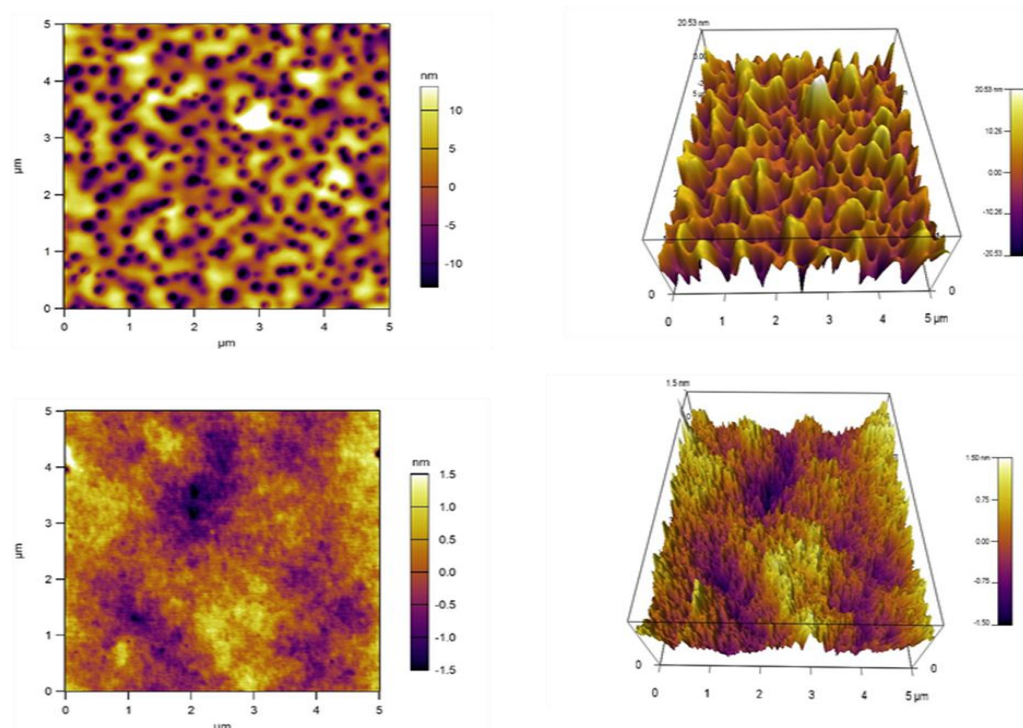


Figure 4.8- AFM height images of (top) L-PBMA:COOH film and (bottom) HB-PBMA:COOH - (scan size $5\mu\text{m} \times 5\mu\text{m}$)

Figure 4.8 shows that the L-PBMA:COOH had a quite rough morphology, but the morphology of the HB-PBMA:COOH had a regularly smooth surface. This could be explained by the different chemical structure of the polymers. The highly branched polymer had lower molecular weight and less intermolecular entanglements than linear polymers, and also the glass transition of linear polymer was higher compared to branched polymer, as well as the wettability and surface energy were higher in branched polymer than linear one.

After imaging a suitable region of interest on each film, the mechanical properties were evaluated through AFM nanoindentation measurements. The elastic moduli data for the polymer films at varying temperatures are shown in Figure 4.9 and tabulated in

Table 4.7. At room temperature the moduli of the polymers were 2.02 ± 1.03 GPa and 1.39 ± 0.07 GPa for linear and branched materials, respectively. The large standard deviation of linear polymer can be attributed to the pit-like surface features that will affect the contact point; however, the deviations decreased with temperature. Furthermore, the amount of indentation measured here is very small (4-5 nm), so even small variations of recorded indentation depth can have a large impact on the measured moduli. In general, both the moduli of the two acidic polymers with different architectures decreased with increasing temperature,

although the highly branched polymer appeared more compliant and its moduli decreased sharper around the T_g around 39 °C.

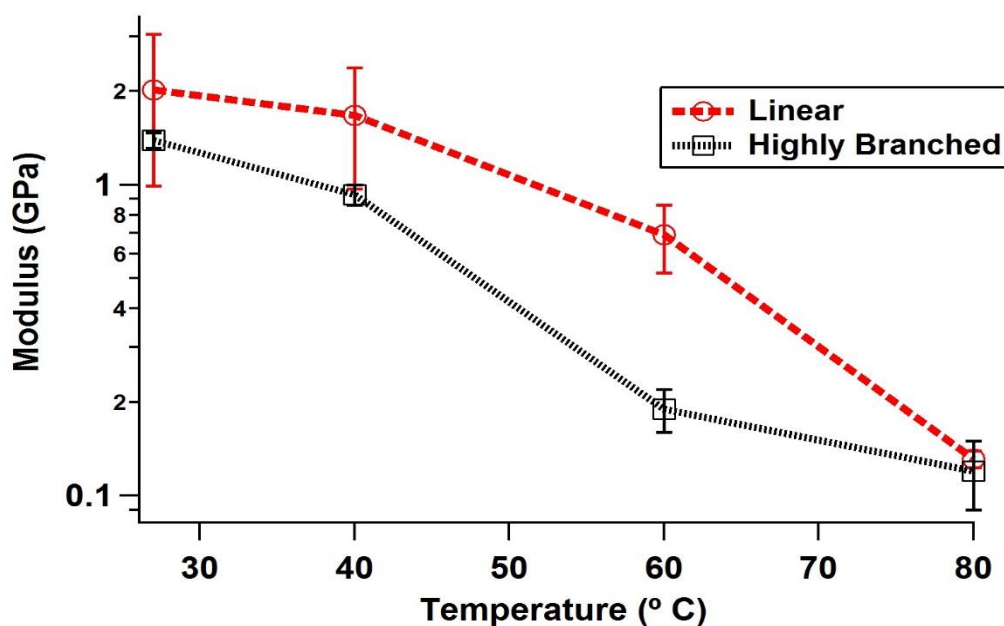


Figure 4.9- Moduli of linear and highly branched polymer films as a function of temperature. Axis logarithmic.

Table 4.7- Elastic modulus of L-PBMA:COOH and HB-PBMA:COOH ± SD at the various temperatures

Temperature (°C)	L-P(BMA-COOH) (GPa)	HB-P(BMA-COOH) (GPa)
Ambient	2.02 ± 1.03	1.39 ± 0.074
40	1.67 ± 0.70	0.93 ± 0.073
60	0.69 ± 0.17	0.19 ± 0.004
80	0.13 ± 0.0082	0.12 ± 0.034

The difference in modulus between linear and branched polymers is best rationalised by considering that the branched polymers are less entangled than the linear polymers in the bulk state. The data indicate the further control of the physical properties that is possible by controlling polymer architecture.

4.3 CONCLUSION

This chapter presented the thermal, physical and mechanical properties of linear and branched poly(*n*-butyl methacrylate) with modified functional groups, compared to homo PnBMA. Thermal properties were analysed by thermogravimetric analysis (TGA) and differential scanning calorimetry (DSC). The surface wettability and surface free energies were determined by contact angle (CA) measurements. The topography and mechanical properties of carboxylic acid functional highly branched and linear polymers were determined by atomic force microscopy (AFM).

The TGA was used for the determination of the highest temperature the polymers can withstand before degradation, which is used for running DSC to obtain the T_g point. The TGA results showed that the thermal degradation process began at different temperatures depending on the copolymerisation method and functional groups compared to the homopolymer PBMA. The degradation temperature of the copolymers was higher than that of the homopolymer because the degradation of homo PnBMA is known to occur predominantly by unzipping from the chain ends to yield monomer. Indeed, the maximum weight loss at 350 °C and 450 °C for both the branched and linear copolymers was similar. Therefore, it can be indicated that the thermal stability of the branched polymers was higher than that of the linear analogues.

The DSC was used for evaluation of the polymers glass transition temperature (T_g). The T_g was obtained from the inflection points of DSC on the second heating cycle. The results showed that, as predicted by the increased free volume required by the branched polymer end groups, the linear polymers have a higher glass transition point compared to the branched polymers. Also, it observed that the T_g increased when the polymers were functionalised with acid groups as the extent of polymer/polymer dipole interactions increased.

Contact angles (CA) were measured on all the polymer coated coverslips, using the sessile drop method, for the evaluation of the materials wettability and surface-free energy. The results showed that amine-terminated polymers had surfaces with increased wettability compared to acid or pyrrole functional groups, and that the architecture significantly affected the wettability. These results demonstrate that the acid or amine functional groups can change the properties of PBMA surfaces from hydrophobic to moderately hydrophilic.

Contact angles of three probe liquids (ultrapure water, methylene iodide and glycerol) were used to calculate the surface energy of all the different polymers. This allowed the calculation of surface energy via two approaches: “dispersion-polar” and “Lifshitz-van der Walls acid-base”, as explained above. The differences were that the calculation of surface energy in the “dispersion-polar” method only depended on dispersive and polar components of the polymer, while in the “Lifshitz-van der Walls acid-base” method more parameters were involved in the calculation of the polymers surface energy; polar, non-polar, electron donor (Lewis acid) and electron acceptor (Lewis base). The main finding was that the highly branched polymer had higher surface free energy and polar character in comparison to the linear one.

Finally, roughness influence on the wetting properties of the various polymer surfaces has been evaluated by Atomic force microscopy (AFM). Polymer coated coverslips were prepared using the same coating method (dip coating) as the one used for the contact angle measurements. The results showed that linear and highly branched polymers with the same functionality did not present significantly different average surface roughness values and therefore the differences observed in the contact angles were due to the differences in the degree of functionality and not because of the differences in the roughness values. When comparing the carboxylic and the amine terminated polymers, the amine terminated ones, both highly branched and linear, presented higher average surface roughness values than the ones with the carboxylic functionality. However, the amine terminated ones presented lower contact angles and higher surface energies than the carboxylic ones, leading again to the conclusion that the chemical functionality was the main driver of the contact angle measurements, rather than the surface roughness. AFM was also used to compare the differences in the mechanical properties of carboxylic acid functional highly branched and linear polymers at ambient temperature, while their stiffness was examined at various temperatures. Using the spin coating method on silicon, the topography of the highly branched polymers was smoother than that of the linear ones, and therefore can be estimated that the average surface roughness was higher for the linear polymers. The coating method can therefore significantly affect the polymers topography and roughness values. That is why the dip coating method was used for the evaluation of the roughness values, as this was the method used for the preparation of the substrates for contact angle measurements and cell adhesion studies. In terms of the polymers mechanical properties, there were significant differences in stiffness between the two-carboxylic acid functionalised polymers; linear and highly branched, and the stiffness was experimentally higher in the case of the linear compared to the highly branched polymers.

Thus, optimising the polymer architectures would be a useful strategy to design the surface properties, which are often a key aspect of biocompatibility, for selected polymers.

4.4 EXPERIMENTAL

4.4.1 Thermal gravimetric analysis

The thermal gravimetric analysis instrument used in the thermal analysis was a Q500 TGA instrument under a nitrogen atmosphere. The samples with a weight of 5–7 mg, were heated from room temperature to 500 °C at a rate of 10 °C/min. Each sample was placed into a platinum pan attached to a microbalance assembly. The computer software program TA Universal Analysis for the apparatus plotted and analysed the thermal analysis curves.

4.4.2 Differential scanning calorimetry

Differential scanning calorimetry was conducted on a Q250 DSC instrument under nitrogen atmosphere. The samples with weight in the range 5 to 8 mg were placed in aluminium pans in the cell. DSC was performed from -30 to 150 °C at a heating rate of 10 °C per minute. Measurements were first taken from -30-150 °C heating at 10 °C/min, then they were cooled back to -30 at a rate of 5 °C/min, and finally they were reheated back to 150 °C at a rate of 10 °C/min.

4.4.3 Contact angle measurements and Surface free energy determination

The wettability of the polymers was determined by measuring the contact angles of three probe liquids with different polarities; ultrapure water, methylene iodide and glycerol, on polymer coated glass coverslips as described in section 5.5.7. Measurements were made at room temperature and ambient humidity using the sessile drop technique²⁶⁰. The deposition of 2 µl droplets on each substrate was recorded using a VCA-Optima system and the contact angles were measured using the ImageJ software. Each measurement was taken at least three times and averaged.

4.4.4 Atomic force microscopy

Polymer samples were prepared at 5mg/ml concentration and transferred to cleaned glass coverslips by dip coating to examine the morphology of the polymer surfaces and estimate their average surface roughness. The surface topographical images of the polymer coated coverslips were obtained using tapping Atomic force microscopy (AFM) and the Igor Pro software. In particular, AFM was carried out using the MFP-3D AFM from Asylum Research (Santa Barbara, CA) and silicon nitride cantilever probes (Applied Nanostructures, Santa Clara, CA, USA) with a nominal tip radius of 15 nm and spring constant of approximately 0.3 N/m.

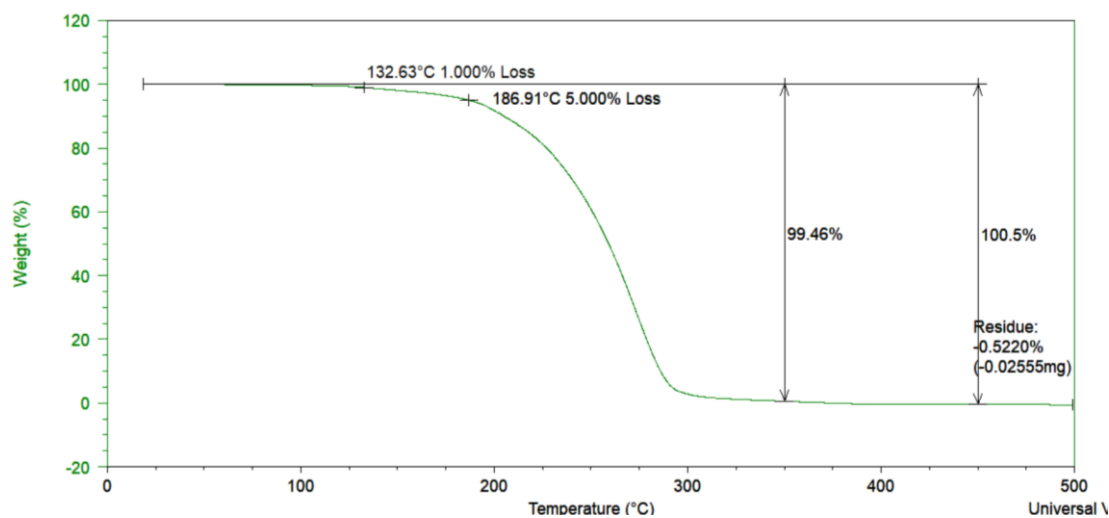
The Igor Pro software was used for the real-time control, the data acquisition, as well as for the offline analysis and the data manipulation. Following laser alignment, calibration of the detector sensitivity and the cantilever spring constant using the thermal method was made²⁶⁵. Imaging was carried out at ambient temperature. The polymers film were examined at three different locations, images were saved and the average roughness was determined for each polymer film based on these images from the three different locations.

Polymer samples were also prepared at 100 mg/ml concentration and transferred (100 μ l) to cleaned silicon wafers via spin coating to study the mechanical properties of carboxylic terminated polymers. AFM was again carried out using the MFP-3D AFM from Asylum Research (Santa Barbara, CA) and silicon nitride cantilever probes (Applied Nanostructures, Santa Clara, CA, USA) with a nominal tip radius of 15 nm and spring constant of approximately 0.3 N/m. The Igor Pro software was used for the real-time control, the data acquisition, as well as for the offline analysis and the data manipulation. Following laser alignment, calibration of the detector sensitivity and the cantilever spring constant using the thermal method was made²⁶⁵. Imaging was carried out at temperatures ranging between 27 to 80 °C, using a BioHeater stage, with either tapping or contact mode. Force volume measurements were made in organized arrays (50 \times 50) of indentations at a piezo velocity of 2 μ m/s and at temperatures ranging between 27 to 80 °C, using the BioHeater stage. The elastic modulus was estimated using a linear elastic Hertzian-based theory for a conical indenter²⁶⁵⁻²⁶⁶.

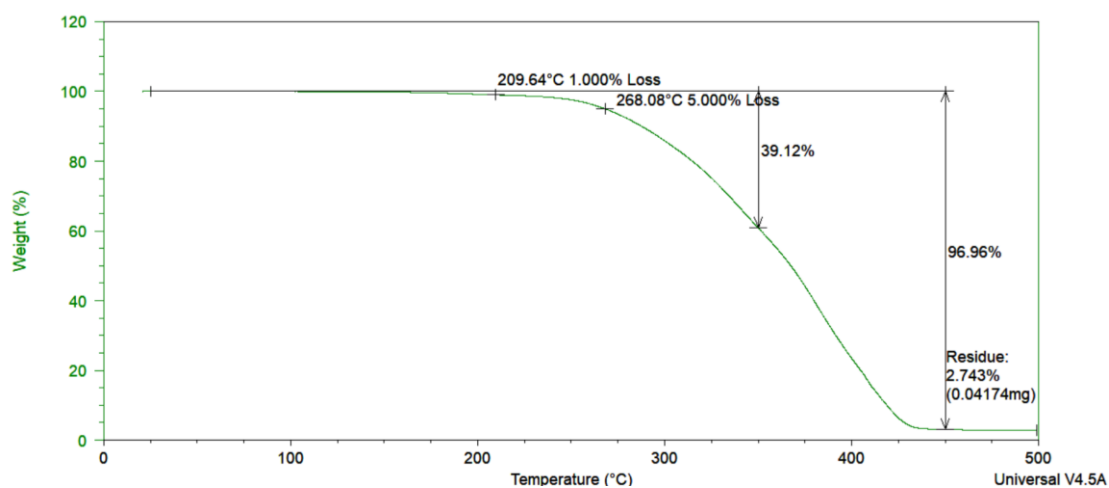
$$F = \frac{2}{\pi} \left(\frac{E}{1-\nu^2} \right) \delta^2 \tan \alpha \quad (4.10)$$

where ν is Poisson's ratio and is assigned a value of 0.5 (i.e. incompressible), δ is the indentation depth and α is the half cone angle of the probe (36°).

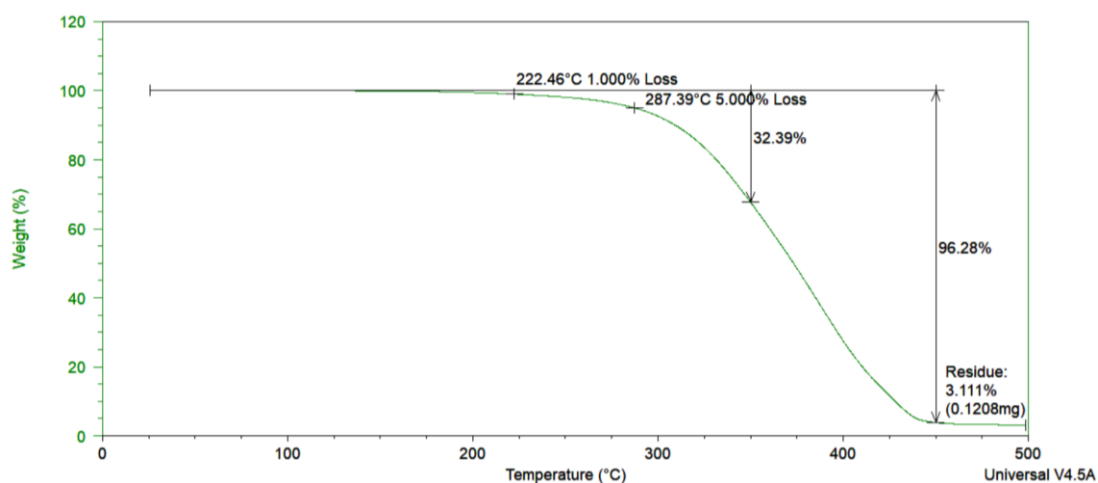
4.5 APPENDIXES



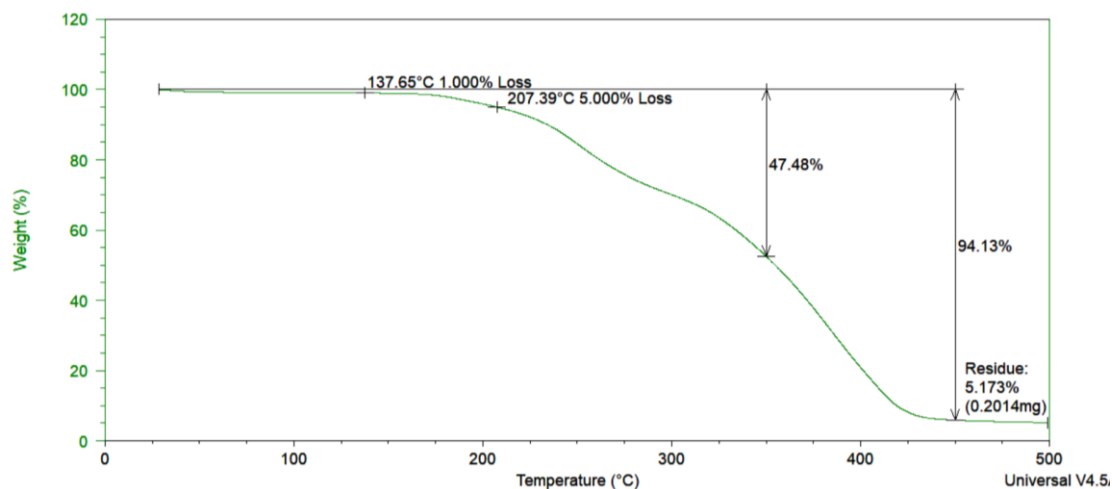
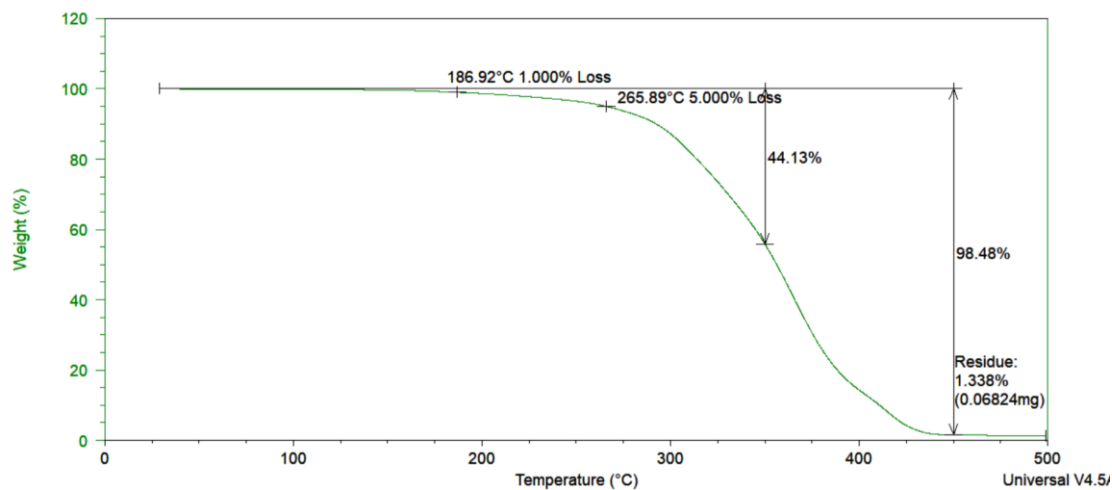
Appendix 4.1- The results analysis of TGA for pure PnBMA



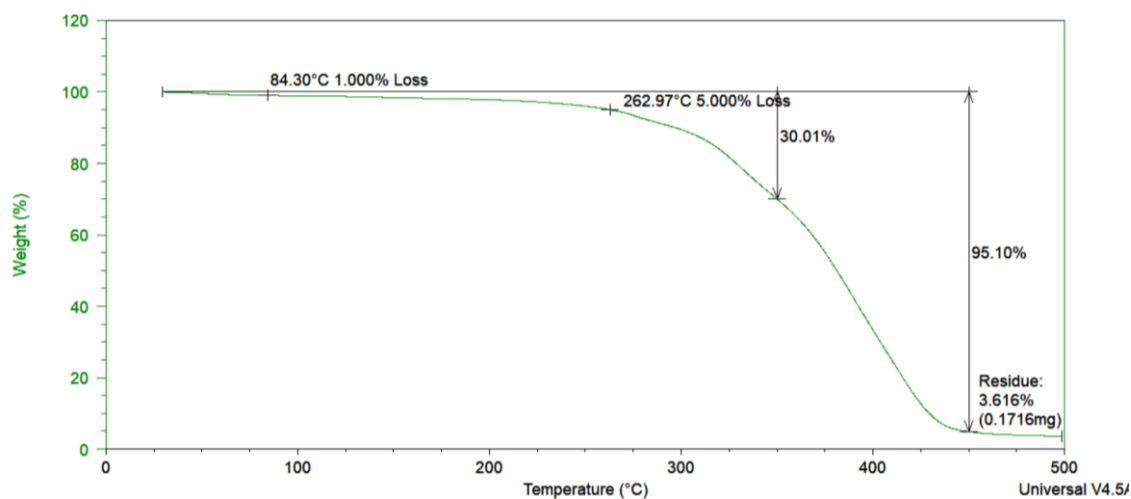
Appendix 4.2- The results analysis of TGA for HB-PBMA:pyrrole (16:1)

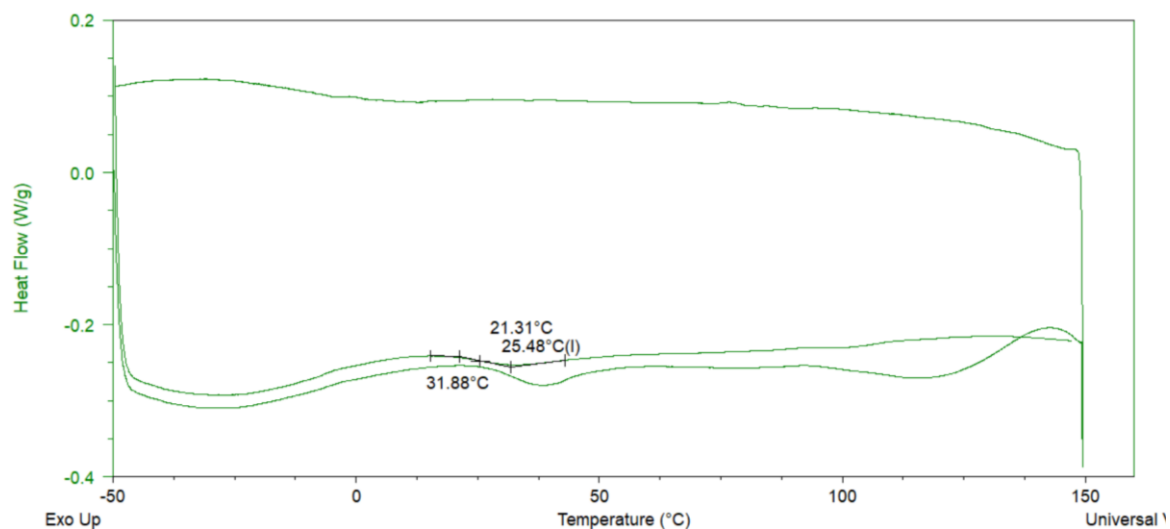


Appendix 4.3- The results analysis of TGA for HB-PBMA:COOH (16:1)

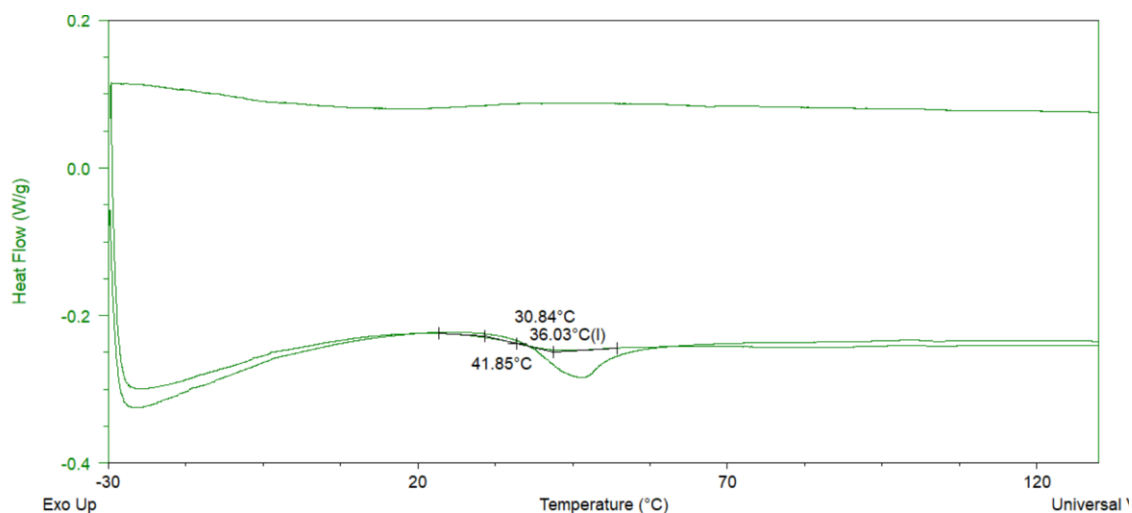
Appendix 4.4- The results analysis of TGA for HB-PBMA:NH₂ (1,6DAH)

Appendix 4.5- The results analysis of TGA for L-PBMA:COOH (16:1)

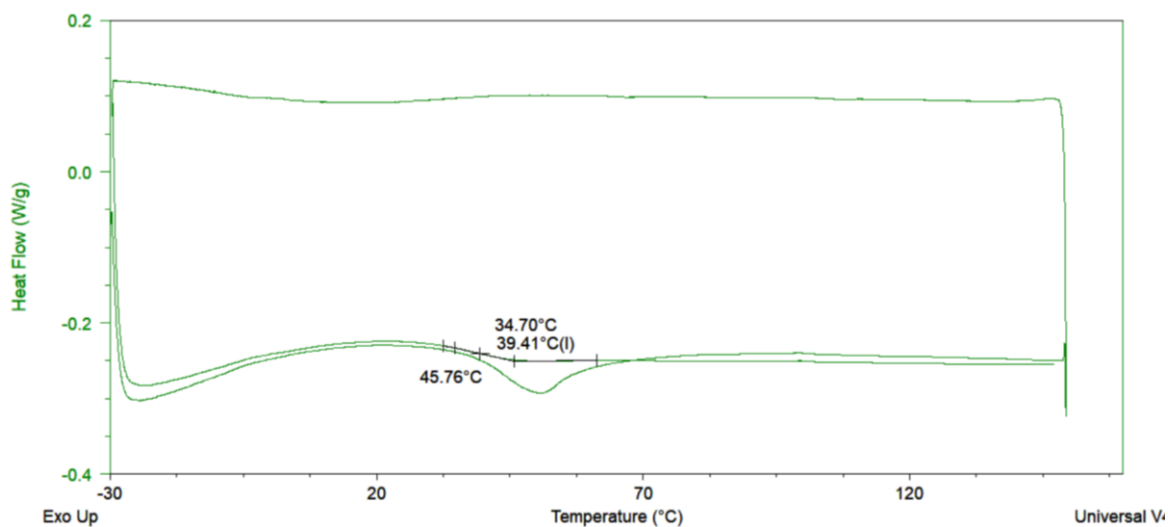
Appendix 4.6- The results analysis of TGA for L-PBMA:NH₂ (1,6DAH)



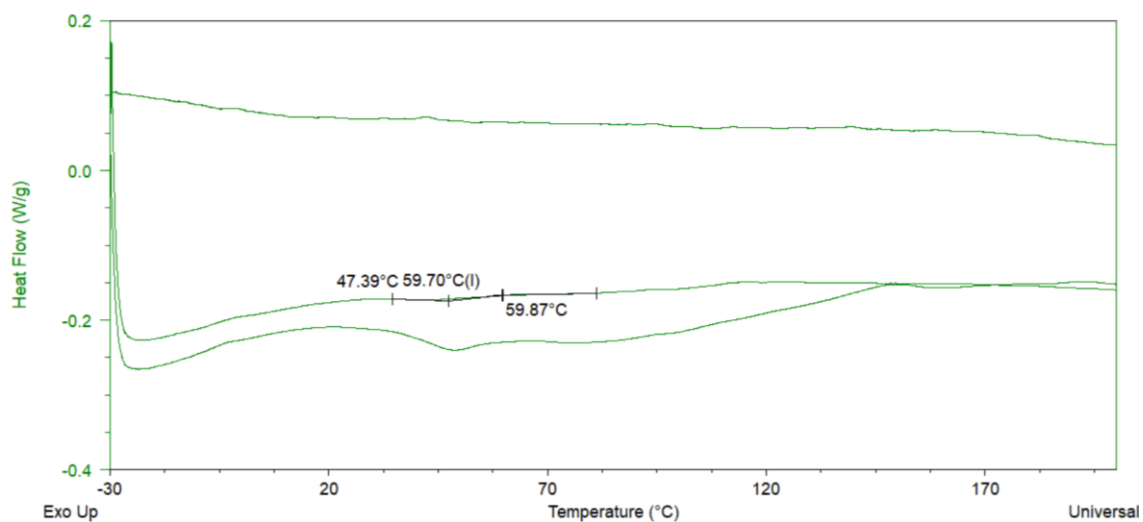
Appendix 4.7- The results analysis of DSC for pure PnBMA



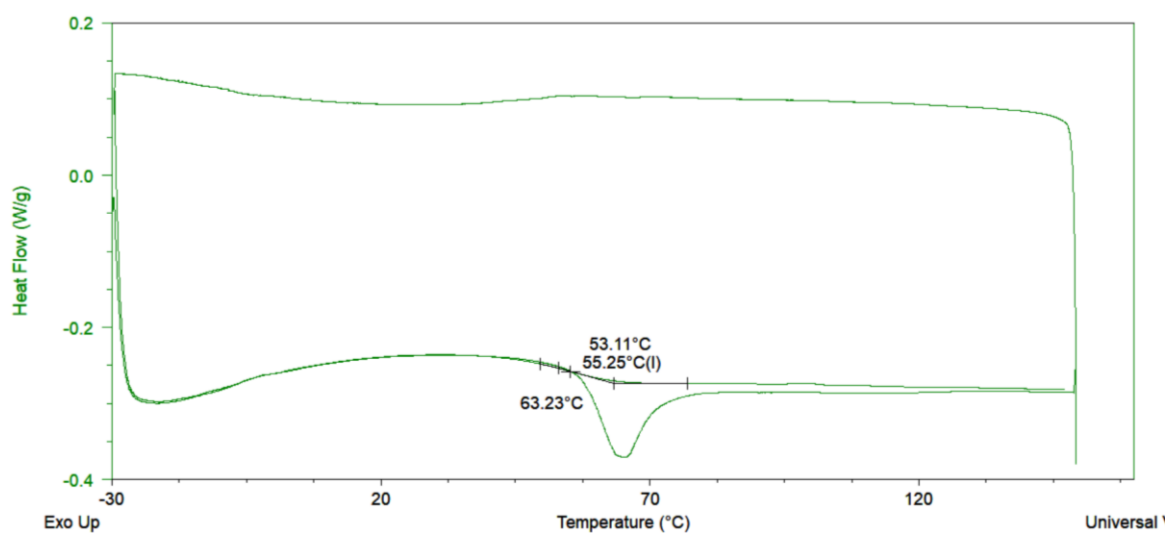
Appendix 4.8- The results analysis of DSC for HB-PBMA:pyrrole (16:1)



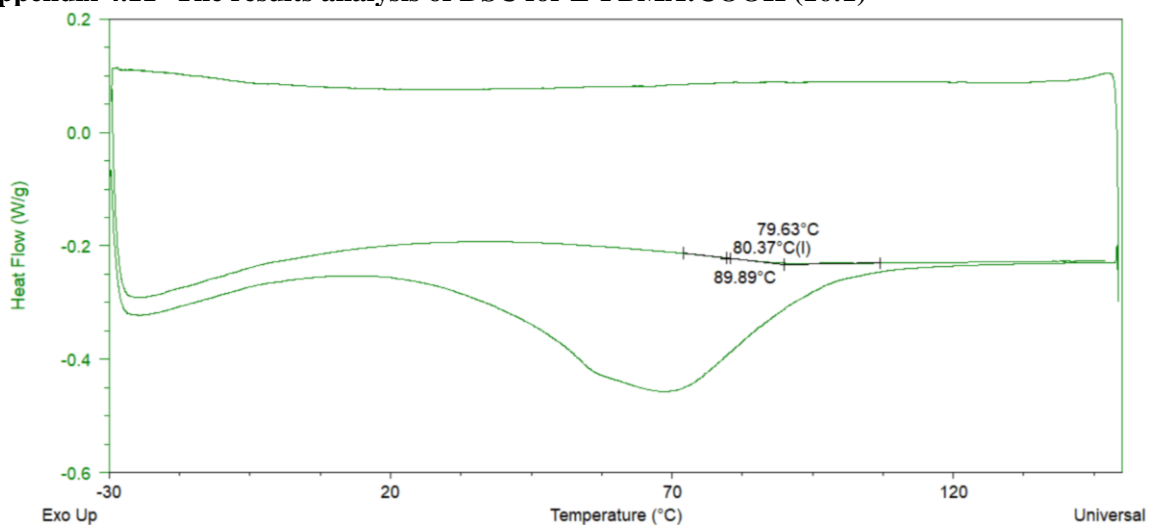
Appendix 4.9- The results analysis of DSC for HB-PBMA:COOH (16:1)



Appendix 4.10- The results analysis of DSC for HB-PBMA:NH₂ (1,6DAH)



Appendix 4.11- The results analysis of DSC for L-PBMA:COOH (16:1)



Appendix 4.12- The results analysis of DSC for L-PBMA:NH₂ (1,6DAH)

5 CHAPTER FIVE: STUDIES OF CELL/BIOMATERIAL INTERACTION OF HUMAN CELLS WITH POLY (BUTYL METHACRYLATE)S

5.1 INTRODUCTION

Biomaterial methacrylate-based polymers, been used in biomedical applications for many years. For example, the poly(hydroxyethyl methacrylate) (PHEMA) hydrogel, as a hydrophilic polymer, has been used as an artificial support materials in rat corneas²⁶⁷ as well as being used in soft contact lenses for many years. Furthermore, poly(methyl methacrylate) (PMMA) has been previously used for the fixation of orthopaedic joint replacements as bone cement. Preclinical studies published by Thomson *et al.* analysed the biocompatibility of four different commercial particles of PMMA and its impact on cellular function and inflammatory response. Salient features of their study revealed the inflammatory potential of four bone cements in human synovial fibroblast, while *in vivo* studies showed the compatibility of all four bone cements in the mouse knee²⁶⁸.

Another application of methacrylate-based polymer has been reported for drug delivery systems. Langer *et al.* showed the use of copolymer nanoparticles of MMA and sulfopropylmethacrylate (SPMA) as carriers for the topical ophthalmic application of the muscarinic agonists arecaidine propargyl ester (APE) and (S)-(C)-aceclidine hydrobromide drugs. Based on their results, the copolymer nanoparticles did not elicit inflammatory response in the rabbit eye²⁶⁹.

Further, Rimmer *et al.* reported the application of PMMA hydrogels as cell culture substrates, although synthetic hydrogels are generally non-cell adhesive materials. This was achieved by modifying hydrogels with hydrophobic or hydrophilic units. Based on their results, the modification of 2,3-propanediol-1-methacrylate with a hydrophobic unit such as lauryl methacrylate significantly increased the adhesion of human dermal fibroblast cells in comparison with a hydrophilic unit such as sulphonic acid or methacrylic acid. In addition, the modified 2,3-propanediol-1-methacrylate network with hydrophilic units such as the alkyl amine series can serve as a biomaterial for both monoculture of bovine keratocytes or human corneal epithelial cells as well as their co-culture²⁷⁰. Later work by Hassan *et al.* showed that these substrates favoured the adhesion and growth of these epithelial cells¹² in comparison to the keratocytes²⁷⁰; indicating that co-culture in this system provided no advantages in the development of the epithelial cells.

The development of effective biomaterials as a substrate for cell culture research finds diverse applications in the biological and clinical settings. To ensure success, these materials must exhibit low cytotoxicity and promote cell adhesion, hence the initial step in evaluating the biocompatibility of biological materials is to study their cytotoxicity *in vitro*.

Polymers with aminated functionality have been shown to selectively support epithelia cell proliferation and adhesion. To date this system has been mainly on a swollen network (hydrogel) format but a system that provides for coating of devices would be useful in situations where developing an epithelium could improve biocompatibility. The purpose of this section was to examine the cytocompatibility of the poly(butyl methacrylate) PBMA coatings (a widely used polymer in the surface coating technologies) functionalised with primary amines. Also, the feasibility of using these coating to support the development of an epithelium was examined. Several epithelial cells are available commercially; both transformed and primary cells. Two epithelial cell-types were chosen. The A549 carcinoma line is a well-studied highly robust cell type that can be easily cultured to high passage using standard culture medium. Primary renal epithelial cells could be used in the future in the preparation of a bio-synthetic kidney. However, they are much more difficult to culture in our hands, they require special media and their culture is sensitive to seeding density. The performance of these two cell types are then compared to a non-epithelial cell type; primary dermal fibroblasts. The development of these cells was used because in previous work it was shown that aminated hydrogels supported corneal epithelial cell proliferation but fibroblast cells. It is, however, accepted that several other strategies could be used and there may be some advantage in using a range of cells from similar tissues.

The aim of this chapter was to test a cell culture study hypothesis, namely that primary alkyl amine functional polymers may mimic the local extracellular matrix (ECM), thereby facilitating a conducive environment for epithelial cells to adhere on and grow. To test the hypothesis, the synthesised polymer materials selected from chapter 3, as shown in Figure 5.1, were examined in direct contact with different types of human cells (epithelial and fibroblast cells). The work aimed to study the effects of polymer architectures and functionalities on cell adhesion and spreading. The evaluation of the biocompatibility or safety of the polymer material in this research was based on three assessments: metabolic activity of cells, cell number determination, and cell cytotoxicity. The AlamarBlue[®] assay was used to measure metabolic activity, while cell numbers and DNA quantification were measured via the

PicoGreen assay. Cell toxicity was measured via the LDH assay. Further, DAPI and TRITC-phalloidin staining was used to visualise the localisation of the nucleus and actin filaments, respectively, within the cells. These methodologies were performed after culturing human renal epithelial (HREp), human dermal fibroblast (HDF), and human carcinoma lung epithelial (A549) cells on polymer coated materials.

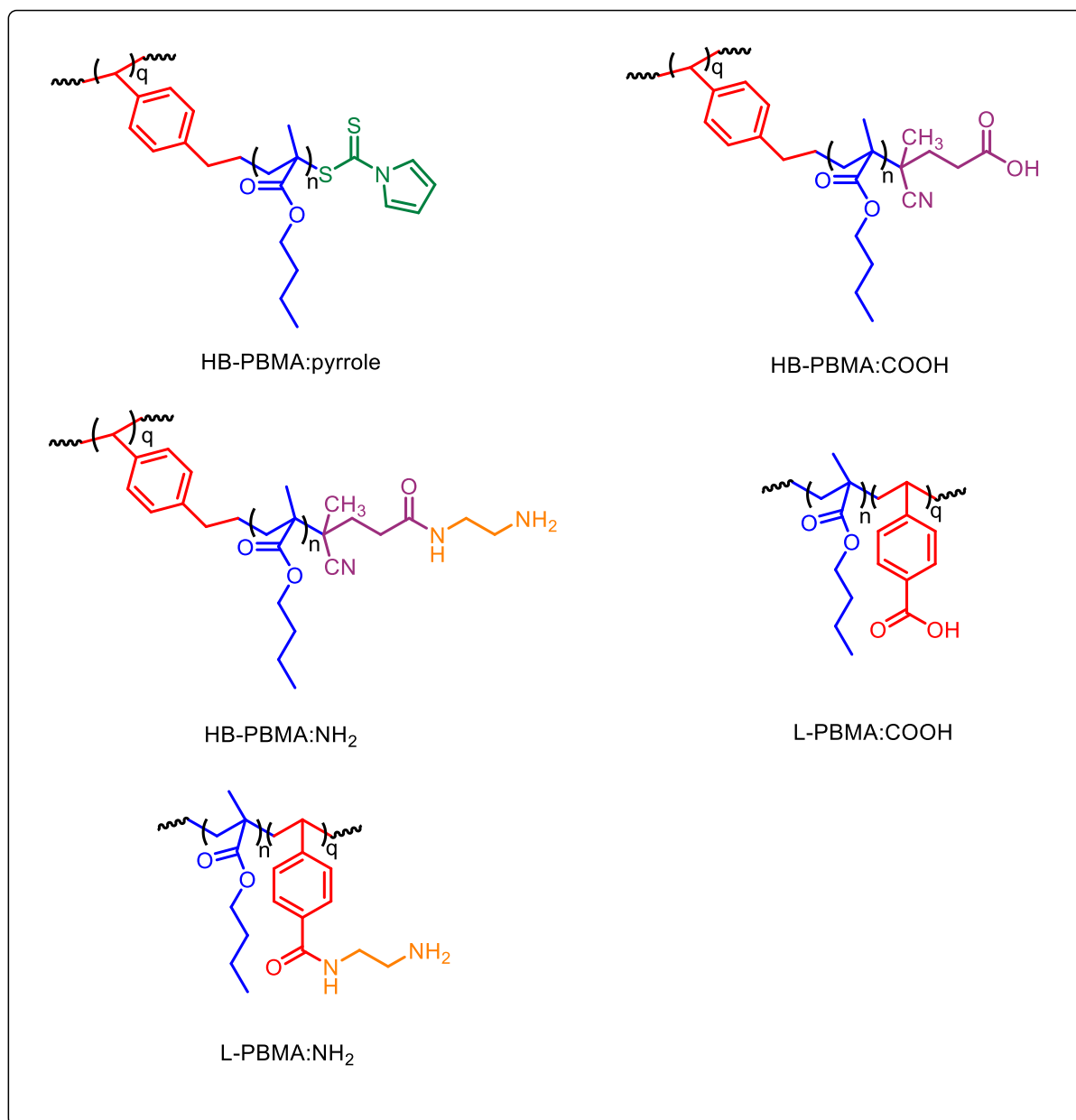


Figure 5.1- Structures of the different architectures and functionalities of poly (n-butyl methacrylate), which are used as the substrates for cell adhesion

5.2 RESULTS

5.2.1 Cell viability assay

To evaluate the metabolic functionality of viable cells grown on polymers, the AlamarBlue assay was used. When AlamarBlue (AB) was added to cell cultures, the oxidized form of the AB enters the cytosol and is converted to the reduced form by mitochondrial enzyme activity, as facilitated by accepting electrons from NADPH, FADH, FMNH, and NADH, as well as from the cytochromes. This redox reaction is accompanied by a shift in colour of the culture medium from indigo blue to fluorescent pink, which can be easily measured by colourimetric or fluorometric reading²⁷¹⁻²⁷². In this research, the AB assay revealed the metabolism of different human cells in direct contact with poly(butyl methacrylate) with different functionalities and architectures compared to tissue culture plastic (TCP), which was used as a control with an absorbance at 570 nm and a 620 nm background. These polymers are highly branched (with pyrrole, acid, and amine ends) and linear (with acid and amine ends), and the human cells are human renal epithelial cells (HREpCs), normal human dermal fibroblast cells (HDFCs), as well as human carcinoma lung epithelial cells (A549). Before testing, the polymers were used to coat sterilised coverslips and placed in 12 well plates, after which the cells were counted via a haemocytometer and seeded at a 1×10^4 cells/ml density on the coated material and allowed to adhere. The cells were then incubated for 72 hours prior to undergoing biocompatibility testing or staining. A culture period of 72 hours was used in order to determine any toxic effects at longer timeframes, which are considered appropriate to coatings that are expected to be present *in vivo*. Often in the literatures 48 hours is used as a culture but in some work much shorter periods, sometimes as short as 24 hours is used. Further work will require different timeframes but here 72 hours was selected as a medium-term time point at which toxic effects would become apparent. The renal epithelial cells in particular require moderate time periods for proliferation.

Figure 5.2 shows that the culturing HREpCs on highly branched polymers with pyrrole ends showed no significant reduction in metabolic activity, compared to on the TCP control ($p = 0.0633$) but there was an apparent decrease in viability. These cells cultured on branched polymers with an acidic functionality significantly ($p < 0.0001$) decreased their viability. A further and substantial significant decrease was observed with cells cultured on amine-terminated branched polymers with the shorter alkyl groups (1,2-DAE and 1,3-DAP). Cellular viability was unaltered with cells cultured on 1,6-DAH end polymer compared to the pyrrole ended polymer and although there was an apparent decrease compared to TCP the difference

was not significant ($p = 0.2923$). On the other hand, 1,4-DAB functionalised polymer gave a lower value than TCP ($p < 0.001$) but this substrate provided much higher viabilities than the 1,2-DAE and 1,3-DAP functionalised.

The linear polymers behaved differently to the branched polymers. There was a significant decrease in viability on the COOH-functional polymers ($p < 0.0001$) and the substantial decrease in viability observed on the branched 1,2-DAE and 1,3-DAP materials was not observed when compared to the COOH-functional polymers. Interestingly, polymers containing 1,2-DAE, 1,3-DAP, 1,4-DAB and 1,6-DAH functionality provided increased cell viability compared to linear COOH-functional polymer and although there was an apparent difference between the viability of the cells on these coatings compared to TCP the difference compared to 1,2-DAE, 1,4-DAB and 1,6-DAH was not significant ($p = 0.1469$, 0.1113 and 0.7554), respectively.

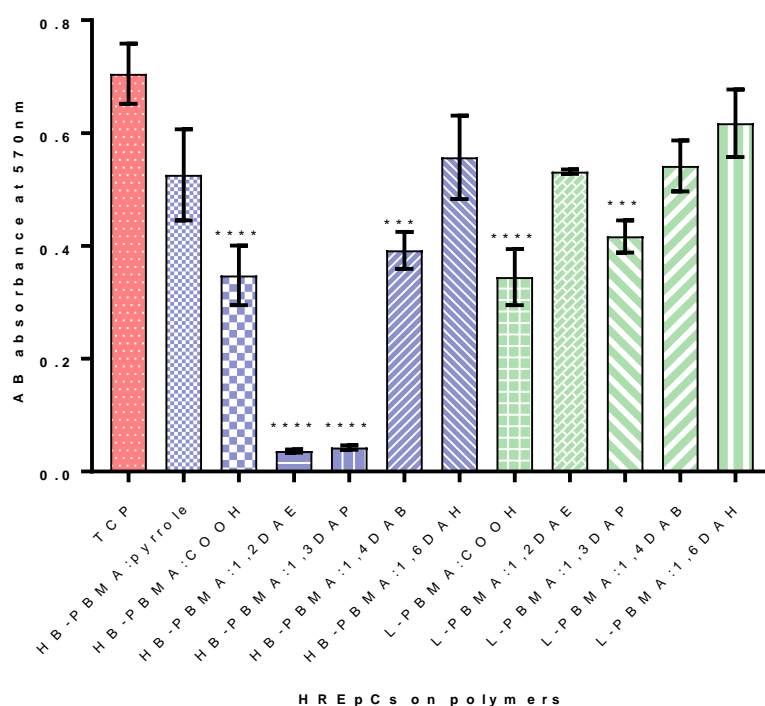


Figure 5.2- Results of AlamarBlue assay for HREp cells on poly(butyl methacrylate)s with different functionalities and architectures

Data analysed with one-way analysis of variance (ANOVA) and Bonferroni post-hoc test. Error bars are the standard error of the mean \pm SEM of three dependent experiments, significance is relative to the TCP control *** $p < 0.001$ and **** $p < 0.0001$

Figure 5.3 indicates that the similar results were observed when A549 cells were cultured on the same coatings. Both the pyrrole and COOH-functional branched polymers provided reduced viability, but the difference was not significant ($p = 0.5842$ and 0.1602), respectively. As observed with the HREp cells the branched polymers with 1,2-DAE and 1,3-DAP functionality were poor substrates for culture ($p < 0.0001$). The branched polymers with 1,4-DAB and 1,6-DAH functionality provided improved substrates but the viability was still significantly ($p < 0.05$) reduced compared to TCP. The linear polymers behaved very differently, and cells cultured on each of these had similar viability to those on TCP regardless of functionality.

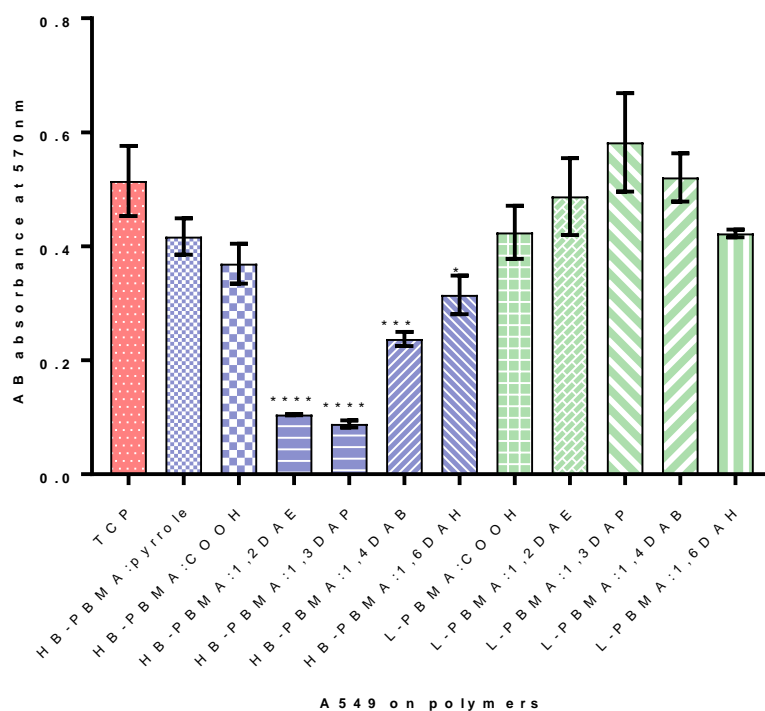


Figure 5.3- Results of AlamarBlue assay for A549 cells on poly(butyl methacrylate)s with different functionalities and architectures

Data analysed with one-way analysis of variance (ANOVA) and Bonferroni post-hoc test. Error bars are the standard error of the mean \pm SEM of three dependent experiments, significance is relative to the TCP control * $p < 0.05$, *** $p < 0.001$ and **** $p < 0.0001$

Figure 5.4 shows that the HDF cells behaved very differently compared to the two epithelial cell types. These cells had increased cell viability compared to TCP when cultured on acidic terminated polymers and the increase was significant on the linear polymer ($p < 0.005$). In contrast to the behaviour of the epithelial cells of all the amine functional polymers did not support the HDFs and this was seen as significant ($p < 0.0001$) decreases compared to TCP.

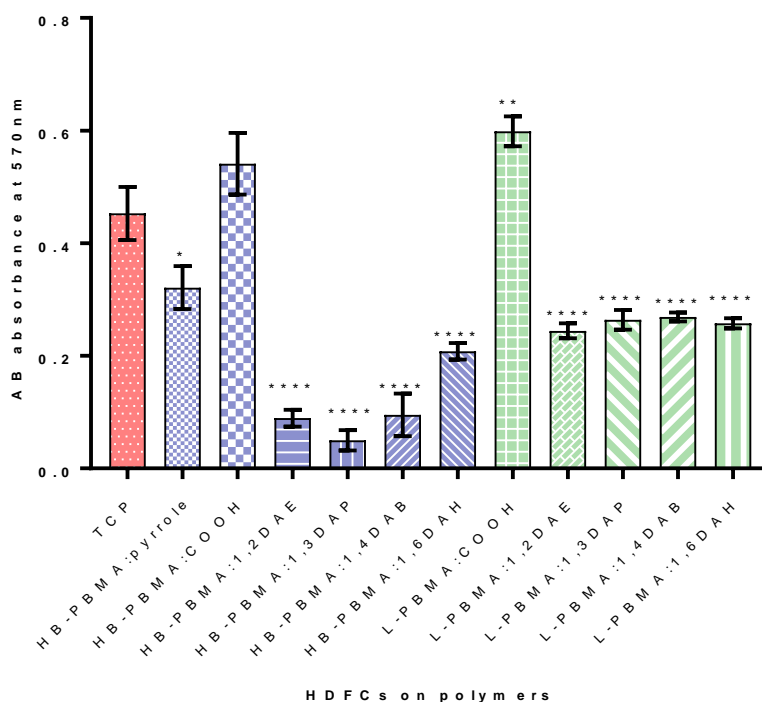


Figure 5.4- Results of AlamarBlue assay for HDF cells on poly(butyl methacrylate)s with different functionalities and architectures

Data analysed with one-way analysis of variance (ANOVA) and Bonferroni post-hoc test. Error bars are the standard error of the mean \pm SEM of three dependent experiments, significance is relative to the TCP control * $p < 0.05$, ** $p < 0.005$ and **** $p < 0.0001$

5.2.2 Determination number of cells

The cell numbers were quantified by using the PicoGreenTM assay of to determine total cellular DNA. The PicoGreen (PG) is a double-stranded (dsDNA) fluorochrome, which provides an accurate measure of cell DNA according to its insensitivity to single stranded DNA (ssDNA) and to other contaminants, as well as a high sensitivity to low levels of dsDNA²⁷³. Since actively dividing cells synthesizes new DNA, the PicoGreen assay can be used to measure cellular DNA and allow for the determination of the number of cells. To determine DNA concentration in cells, a calibration curve was generated using a DNA standard at known concentration. The cell number was quantified by generation of three different standard curves depending on cell type via fluorescence reading against a known number of cells, as described in the experimental section. The goal of this study was to confirm that the increase in cell number was parallel to the increase in metabolic activity as measured via Alamar Blue assay. All three types of cells (HREp, HDF, and A549) were seeded into 12 well plates coated with polymers and TCP and incubated for three days with 5% CO₂ at 37 °C.

Figure 5.5 shows that the total DNA content and the cell number of HREp cells on the polymer coatings. The highly branched polymer with the pyrrole terminus appeared to be a good substrate for cell adhesion. However, both branched and linear polymers with COOH functionality gave a lower number of cells and DNA with a significant reduction ($p < 0.0001$) compared to the control. This result was consistent to that observed with the Alamar Blue assay. Further, the data assessing the numbers of cells on the amine functional polymers supported that obtained also by the Alamar Blue assay. Thus, there was a large and significant reduction in cell number observed on the branched polymers with 1,2-DAE and 1,3-DAP functionality but on 1,4-DAB and 1,6-DAH functional polymers cell numbers, although significantly reduced ($p < 0.001$) and ($p < 0.005$) respectively, approached the values observed on the TCP control. On the linear polymers the HREp cells grown on the 1,6-DAH and 1,4-DAB polymers showed no significant reduction in cell number ($p = 0.1680$ and 0.0713) or in DNA content ($p = 0.9999$ and 0.9958), respectively. Also, as in the Alamar Blue data there was a small but significant reduction ($p < 0.05$) on the 1,2-DAE 1,3-DAP functional linear polymer substrates.

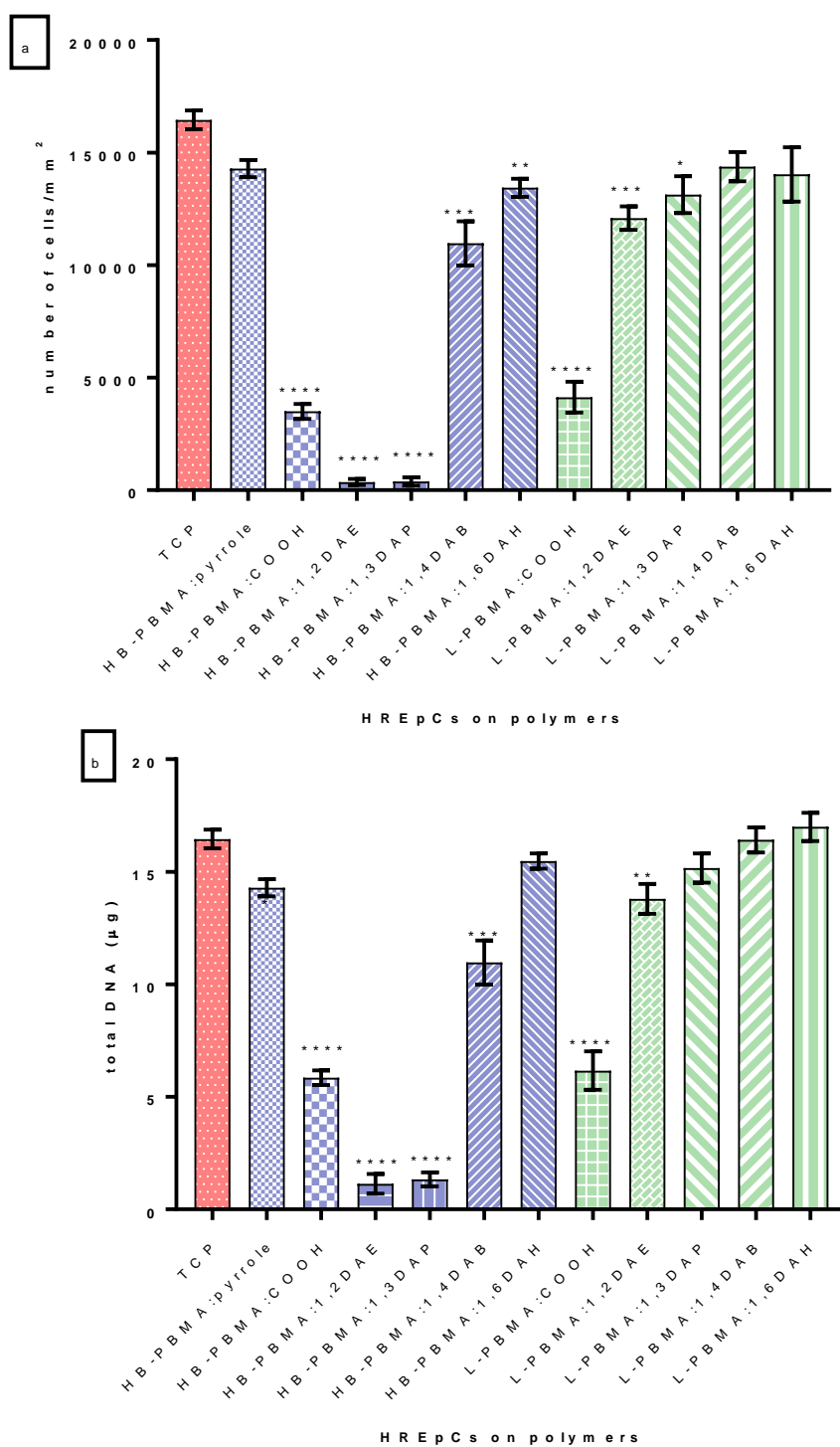


Figure 5.5- PicoGreen results for HREpCs after incubation on PBMA with different functionalities and architectures (a) number of cells (b) quantity of DNA

Data analysed with one-way analysis of variance (ANOVA) and Bonferroni procedure. Error bars are the standard error of the mean \pm SEM of three dependent experiments, significance is relative to the TCP control * $p < 0.05$, ** $p < 0.005$, *** $p < 0.001$ and **** $p < 0.0001$

Figure 5.6 shows that the similar to AlamarBlue results, a cell-specific variable effect on cell metabolism was observed on A549 cells grown on synthesised polymers. Culturing A549 cells on highly branched polymers showed a differential effect on DNA content and the number of cells. Except for acidic and pyrrole functionality, other aminated highly branched polymers showed a significant reduction in DNA content cell number of this cell line. As in the previous data the branched polymers with 1,2-DAE and 1,3-DAP functionality were much poorer substrates for culture than the polymers with 1,4-DAB or 16 DAH functionalities. However, the number of cells on these latter polymers was reduced. As in the Alamar Blue data the linear polymers performed well a cell substrate and the data from the polymer with 1,4-DAB functionality provided an increase compared to TCP, which was significant ($p < 0.001$).

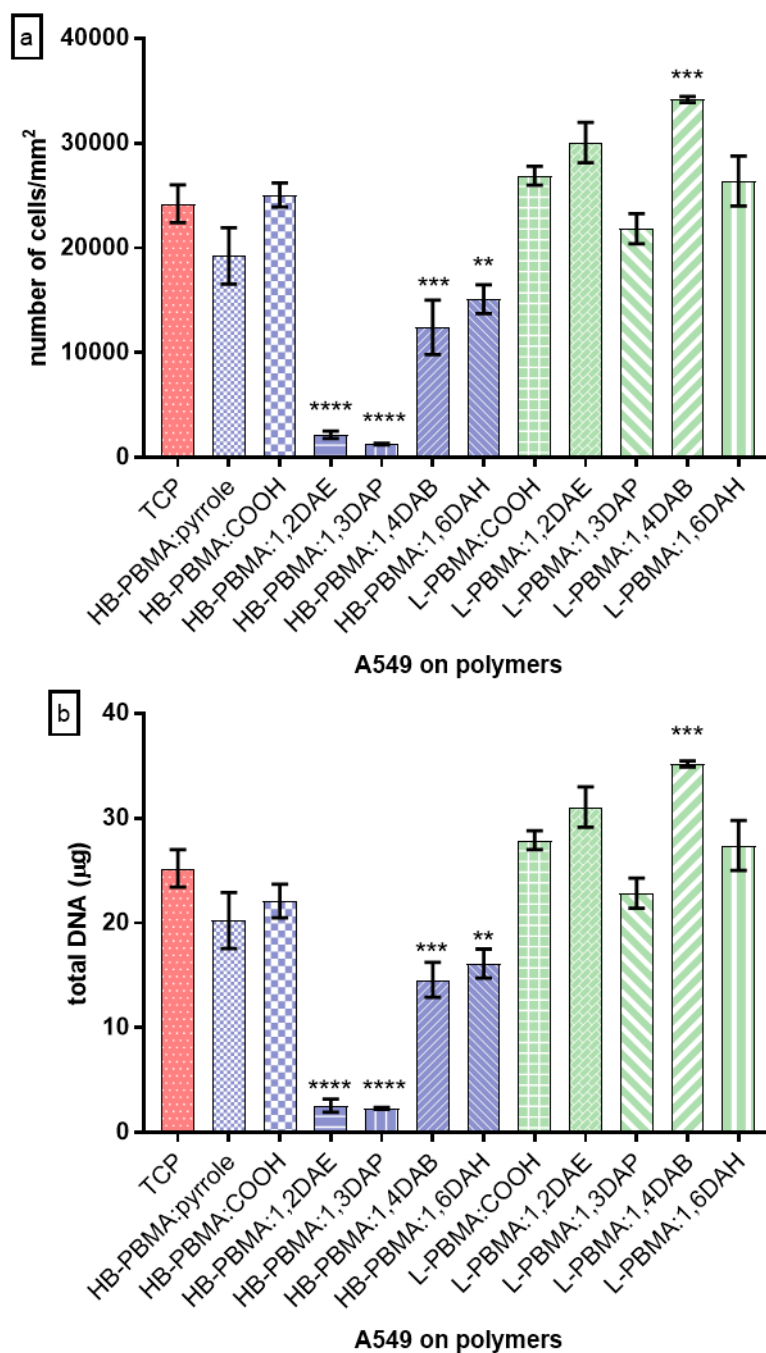


Figure 5.6- PicoGreen results for A549 cells after incubation on P(BMA) with different functionalities and architectures (a) total number of DNA (b) number of cells

Data analysed with one-way analysis of variance (ANOVA) and Bonferroni producer. Error bars are the standard error of the mean \pm SEM of three dependent experiments, significance is relative to the TCP control ** $p < 0.005$, *** $p < 0.001$ and **** $p < 0.0001$.

Figure 5.7 shows that the PicoGreen data confirmed the results of the Alamar Blue assay in culturing HDF cells. Interestingly, both sets of data indicated that both the branched and linear polymer with COOH functionality produced an improved substrate for the culture of HDFs; the number of cells present after 72 hours culture was increased significantly ($p < 0.0001$) compared to TCP. On the other hand, all of the aminated branched polymers showed a large and significant reduction ($p < 0.0001$) in DNA content and cell number of HDFCs. For this cell type there was no effect of architecture.

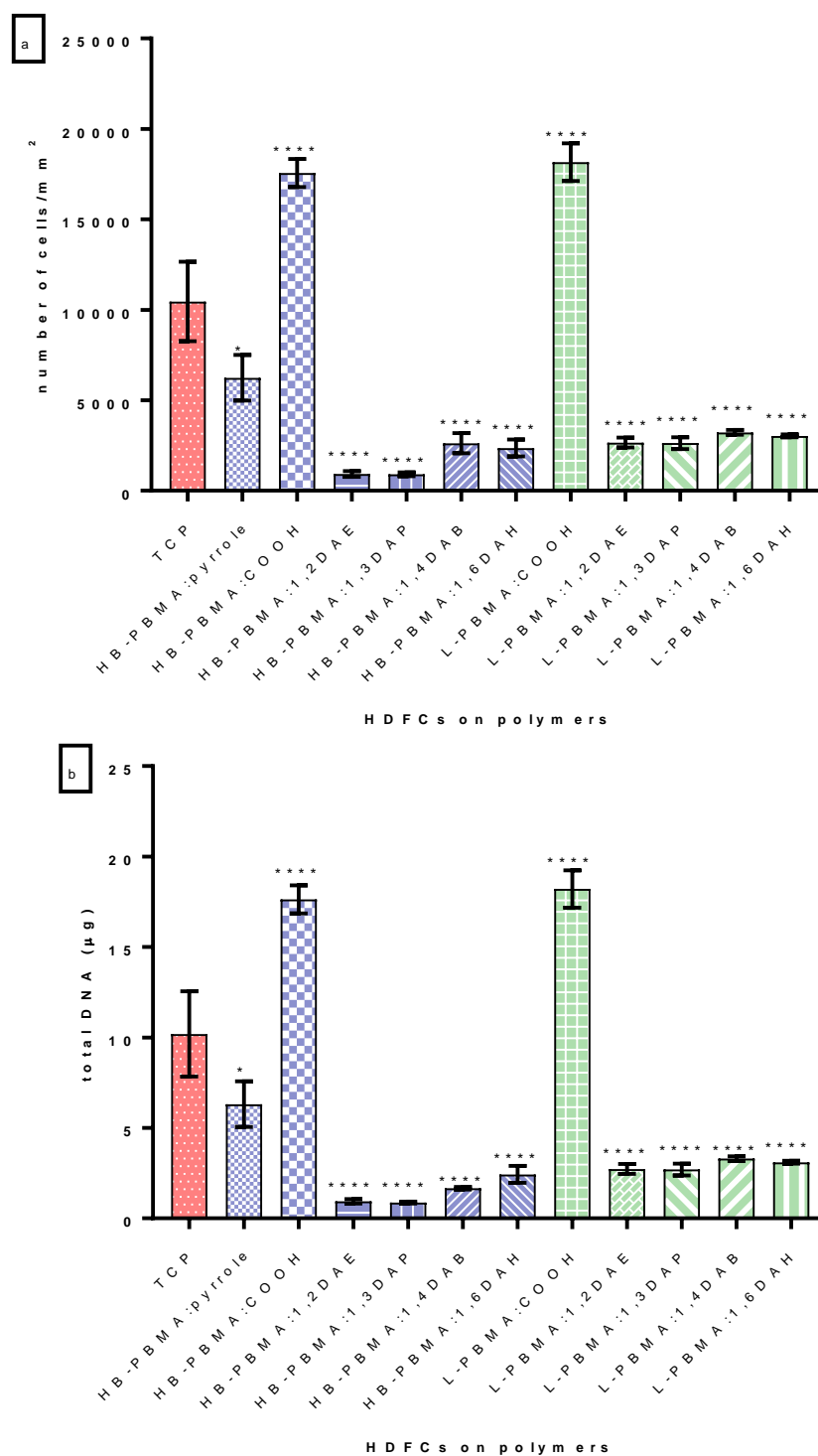


Figure 5.7- PicoGreen results for HDFCs after incubation on P(BMA) with different functionalities and architectures (a) number of cells (b) quantity of DNA

Data analysed with one-way analysis of variance (ANOVA) and Bonferroni producer. Error bars are the standard error of the mean \pm SEM of three dependent experiments, significance is relative to the TCP control * $p < 0.05$ and **** $p < 0.0001$

5.2.3 Cytotoxicity assay

Analysing the effects of cell growth cytotoxicity or cell death has been an important factor in biological research, especially in the investigation of new materials. The quantification of plasma membrane damage was evaluated using the release cytosolic enzyme lactate dehydrogenase (LDH) since it has a potential site for interaction of cationic macromolecules in the cell membrane²⁷⁴⁻²⁷⁵. LDH is widely used in cytotoxicity studies to provide information on the effects of biomaterials after incubation. The aim of this study was to confirm that the results of LDH release assay were correlated to Alamar Blue and PicoGreen assays. Cytotoxicity is defined as the fraction of LDH produced compared to the maximum possible following full lysis of the cells (see experimental for full details). As with the previous cellular assays, LDH assay was performed by seeding 1×10^4 cells in 12 well plates in direct contact with different polymer substrates. Additionally, the same number of cells were seeded on TCP to determine the cytotoxicity as per the manufacture's protocol. Further details of this method are provided in the experimental section. Three different types of cells (HREp, HDF, A549) with various different polymer materials were compared to TCP as the control to determine the toxicity percentage of cells when exposed to polymer materials.

Figure 5.8 shows that the LDH cytotoxicity assay of HREp cells on the polymer coating as the substrate compared to TCP. The results revealed that no cytotoxic effects due to the polymers were observed on HREpCs, with the exception of the HB-PBMA:1,2-DAE and HB-PBMA:1,3-DAP highly branched polymers contributing a 40% significant increase in cytotoxicity ($p < 0.0001$) compared to the TCP control.

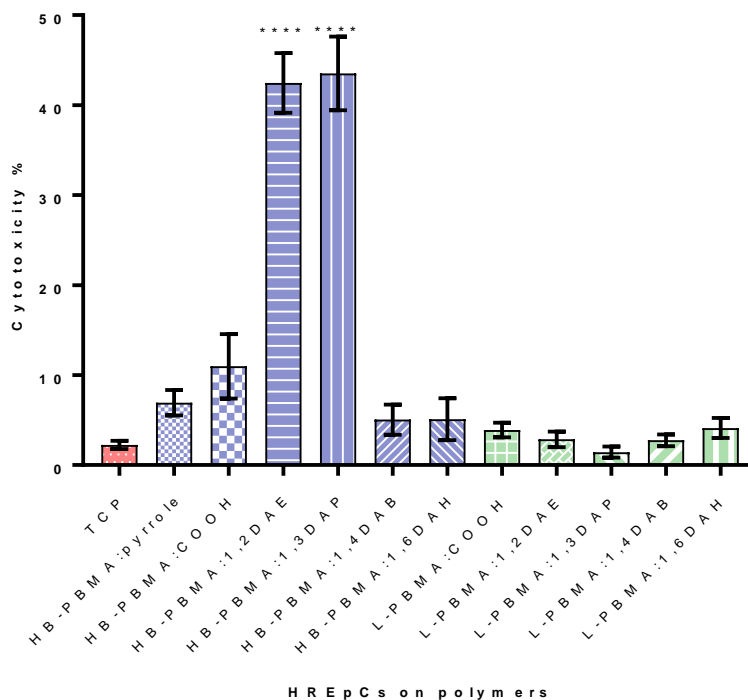


Figure 5.8- The percentage of cytotoxicity from the LDH assay in HREp cells after exposure to different polymer materials for 72 hours

Data analysed with one-way analysis of variance (ANOVA) and Bonferroni producer. Error bars are the standard error of the mean \pm SEM of three dependent experiments, significance is relative to the TCP control **** $P < 0.0001$.

The results of assessing the A549 damage to the cell membranes showed variable effects on different polymer substrates as seen in Figure 5.9. As in the previous data the branched 1,2-DAE and 1,3-DAP terminated polymers gave the highest values of toxicity and there were no significant differences between the pyrrole or COOH functional branched polymers. However, the other amine functional polymers did provide some small indications of cell lysis.

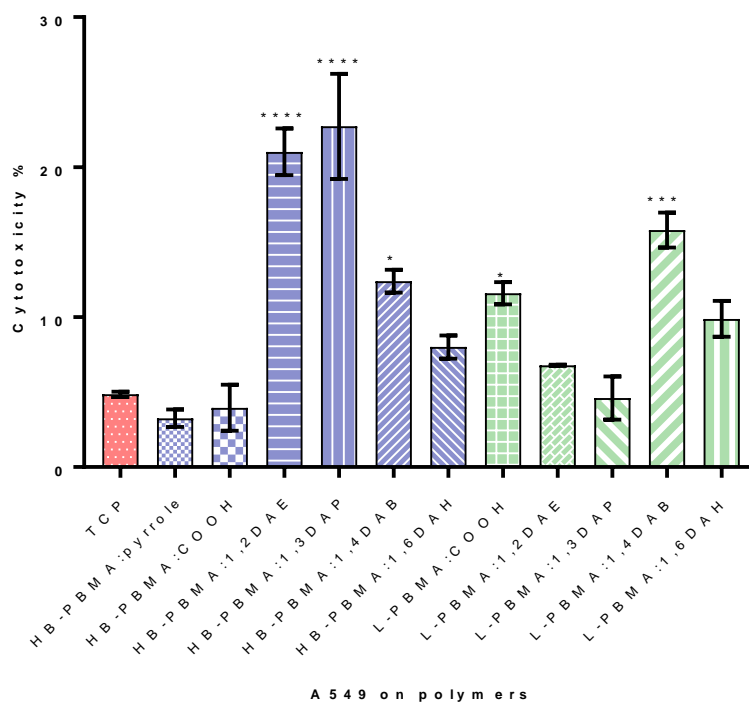


Figure 5.9- The percentage of cytotoxicity from the LDH assay in A549 cells after exposure to different polymer materials for 72 hours

Data analysed with one-way analysis of variance (ANOVA) and Bonferroni post-hoc test. Error bars are the standard error of the mean \pm SEM of three dependent experiments, significance is relative to the TCP control * $p < 0.05$, *** $p < 0.001$ and **** $p < 0.0001$.

Figure 5.10 shows that the LDH release detected in HDFCs cultured on different polymer substrates were not significantly different from the control, except for the highly branched 1,2-DAE and 1,3-DAP terminated polymers as they had more than 40% toxicity. In control cells which were on the TCP without polymer, the release of the enzyme was detected to be 19%, which is significantly higher. The reason for this might be due to the increasing absorbance at 490 nm in the cell culture media that contain phenol red or a high level of serum²⁷⁶.

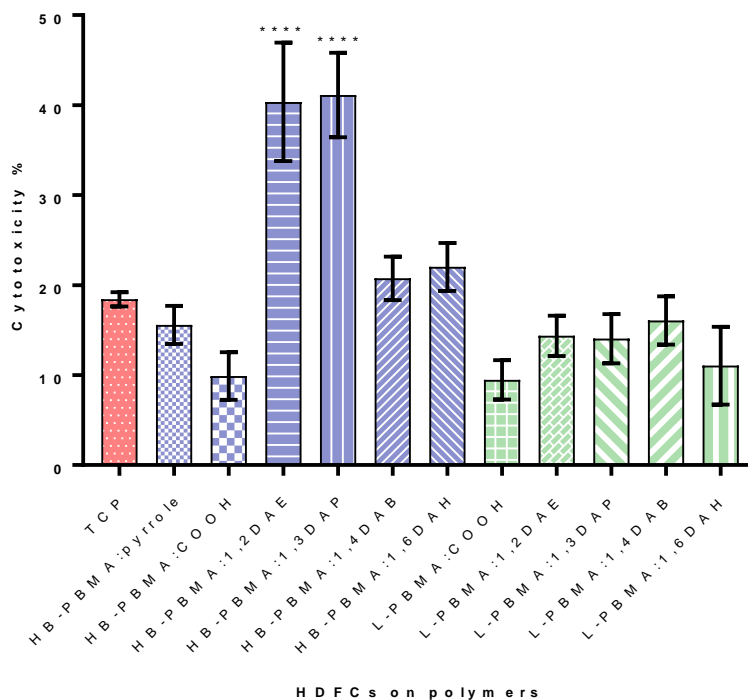


Figure 5.10- The percentage of cytotoxicity from the LDH assay in HDF cells after exposure to different polymer materials for 72 hours

Data analysed with one-way analysis of variance (ANOVA) and Bonferroni producer. Error bars are the standard error of the mean \pm SEM of three dependent experiments, significance is relative to the TCP control **** $p < 0.0001$

5.2.4 Immunofluorescence

The morphological features of the cells were investigated using fluorescence microscopy to further examine the performance of the polymer substrates and TCP. The structure of the cells was examined by staining the actin filaments (also called microfilaments) and the nucleus of the cells. TRITC (tetramethylrhodamine-5,6-isothiocyanate)-phalloidin is a red fluorescent stain that binds to actin filaments in cells, while DAPI (4',6-diamidion-2-phenylindole) is a blue fluorescent stain that binds to their nuclei. The actin filaments are frequently abundant beneath the plasma membrane, and they provide cell shape and movement through the formation of a network (called actin stress fibres), thereby enabling cells to migrate and divide. They consist of globular actin (G-actin) subunits and have the appearance of a double standard helix with a distinct polarity called a barbed (plus) end and pointed (minus) end. This polarity gives the orientation of all actin monomers allowing them to move in the same direction ²⁷⁷. The adhesion and spreading of cells includes the organisation of the cytoskeleton and formation of focal adhesions (integrins). The integrins are bound to ECM components on one side, and

to actin stress fibres on the other. The force on one side causes a reaction on the other, and this, together with integrin signalling pathways, determines the cell shape²⁷⁸. In this study, each type of cell was cultured and incubated on the coating materials for 72 hours, fixed, stained and then imaged to see the effects of morphological changes on the shape of the cytoskeleton and the nucleus. Further details of this procedure are given in the experimental section.

Fluorescence micrographs recorded for HREp cells 72 hours post-cell seeding on different polymer and control surfaces can be seen in Figure 5.11. Adhesion and cell growth were observed on all surfaces, except for the highly branched with 1,2-DAE and 1,3-DAP polymers and the data support the hypothesis that these polymers were cytotoxic. The images of these cells lacked nuclei and probably are of mainly cell debris following cell lysis. On the control and pyrrole terminated branched substrates, the cell body was more organized and spread well with mixed polygonal and morphology with stress fibres. Although fewer cells were observed on the pyrrole end surface, the actin was well organised and the dense cortex that is typical of these was observed. On the acidic terminated linear and branched surfaces, fewer cells grew but the cells on the branched variant did have a well organised actin structure. There were fewer cells observed on the highly branched aminated polymer surfaces with 1,4-DAB or 1,6-DAH functionality but the cells do appear to be starting to show an organised actin structure. The cells adhered more to the 1,6-DAH terminated polymer surface compared to the 1,4-DAB functional polymer. On the linear aminated polymer surfaces, HREp cells spread differently depending on the length of the carbon chain of the functionality. On 1,2-DAE and 1,3-DAP functional polymer substrates, the nuclei of the cells displayed a weak DAPI intensity, and the fibres were randomly organised. Thus, these 1,2-DAE and 1,3-DAP materials also appear to be poor substrates for cell culture, despite the results from Alamar Blue and PicpGreen assays indicating their suitability. In contrast, the cells in the well coated with linear PBMA with 1,4-DAB functionality supported a large number of cells but the actin organisation appeared a typical for epithelial cells with a more spindle-like shape compared to the control and other surfaces. On the other hand, although there were fewer cells observed on the linear PBMA with 1,6-DAH functionality the cells had a well-developed actin cortex and they were taking up the typical cobble-stone morphology of epithelial cells

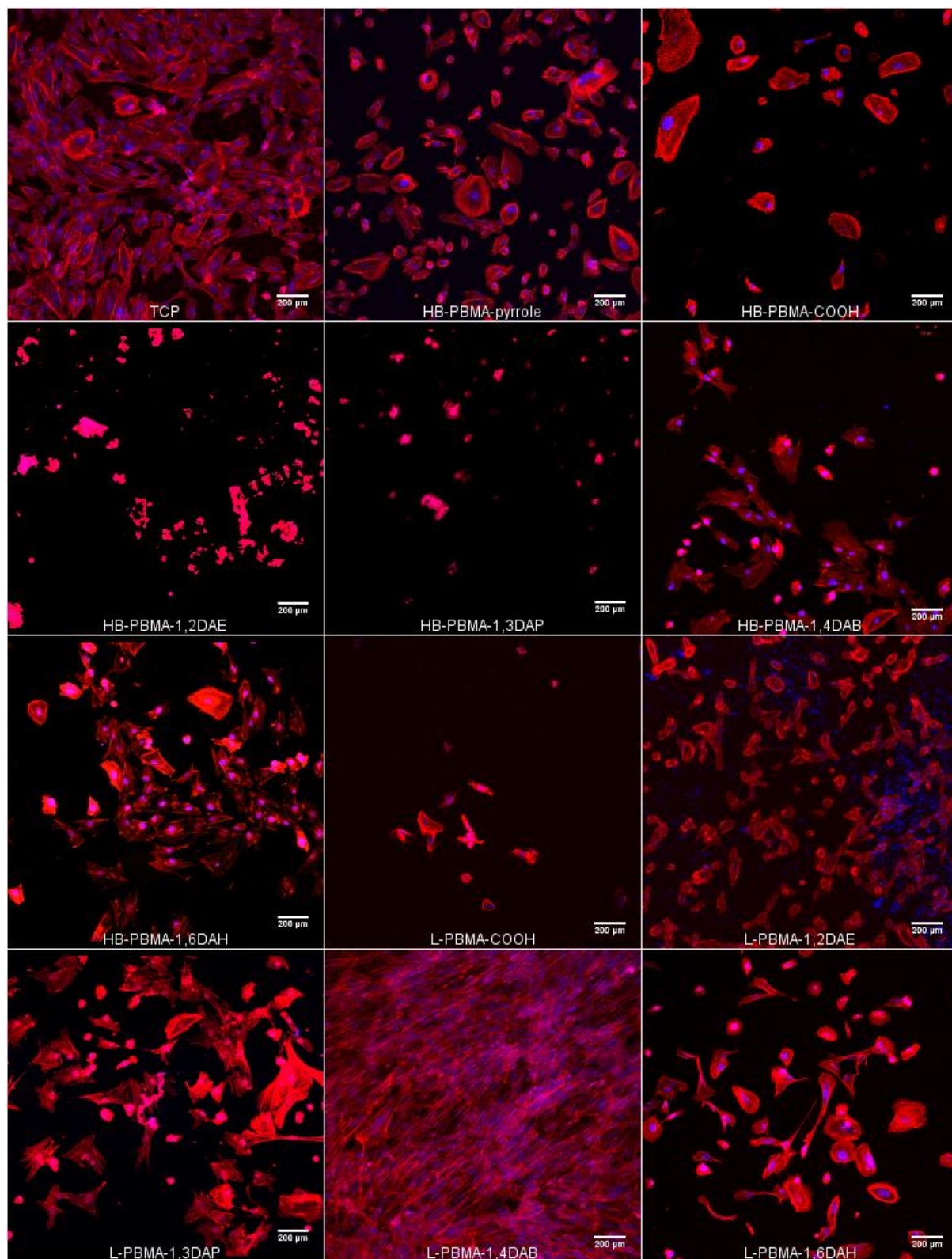


Figure 5.11- Immunofluorescence micrographs of HREp cells on different polymer coatings stained with TRITC-phalloidin for actin (red) and DAPI for nucleus (blue)

Findings presented below in Figure 5.12 indicated that the cancer cells behaved differently to primary HREp cells. This could be explained by considering the biological differences between the normal somatic cells and the immortalised transformed cancer cells. The latter are characterised by their rapid growth potential independent of growth regulation, in addition to their high migration and invasion capabilities compared to the non-transformed epithelial cells. However, even when the rapid growth rate of these cells was considered it was clear that the branched polymers with 1,2-DAE or 1,3-DAP functionality and the linear polymer with 1,2-DAE functionality were cytotoxic and did not support these cells. The behaviour of these aminated polymers appears to be rather complex so that the branched polymers with 1,4-DAB and 1,6-DAH functionality support these cells but the images from the linear analogues seem to be less satisfactory. Also, the linear polymer with 1,3-DAP functionality provided images of cells that were located into colonies of well defined actin structures with co-located nuclei.

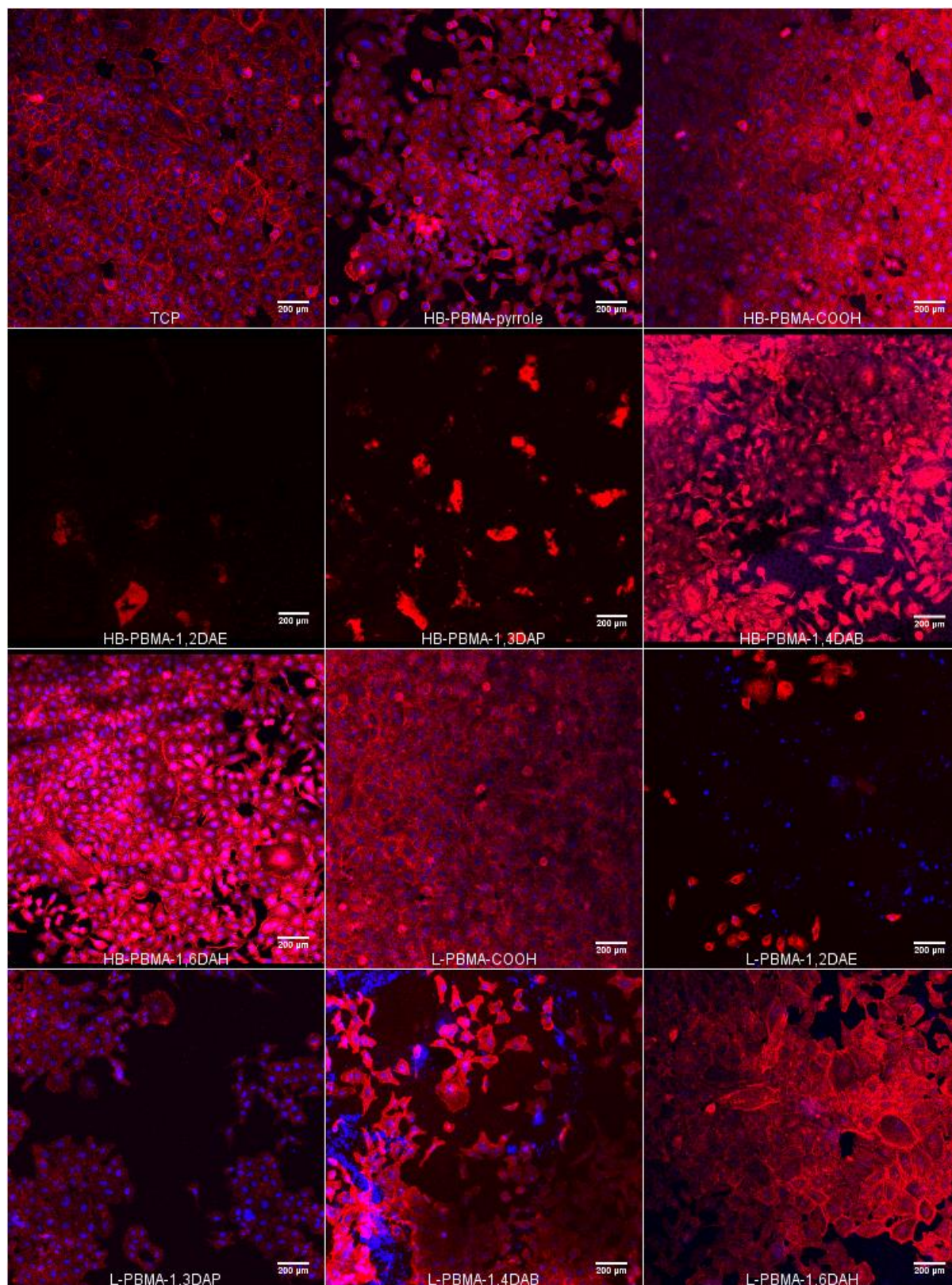


Figure 5.12- Immunofluorescence micrographs of A549 cells on different polymer coatings stained with phalloidin-TRITC for actin (red) and DAPI

Figure 5.13 shows images of the HDF cells on the various substrates. The control cells on TCP showed the typical fibroblast morphology with spindle-like organisation of actin and well -defined stained nuclei. The linear and branched COOH functional polymers provide similar images but the quantity of cells was decreased. On the highly branched polymer with a pyrrole end group the cells were grown well but with an atypical polygonal morphology and less organised actin filaments. The branched 1,2-DAE and 1,3-DAP functional polymers supported very few cells and the images seem to be of cell debris. On linear polymer surfaces with 1,2-DAE and 1,3-DAP, the nucleus was not localised within the actin structures, which provides an indication of cell lysis. On the other hand, although there were fewer cells on the branched polymers with 1,4-DAB or 1,6-DAH functionality the cells did have the typical spindle like morphology with the nuclei co-located within the actin structures. These polymers appear to be better substrates for HDFs than the equivalent linear polymers which did provide images of the actin structures, but the nuclei were not collocated within these structures.

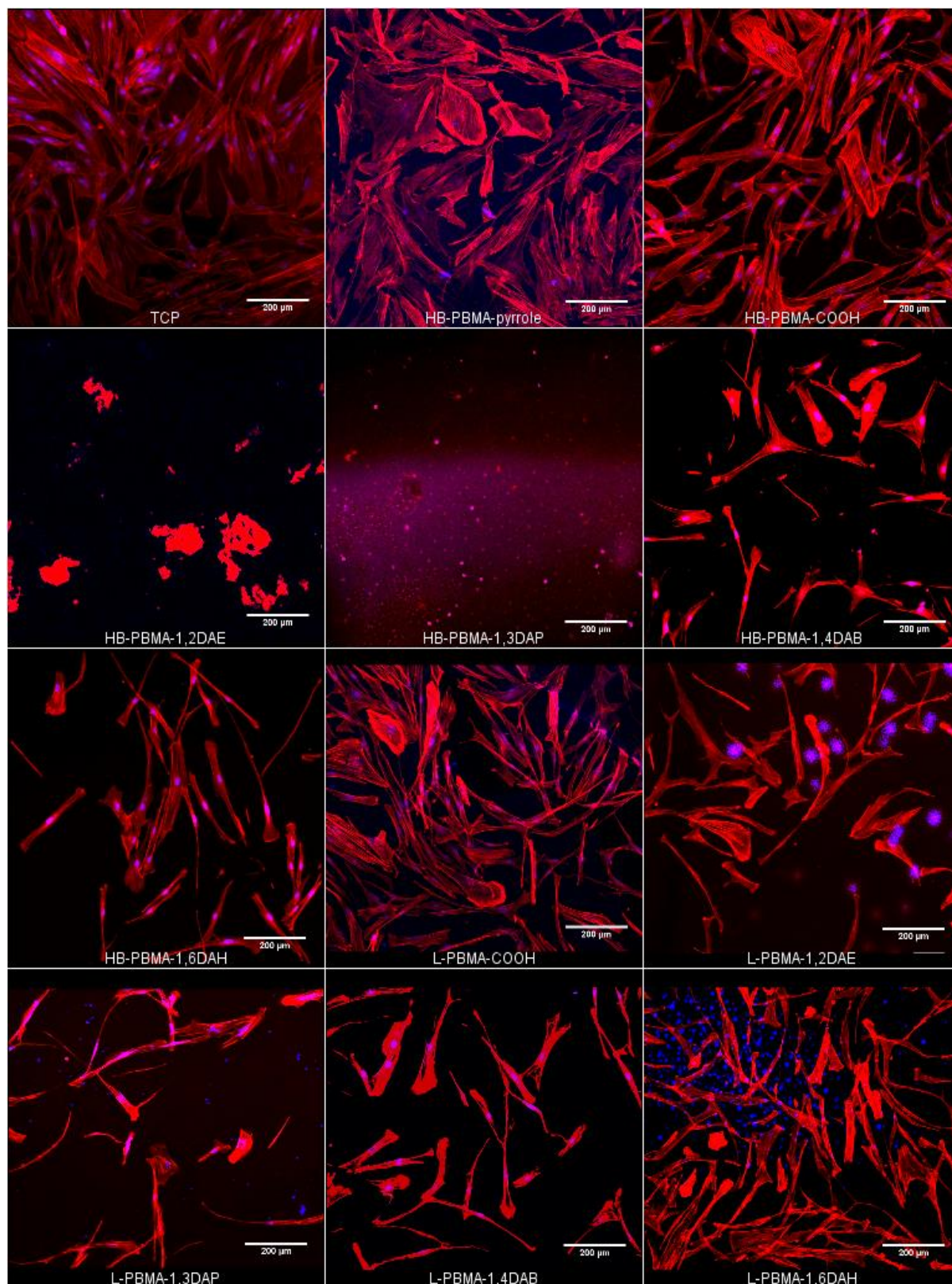


Figure 5.13- Immunofluorescence micrographs of HDF cells on different polymer coatings stained with phalloidin-TRITC for actin (red) and DAPI for nucleus (blue)

5.2.5 Polymer architecture (linear and branched) impact on cell adhesion

Based on the consistent results derived from the metabolic activity using the Alamar Blue assay and the number of cells using the Pico Green assay, one type of test was selected to study the correlation between two polymer architectures (linear and highly branched) of the same functionality and the cell behaviour, and this was the number of cells according to the Pico Green assay. The two polymers that were observed to be toxic in the previous assays; HB-PBMA:1,2-DAE and HB-PBMA:1,3-DAP, were excluded from the analysis. Therefore, the comparison was made between linear and highly branched with COOH, 1,4-DAB and 1,6-DAH functional groups as seen in Figure 5.14.

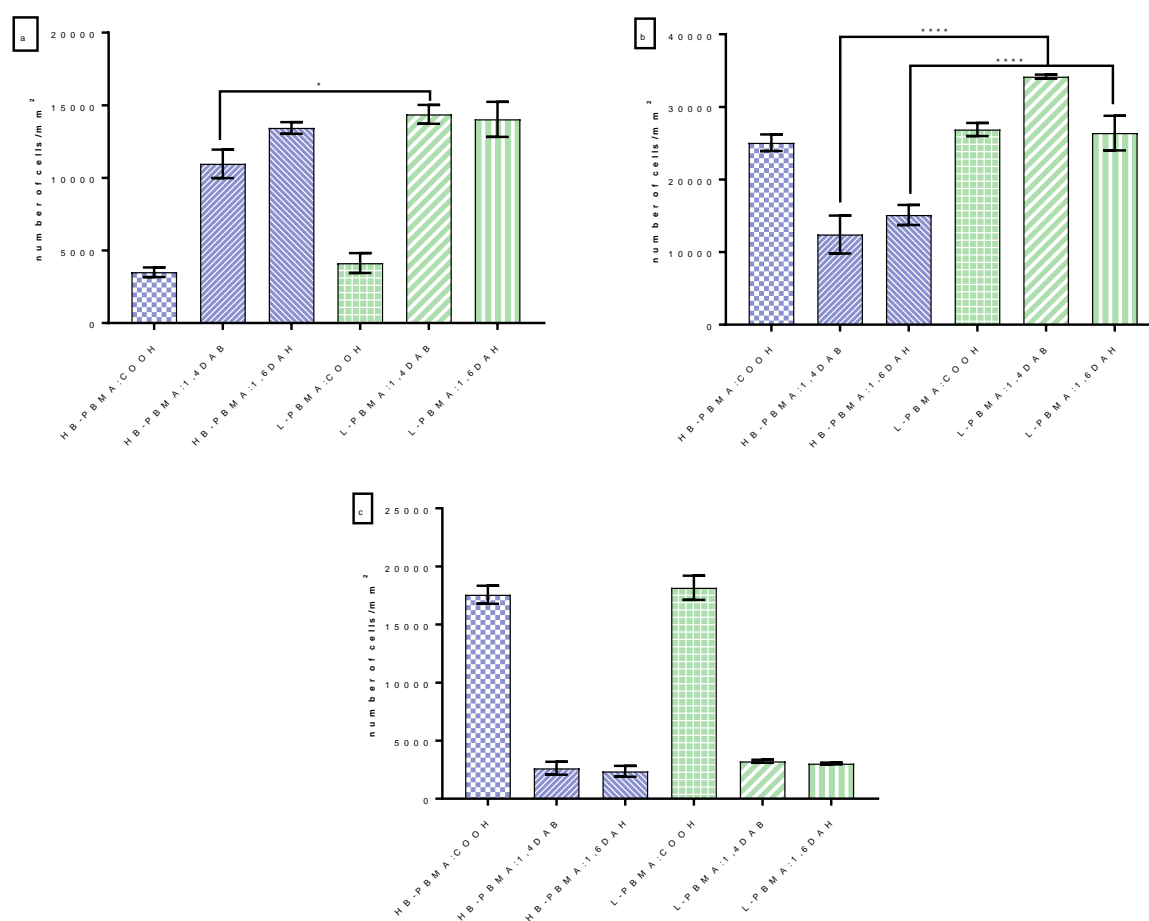


Figure 5.14- The results of two architectures of the same functionality in cell adhesion (a) HREp cells, (b) A549 cells and (c) HDF cells

Data analysed with one-way analysis of variance (ANOVA) and post-hoc Tukey's analysis. Error bars are the standard error of the mean \pm SEM of three dependent experiments, significance value marked with * $p < 0.05$ and **** $p < 0.0001$.

In HREp cells, there was a significant reduction in number of cells that adhered on HB-PBMA:1,4-DAB ($p < 0.05$) compared to L-PBMA-1,4-DAB. However, there was no significant reduction of cell number on 1,6-DAH functionality at both architectures. In the A549 cancer cell line, the linear polymer structure observed a significant ($p < 0.0001$) increasing of cells on 1,4-DAB and 1,6-DAH compared to highly branched polymer structure with the same functionalities. In contrast, there was no effect of architectures in HDF cells.

5.3 DISCUSSION

The aim of this study was to begin to set out the structure-biological property relationships associate with both chemical structure and polymer architecture. The experimental design involved comparing linear and branched polymers and comparing COOH and primary amine functionalities. The BMA polymers were used as substrate coating materials with different functional groups to support the adhesion of human renal epithelial cells, human lung carcinoma cells and human dermal fibroblast cells. These materials were assessed according to two coating architectures: highly branched polymers with three different end groups (pyrrole, acid and a selection of primary alkyl amines), and linear polymers with two similar pendant groups (acid and a selection of primary alkyl amines). Four different approaches were used to study the biocompatibility and cytotoxicity of these materials: AlamarBlue metabolic assay, PicoGreen quantification assay, LDH toxicity assay and imaging. HREp and HDF cells were used to continue the previous work based on the synthesised oligomer butyl methacrylate as a substrate with acid and amine functionalities. The results showed that HREp and HDF cells could be grown on acidic functionality, while the amine-modified olig(BMA) can support epithelisation with HRECs only¹⁸³. A549 cells were used because they are abundant, easy to culture, and show adherence and confluence more quickly than HREp cells. Further, to show the differences between primary cells and the epithelial cell lines in terms of their response to synthetic biomaterials.

The major aim of this work is to extract the design rules that will allow coatings to be developed that can support the development of epithelia. Moreover, it was not a focus of this research to engineer tissue replacements, therefore the dermal fibroblast and kidney epithelial cells were used to add to and expand the previous work based on the synthesised oligomer butyl methacrylate as a substrate with acid and amine functionalities. The amine-modified olig(BMA) can support epithelisation with HREpCs only¹⁸³. The previous study by Rimmer *et al.* showed that the alkyl aminated hydrogels and conetwork of 1,2-propandiol-3-methacrylate (GMA) was selective substrates for cell adhesion of A549 epithelial cells²⁷⁹.

The data presented in this chapter highlighted the correlation between surface chemistry and cell adhesion, giving an understanding of how the different functionalities on the same material can influence epithelial and fibroblast cell behaviour. The principle of adding amine or acid functionalities is to increase both the net surface charge and the hydrophilicity of the polymer¹¹. Increasing surface charge leads to improved wettability and hence protein and cell

adhesion¹⁴⁴. The cell and protein adhesion can be achieved in some cases by adding a negatively charge group such as a carboxylate and acrylate (the conjugate bases of carboxylic and acrylic acids, respectively). MacNeil *et al.* observed that carboxylic acid end functionality has a degree of biocompatibility, with 3% of the acid in the polymers enhancing the attachment of keratinocytes and osteoblast-like cells^{9-10, 108}. Also, cell adhesion and the proliferation of human aortic endothelial cells were improved on plasma polymerised poly(vinylacetic acid) containing 3.6 to 9% COOH groups²⁸⁰. In contrast, other studies indicate that the COOH group can lead to reduced cell adhesion in certain types of cells such as smooth cells²⁸¹ and fibroblast cells²⁸². Other reports have indicated that cell adhesion is enhanced by adding a positively charged functional group such as ammonia or an alkyl amine. The positive charge of the quaternary amino group on biomaterials has been extensively used in tissue engineering and regenerative medicine due to their properties (good hydrophilicity, high biocompatibility, and adequate chemical and thermal stability)²⁸³. However, some reports have showed that there is little effect on cell adhesion due to surface charge derived from quaternary amine functionality²⁸⁴. Recently, Rimmer *et al.* observed that the primary alkyl amine functionality of hydrogels enhances the attachment of corneal and epithelial cells but not fibroblasts^{11-12, 183}.

Synthetic hydrogels and conetworks have interesting applications in medical devices and in tissue engineering²⁸⁵ due to their swollen nature and given their similarities to the physical properties of natural tissues, which are non-immunogenic and non-inflammatory²⁸⁶. However, these materials are poor substrates for cell cultures if they are not modified with either cell-adhesive peptides^{279, 287} or in some cases other chemical functionalities, such as primary alkyl amines.^{1,2} For example, PEG is approved by the FDA as it plays an important role in various biological applications from wound healing to drug delivery, but it does not support cell adhesion or proliferation as a scaffold or substrate materials without incorporating RGD peptides²⁸⁸. Therefore, to promote cell adhesion with the hydrogel materials different strategies have been identified. Some common strategies are modification of the hydrogel surface with an incorporated cell adhesive peptide, modification of hydrogels by adding hydrophobic segments and modification of the hydrogel surface by adding an alkyl amine^{11, 16, 109, 270, 289}. Previous work has suggested that the increasing growth of corneal epithelial cells can be achieved on polymethacrylate hydrogels, which were synthesised by glycidyl methacrylate (GMA), ethylene glycol dimethacrylate (EGDMA) and glycidyl monomethacrylate (GMMA) monomers and modified with alkyl amine carbon chain with lengths between 3 and 6¹¹. This polymethacrylate hydrogel was then modified by adding lauryl methacrylate (LMA) monomer

and alkyl amines with different extracellular matrix proteins, the results of which showed that the 1,4-diamonbutane coated with collagen IV has a strong preference for the re-epithelisation and growth of corneal epithelial cells and the clinical development of artificial corneas¹⁸⁴. Another study by Hassan *et al* also used the polymethacrylate hydrogels with GMA, EGDMA, GMMA and LMA with different alkyl amines and two equilibrium water contents (EWCs): EWCs = 55% or EWCs = 35%. The results demonstrated that the material with EWC = 55% with 1,4-DAB could support the growth of limbal epithelial cells while inhibiting limbal fibroblast cells, and the bulk properties of the two hydrogels varied markedly according to the differences in cross-linking density. This might be related to the fact that a normal corneal stroma has 75% water content and prefers materials that contain more water¹².

Producing polymethacrylate for surface coatings as a solid material has not been achieved until the use of synthetic butyl methacrylate (BMA) as oligomers with acid and a selection of alkyl amines (1,2-DAE, 1,3-DAP and 1,4-DAB)^{183, 289-290}. The cell culture results showed that the oligo(BMA) with an acid end group supported the adhesion of renal epithelial and dermal fibroblast cells, whereas the oligo(BMA) with amine functionality had a greater adherence and viability for epithelial cells but was not good for fibroblast cells¹⁸³. The current study goes beyond these results to reveal the performance of more advanced complex architectures of PBMA with COOH and a selection of primary alkyl amine functionalities for promoting cell adhesion. The hypothesis tested in this thesis was that the effectiveness of primary alkyl amines as terminating groups for promoting of epithelisation could relate to the similarity in structure between the alkyl amine and the amino acid lysine, which is involved in protein cross-linking with glutamine residues. In the epithelial cells, the cross-linking between the free amine and γ -carboxyamide in glutamine form ϵ -(γ - glutamyl) lysine through an isopeptide and mediated by the transglutaminase²⁹¹⁻²⁹². The transglutaminase is a ubiquitously expressed enzyme involved in a variety of physiological cellular processes such as adhesion and migration of epithelial cells as well as some pathological conditions such as wound healing²⁹³⁻²⁹⁴.

The first observation to be made in these data is the observation that across three all types of cells using a range of assays and imaging techniques there was no evidence for any cytotoxic effects when the cells were exposed the branched polymers containing the dithioate end group derived from the RAFT process. These data will be widely applicable in the field given the

extensive use of RAFT to produce new polymeric biomaterials. On the other hand, the data provided extensive evidence to show that polymers containing 1,2-DAE or 1,3-DAP functionalities were toxic and did not support the culture of any of the three cell types. This was unexpected, but the result is supported by the previous observations on hydrogels showing that hydrogels functionalised with 1,2-DAE did not support epithelial cell growth¹¹⁻¹².

The first part of this chapter discussed the metabolic activity as determined by AlamarBlue by growing three types of cells on different polymer coating materials and comparing to those grown on TCP after incubating the cells on those materials for three days. The results suggest that the PBMA with an acid end coated surface was preferable to adhered fibroblast cells, whilst amine terminated surfaces, in which the amine group is separated from the polymer by an alkyl chain of 4 or 6 carbon atoms, promote cell attachment of epithelial cells. The second section discussed the total DNA content and cell numbers via PicoGreen (PG) assay on three different cells with different functionalities and architectures of PBMA compared to TCP after three days' incubation time. These results indicated the number of cells on each polymer surface and confirmed that HREp cells as seen in Figure 5.5 responded differently to amine functionalised coatings compared to HDFCs, which preferred an acidic polymer coating, as seen in Figure 5.7.

In a separate experiment, LDH was used to conduct a cytotoxicity assay of different polymers in cells. The cytotoxicity results on primary cells showed that the polymers behaved differently and as stated above, polymers with 1,2-DAE and 1,3-DAP functionality had a toxic effect on the cell compared to TCP as the control. Further, the HREp and HDF cells did not respond any percentage of toxicity compared to TCP. However, the A549 cell line responded to different percentages of toxicity on HB-PBMA:1,4DAB, L-PBMA:COOH and L-PBMA:1,4DAB polymer surfaces in comparison to TCP. Although the HDF and HREp cells are both primary cells, the toxicity of TCP as the control was higher in fibroblast than epithelial cells; this might be explained by the presence of phenol red in the fibroblast cell culture media (15 mg/ml), which might interfere with the absorbance of LDH at the same wavelength of 490 nm^{276, 295} in HDFCs, as seen in Figure 5.10. Additionally, the use of 10% serum as a medium supplement may also have had significant consequences for the toxicity analysis as the serum can serve as an exogenous source of LDH, though this can be avoided by using low serum medium (1-2%). Although this was one of the limitations of this work, which affects the reliability of our findings, serum reductions can influence cell viability²⁹⁶ and those cells are

highly serum-dependent, and ultimately it was not possible to maintain them in low serum medium. However, the epithelial cells culture medium used in this work was phenol red-free and contains 5% serum, which is the minimum concentration to which the serum can be reduced without affecting cell viability. In this context, future LDH-cytotoxicity experiment involving the use of phenol red-free media and low serum content is warranted to eliminate their potential contributions to the findings. Despite the problems associated with this assay, the overall results confirmed that PBMA with different functionalities demonstrated a lower rate of cell toxicity compared to TCP as the control. However, the 1,2-DAE and 1,3-DAP highly branched polymer-based substrates performed poorly and were found to have a higher toxicity for all cells due to their chemical or physical properties.

In the final part, based on the results observed under fluorescence microscopy, actin assembly, as well as its arrangement, can significantly influence the mobility of the HREp cells, as seen in Figure 5.11. Therefore, it can conclude that the L-PBMA:1,4-DAB polymer was the best in terms of actin structure and organization. Other polymer surfaces such as HB-PBMA:pyrrole, HB-PBMA:1,6DAH, HB-PBMA:1,4DAB and L-PBMA:1,6DAH terminated polymers also enhanced the growing of cells, as they appear to be starting to show an organised actin structure but might be influenced better with long incubation time. Hence, it can assume that these polymers can foster cell mobility by providing adequate traction force for cell migration²⁹⁷. In contrast, the other linear polymers (L-PBMA:1,2-DAE and L-PBMA:1,3-DAP) enhanced the cell number and metabolic activity of the cells; however, they resulted in a random arrangement of actin fibres. On the other hand, the acidic terminated linear and branched surfaces did not support growth of the cells. The morphology of HDF cells on the polymer and control surfaces was also observed by F-actin and nucleus staining, as shown in Figure 5.13. It can be concluded that HB-PBMA-pyrrole, L-PBMA:COOH and HB-PBMA:COOH polymer surfaces were the best in terms of organised pattern, where cells were aligned parallel to each other and were similar to the control. Therefore, it can be assumed that these polymers can foster cell mobility by providing adequate traction force for cell migration. By contrast, the HDF cells with spindle morphology did not spread well on any of the animated terminated polymers, hence the mobility of the cells was reduced. Furthermore, it may be noted that the presence of A549 cells on polymer surfaces could be associated with enhanced cell number, as seen in Figure 5.12. The HB-PBMA:1,2-DAE and HB-PBMA:1,3-DAP functional coatings were also shown to be toxic and the images were of mainly cell debris.

The impact of polymer architectures observed in PicoGreen assay was that the number of cells were significantly increased on the linear material compared to branched material with 1,4-DAB functional group on HREp and A549 cells but there was no effect on HDF cells because they did not grow on aminated polymers as seen in Figure 5.14. Further, the linear polymer with 1,6-DAH end group was a more suitable substrate for growth of cells compared to branched polymer of the same functionality with A549 cells. The different impact of the linear and branched polymers within just 1,4-DAB and 1,6-DAH functional groups might be due to the differences of wettability between them, as aminated branched materials are more wet surfaces than linear one, and this can affect on protein adsorption and hence cell adhesion. On the other hand, the carboxylic terminated polymer for both architectures was not seen any statistical significant changes on growing cells. This might be due to their roughness and elastic modulus of both structures were similar. The impact of polymer architectures had been studied previously in different cell biology works, different architectures were assessed to investigate whether biocompatibility would be affected by polymer size or molecular weight. Linear or branched poly(ethylenimine) (PEI), as used in gene delivery, was assessed *in vitro* where it was shown that the linear architecture is a great deal better than hyperbranched²⁹⁸, and the high molecular weight of the polymer was good for gene delivery²⁹⁹. Poly(glycidol) as another example had been studied in relation to the effectiveness of the biocompatibility of branched and linear polymers in blood testing, and the results demonstrated that both architectures have very good biocompatibility in both *in vitro* and *in vivo* assays¹⁷⁸.

The results of the surface-coated BMA materials showed the correlation between the surface functionalised with alkyl amine carbon chain length and cell adhesion. The results are in agreement with previous work which reported that longer alkyl chains are more conducive to growing epithelial cells¹¹⁻¹². It is also important to mention that the data of this work are consistent with those of E. Hassan *et al*¹², showing that cell adhesion was supported on long-chain amine functionalities, specifically on 1,4-diaminobutane based on hydrogel in limbal epithelial cells (LECs), while the cell adhesion is inhibited in limbal fibroblast cells (LFCs). In addition, this work also observed that the cell adhesion and proliferation of HREp cells were promoted on long-chain amine functionalities of solid PBMA but were inhibited in HDF cells. Here, the polymer functionality with carbon chain lengths between 4 and 6 is seen as a good surface to support human renal epithelial cells. On the other hand, the surface functionalised with carboxylic acid is a good surface to promote HDF cells. The A549 cell line had variable results, but most of functional groups supported cell adhesion excepted the branched materials

with 1,2-DAE and 1,3-DAP end as they showed toxic for all cells. These results prove that epithelial and fibroblast cells have different or opposite reactions in the same substrate, and this might be due to the differences in protein expression and extracellular matrix (ECM) development.

5.4 CONCLUSION

In this study, the behaviour of highly branched and linear butyl methacrylate polymers with different terminated groups in direct contact with human renal epithelial cells (HREpCs), human dermal fibroblast cells (HDFCs) and human lung carcinoma cells (A549) was investigated by measuring cell viability and cytotoxicity of the polymers. The results from this study demonstrate how PBMA with acid functionality provided a good surface for fibroblast cells, whereas PBMA with different primary alkyl amine functionality, if the alkyl group contained 4 or 6 carbons, provided a good surface for epithelial cells. Although linear polymers with pendant alkyl amines with 2 or 3 carbons in the alkyl chain could support some cells, but analogous branched polymers always appeared to be cytotoxic.

5.5 EXPERIMENTAL

5.5.1 Equipment and reagents

Details of all equipment and reagents used for cell culture experiments are shown in Table 5.1 and Table 5.2.

Table 5.1- List of equipment used

Equipment	Brand	Supplier
Centrifuge	Eppendorf	Thermo Fisher Scientific
Class II laminar flow hood	Airstrema	ESCO worldwide
CoolCell	Biocision	Sigma Aldrich
Glass coverslips	VWR	VWR
Haemocytometer chamber	Neubauer	Sigma Aldrich
Incubator	Galaxy R CO ₂ incubator	SLS Scientific laboratory suppliers
Pipette boy	Fastpetite	Sigma Aldrich
Pipette glass	Fisher	Fisher Scientific
Pipette straw	Sarstedt	Fisher Scientific
Pipette tips	Triple red	Triplered
T- flask	Nunc	Thermo Fisher Scientific
Well-plates	Coring	Sigma Aldrich

Table 5.2- List of reagents used

Reagent	Supplier
4' 6- diamidino-2-phenylindole (DAPI)	Molecular probes, Life technologies
Alamar blue® cell viability reagent	Invitrogen Life technologies
Dimethyl sulfoxide (≥99.9%)	Bioreagent, Sigma Aldrich
Dulbecco's modified Eagle medium with D-glucose, L-glutamine and pyruvate	Gibco Life technologies
Dulbecco's modified Eagle medium with HEPES buffer, high glucose, L-glutamine and pyruvate	Gibco Life technologies
Fetal bovine serum	Sigma Aldrich
Formaldehyde	Sigma Aldrich
Human carcinoma epithelia lung cells	ATCC
Human dermal fibroblast cells	ATCC

Human renal epithelial cells	PromoCell, Germany
Penicillin/streptomycin	Gibco Life technologies
Pierce™ LDH Cytotoxicity assay kit	Thermo Fisher Scientific
Quant-iT™ PicoGreen™ dsDNA assay kit	Thermo Fisher Scientific
Renal epithelial cell growth medium 2 (ready-to-use)	PromoCell, Germany
Rhodamine phalloidin-TRITC	Molecular probes, Life technologies
sterile phosphate buffered saline	Invitrogen Life technologies
Triton X100	Sigma Aldrich
Trypan blue	Sigma Aldrich
Trypsin 0.25% with EDTA 4Na	Invitrogen Life technologies
Trypsin neutralise solution	Invitrogen Life technologies

5.5.2 Cell culture

All culture protocols were performed under sterile condition in a class II laminar flow hood, using 70% ethanol with distilled water and virkon® as a cleaning agent.

5.5.2.1 Human renal epithelial cells (HREps) culture

HREp cells were cultured in tissue culture plastic containing renal epithelial cell growth medium 2. The medium was supplemented with 5% fetal calf serum, epidermal growth factor (10 ng/ml), insulin (5 µg/ml), epinephrine (0.5 µg/ml), hydrocortisone (36 ng/ml), transferrin (5 µg/ml) and triiodo-L-thyronine (4 pg/ml). 10 ml of the complete medium was placed into two T25 flasks in the incubator in a humidified atmosphere for 30 minutes. 5×10^6 cryopreserved HREp cells were placed in a 37 °C water bath for 90 seconds with constant agitation. The cells were pipetted up and down and were then quickly transferred to the pre-warmed flasks. The cells were incubated at 5% CO₂, at 37 °C for a minimum of 16 hours before changing the media. Subsequent media changes were performed every 2–3 days until confluent and HREp cells were passaged at 60-70 % confluent, with routine checking under the optical microscope.

5.5.2.2 Human dermal fibroblast cells (HDFs) culture

HDF cells from skin were cultured in tissue culture plastic containing a DMEM medium with HEPES buffer, high glucose, L-glutamine and pyruvate. 60 ml of DMEM was removed

from the 500 ml bottle and replaced with 50 ml of FBS (10%) and 10 ml penicillin/streptomycin. 15 ml of the complete medium was placed into a T75 cell culture flask and warmed in the incubator for 30 minutes. 2×10^6 cryopreserved HDF cells were placed in a 37 °C water bath for 90 seconds with constant agitation. The cells were pipetted up and down and then quickly transferred to the pre-warmed flask. The cells were placed in the incubator at 37 °C, 5% CO₂ for a minimum of 16 hours in order to adhere before changing media. Subsequent media changes were performed every 2–3 days. HDF cells were passaged at 70-90 % confluence, with routine checking under the optical microscope.

5.5.2.3 Human carcinoma epithelial lung cells (A549) culture

Human lung epithelial cells (A549) were cultured in tissue culture plastic containing DMEM medium with D-glucose, L-glutamine and pyruvate. The complete medium was prepared by removing 60 ml of DMEM from the 500 ml bottle and then replacing with (10 ml) penicillin/streptomycin and 50 ml fetal bovine serum (10%). 15 ml of the complete medium was placed into a T75 flask and warmed in an incubator in a humidified atmosphere for 30 minutes. 2×10^6 cryopreserved A549 cells were placed in a 37 °C water bath for 90 seconds with constant agitation. The cells were pipetted up and down and were then quickly transferred to the pre-warmed flask. The cells were placed in the incubator set to 37 °C, 5% CO₂ for a minimum of 16 hours before changing media. Subsequent media changes were performed every 2–3 days and A549 cells were passaged at 70-90% confluence, with routine checking under the optical microscope.

5.5.3 Sub-culturing of cells

Cells were passaged upon reaching 70-90% confluence as determined by microscopy. The old medium was removed from the flask and the cells were washed with 10 ml of sterile phosphate buffered saline (PBS). Cells were trypsinised using 5 ml of trypsin and the flask was agitated vigorously at room temperature. Optical microscopy was used to observe the detachment of cells, and when 90% complete detachment was observed 5 ml of trypsin neutralise solution was added (containing PBS and fetal calf serum and working as trypsin inhibitor). The entire contents of the flask were then added to a sterile centrifuge tube and spun at 453 x g for 5 minutes to form a pellet. The supernatant was removed from the tube and the cells were re-suspended in 2 ml of media and cell a count was performed before splitting into a new sterile flask or well plate.

5.5.4 Cryopreservation of cells (cell freezing)

The CoolCell[®] (which is an alcohol-free container and it used instead of a Mr Frosty container and -80 °C freezer) was placed in a polystyrene container and surrounded with dry ice to cool down cells before transforming into liquid nitrogen. The cell freezing medium was prepared by adding 10 % DMSO in FBS. The cells were washed with sterile PBS and trypsin was added, as described above in the passage protocol. After centrifugation, the supernatant was removed and the cells were re-suspended in a freezing medium and placed in a cryovial with a density of $\sim 1 \times 10^6$ cells per ml. The cryovials were then promptly placed into CoolCell, and after 24 hours the cryovials were removed and placed into liquid nitrogen for storage at -196 °C.

5.5.5 Thawing of cells

The cryovial was removed from the liquid nitrogen container and thawed in a water bath at 37 °C for 2 minutes. The cryovial was rinsed thoroughly with 70 % ethanol under laminar flow and then the vial was opened to transfer the cells to a centrifuge flask that contained 5 ml of pre-warmed medium.

5.5.6 Cell counting protocol

Under sterile conditions, 15 μ l of cell suspension was placed in a pre-labelled flask and mixed with 15 μ l of trypan blue solution. 10 μ l of this solution was then withdrawn and placed into the chamber of the Neubauer haemocytometer. Viable cells are not stained by trypan blue, while the dead cells appear due to trypan blue under light microscopy using a x10 objective lens. The actual number of cells were determined by using the equation below.

Average number of cells = total number of all accounting cells/number of squares

Then, Actual number of cells = $n \times 10,000 \times m$

Where n = Average number of viable cells counted, m = Volume of culture media cells were re-suspended in (a dilution factor).

5.5.7 Preparing test material

5.5.7.1 Polymer solution

Polymers were dissolved and agitated vigorously in the appropriate solvent at a concentration of 5mg/ml as shown below.

Polymer	Solvent
HB-PBMA:pyrrole	Tetrahydrofuran
HB-PBMA-COOH	Tetrahydrofuran
HB-PBMA:amine	Tetrahydrofuran
L-PBMA:COOH	Tetrahydrofuran
L-PBMA:amine	Tetrahydrofuran

5.5.7.2 Sterilising glass coverslips:

Glass coverslips (22x22 mm for 6 well plate, and 19x19 mm for 12 well plate) were cleaned by sonicating them in a beaker first in 1M HCl for 24 hours and then in dH₂O and finally in ethanol. Individual coverslips were then removed from the ethanol and dried under a stream of nitrogen, making sure each coverslip was dried well. 100 µl of the polymer solution was pipetted onto the sterilised coverslips. An IR lamp was used to expose the polymer films until the solvent appeared visibly removed. Each coverslip was placed into its own well of 12 well plates and washed twice with PBS to remove any residual solvent.

A549, HDF or HREp cells were treated with trypsin as the passage protocol but instead of re-seeding into a flask, they were seeded onto the polymer film at an appropriate density (2×10^4 for 6 well plate and 1×10^4 for 12 well plate). The complete medium (2 ml for 6 well plate and 1 ml for 12 plate) was added to each well plate and then incubated for 24 hours at 37 °C, 5% CO₂. After 24 hours, the culture medium was changed for fresh medium and the cells incubated for 3 days before being fixed for staining cells or assay.

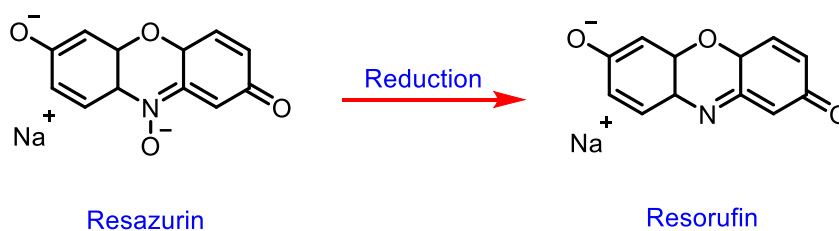
5.5.8 DAPI and phalloidin- TRITC staining

After growing the cells on a glass coverslip (22 x 22mm) in a 6-well plate, the medium was removed, and the cells were washed twice with PBS. The cells were then fixed with 3.7% formaldehyde in PBS for 30 minutes at room temperature. The formaldehyde was then removed, and the cells were washed with PBS twice. 1% of Triton X100 in PBS was added to the cells and left in the fridge for 5 minutes. The Triton was then removed, and the cells were

washed with PBS three times. 1 ml of diluted phalloidin-TRITC in PBS (1 $\mu\text{g/ml}$) and diluted DAPI in PBS (0.1 $\mu\text{g/ml}$) were added to each coverslip and the samples incubated for an hour in an incubator at 37 $^{\circ}\text{C}$, 5% CO_2 . The phalloidin and DAPI medium was then removed and the cells were washed three times with PBS before imaging with confocal microscopy. The excitation and emission wavelengths were 480 nm and 500 nm for phalloidin-TRITC, and 340 nm and 488 nm for DAPI.

5.5.9 Cell viability, determination number of cells and cytotoxicity methods

5.5.9.1 Alamar Blue[®] assay



Scheme 5.1- Reduction of Resazurin to Resorufin via mitochondrial dehydrogenase

AlamarBlue[®] (AB) assay is a colorimetric growth indicator for the detection of metabolic activity. The colour changes in solution from blue to red in response to the chemical reduction of AB into purple by the mitochondrial dehydrogenase activity in cell nuclei, as seen in Scheme 5.1. It is a non-cytotoxic assay allowing continuous observation of cell cultures and cells can be reused for further experiments^{271, 300-301}. To measure cell viability, the polymers were dissolved in an appropriate solvent (as described previously) and cast onto a sterile glass coverslip of 19 x 19 mm and then placed onto 12 well plates. The cells were seeded at 1×10^4 cells per well in a volume of 2 ml medium directly onto the polymer films and incubated at 5% CO_2 , 37 $^{\circ}\text{C}$ for 72 hours. TCP wells were also used with cells alone as a positive control. After incubation, the medium was removed, and the cells were washed with PBS, and 1 ml medium was added to each well following the addition of 100 μl of AB reagent. The samples were protected from light and incubated for four hours under humidified conditions, as were the AB and media for use as a negative control. After four hours, 200 μl of cell solution was transferred to 96 well plates in triplicate and the absorbance was then measured using a 96-well plate reader at 570 nm (and reference at 600 nm).

5.5.9.2 PicoGreen assay

Quant-iT™ PicoGreen™ dsDNA (PG) assay kit was used as a fluorescent nucleic acid stain for the quantification of total cellular dsDNA (double stranded DNA) and for determining the density of cells in the culture. The PG is used as a quantity DNA by binding the dsDNA of a fluorophore to nucleotides, and it is based on the fluorescent signal³⁰¹⁻³⁰². A standard curve for the PG assay was generated using the manufacture's protocol to obtain the concentration of DNA using a lambda DNA standard at a known concentration. In addition, to estimate a quantitative number of cells according to this paper²⁷³, three calibration curves were generated using a known cell number against a fluorescence reading. The linear calibration curves are shown in Figure 5.15.

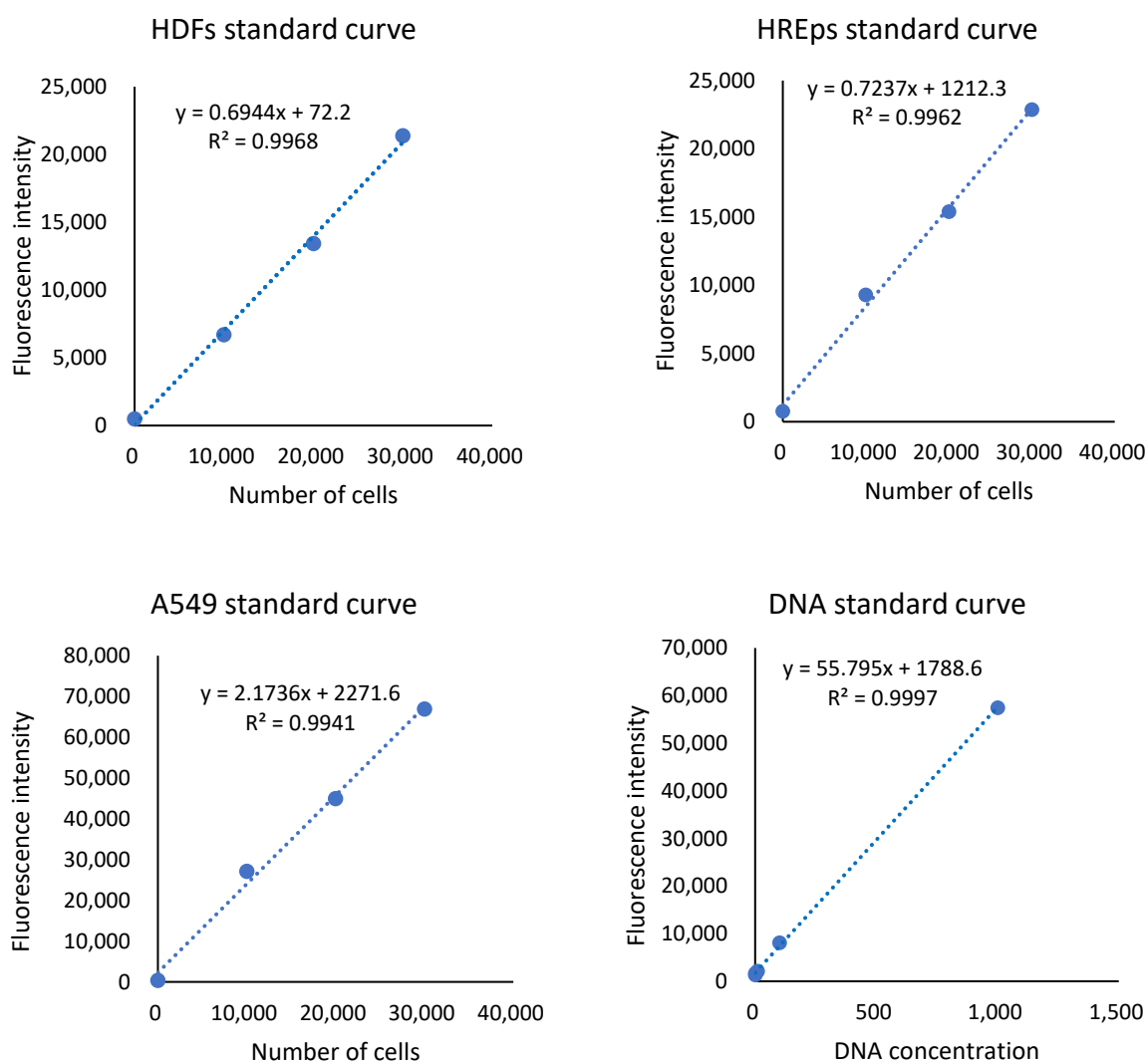


Figure 5.15- Standard curves for PicoGreen assay derived from lambda DNA standards, and known cells concentrations

The number of cells or DNA concentration in each polymer substrate was calculated using the following equation;

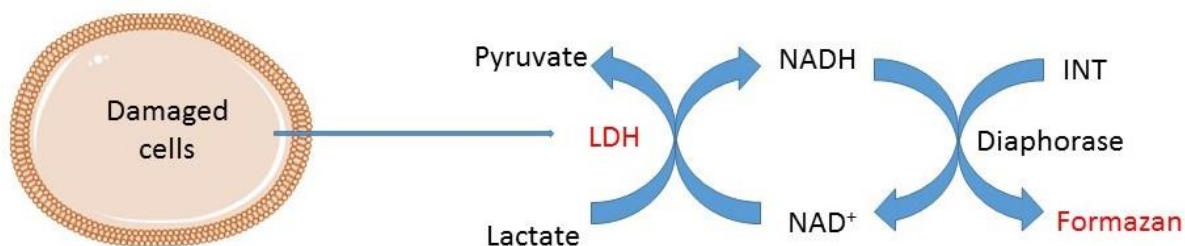
$$\text{number of cells} = \frac{OD_{520nm} - C}{m}$$

Where OD_{520nm} is the fluorescence intensity of each well, C is the constant from the standard curve and m is the gradient of the standard curve.

Cells were plated at a density of 1×10^4 onto the polymer surface, as described above, in 12 well plates in 1 ml medium; they were then incubated in the incubator at 37°C , 5% CO_2 for 72 hours. After the incubation time, all media were removed, and the cells were washed with 1 ml of PBS three times. Two ml of TE buffer was added to each sample and then frozen at -80°C until the cells were ready to assess (at least 48 hours for efficient cell lysis) and were then thawed at room temperature. 100 μl samples were transferred to 96 black well plates in triplicate, and then 100 μl of PicoGreen working solution reagent were added to each plate, and samples excited at 480 nm with an emission wavelength at 520 nm. The working solution of the reagent of dsDNA PicoGreen was prepared by mixing one vial of reagent, 100 μl , with 19.9 ml of TE buffer in a plastic container which was protected from the light.

5.5.9.3 LDH cytotoxicity assay

Lactate dehydrogenase is a cytosolic enzyme present in different cell types; it is a colorimetric assay to evaluate cell damage. Damaged plasma membranes were released into the cell culture media, extracellular LDH could be quantified by two enzymatic reactions. LDH converts lactate to pyruvate by generating NADH from NAD^+ . Diaphorase then uses NADH to reduce a tetrazolium (INT) salt to a red formazan product that can be measured at 490nm as shown in Scheme 5.2.



Scheme 5.2- Schematic of the principle of LDH cytotoxicity assay mechanism

A Pierce™ LDH cytotoxicity assay kit was used to measure the lactate dehydrogenase (LDH) released into the media from damaged cells for cellular cytotoxicity following the manufacturer's instructions. Polymers were dissolved in an appropriate solvent (as described previously) and cast onto a sterile glass coverslip of 19 x 19 mm and then placed onto a 12-well plate. 1×10^4 cells/well were plated onto different polymer surfaces in 1 ml medium in 12-well tissue culture plates (including a complete medium control without cells, and cells in well plate for spontaneous LDH activity control and maximum LDH activity control) and incubated overnight. After the incubation time, 100 μ l sterile ultrapure water was added to each cell well as the spontaneous LDH activity control, and then the plate was incubated at 37 °C, 5% CO₂ for 48 hours. After incubation, 100 μ l Lysis buffer (10X) was added to the cells serving as the maximum LDH activity control, and mixed and incubated under normal conditions for 45 minutes. After this time, 50 μ l of each sample medium (complete medium without cells, spontaneous LDH activity control, maximum LDH activity control and compound treated cells) were transferred onto a 96-well plate in triplicate wells. Then, 50 μ l of reaction mixture was added to each sample well, mixed and incubated at room temperature for 30 minutes whilst being protected from the light. Reaction mixture is one vial of the substrate mix (lyophilizate), dissolved in 11.4 ml of ultrapure water in a 15-ml conical flask and combined with 0.6 ml of assay buffer, mixed well, and protected from the light. 50 μ l of stop solution was added to each well, mixed gently, and the absorbance was measured at 490 nm and 680 nm as reference using a 96-well plate reader. Cytotoxicity was calculated using the following equation:

$$\%Cytotoxicit = \frac{\text{Compound treated LDH activity} - \text{Spontaneous LDH activity}}{\text{Maximum LDH activity} - \text{Spontaneous LDH activity}} \times 100$$

5.5.10 Statistical analysis

The data from the biology work were analysed using the GraphPad Prism 6 statistics program. Statistical analysis was performed via a one-way ANOVA followed by Bonferroni test for testing all surface materials that compared to TCP as the control, further the analysis of impact the polymer architectures of the same functionality was performed by a post Hoc Tukey test. Data were expressed as means \pm standard error of the mean (SEM) of at least three dependent experiments, with probability values were less than 0.05 ($p < 0.05$) considered statistically significant. Annotations as follows * $p < 0.05$, ** $p < 0.005$, *** $p < 0.001$ and **** $p < 0.0001$.

5.6 INSTRUMENTATION

5.6.1 Optical microscopy

In this work, phase contrast microscopy was used with an inverted bright field microscope (Olympus Co, CKX41, New York) throughout the cell biology progress with an objective UPLFLN 4x /0.10 PhP FN22 and CACHN 10x /0.25 PhP FN22 lenses (Olympus, Japan). All objective lenses were attached and rotated under the microscope stage. The Olympus camera (Olympus, UC30, Japan) was fitted to a microscope for imaging.

5.6.2 Confocal microscopy

Images were obtained using a Zeiss series confocal laser scanning microscope located at Bradford and Sheffield Universities. In Bradford, inverted confocal microscope (Carl Zeiss LSM710, Germany) with an objective EC Plan-Neofluar 10x /0.3 M27 lens (Carl Zeiss, Jena, Germany). In Sheffield, Zeiss upright confocal microscope (Carl Zeiss LSM510-META, Germany) long range water dipping lenses used with an objective EC Plan-Neofluar 10x /0.3 M27 lens (Carl Zeiss, Jena, Germany). TRITC was excited using a laser wavelength of 480 nm and emission was detected at 500 nm, whilst DAPI was excited using a laser wavelength of 340 nm and emission was detected at 488 nm. Image acquisition was carried out with Carl Zeiss Laser Scanning System software, and analysis was performed using ImageJ software.

1 RELATIONSHIP BETWEEN SURFACE PROPERTIES (WETTABILITY AND SURFACE FREE ENERGY) OF SYNTHESISED POLYMERS AND CELL BEHAVIOUR

1.1 INTRODUCTION

The modification of polymer surface properties such as chemical functionality, wettability, topography and mechanical properties have been studied in recent years and have been shown to influence cell adhesion and to affect cell behaviour^{12, 109, 176, 270, 303}. The change in the chemical composition, following the modification of the architectures and functionalities of PBMA polymers affects their surface properties considerably, as seen in chapter 4. Chapter 5 presents the adhesion and growth of three different cell types; human renal epithelial (HREp), human dermal fibroblast (HDF), human carcinoma cells (A549), on different functional polymers and architecture surfaces, following *in vitro* studies via different functional assays. The results showed that the adhesion and growth of cells varies, depending on both the substrates properties and the cell type. However, the effect of the polymers wettability and interfacial free energy on cell metabolic activity and adhesion has not yet been considered. The wettability of the various polymer surfaces was evaluated by water contact angle measurements; the higher the water contact angle, the lower the wettability (chapter 4). The materials surface free energy (SFE) and its components were calculated based on the contact angles of different solvents, as presented in chapter 4. This chapter explores whether there is any correlation between the water contact angles (wettability) and SFE components of the synthesised polymers with cell behaviour, as measured by their metabolic activity and cell number. The Spearman's rank-order correlation was used to study the relationship between SFE and its components, as well as polymers wettability, and cell adhesion-viability. The Spearman's correlation coefficient (r) is a statistical measure of the non-normally distributed data relationship between paired data, measuring the strength and direction of association between two ranked variables. In this study, a high Spearman's correlation is considered for r values higher than 0.7 ($r > 0.7$). This correlation is considered statistically significant if the probability (p) is less than 0.05 ($p < 0.05$).

1.2 RESULTS AND DISCUSSION

1.2.1 Correlation between surface wettability and cell behaviour

The polymers wettability was directly evaluated by water contact angle measurements on glass coverslips coated with the polymers, as shown in section 4.2.2. The Spearman's correlation was used to observe the relationship between the metabolic activity/number of cells on the different polymer surfaces and their water contact angles. The change in chemical structure that occurred during the incorporation of amine or carboxylic acid functionalities within linear and highly branched polymers has been observed to increase their wettability, in comparison to the homo poly(butyl methacrylate). In this section, the influence of polymers wettability on cell behaviour is examined. The two polymers; namely HB-PBMA:1,2-DAE and HB-PBMA:1,3-DAP, that were found to be toxic in the cell culture assays, although presented in the figures, were excluded from the analysis, as it is considered that toxicity cannot be surface wettability driven only.

Figure 1.1 displays the relationship between the HREp cell viability assays and the polymers surface wettability. Under both assays; number of cells and metabolic activity, no significant correlation was observed between cell number/metabolic activity and polymers water contact angles.

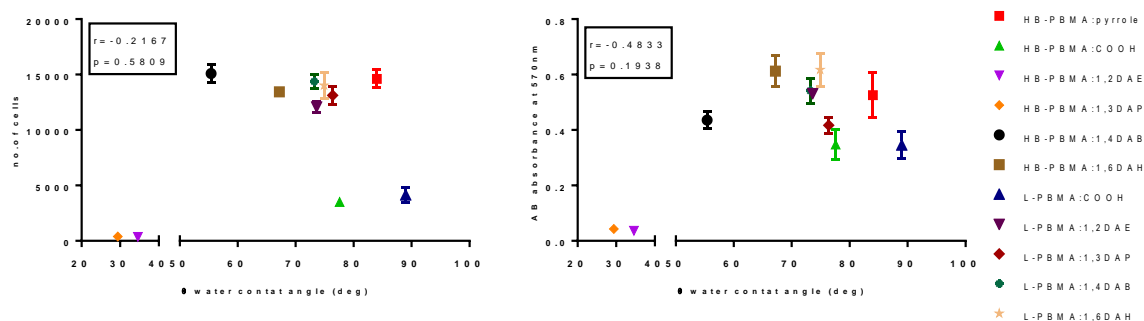


Figure 1.1- Relationship between the human renal epithelial (left) cell number and (right) metabolic activity assays with surface wettability

On the other hand, the metabolic activity and the number of adherent HDF cells were significantly and positively correlated with the polymers water contact angles as seen in Figure 1.2. The increase in the polymers contact angle increased the cell number and metabolic activity for the linear and highly branched polymers with carboxylic acid functionality that presented water contact angles between 75 to 90°.

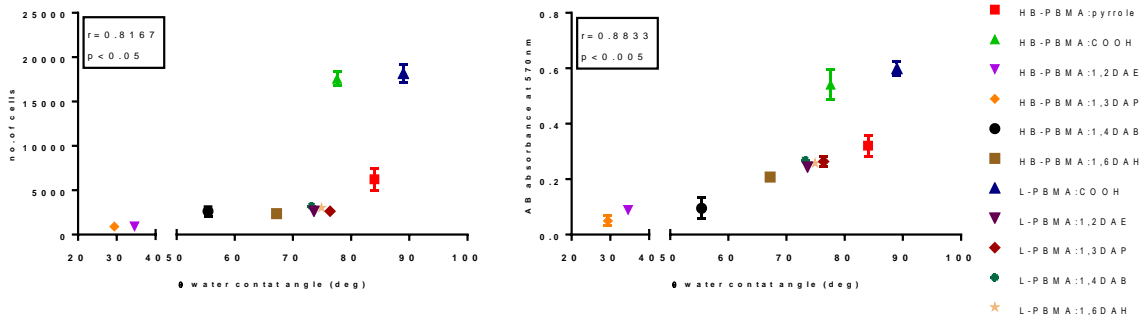


Figure 1.2- Relationship between the human dermal fibroblast (left) cell number and (right) metabolic activity assays with surface wettability

For the A549 cell line, the relationship of the cell number and metabolic activity with the polymers surface wettability is presented in Figure 1.3. Under both assays no significant correlation was observed between cell number/metabolic activity and polymers water contact angles, for the A549 cell line.

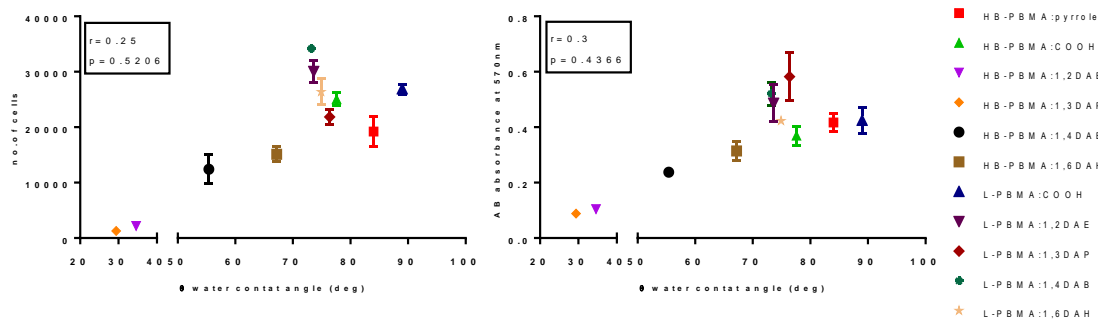


Figure 1.3- Relationship between the human carcinoma epithelial “A549” (left) cell number and (right) metabolic activity assays with surface wettability

The wettability of the surface may play an important role in determining the interaction of cells with a specific polymer coating, as discussed in chapter 2. Several studies found that moderate surfaces, displaying properties that can be described as somewhere between hydrophobicity and hydrophilicity, favour good cell adhesion and growth³⁰⁴⁻³⁰⁶. Water contact angles of the PBMA in highly branched and linear architectures, as well as in carboxylic acid and different alkyl diamine functionalities, are listed in Figure 4.3 and Figure 4.4, respectively. A comparison was made between the level of adhesion of the epithelial, fibroblast and cancer cells on the functionalised polymers. From the above results, it can be concluded that there is no correlation between the water contact angles on the various polymer surfaces and the cell number or metabolic activity in the case of epithelial and cancer cells. In the case of fibroblast

cells, although there is a significant and positive correlation between the polymers water contact angles and the fibroblast number as well as metabolic activity, it is interesting to observe that the pyrrole terminated HB polymers with a water contact angle of 84° presented significantly lower cell numbers and metabolic activity than the carboxyl terminated highly branched and linear polymers, that presented similar water contact angle measurements of 77° and 89° respectively. This means that the cell adhesion is not only driven by the wettability but by the chemical functionality too. Specifically, from the above results it can be concluded that the epithelial cells grown better on the aminated and pyrrole functionalised polymers but not on carboxyl terminated functional polymers, while a contrasting behaviour is observed in the case of fibroblast cells on the same substrates. The cancer cells adhered well and proliferated on most the tested polymers. From the results obtained for water contact angles, it might be suggested that these three modified functional polymers have moderately wettable surfaces that can enhance cell adhesion. However, the different types of cells showed different responses to these modified polymers according to functional groups and might be due to the variances in protein expression.

1.2.2 Correlation between surface free energy components and cell behaviour

The surface free energies of synthesised polymers were determined by contact angle and the SFE components calculated according to different approaches, as shown in section 4.2.3. The dispersive, polar and thus total SFE components were determined by the “dispersion-polar” approach, while acid, base, polar, apolar and the total of their SFE components were determined by the “Lifshitz-van der Waals acid-base” approach. Again, the Spearman’s correlation coefficient was used to observe the relationship between the viability of cells on different polymer surfaces and the SFE and its components. The two polymers that were observed to be toxic in the cell culture assays; HB-PBMA:1,2-DAE and HB-PBMA:1,3-DAP, were excluded from the analysis and are only presented in the graphs for comparison reasons. Based on the consistent results derived from the metabolic activity using the Alamar Blue assay and the number of cells using the PicoGreen assay, one type of test was selected to study the correlation between the surface free-energy components and the cell behaviour, and this was the number of cells according to the Pico Green assay. The implementation of the “Lifshitz-van der Waals acid-base” approach allowed for the investigation of how the metabolic activity or the number of cells are correlated with not only the polymers polar γ_S^{AB} and apolar γ_S^{LW} components, but also with the electron donor γ_S^- (basic) and electron acceptor γ_S^+ (acidic)

characters of polymer substrates. The non-polar component is not analysed in this method because its values are the same as the dispersive components in the “dispersion-polar” approach.

1.2.2.1 Human renal epithelial cells

The relationship between the number of HREp cells adhering to the various polymer substrates and the polymers total SFE γ_S^{d-p} and its components, based on “dispersion-polar” theory, is presented in Figure 1.4. No significant correlation was observed between the cell number and the polymers γ_S^p or γ_S^d components and the γ_S^{d-p}

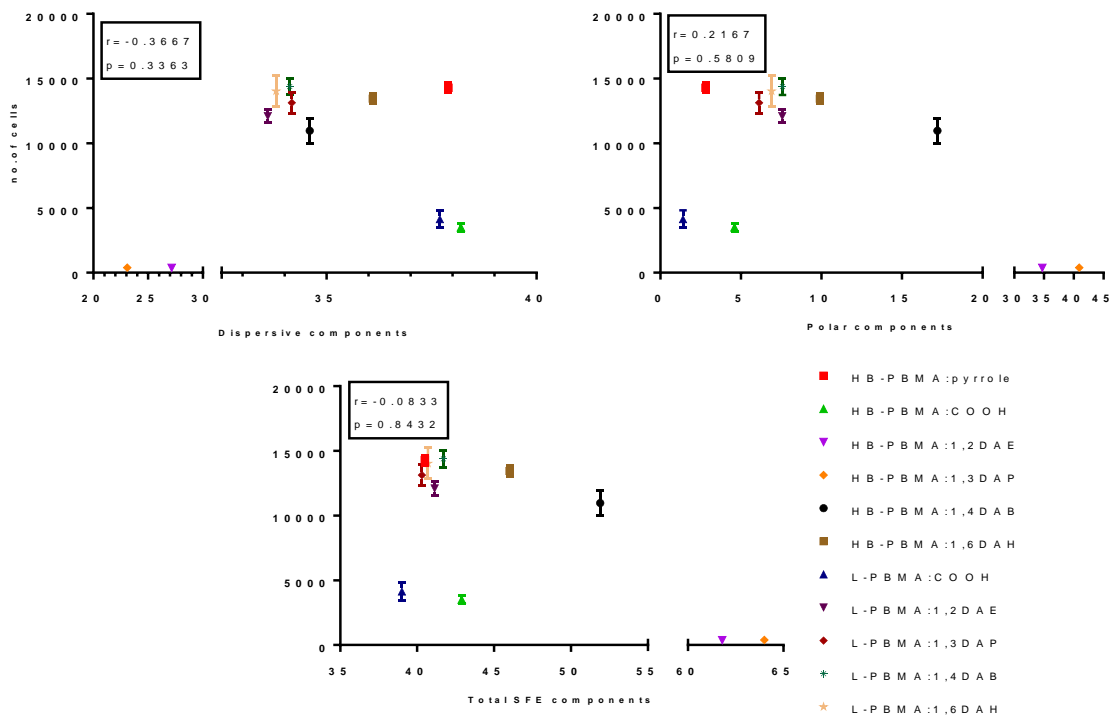


Figure 1.4- Spearman’s correlation between the number of human renal epithelial cells and the total surface energy (γ_S^{d-p}), its dispersive (γ_S^d) and polar(γ_S^p) components, according to the “dispersion-polar” approach

In addition, the “Lifshitz-van der Waals acid-base” approach allowed for the investigation of the relationship between the number of HREp cells and SFE, polar γ_S^{AB} and apolar γ_S^{LW} components, but also with the electron donor γ_S^- (basic) and electron acceptor γ_S^+ (acidic) characters of the polymer substrates, as seen in Figure 1.5. The results revealed no significant correlation between the number of cells and the γ_S^+ , γ_S^- , and γ_S^{AB} components, neither with the γ_S^{LW-AB} .

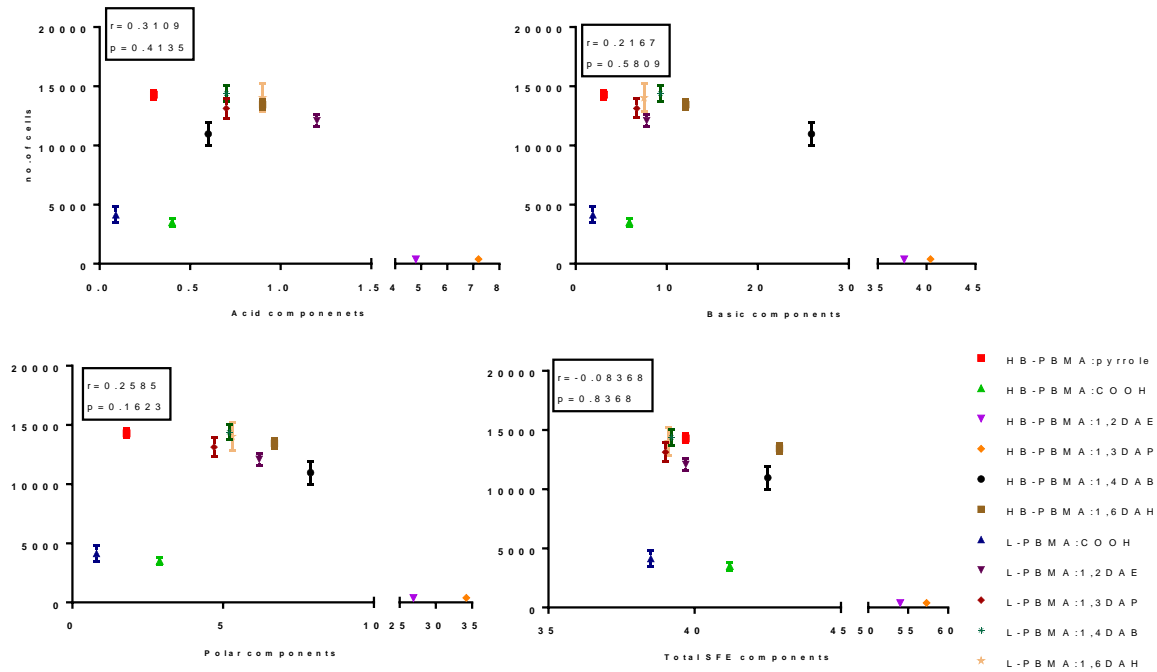


Figure 1.5- Spearman correlation between the number of human renal epithelial cells and the total surface energy (γ_S^{LW-AB}), its electron acceptor (γ_S^+), electron donor (γ_S^-), and polar (γ_S^{AB}) components, according to the “Lifshitz-van der Waals acid-base” approach

1.2.2.2 Human dermal fibroblast cells

The relationship between the number of adherent HDF cells and the total SFE γ_S^{d-p} of the polymer substrates and its components, based on “dispersion-polar” theory, is presented in Figure 1.6. No significant correlation was observed between the number of adherent cells and γ_S^{d-p} and its γ_S^d component, while the number of adherent cells was significantly and negatively correlated to the γ_S^p component ($p < 0.05$). This means that a decrease in the polymers polar component increased the number of HDF adherent cells. As discussed in the case of the water contact angles though (Figure 6.2), it is interesting to observe that substrates with similar values of polar component; pyrrole and carboxylic acid terminal functionality, presented significantly different numbers of adherent cells. Apart therefore from the polar component, it is the chemical functionality that greatly affected the number of adherent cells. It is clear from the Figure 6.6 that the HDF cells preferentially adhered to the carboxyl terminated functionalities, either highly branched or linear.

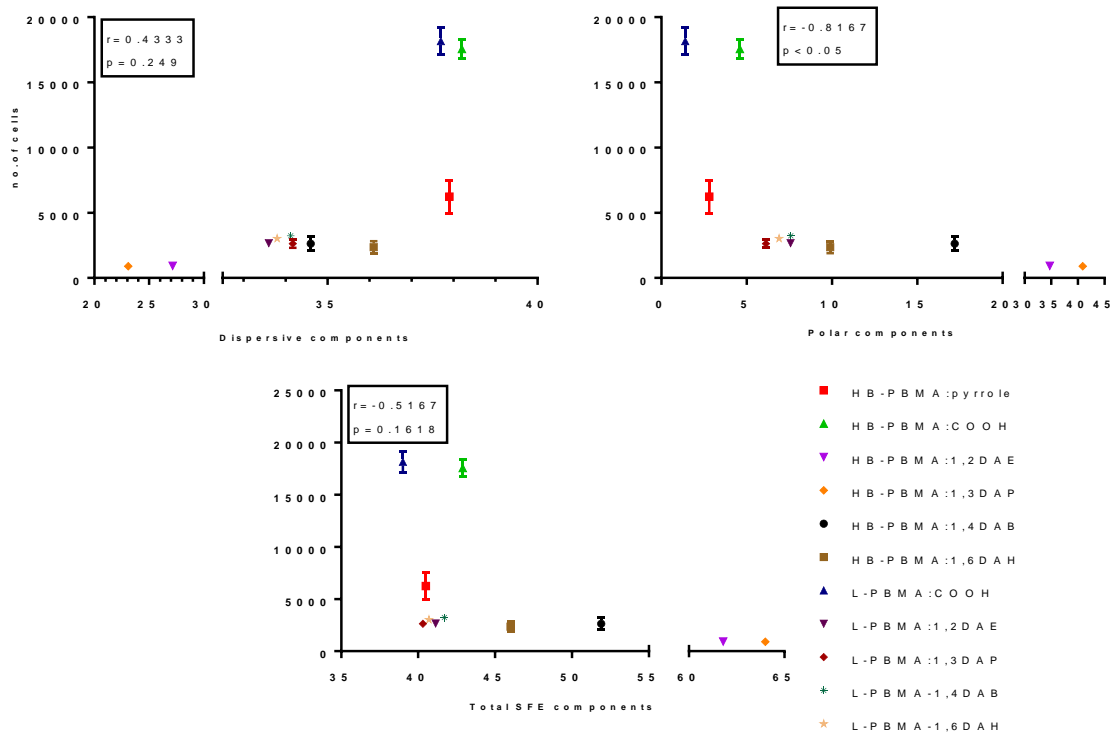


Figure 1.6- Spearman's correlation between the number of human dermal fibroblast cells and the total surface energy (γ_S^{d-p}), its dispersive (γ_S^d) and polar (γ_S^d) components, according to the “dispersion-polar” approach

Following the “Lifshitz-van der Waals acid-base” approach, the relationship between the number of cells and the γ_S^+ , γ_S^- , γ_S^{AB} and γ_S^{LW-AB} characters of the various polymer substrates was investigated and is presented in Figure 1.7. The Spearman's analysis showed that, as in the case of the “dispersion – polar” approach, the number of HDF cells was significantly and negatively correlated with the polar component (γ_S^{AB}) ($p < 0.005$) but not with the γ_S^{LW-AB} . With regards to the electron acceptor (γ_S^+) and electron donor (γ_S^-) characters of the polymer substrates, the results revealed that the number of cells was significantly and negatively correlated with the γ_S^- component ($p < 0.005$) but not with the γ_S^+ . Therefore, the number of HDF cells in cells significantly increased with the decrease in the polymers polar and basic components. As previously, it is again obvious the preference of the HDF cells for the carboxyl terminated functional substrates, either highly branched or linear, in comparison to all the other substrates, even the pyrrole that has similar polar and basic components as the carboxyl terminated ones.

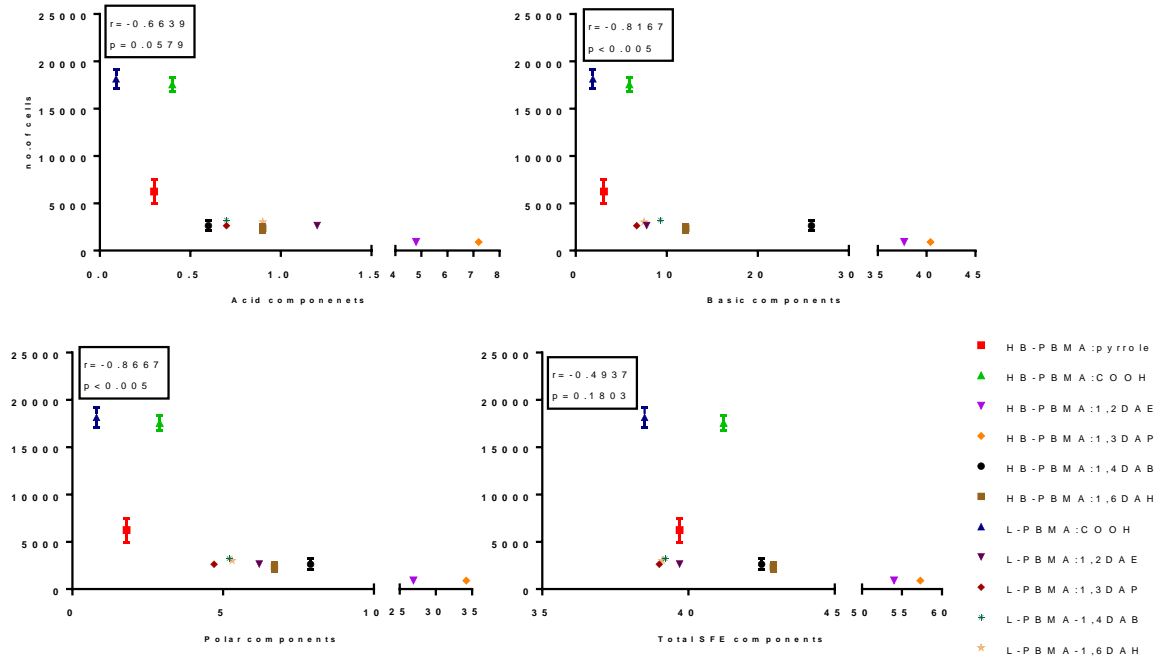


Figure 1.7- Spearman's correlation between the number of human dermal fibroblast cells and the total surface energy (γ_S^{LW-AB}), its electron acceptor (γ_S^+), electron donor (γ_S^-), and polar (γ_S^{AB}) components, according to the "Lifshitz-van der Waals acid-base" approach

1.2.2.3 Human carcinoma epithelial lung cells

The relationship between the number of adherent A549 cells and the total SFE γ_S^{d-p} of the polymer substrates and its components based on the "dispersion-polar" theory has been explored, as seen in Figure 1.8. No significant correlation was observed between the number of cancer cells and the γ_S^d , γ_S^{d-p} and γ_S^p .

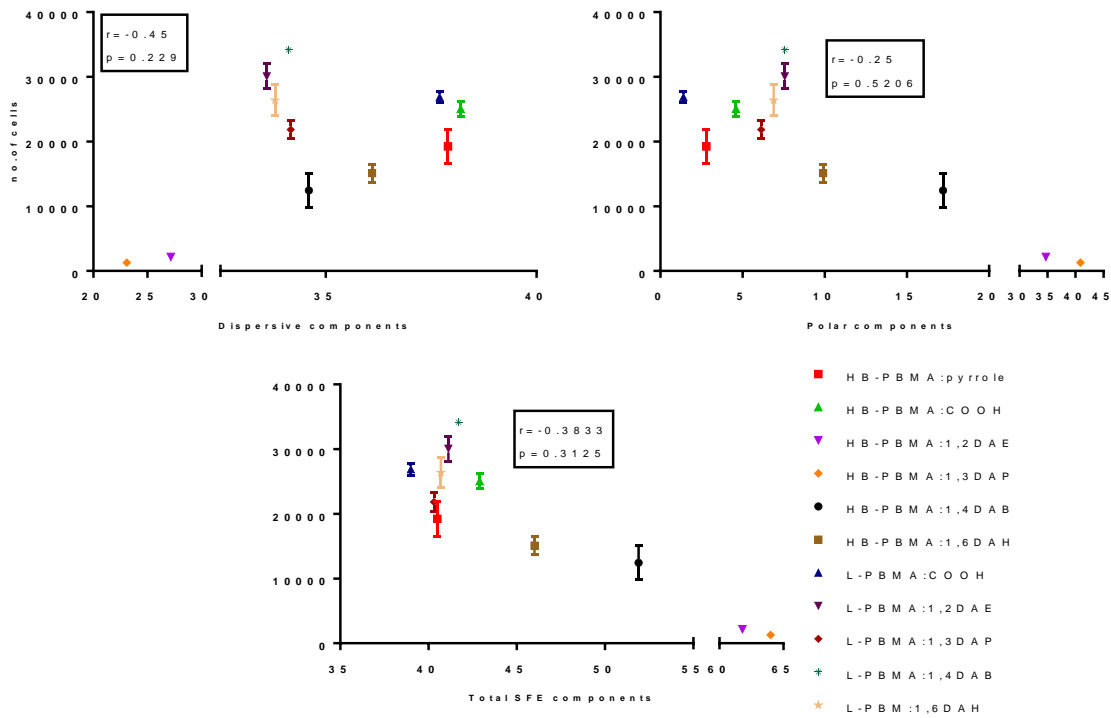


Figure 1.8- Spearman's correlation between the number of human carcinoma cells and the total surface energy (γ_S^{d-p}), its dispersive (γ_S^d) and polar (γ_S^p) components, according to the “dispersion-polar” approach

Furthermore, the “Lifshitz-van der Waals acid-base” approach was used to evaluate the effect of the electron donor γ_S^- (basic) and electron acceptor γ_S^+ (acidic) components of the polymers, alongside their polar γ_S^{AB} and total SFE γ_S^{LW-AB} characters, as shown in Figure 1.9. The results revealed no significant correlation between the cell number and these parameters. The results are essentially similar to those obtained from the “acid-base” approach that showed no significant correlation between the number of the adherent cancer cells and the polymers surface free energy, its polar and dispersion components.

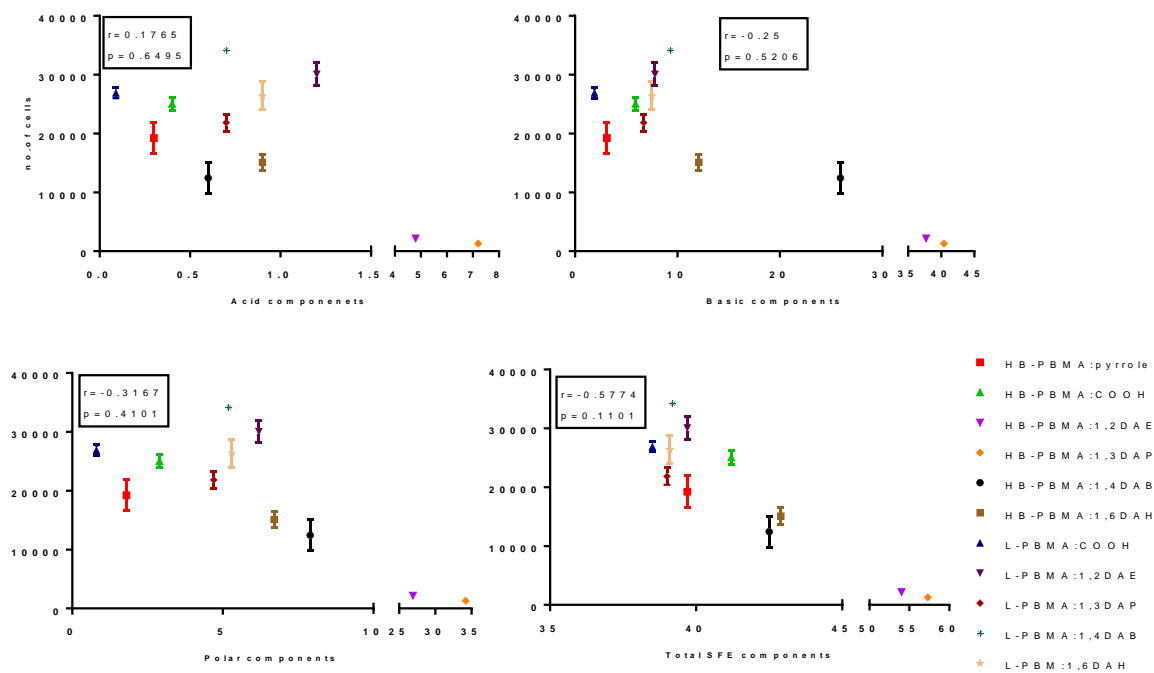


Figure 1.9- Spearman's correlation between the number of human carcinoma cells and the total surface energy (γ_S^{LW-AB}), with its electron acceptor (γ_S^+), electron donor (γ_S^-), and polar (γ_S^{AB}) components, according to "Lifshitz-van der Waals acid-base" approach

The surface free energy (SFE) components of the various polymers were determined by contact angle measurements, according to the "dispersion-polar" and the "Lifshitz-van der Waals acid-base" approaches. The investigation of the relationship between the SFE components and the viability of HRE, A549 and HDF cells was carried out. From all the correlation data between SFE and cell adhesion, it becomes clear that cell adhesion is influenced by the nature of the interaction between the cells and the substrate. Therefore, there was no significant correlation between the SFE components of the various polymer substrate and the adhesion of human renal epithelial and human carcinoma cells, according to both the "dispersion – polar" "Lifshitz-van der Waals acid-base" approaches. It was only the polymers polar and basic components that were significantly and negatively correlated with the adhesion of human dermal fibroblast cells. However, a closer look at these results showed that this correlation was not mainly due to the polymers polar or basic components but rather an effect of the functional groups presents in these materials. In particular, it was due to the preference of the HDF cells for the carboxyl terminated polymers, which have lower polarity and electron donor character compared to the amine terminated polymers. In conclusion, these results suggest that the HRE and HDF cell attachment to polymer surfaces were more sensitive to

differences in the surface chemistry and the end group functionality, rather than the polymers wettability and surface free energy.

It is important to note that for the Spearman's correlation analysis, the linear and highly branched polymers were analysed together. According to the main findings as to the differences between these two structures discussed in chapter 4, the highly branched polymers had a higher surface free energy and polar character in comparison to the linear ones; for both the amine and carboxyl terminated functionality, due to the high density of functional groups and less entanglement materials, which, overall, result in greater steric hinderance³⁰⁷⁻³⁰⁸. Therefore, it may be that the correlation of the polymers wettability or surface energy and cell adhesion was not statically significant due to more than one parameters varying at the same time; chemistry, architecture and wettability. It may be that the correlations could be improved by the separate analysis of the two polymer architectures in regard to the effect of the polymers wettability on the cell adhesion. However, it is not always possible to separate parameters that simultaneously affect the cell adhesion and these are not only the chemistry, the architecture, the wettability, but the topography, the mechanical properties and the surface charges amongst others^{12, 109, 176, 270, 303}.

1.3 CONCLUSION

The main findings of this chapter therefore are that the adhesion of the human renal epithelial cells on the highly branched and linear copolymer coatings was better facilitated by the existence of the amine-terminated polymer, whereas the adhesion of the human dermal fibroblast cells on the copolymer coatings was better facilitated by the existence of the carboxylic acid-terminated polymer. The human carcinoma cells adhered well on most of the tested polymers and no significant correlation was observed between the number of adherent cells and the polymers wettability, surface energy or chemistry. The overall relationship between the polymers wettability - surface free energy and the number of adherent cell was not significant.

2 CONCLUSION AND FUTURE WORK

2.1 SUMMARY AND CONCLUSION

The goal of this work was to produce new polymer surface coatings as solid materials based on the *n*-butyl methacrylate monomer for enhanced cell adhesion *in vitro*. The experiments in this research were designed to test the following hypothesis, alkyl amines could play an essential role in the epithelisation of cells as they can mimic lysine and thus encourage the formation of a cross-linked extracellular matrix. The work has involved the synthesis of new polymers, the technology of coating the synthesised polymers on glass and silicon substrates, the chemical, thermal, physical, mechanical and biological characterisation of the synthesised materials. These characterisations can be important for the design and investigation of new biomaterials and allow the investigation of their suitability for biological and biomedical applications.

In the chemistry part of this research, highly branched polymers in three different molar ratios of *n*-butyl methacrylate BMA as a monomer with 4-vinyl benzyl pyrrole carbodithioate (4-VBPC) as a chain transfer agent CTA were synthesised using RAFT polymerisation. An excess of ACVA was used to replace the end group of HB-PBMA with carboxylic acid functionality. The branched PBMA:COOH of 16:1 molar ratio was selected for the modification of its acid groups into amine functionality, due to observing complete and well converted HB-PBMA to acid functionality without sulphuric content, and the removal of all pyrrole was ensured through elemental analysis, FTIR, ¹HNMR and DOSY-NMR. The aminated branched polymers were synthesised in aqueous solution with different alkyl diamines to obtain the desired polymers. Moreover, linear copolymers of *n*-BMA were also synthesised in the same molar ratio as the branched polymers between BMA and 4-vinyl benzoic acid (4-VBA) by free radical polymerisation to observe the effect of different architectures of the same polymer on the cell culture. These linear polymers already had an acid group through the incorporation of 4-VBA as the co-monomer and then, as branched polymers, these polymers were reacted with diamine to produce amine functionality. These polymers were analysed, and their structures were confirmed via SEC, NMR, FTIR and elemental analysis. All polymers were synthesised in order to obtain an understanding of how polymer surface functionalities and architectures can influence cell attachment and adhesion on polymer coatings.

In the physics part of the research, the thermal, physico-chemical and mechanical properties of linear and highly branched (*n*-butyl methacrylate) polymers were obtained. The incorporation of pyrrole, carboxylic acid or amine functionalities as a copolymer into PBMA had significant effects on the rise in degradation temperature. Thus, it is evident from TGA study that the degradation of copolymers can often proceed via multiple mechanisms. However, the degradation of homo PnBMA is known to occur predominantly by unzipping from the chain ends to yield the monomer. The glass transition (T_g) of polymers was determined from the inflection point of DSC on the second heating cycle. It was seen that the linear polymers had a higher glass transition point compared to highly branched polymers and the T_g increased when modifying terminated polymers into acid or amine functionality. The mechanical properties of different polymer architectures with acidic functionality were determined via AFM. The topography of the highly branched polymers was smoother than that of the linear ones, for spin coated polymers on silicon, however polymer surfaces that were produced by dip coating of coverslips did not show any significant difference in the average surface roughness values. Regarding the mechanical properties, there were no significant differences in stiffness between the two carboxylic acid-functionalised polymers; both the moduli decreased with increasing temperature, but the stiffness was experimentally higher in the case of the linear compared to the highly branched polymers. The wettability of all polymers coatings on the coverslips was measured using water contact angles. The results confirmed that chemically modified polymer surfaces incorporating acid or amine functionalities can change the behaviour of PBMA from a hydrophobic state to a moderately hydrophilic state. In the final experiment in this part, contact angles of three probe liquids (ultrapure water, methylene iodide and glycerol) were used to calculate the surface energy and polarity of all coated polymer surfaces. The results are consistent with the wettability analysis of the adhesion process, for both the “dispersion-polar” and “Lifshitz-van der Waals acid base” approaches and revealed that the polarity of the surface increased, and the polymer appeared to be a moderately hydrophilic/ hydrophobic material with the re-functionalisation of the polymer by acid and amine.

The biology work studied the dependence on the 16:1 molar ratio for all architectures according to their synthesis, re-functionalisation, being soluble in organic solvent and lack of cross-linking obtained. Cell adhesion was studied through three types of cells *in vitro*, by culturing the cells on coverslips with different polymer coating. The A549 lung carcinoma cell line was selected since it is widely used in biological research and to allow comparison with

the results of the adhesion study on coated materials with primary human renal epithelial and human fibroblast cells. Cell adhesion studies were performed on three functional polymers (pyrrole, carboxylic acid and amine) and TCP was used as the control. These studies showed that different functionalities were preferred by different cell types. The biocompatibility and cytotoxicity of these materials were assessed by using the AlamarBlue metabolic assay, PicoGreen quantification assay, and LDH toxicity assay. Also, fluorescence staining with DAPI and phalloidin-TRITC was used to visualise the morphology of the attached cells. Briefly, the results of the AlamarBlue and PicoGreen assays were consistent with each other; namely, when the absorbance of AB is high, the number of cells is also high. The LDH cytotoxicity assay showed contrasting behaviour. This means that if the metabolic activities and number of cells are high, the level of LDH absorbance is low in the same materials. The results of cell adhesion showed that PBMA with acid functionality provided a good surface for fibroblast cells, while PBMA with different primary alkyl amine functionality provided a good surface for epithelial cells. However, A549, as a cancer cell line, adhered well to most polymer surfaces with the exception of the two toxic materials synthesised. The observation confirmed that fibroblast cells behaved differently to epithelial cells, and that they preferred acid functionalised substrates. The explanation for this might be due to their differing biological roles. As mentioned in chapter 2, fibroblast and epithelial cells have variances in their protein expression and thus these cells may have conflicting reactions in some materials.

The last chapter of this thesis demonstrated the relationship between surface wettability of synthesised polymers and cell adhesion work, as well as the correlation between surface free energy components and cell adhesion. The results showed that according to the different architectures of the materials considered, it is difficult to find any real correlation between surface free energy and cell adhesion. The important parameter in this study for growing primary epithelial and fibroblast cells was considered to be the polymer surface functionality. However, the correlation could be improved if the two polymer architectures; linear and highly branched, were analysed separately.

2.2 FUTURE WORK

In the polymer synthesis, the aminated HBPs could be repeated using the DOWFAX 2A1 emulsifier stabiliser instead of SDS as aminated linear polymers. These may improve the incorporation of 1,2-diamonethane and 1,3-diaminopropane into HB-PBMA:COOH end, and further show a decrease in the polarity of the surfaces. Therefore, these surfaces could behave differently to the current one and could potentially be more suitable in cell cultures with reduced toxicity. The comparison of highly branched and linear polymers could be improved if linear polymers were synthesised with a chain transfer agent, and also had their pyrrole end group converted to carboxylic acid and then to alkyl amine functionalities.

In polymer characterisation, acidic functional polymers could be subject to a titration reaction to obtain the amount of acid groups in the polymers, and hence allow the determination of the optimal percentage of acid required for the adhesion of fibroblast cells. Moreover, dynamic light scattering (DLS) could be beneficial for measuring the hydrodynamic radius of polymers and for comparing these results with the DOSY experiments. Additionally, molecular weights, M_w , could be calculated via DOSY NMR through the creation of external curve calibration curves for PBMA to allow for predictions of molecular weight, which could then be compared to the results obtained from the SEC technique.

More investigations using dual detection SEC with viscometry are required to obtain an absolute molar mass and α values to provide information about the topological structure of polymers in solution. Furthermore, using triple detection SEC with the additional capability for light scattering would be useful for providing more information about the branching of the copolymers and calculate the number of branching of each copolymer.

In terms of physical characterisation, it would be useful to determine the mechanical properties of the aminated linear and highly branched polymers by AFM. Moreover, using the hysteresis method, via advancing and receding contact angle would provide information regarding the materials homogeneity; chemical and topological and the results could be compared to the average surface roughness values obtained using the AFM. Furthermore, the surface charge characterisation could be useful to complete the full picture of surface properties and how these affect cell adhesions.

In the biological work, a firm conclusion cannot be reached based on the wealth of the assays that we used, and further work is needed such as a migration assay to evaluate the migrative ability of the cells, a proliferation assay using several time points such as 24, 48, 72 hours to monitor cell growth, and the polymerase chain reaction (PCR) technique to investigate the gene expression of the transglutaminase.

3 REFERENCES

1. Ul Ahad, I.; Bartnik, A.; Fiedorowicz, H.; Kostecki, J.; Korczyk, B.; Ciach, T.; Brabazon, D., Surface modification of polymers for biocompatibility via exposure to extreme ultraviolet radiation. *Journal of Biomedical Materials Research Part A* **2014**, *102* (9), 3298-3310.
2. Ramakrishna, S.; Mayer, J.; Wintermantel, E.; Leong, K. W., Biomedical applications of polymer-composite materials: a review. *Composites science and technology* **2001**, *61* (9), 1189-1224.
3. Burakowska, E.; Quinn, J. R.; Zimmerman, S. C.; Haag, R., Cross-linked hyperbranched polyglycerols as hosts for selective binding of guest molecules. *Journal of the American Chemical Society* **2009**, *131* (30), 10574-10580.
4. Voit, B. I.; Lederer, A., Hyperbranched and Highly Branched Polymer Architectures • Synthetic Strategies and Major Characterization Aspects. *Chemical reviews* **2009**, *109* (11), 5924-5973.
5. Sunder, A.; Hanselmann, R.; Frey, H.; Mülhaupt, R., Controlled synthesis of hyperbranched polyglycerols by ring-opening multibranching polymerization. *Macromolecules* **1999**, *32* (13), 4240-4246.
6. Lim, Y.-b.; Kim, S.-M.; Lee, Y.; Lee, W.-k.; Yang, T.-g.; Lee, M.-j.; Suh, H.; Park, J.-s., Cationic hyperbranched poly (amino ester): a novel class of DNA condensing molecule with cationic surface, biodegradable three-dimensional structure, and tertiary amine groups in the interior. *Journal of the American Chemical Society* **2001**, *123* (10), 2460-2461.
7. Tian, H.; Deng, C.; Lin, H.; Sun, J.; Deng, M.; Chen, X.; Jing, X., Biodegradable cationic PEG-PEI-PBLG hyperbranched block copolymer: synthesis and micelle characterization. *Biomaterials* **2005**, *26* (20), 4209-4217.
8. Deshpande, P.; McKean, R.; Blackwood, K. A.; Senior, R. A.; Ogunbanjo, A.; Ryan, A. J.; MacNeil, S., Using poly (lactide-co-glycolide) electrospun scaffolds to deliver cultured epithelial cells to the cornea. *Regenerative medicine* **2010**, *5* (3), 395-401.
9. France, R.; Short, R.; Dawson, R., Attachment of human keratinocytes to plasma copolymers of acrylic acid/octa-1, 7-diene and allyl amine/octa-1, 7-diene. *Journal of Materials Chemistry* **1998**, *8* (1), 37-42.
10. Daw, R.; Candan, S.; Beck, A.; Devlin, A.; Brook, I.; MacNeil, S.; Dawson, R.; Short, R., Plasma copolymer surfaces of acrylic acid/1, 7 octadiene: surface characterisation and the attachment of ROS 17/2.8 osteoblast-like cells. *Biomaterials* **1998**, *19* (19), 1717-1725.
11. Rimmer, S.; Johnson, C.; Zhao, B.; Collier, J.; Gilmore, L.; Sabnis, S.; Wyman, P.; Sammon, C.; Fullwood, N. J.; MacNeil, S., Epithelialization of hydrogels achieved by amine functionalization and co-culture with stromal cells. *Biomaterials* **2007**, *28* (35), 5319-5331.

12. Hassan, E.; Deshpande, P.; Claeysens, F.; Rimmer, S.; MacNeil, S., Amine functional hydrogels as selective substrates for corneal epithelialization. *Acta biomaterialia* **2014**, *10* (7), 3029-3037.
13. Carter, S.; Hunt, B.; Rimmer, S., Highly branched poly (N-isopropylacrylamide) s with imidazole end groups prepared by radical polymerization in the presence of a styryl monomer containing a dithioester group. *Macromolecules* **2005**, *38* (11), 4595-4603.
14. Carter, S.; Rimmer, S.; Sturdy, A.; Webb, M., Highly Branched Stimuli Responsive Poly [(N-isopropyl acrylamide)-co-(1, 2-propandiol-3-methacrylate)] s with Protein Binding Functionality. *Macromolecular bioscience* **2005**, *5* (5), 373-378.
15. Rimmer, S.; Carter, S.; Rutkaite, R.; Haycock, J. W.; Swanson, L., Highly branched poly-(N-isopropylacrylamide) s with arginine–glycine–aspartic acid (RGD)-or COOH-chain ends that form sub-micron stimulus-responsive particles above the critical solution temperature. *Soft Matter* **2007**, *3* (8), 971-973.
16. Rimmer, S.; German, M. J.; Maughan, J.; Sun, Y.; Fullwood, N.; Ebdon, J.; MacNeil, S., Synthesis and properties of amphiphilic networks 3: preparation and characterization of block conetworks of poly (butyl methacrylate-block-(2, 3 propandiol-1-methacrylate-statethandiol dimethacrylate)). *Biomaterials* **2005**, *26* (15), 2219-2230.
17. Odian, G., *Principles of Polymerisation*. 4 ed.; John Wiley & Sons: 2004.
18. Gao, C.; Yan, D., Hyperbranched polymers: from synthesis to applications. *Progress in Polymer Science* **2004**, *29* (3), 183-275.
19. England, R. M.; Rimmer, S., Hyper/highly-branched polymers by radical polymerisations. *Polymer Chemistry* **2010**, *1* (10), 1533.
20. Wang, D.; Zhao, T.; Zhu, X.; Yan, D.; Wang, W., Bioapplications of hyperbranched polymers. *Chemical Society Reviews* **2015**.
21. Bruchmann, B., Dendritic polymers based on urethane chemistry—syntheses and applications. *Macromolecular Materials and Engineering* **2007**, *292* (9), 981-992.
22. Bruchmann, B.; Königer, R.; Renz, H., Tailor-made crosslinkers for high performance PUR coatings—hyperbranched polyisocyanates. *Macromolecular Symposia* **2002**, *187* (1), 271-280.
23. Wang, Y.; Grayson, S. M., Approaches for the preparation of non-linear amphiphilic polymers and their applications to drug delivery. *Advanced drug delivery reviews* **2012**, *64* (9), 852-865.
24. Chen, S.; Zhang, X.-Z.; Cheng, S.-X.; Zhuo, R.-X.; Gu, Z.-W., Functionalized amphiphilic hyperbranched polymers for targeted drug delivery. *Biomacromolecules* **2008**, *9* (10), 2578-2585.

25. Hong, Y.; Coombs, S.; Cooper-White, J.; Mackay, M.; Hawker, C.; Malmström, E.; Rehnberg, N., Film blowing of linear low-density polyethylene blended with a novel hyperbranched polymer processing aid. *Polymer* **2000**, *41* (21), 7705-7713.
26. Unal, S.; Yilgor, I.; Yilgor, E.; Sheth, J.; Wilkes, G.; Long, T., A new generation of highly branched polymers: hyperbranched, segmented poly (urethane urea) elastomers. *Macromolecules* **2004**, *37* (19), 7081-7084.
27. Alfurhood, J. A.; Bachler, P. R.; Sumerlin, B. S., Hyperbranched polymers via RAFT self-condensing vinyl polymerization. *Polymer Chemistry* **2016**, *7* (20), 3361-3369.
28. Zheng, Y.; Li, S.; Weng, Z.; Gao, C., Hyperbranched polymers: advances from synthesis to applications. *Chemical Society Reviews* **2015**, *44* (12), 4091-4130.
29. Hölter, D.; Burgath, A.; Frey, H., Degree of branching in hyperbranched polymers. *Acta Polymerica* **1997**, *48* (1-2), 30-35.
30. Peter, J.; Khalyavina, A.; Kříž, J.; Bleha, M., Synthesis and gas transport properties of ODPa-TAP-ODA hyperbranched polyimides with various comonomer ratios. *European Polymer Journal* **2009**, *45* (6), 1716-1727.
31. Rogers, M. E.; Long, T. E., *Synthetic methods in step-growth polymers*. John Wiley & Sons: 2003.
32. Cowie, J. M. G.; Arrighi, V., *Polymers: chemistry and physics of modern materials*. CRC press: 2007.
33. Pepper, D., Ionic polymerisation. *Quarterly Reviews, Chemical Society* **1954**, *8* (1), 88-121.
34. Jenkins, A. D.; Jones, R. G.; Moad, G., Terminology for reversible-deactivation radical polymerization previously called "controlled" radical or "living" radical polymerization (IUPAC Recommendations 2010). *Pure and Applied Chemistry* **2009**, *82* (2), 483-491.
35. Fierens, S. K.; D'hooge, D. R.; Van Steenberge, P. H.; Reyniers, M.-F.; Marin, G. B., Exploring the full potential of reversible deactivation radical polymerization using pareto-optimal fronts. *Polymers* **2015**, *7* (4), 655-679.
36. Chiefari, J.; Chong, Y.; Ercole, F.; Krstina, J.; Jeffery, J.; Le, T. P.; Mayadunne, R. T.; Meijs, G. F.; Moad, C. L.; Moad, G., Living free-radical polymerization by reversible addition-fragmentation chain transfer: the RAFT process. *Macromolecules* **1998**, *31* (16), 5559-5562.
37. Gilbert, M., *Brydson's Plastics Materials*. William Andrew: 2016.
38. Lei, L.; Tanishima, M.; Goto, A.; Kaji, H., Living Radical Polymerization via Organic Superbase Catalysis. *Polymers* **2014**, *6* (3), 860-872.
39. Goto, A.; Fukuda, T., Kinetics of living radical polymerization. *Progress in Polymer Science* **2004**, *29* (4), 329-385.

40. Fischer, H., The persistent radical effect: a principle for selective radical reactions and living radical polymerizations. *Chemical Reviews* **2001**, *101* (12), 3581-3610.
41. Michael, K. G.; Veregin, P., Narrow Molecular Weight Resins by a Table I. Polymerization of Styrene (TEMPO/BPO= 13) Free-Radical Polymerization Process sample convn (%) rmtime (h) M.(1W) M,(1W3) PD. *Macromolecules* **1993**, *26*, 2987-2988.
42. Wang, J.-S.; Matyjaszewski, K., Controlled/" living" radical polymerization. Atom transfer radical polymerization in the presence of transition-metal complexes. *Journal of the American Chemical Society* **1995**, *117* (20), 5614-5615.
43. Kato, M.; Kamigaito, M.; Sawamoto, M.; Higashimura, T., Polymerization of methyl methacrylate with the carbon tetrachloride/dichlorotris-(triphenylphosphine) ruthenium (II)/methylaluminum bis (2, 6-di-tert-butylphenoxide) initiating system: possibility of living radical polymerization. *Macromolecules* **1995**, *28* (5), 1721-1723.
44. Gaynor, S. G.; Wang, J.-S.; Matyjaszewski, K., Controlled radical polymerization by degenerative transfer-effect of the structure of the transfer agent. *Macromolecules* **1995**, *28* (24), 8051-8056.
45. Flory, P. J., Molecular size distribution in three dimensional polymers. I. Gelation1. *Journal of the American Chemical Society* **1941**, *63* (11), 3083-3090.
46. Flory, P. J., Molecular size distribution in three dimensional polymers. VI. Branched polymers containing A—R—Bf-1 type units. *Journal of the American Chemical Society* **1952**, *74* (11), 2718-2723.
47. Emrick, T.; Chang, H.-T.; Frechet, J. M., An A2+ B3 approach to hyperbranched aliphatic polyethers containing chain end epoxy substituents. *Macromolecules* **1999**, *32* (19), 6380-6382.
48. Fréchet, J. M.; Hawker, C. J., Hyperbranched polyphenylene and hyperbranched polyesters: new soluble, three-dimensional, reactive polymers. *Reactive and Functional Polymers* **1995**, *26* (1), 127-136.
49. Alfurhood, J. A.; Sun, H.; Bachler, P. R.; Sumerlin, B. S., Hyperbranched poly (N-(2-hydroxypropyl) methacrylamide) via RAFT self-condensing vinyl polymerization. *Polymer Chemistry* **2016**, *7* (11), 2099-2104.
50. Liu, M.; Vladimirov, N.; Fréchet, J. M., A new approach to hyperbranched polymers by ring-opening polymerization of an AB monomer: 4-(2-hydroxyethyl)-ε-caprolactone. *Macromolecules* **1999**, *32* (20), 6881-6884.
51. Suzuki, M.; Li, A.; Saegusa, T., Multibranching polymerization: palladium-catalyzed ring-opening polymerization of cyclic carbamate to produce hyperbranched dendritic polyamine. *Macromolecules* **1992**, *25* (25), 7071-7072.
52. O'brien, N.; McKee, A.; Sherrington, D.; Slark, A.; Titterton, A., Facile, versatile and cost effective route to branched vinyl polymers. *Polymer* **2000**, *41* (15), 6027-6031.

-
53. Chisholm, M.; Hudson, N.; Kirtley, N.; Vilela, F.; Sherrington, D. C., Application of the “strathclyde route” to branched vinyl polymers in suspension polymerization: architectural, thermal, and rheological characterization of the derived branched products. *Macromolecules* **2009**, *42* (20), 7745-7752.
54. Ishida, Y.; Sun, A. C.; Jikei, M.; Kakimoto, M.-a., Synthesis of hyperbranched aromatic polyamides starting from dendrons as AB_x monomers: effect of monomer multiplicity on the degree of branching. *Macromolecules* **2000**, *33* (8), 2832-2838.
55. Huang, W.; Gu, W.; Yang, H.; Xue, X.; Jiang, B.; Zhang, D.; Fang, J.; Chen, J.; Yang, Y.; Guo, J., Preparation and Properties of Branched Polystyrene through Radical Suspension Polymerization. *Polymers* **2017**, *9* (1), 14.
56. Simon, P. F.; Radke, W.; Müller, A. H., Hyperbranched methacrylates by self-condensing group transfer polymerization. *Macromolecular rapid communications* **1997**, *18* (9), 865-873.
57. Charleux, B.; Faust, R., Synthesis of branched polymers by cationic polymerization. In *Branched Polymers I*, Springer: 1999; pp 1-69.
58. Baskaran, D., Hyperbranched polymers from divinylbenzene and 1, 3-diisopropenylbenzene through anionic self-condensing vinyl polymerization. *Polymer* **2003**, *44* (8), 2213-2220.
59. Ishizu, K.; Shibuya, T.; Kawauchi, S., Kinetics on formation of hyperbranched poly(ethyl methacrylate) via a controlled radical mechanism of photofunctional inimer. *Macromolecules* **2003**, *36* (10), 3505-3510.
60. Graff, R. W.; Wang, X.; Gao, H., Exploring Self-Condensing Vinyl Polymerization of Inimers in Microemulsion To Regulate the Structures of Hyperbranched Polymers. *Macromolecules* **2015**, *48* (7), 2118-2126.
61. Sun, H.; Kabb, C. P.; Sumerlin, B. S., Thermally-labile segmented hyperbranched copolymers: using reversible-covalent chemistry to investigate the mechanism of self-condensing vinyl copolymerization. *Chemical Science* **2014**, *5* (12), 4646-4655.
62. Tao, Y.; He, J.; Wang, Z.; Pan, J.; Jiang, H.; Chen, S.; Yang, Y., Synthesis of branched polystyrene and poly(styrene-*b*-4-methoxystyrene) by nitroxyl stable radical controlled polymerization. *Macromolecules* **2001**, *34* (14), 4742-4748.
63. Hill, M. R.; Carmean, R. N.; Sumerlin, B. S., Expanding the Scope of RAFT Polymerization: Recent Advances and New Horizons. *Macromolecules* **2015**, *48* (16), 5459-5469.
64. Wang, Z.; He, J.; Tao, Y.; Yang, L.; Jiang, H.; Yang, Y., Controlled chain branching by RAFT-based radical polymerization. *Macromolecules* **2003**, *36* (20), 7446-7452.
65. Roy, S. G.; De, P., Facile RAFT synthesis of side-chain amino acids containing pH-responsive hyperbranched and star architectures. *Polymer Chemistry* **2014**, *5* (21), 6365-6378.

-
66. Jang, J.; Oh, J. H.; Moon, S. I., Crystallization behavior of poly (ethylene terephthalate) blended with hyperbranched polymers: the effect of terminal groups and composition of hyperbranched polymers. *Macromolecules* **2000**, *33* (5), 1864-1870.
67. Ajroldi, G.; Pezzin, G.; Palma, G., Influence of branching on melt viscosity of polydisperse polymers. *Rheologica Acta* **1971**, *10* (3), 418-421.
68. Chen, H.; Kong, J., Hyperbranched polymers from A₂+ B₃ strategy: recent advances in description and control of fine topology. *Polymer Chemistry* **2016**, *7* (22), 3643-3663.
69. Striegel, A.; Yau, W. W.; Kirkland, J. J.; Bly, D. D., *Modern size-exclusion liquid chromatography: practice of gel permeation and gel filtration chromatography*. John Wiley & Sons: 2009.
70. Grubisic, Z.; Rempp, P.; Benoit, H., A universal calibration for gel permeation chromatography. *Journal of Polymer Science Part C: Polymer Letters* **1967**, *5* (9), 753-759.
71. Striegel, A. M., *Multiple detection in size-exclusion chromatography of macromolecules*. ACS Publications: 2005.
72. Kostanski, L. K.; Keller, D. M.; Hamielec, A. E., Size-exclusion chromatography—a review of calibration methodologies. *Journal of biochemical and biophysical methods* **2004**, *58* (2), 159-186.
73. Saunders, G.; Cormack, P. A.; Graham, S.; Sherrington, D. C., Use of rapid triple detection size exclusion chromatography to evaluate the evolution of molar mass and branching architecture during free radical branching copolymerization of methyl methacrylate and ethylene glycol dimethacrylate. *Macromolecules* **2005**, *38* (15), 6418-6422.
74. Gaborieau, M.; Castignolles, P., Size-exclusion chromatography (SEC) of branched polymers and polysaccharides. *Analytical and bioanalytical chemistry* **2011**, *399* (4), 1413-1423.
75. Brandrup, J.; Immergut, E. H.; Grulke, E. A.; Abe, A.; Bloch, D. R., *Polymer handbook*. Wiley New York etc: 1989; Vol. 7.
76. Yan, D., Intrinsic viscosity of polymer solutions: fresh ideas to an old problem. *Science China Chemistry* **2015**, *58* (5), 835-838.
77. Das, T.; Sengupta, S.; Ghorai, U. K.; Dey, A.; Bandyopadhyay, A., Sequential amphiphilic and pH responsive hyperbranched copolymer: influence of hyper branching/pendant groups on reversible self assembling from polymersomes to aggregates and usefulness in waste water treatment. *RSC Advances* **2015**, *5* (124), 102932-102941.
78. Willcock, H.; O'Reilly, R. K., End group removal and modification of RAFT polymers. *Polymer Chemistry* **2010**, *1* (2), 149-157.
79. Moad, G.; Rizzardo, E.; Thang, S. H., Living radical polymerization by the RAFT process. *Australian Journal of Chemistry* **2005**, *58* (6), 379-410.

-
80. Quinn, J. F.; Rizzardo, E.; Davis, T. P., Ambient temperature reversible addition–fragmentation chain transfer polymerisation. *Chemical Communications* **2001**, (11), 1044-1045.
81. Aldrich, S., RAFT: Choosing the Right Agent to Achieve Controlled Polymerization. In <http://www.sigmaaldrich.com/materials-science/polymer-science/raft-polymerization.html>, 2012.
82. Moad, G.; Rizzardo, E.; Thang, S. H., End-functional polymers, thiocarbonylthio group removal/transformation and reversible addition-fragmentation-chain transfer (RAFT) polymerization. *Polymer International* **2011**, *60* (1), 9-25.
83. Gibson, M. I.; Fröhlich, E.; Klok, H. A., Postpolymerization modification of poly (pentafluorophenyl methacrylate): Synthesis of a diverse water-soluble polymer library. *Journal of Polymer Science Part A: Polymer Chemistry* **2009**, *47* (17), 4332-4345.
84. Pissuwan, D.; Boyer, C.; Gunasekaran, K.; Davis, T. P.; Bulmus, V., In vitro cytotoxicity of RAFT polymers. *Biomacromolecules* **2010**, *11* (2), 412-420.
85. Chang, C.-W.; Bays, E.; Tao, L.; Alconcel, S. N.; Maynard, H. D., Differences in cytotoxicity of poly (PEGA) s synthesized by reversible addition–fragmentation chain transfer polymerization. *Chemical Communications* **2009**, (24), 3580-3582.
86. Keddie, D. J.; Moad, G.; Rizzardo, E.; Thang, S. H., RAFT agent design and synthesis. *Macromolecules* **2012**, *45* (13), 5321-5342.
87. Perrier, S.; Takolpuckdee, P.; Mars, C. A., Reversible addition-fragmentation chain transfer polymerization: End group modification for functionalized polymers and chain transfer agent recovery. *Macromolecules* **2005**, *38* (6), 2033-2036.
88. Chong, Y. K.; Moad, G.; Rizzardo, E.; Thang, S. H., Thiocarbonylthio end group removal from RAFT-synthesized polymers by radical-induced reduction. *Macromolecules* **2007**, *40* (13), 4446-4455.
89. Hopkins, S.; Carter, S. R.; Haycock, J. W.; Fullwood, N. J.; MacNeil, S.; Rimmer, S., Sub-micron poly(N-isopropylacrylamide) particles as temperature responsive vehicles for the detachment and delivery of human cells. *Soft Matter* **2009**, *5* (24), 4928.
90. Klee, D.; Höcker, H., Polymers for biomedical applications: improvement of the interface compatibility. In *Biomedical Applications Polymer Blends*, Springer: 1999; pp 1-57.
91. Tabata, Y., Biomaterials design of culture substrates for cell research. *Inflammation and regeneration* **2011**, *31* (2), 137-145.
92. Poncin-Epaillard, F.; Vrlinic, T.; Debarnot, D.; Mozetic, M.; Coudreuse, A.; Legeay, G.; El Moualij, B.; Zorzi, W., Surface treatment of polymeric materials controlling the adhesion of biomolecules. *Journal of functional biomaterials* **2012**, *3* (3), 528-543.
93. Nair, L. S.; Laurencin, C. T., Biodegradable polymers as biomaterials. *Progress in polymer science* **2007**, *32* (8), 762-798.

-
94. Ratner, B. D.; Hoffman, A. S.; Schoen, F. J.; Lemons, J. E., *Biomaterials science: an introduction to materials in medicine*. Academic press: 2004.
95. Dhandayuthapani, B.; Yoshida, Y.; Maekawa, T.; Kumar, D. S., Polymeric scaffolds in tissue engineering application: a review. *International Journal of Polymer Science* **2011**, 2011.
96. Pinchuk, L., A review of the biostability and carcinogenicity of polyurethanes in medicine and the new generation of 'biostable' polyurethanes. *Journal of Biomaterials Science, Polymer Edition* **1995**, 6 (3), 225-267.
97. Shoichet, M. S., Polymer scaffolds for biomaterials applications. *Macromolecules* **2009**, 43 (2), 581-591.
98. Elbert, D. L.; Hubbell, J. A., Surface treatments of polymers for biocompatibility. *Annual Review of Materials Science* **1996**, 26 (1), 365-394.
99. Neff, J.; Caldwell, K.; Tresco, P. A., A novel method for surface modification to promote cell attachment to hydrophobic substrates. *Journal of biomedical materials research* **1998**, 40 (4), 511-519.
100. Park, J. B.; Bronzino, J. D., *Biomaterials: principles and applications*. crc press: 2002.
101. Godbey, W.; Atala, A., In vitro systems for tissue engineering. *Annals of the New York Academy of Sciences* **2002**, 961 (1), 10-26.
102. Black, J.; Hastings, G., *Handbook of biomaterial properties*. Springer Science & Business Media: 2013.
103. Kostanski, L. K.; Huang, R.; Filipe, C. D.; Ghosh, R., Interpenetrating polymer networks as a route to tunable multi-responsive biomaterials: development of novel concepts. *Journal of Biomaterials Science, Polymer Edition* **2009**, 20 (3), 271-297.
104. Ilagan, B. G.; Amsden, B. G., Surface modifications of photocrosslinked biodegradable elastomers and their influence on smooth muscle cell adhesion and proliferation. *Acta biomaterialia* **2009**, 5 (7), 2429-2440.
105. Perlin, L.; MacNeil, S.; Rimmer, S., Cell adhesive hydrogels synthesised by copolymerisation of arg-protected Gly-Arg-Gly-Asp-Ser methacrylate monomers and enzymatic deprotection. *Chemical Communications* **2008**, (45), 5951-5953.
106. Knight, C. G.; Morton, L. F.; Peachey, A. R.; Tuckwell, D. S.; Farndale, R. W.; Barnes, M. J., The Collagen-binding A-domains of Integrins $\alpha 1\beta 1$ and $\alpha 2\beta 1$ recognize the same specific amino acid sequence, GFOGER, in native (Triple-helical) collagens. *Journal of Biological Chemistry* **2000**, 275 (1), 35-40.
107. Hersel, U.; Dahmen, C.; Kessler, H., RGD modified polymers: biomaterials for stimulated cell adhesion and beyond. *Biomaterials* **2003**, 24 (24), 4385-4415.

-
108. Haddow, D. B.; Steele, D.; Short, R.; Dawson, R.; MacNeil, S., Plasma-polymerized surfaces for culture of human keratinocytes and transfer of cells to an in vitro wound-bed model. *Journal of biomedical materials research Part A* **2003**, *64* (1), 80-87.
109. Johnson, C.; Perlin, L.; Wyman, P.; Zhao, B.; Fullwood, N. J.; MacNeil, S.; Rimmer, S., Cell Adhesion to Polymethacrylate Networks Prepared by Photopolymerization and Functionalized with GRGDS Peptide or Fibrinogen. *Macromolecular Symposia* **2010**, *291-292* (1), 314-325.
110. Lakard, S.; Morrand-Villeneuve, N.; Lesniewska, E.; Lakard, B.; Michel, G.; Herlem, G.; Gharbi, T.; Fahys, B., Synthesis of polymer materials for use as cell culture substrates. *Electrochimica Acta* **2007**, *53* (3), 1114-1126.
111. Saltzman, W. M.; Kyriakides, T. R., Cell interactions with polymers. *Principles of tissue engineering* **2000**, *3*.
112. Vroman, L.; Adams, A.; Fischer, G.; Munoz, P., Interaction of high molecular weight kininogen, factor XII, and fibrinogen in plasma at interfaces. *Blood* **1980**, *55* (1), 156-159.
113. Vilaseca, P.; Dawson, K. A.; Franzese, G., Understanding and modulating the competitive surface-adsorption of proteins through coarse-grained molecular dynamics simulations. *Soft Matter* **2013**, *9* (29), 6978-6985.
114. Fabrizio-Homan, D.; Cooper, S., A comparison of the adsorption of three adhesive proteins to biomaterial surfaces. *Journal of Biomaterials Science, Polymer Edition* **1992**, *3* (1), 27-47.
115. Smith, B. A.; Sefton, M. V., Thrombin and albumin adsorption to PVA and heparin-PVA hydrogels. 2: Competition and displacement. *Journal of Biomedical Materials Research Part A* **1993**, *27* (1), 89-95.
116. Keselowsky, B. G.; Collard, D. M.; García, A. J., Surface chemistry modulates fibronectin conformation and directs integrin binding and specificity to control cell adhesion. *Journal of Biomedical Materials Research Part A* **2003**, *66* (2), 247-259.
117. Nuttelman, C. R.; Mortisen, D. J.; Henry, S. M.; Anseth, K. S., Attachment of fibronectin to poly (vinyl alcohol) hydrogels promotes NIH3T3 cell adhesion, proliferation, and migration. *Journal of biomedical materials research* **2001**, *57* (2), 217-223.
118. Chen, C. S.; Mrksich, M.; Huang, S.; Whitesides, G. M.; Ingber, D. E., Geometric control of cell life and death. *Science* **1997**, *276* (5317), 1425-1428.
119. Chen, L.; Yan, C.; Zheng, Z., Functional polymer surfaces for controlling cell behaviors. *Materials Today* **2017**.
120. Khalili, A. A.; Ahmad, M. R., A review of cell adhesion studies for biomedical and biological applications. *International journal of molecular sciences* **2015**, *16* (8), 18149-18184.
121. Anselme, K., Osteoblast adhesion on biomaterials. *Biomaterials* **2000**, *21* (7), 667-681.

-
122. Wilson, C. J.; Clegg, R. E.; Leavesley, D. I.; Percy, M. J., Mediation of biomaterial-cell interactions by adsorbed proteins: a review. *Tissue engineering* **2005**, *11* (1-2), 1-18.
123. Horbett, T. A.; Schway, M. B.; Ratner, B. D., Hydrophilic-hydrophobic copolymers as cell substrates: Effect on 3T3 cell growth rates. *Journal of colloid and interface science* **1985**, *104* (1), 28-39.
124. Khang, G.; Choe, J. H.; Rhee, J. M.; Lee, H. B., Interaction of different types of cells on physicochemically treated poly (L-lactide-co-glycolide) surfaces. *Journal of applied polymer science* **2002**, *85* (6), 1253-1262.
125. Dowling, D. P.; Miller, I. S.; Ardhaoui, M.; Gallagher, W. M., Effect of surface wettability and topography on the adhesion of osteosarcoma cells on plasma-modified polystyrene. *Journal of biomaterials applications* **2010**.
126. Chang, H.-I.; Wang, Y., Cell responses to surface and architecture of tissue engineering scaffolds. In *Regenerative medicine and tissue engineering-cells and biomaterials*, InTech: 2011.
127. Webb, K.; Hlady, V.; Tresco, P. A., Relative importance of surface wettability and charged functional groups on NIH 3T3 fibroblast attachment, spreading, and cytoskeletal organization. *Journal of biomedical materials research* **1998**, *41* (3), 422.
128. Yang, Z.; Galloway, J. A.; Yu, H., Protein interactions with poly (ethylene glycol) self-assembled monolayers on glass substrates: diffusion and adsorption. *Langmuir* **1999**, *15* (24), 8405-8411.
129. Tziampazis, E.; Kohn, J.; Moghe, P. V., PEG-variant biomaterials as selectively adhesive protein templates: model surfaces for controlled cell adhesion and migration. *Biomaterials* **2000**, *21* (5), 511-520.
130. Lensen, M. C.; Schulte, V. A.; Diez, M., Cell adhesion and spreading on an intrinsically anti-adhesive PEG biomaterial. In *Biomaterials-Physics and Chemistry*, InTech: 2011.
131. Dong, B.; Manolache, S.; Wong, A. C.; Denes, F. S., Antifouling ability of polyethylene glycol of different molecular weights grafted onto polyester surfaces by cold plasma. *Polymer Bulletin* **2011**, *66* (4), 517-528.
132. Pasche, S.; Textor, M.; Meagher, L.; Spencer, N. D.; Griesser, H. J., Relationship between interfacial forces measured by colloid-probe atomic force microscopy and protein resistance of poly (ethylene glycol)-grafted poly (L-lysine) adlayers on niobia surfaces. *Langmuir* **2005**, *21* (14), 6508-6520.
133. Shahkaramipour, N.; Tran, T. N.; Ramanan, S.; Lin, H., Membranes with Surface-Enhanced Antifouling Properties for Water Purification. *Membranes* **2017**, *7* (1), 13.
134. Ma, Z.; Gao, C.; Gong, Y.; Shen, J., Chondrocyte behaviors on poly-L-lactic acid (PLLA) membranes containing hydroxyl, amide or carboxyl groups. *Biomaterials* **2003**, *24* (21), 3725-3730.

-
135. Ma, Z.; Gao, C.; Yuan, J.; Ji, J.; Gong, Y.; Shen, J., Surface modification of poly-L-lactide by photografting of hydrophilic polymers towards improving its hydrophilicity. *Journal of applied polymer science* **2002**, *85* (10), 2163-2171.
136. Kishida, A.; Iwata, H.; Tamada, Y.; Ikada, Y., Cell behaviour on polymer surfaces grafted with non-ionic and ionic monomers. *Biomaterials* **1991**, *12* (8), 786-792.
137. Wang, K.; Zhou, C.; Hong, Y.; Zhang, X., A review of protein adsorption on bioceramics. *Interface focus* **2012**, rsfs20120012.
138. Zhu, X.; Fan, H.; Zhao, C.; Lu, J.; Ikoma, T.; Tanaka, J.; Zhang, X., Competitive adsorption of bovine serum albumin and lysozyme on characterized calcium phosphates by polyacrylamide gel electrophoresis method. *Journal of Materials Science: Materials in Medicine* **2007**, *18* (11), 2243-2249.
139. Bet, M.; Goissis, G.; Vargas, S.; Selistre-de-Araujo, H., Cell adhesion and cytotoxicity studies over polyanionic collagen surfaces with variable negative charge and wettability. *Biomaterials* **2003**, *24* (1), 131-137.
140. Atala, A.; Lanza, R.; Thomson, J. A.; Nerem, R., *Principles of regenerative medicine*. Academic Press: 2010.
141. Schneider, G. B.; English, A.; Abraham, M.; Zaharias, R.; Stanford, C.; Keller, J., The effect of hydrogel charge density on cell attachment. *Biomaterials* **2004**, *25* (15), 3023-3028.
142. Dadsetan, M.; Pumberger, M.; Casper, M. E.; Shogren, K.; Giuliani, M.; Ruesink, T.; Hefferan, T. E.; Currier, B. L.; Yaszemski, M. J., The effects of fixed electrical charge on chondrocyte behavior. *Acta biomaterialia* **2011**, *7* (5), 2080-2090.
143. Chen, L.; Mccrate, J. M.; Lee, J. C.; Li, H., The role of surface charge on the uptake and biocompatibility of hydroxyapatite nanoparticles with osteoblast cells. *Nanotechnology* **2011**, *22* (10), 105708.
144. Lee, J. H.; Jung, H. W.; Kang, I.-K.; Lee, H. B., Cell behaviour on polymer surfaces with different functional groups. *Biomaterials* **1994**, *15* (9), 705-711.
145. Vagaská, B.; Bacakova, L.; Filová, E.; Balík, K., Osteogenic cells on bio-inspired materials for bone tissue engineering. *Physiological research* **2010**, *59* (3), 309.
146. Lee, S. J.; San Choi, J.; Park, K. S.; Khang, G.; Lee, Y. M.; Lee, H. B., Response of MG63 osteoblast-like cells onto polycarbonate membrane surfaces with different micropore sizes. *Biomaterials* **2004**, *25* (19), 4699-4707.
147. Huang, H.-H.; Ho, C.-T.; Lee, T.-H.; Lee, T.-L.; Liao, K.-K.; Chen, F.-L., Effect of surface roughness of ground titanium on initial cell adhesion. *Biomolecular engineering* **2004**, *21* (3), 93-97.
148. De Bartolo, L.; Rende, M.; Morelli, S.; Giusi, G.; Salerno, S.; Piscioneri, A.; Gordano, A.; Di Vito, A.; Canonaco, M.; Drioli, E., Influence of membrane surface properties on the

- growth of neuronal cells isolated from hippocampus. *Journal of Membrane Science* **2008**, *325* (1), 139-149.
149. Chung, T.-W.; Liu, D.-Z.; Wang, S.-Y.; Wang, S.-S., Enhancement of the growth of human endothelial cells by surface roughness at nanometer scale. *Biomaterials* **2003**, *24* (25), 4655-4661.
150. Janmey, P. A.; Winer, J. P.; Murray, M. E.; Wen, Q., The hard life of soft cells. *Cell motility and the cytoskeleton* **2009**, *66* (8), 597-605.
151. Nemir, S.; West, J. L., Synthetic materials in the study of cell response to substrate rigidity. *Annals of biomedical engineering* **2010**, *38* (1), 2-20.
152. Wong, J. Y.; Leach, J. B.; Brown, X. Q., Balance of chemistry, topography, and mechanics at the cell–biomaterial interface: issues and challenges for assessing the role of substrate mechanics on cell response. *Surface Science* **2004**, *570* (1), 119-133.
153. Yeung, T.; Georges, P. C.; Flanagan, L. A.; Marg, B.; Ortiz, M.; Funaki, M.; Zahir, N.; Ming, W.; Weaver, V.; Janmey, P. A., Effects of substrate stiffness on cell morphology, cytoskeletal structure, and adhesion. *Cell motility and the cytoskeleton* **2005**, *60* (1), 24-34.
154. Yeung, T.; Georges, P. C.; Flanagan, L. A.; Marg, B.; Ortiz, M.; Funaki, M.; Zahir, N.; Ming, W.; Weaver, V.; Janmey, P. A., Effects of substrate stiffness on cell morphology, cytoskeletal structure, and adhesion. *Cytoskeleton* **2005**, *60* (1), 24-34.
155. Khatiwala, C. B.; Peyton, S. R.; Metzke, M.; Putnam, A. J., The regulation of osteogenesis by ECM rigidity in MC3T3-E1 cells requires MAPK activation. *Journal of cellular physiology* **2007**, *211* (3), 661-672.
156. Engler, A. J.; Sen, S.; Sweeney, H. L.; Discher, D. E., Matrix elasticity directs stem cell lineage specification. *Cell* **2006**, *126* (4), 677-689.
157. Engler, A.; Bacakova, L.; Newman, C.; Hategan, A.; Griffin, M.; Discher, D., Substrate compliance versus ligand density in cell on gel responses. *Biophysical journal* **2004**, *86* (1), 617-628.
158. Flanagan, L. A.; Ju, Y.-E.; Marg, B.; Osterfield, M.; Janmey, P. A., Neurite branching on deformable substrates. *Neuroreport* **2002**, *13* (18), 2411.
159. Handorf, A. M.; Zhou, Y.; Halanski, M. A.; Li, W.-J., Tissue stiffness dictates development, homeostasis, and disease progression. *Organogenesis* **2015**, *11* (1), 1-15.
160. Freshney, R. I.; Freshney, M. G., *Culture of epithelial cells*. John Wiley & Sons: 2004; Vol. 10.
161. Kojima, K.; Bonassar, L. J.; Roy, A. K.; Mizuno, H.; Cortiella, J.; Vacanti, C. A., A composite tissue-engineered trachea using sheep nasal chondrocyte and epithelial cells. *The FASEB journal* **2003**, *17* (8), 823-828.
162. <http://www.siumed.edu/~dking2/intro/ct.htm#blood> Connective tissue study guide.

-
163. McAnulty, R. J., Fibroblasts and myofibroblasts: their source, function and role in disease. *The international journal of biochemistry & cell biology* **2007**, *39* (4), 666-671.
164. Alberts, B.; Johnson, A.; Lewis, J.; Morgan, D.; Raff, M.; Roberts, K.; Walter, P., *Molecular biology of the cell*. Sixth ed.; Garland Science, Taylor & Francis Group: New York, 2015.
165. Tettamanti, G.; Grimaldi, A.; Rinaldi, L.; Arnaboldi, F.; Congiu, T.; Valvassori, R.; Eguileor, M., The multifunctional role of fibroblasts during wound healing in *Hirudo medicinalis* (Annelida, Hirudinea). *Biology of the Cell* **2004**, *96* (6), 443-455.
166. Ebert, T.; Bander, N.; Finstad, C.; Ramsawak, R.; Old, L., Establishment and characterization of human renal cancer and normal kidney cell lines. *Cancer research* **1990**, *50* (17), 5531-5536.
167. Kaur, G.; Dufour, J. M., *Cell lines: Valuable tools or useless artifacts*. Taylor & Francis: 2012.
168. Nelson-Rees, W.; Daniels, D.; Flandermeyer, R., Cross-contamination of cells in culture. *Science* **1981**, *212* (4493), 446-452.
169. Jiang, L.; Zeng, X.; Wang, Z.; Chen, Q., Cell line cross-contamination: KB is not an oral squamous cell carcinoma cell line. *European journal of oral sciences* **2009**, *117* (1), 90-91.
170. Fleckenstein, E.; Uphoff, C.; Drexler, H., Effective treatment of mycoplasma contamination in cell lines with enrofloxacin (Baytril). *Leukemia* **1994**, *8* (8), 1424-1434.
171. Hay, R.; Macy, M.; Chen, T., Mycoplasma infection of cultured cells. *Nature* **1989**, *339* (6224), 487-488.
172. CHIScientific, *Handbook of primary cell culture*. USA, 2007; p 1-484.
173. Badylak, S. F. In *The extracellular matrix as a scaffold for tissue reconstruction*, Seminars in cell & developmental biology, Elsevier: 2002; pp 377-383.
174. LeBaron, R. G.; Athanasiou, K. A., Extracellular matrix cell adhesion peptides: functional applications in orthopedic materials. *Tissue engineering* **2000**, *6* (2), 85-103.
175. Perlin, L.; MacNeil, S.; Rimmer, S., Production and performance of biomaterials containing RGD peptides. *Soft Matter* **2008**, *4* (12), 2331-2349.
176. Tang, L.; Thevenot, P.; Hu, W., Surface chemistry influences implant biocompatibility. *Current topics in medicinal chemistry* **2008**, *8* (4), 270-280.
177. Zeng, M.; Zhou, D.; Ng, S.; Ahern, J. O.; Alshehri, F.; Gao, Y.; Pierucci, L.; Greiser, U.; Wang, W., Highly Branched poly (5-amino-1-pentanol-co-1, 4-butanediol diacrylate) for High Performance Gene Transfection. *Polymers* **2017**, *9* (5), 161.

178. Kainthan, R. K.; Janzen, J.; Levin, E.; Devine, D. V.; Brooks, D. E., Biocompatibility testing of branched and linear polyglycidol. *Biomacromolecules* **2006**, *7* (3), 703-709.
179. Lee, W. H.; Loo, C. Y.; Chrzanowski, W.; Rohanizadeh, R., Osteoblast response to the surface of amino acid-functionalized hydroxyapatite. *Journal of Biomedical Materials Research Part A* **2015**, *103* (6), 2150-2160.
180. Lee, J. Y.; Schmidt, C. E., Amine-functionalized polypyrrole: Inherently cell adhesive conducting polymer. *Journal of Biomedical Materials Research Part A* **2015**, *103* (6), 2126-2132.
181. Lee, J.-W.; Serna, F.; Nickels, J.; Schmidt, C. E., Carboxylic acid-functionalized conductive polypyrrole as a bioactive platform for cell adhesion. *Biomacromolecules* **2006**, *7* (6), 1692-1695.
182. Faucheux, N.; Schweiss, R.; Lützow, K.; Werner, C.; Groth, T., Self-assembled monolayers with different terminating groups as model substrates for cell adhesion studies. *Biomaterials* **2004**, *25* (14), 2721-2730.
183. CoxNowak, K.; AlYamani, O.; Grant, C.; Green, N.; Rimmer, S., Poly (n-butyl Methacrylate) with Primary Amine End Groups for Supporting Cell Adhesion and Proliferation of Renal Epithelial Cells. *International Journal of Polymeric Materials and Polymeric Biomaterials* **2017**, (just-accepted).
184. Ma, A.; Zhao, B.; Bentley, A. J.; Brahma, A.; MacNeil, S.; Martin, F. L.; Rimmer, S.; Fullwood, N. J., Corneal epithelialisation on surface-modified hydrogel implants. *Journal of Materials Science: Materials in Medicine* **2011**, *22* (3), 663-670.
185. Nakajima, N.; Ikada, Y., Mechanism of amide formation by carbodiimide for bioconjugation in aqueous media. *Bioconjugate chemistry* **1995**, *6* (1), 123-130.
186. Betts, M. J.; Russell, R. B., Amino acid properties and consequences of substitutions. *Bioinformatics for geneticists* **2003**, *317*, 289.
187. Errington, N.; Doig, A. J., A phosphoserine-lysine salt bridge within an α -helical peptide, the strongest α -helix side-chain interaction measured to date. *Biochemistry* **2005**, *44* (20), 7553-7558.
188. Kagan, H. M.; Li, W., Lysyl oxidase: properties, specificity, and biological roles inside and outside of the cell. *Journal of cellular biochemistry* **2003**, *88* (4), 660-672.
189. Lucero, H.; Kagan, H., Lysyl oxidase: an oxidative enzyme and effector of cell function. *Cellular and Molecular Life Sciences CMLS* **2006**, *63* (19-20), 2304-2316.
190. Smith-Mungo, L. I.; Kagan, H. M., Lysyl oxidase: properties, regulation and multiple functions in biology. *Matrix biology* **1998**, *16* (7), 387-398.
191. Yan, D.; Gao, C.; Frey, H., *Hyperbranched polymers: synthesis, properties, and applications*. John Wiley & Sons: 2011; Vol. 8.

192. Wang, K.; Peng, H.; Thurecht, K. J.; Puttick, S.; Whittaker, A. K., Segmented highly branched copolymers: Rationally designed macromolecules for improved and tunable 19f mri. *Biomacromolecules* **2015**, *16* (9), 2827-2839.
193. Han, J.; Li, S.; Tang, A.; Gao, C., Water-soluble and clickable segmented hyperbranched polymers for multifunctionalization and novel architecture construction. *Macromolecules* **2012**, *45* (12), 4966-4977.
194. Grechanovskii, V. A., Degree of Branching in Polymeric Chains. *Russian Chemical Reviews* **1969**, *38* (12), 987-1000.
195. De, P.; Sumerlin, B. S., Precision control of temperature response by copolymerization of di (ethylene glycol) acrylate and an acrylamide comonomer. *Macromolecular Chemistry and Physics* **2013**, *214* (2), 272-279.
196. Zhang, C.; Zhou, Y.; Liu, Q.; Li, S.; Perrier, S. b.; Zhao, Y., Facile synthesis of hyperbranched and star-shaped polymers by RAFT polymerization based on a polymerizable trithiocarbonate. *Macromolecules* **2011**, *44* (7), 2034-2049.
197. Fatma, N.; Ansari, W. H.; Panda, M., A systematic study of mixed surfactant solutions of a cationic ester-bonded dimeric surfactant with cationic, anionic and nonionic monomeric surfactants in aqueous media. *Journal of Surfactants and Detergents* **2013**, *16* (4), 609-620.
198. Panda, M.; Kamil, M., Polymer-Amphiphile Interactions: An Overview. *Eurasian Chemico-Technological Journal* **2017**, *19* (2), 99-113.
199. Mayo, F. R.; Lewis, F. M., Copolymerization. I. A basis for comparing the behavior of monomers in copolymerization; the copolymerization of styrene and methyl methacrylate. *Journal of the American Chemical Society* **1944**, *66* (9), 1594-1601.
200. Moad, G.; Solomon, D. H., *The chemistry of radical polymerization*. Elsevier: 2006.
201. Alfrey, T.; Price, C. C., Relative reactivities in vinyl copolymerization. *Journal of Polymer Science Part A: Polymer Chemistry* **1947**, *2* (1), 101-106.
202. Wypych, G., *Handbook of polymers*. Elsevier: 2016.
203. Johnson Jr, C. S., Diffusion ordered nuclear magnetic resonance spectroscopy: principles and applications. *Progress in Nuclear Magnetic Resonance Spectroscopy* **1999**, *34* (3-4), 203-256.
204. Ambrus, A.; Yang, D., Diffusion-ordered nuclear magnetic resonance spectroscopy for analysis of DNA secondary structural elements. *Analytical biochemistry* **2007**, *367* (1), 56-67.
205. Cherifi, N.; Khoukh, A.; Benaboura, A.; Billon, L., Diffusion-ordered spectroscopy NMR DOSY: an all-in-one tool to simultaneously follow side reactions, livingness and molar masses of polymethylmethacrylate by nitroxide mediated polymerization. *Polymer Chemistry* **2016**, *7* (33), 5249-5257.

206. Li, W.; Chung, H.; Daeffler, C.; Johnson, J. A.; Grubbs, R. H., Application of 1H DOSY for facile measurement of polymer molecular weights. *Macromolecules* **2012**, *45* (24), 9595-9603.
207. Maina, N. H.; Pitkänen, L.; Heikkinen, S.; Tuomainen, P.; Virkki, L.; Tenkanen, M., Challenges in analysis of high-molar mass dextrans: comparison of HPSEC, AsFIFFF and DOSY NMR spectroscopy. *Carbohydrate polymers* **2014**, *99*, 199-207.
208. Swift, T.; Hoskins, R.; Telford, R.; Plenderleith, R.; Pownall, D.; Rimmer, S., Analysis Using Size Exclusion Chromatography of poly (N-isopropyl acrylamide) using Methanol as an Eluent. *Journal of Chromatography A* **2017**.
209. Gu, K.; Onorato, J.; Xiao, S. S.; Luscombe, C. K.; Loo, Y.-L., Determination of the molecular weight of conjugated polymers with diffusion-ordered NMR spectroscopy. *Chemistry of Materials* **2018**.
210. Vitte, J.; Benoliel, A.; Pierres, A.; Bongrand, P., Is there a predictable relationship between surface physical-chemical properties and cell behaviour at the interface. *Eur Cell Mater* **2004**, *7*, 52-63.
211. Vadgama, P., 2 Surface biocompatibility. *Annual Reports Section " C"(Physical Chemistry)* **2005**, *101*, 14-52.
212. Desseaux, S.; Hinestrosa, J. P.; Schüwer, N.; Lokitz, B. S.; Ankner, J. F.; Kilbey, S. M.; Voitchovsky, K.; Klok, H.-A., Swelling Behavior and Nanomechanical Properties of (Peptide-Modified) Poly (2-hydroxyethyl methacrylate) and Poly (poly (ethylene glycol) methacrylate) Brushes. *Macromolecules* **2016**, *49* (12), 4609-4618.
213. Shintani, H., Modification of medical device surface to attain anti-infection. *Trends Biomater Artif Organs* **2004**, *18* (1), 1-8.
214. Deligianni, D. D.; Katsala, N. D.; Koutsoukos, P. G.; Missirlis, Y. F., Effect of surface roughness of hydroxyapatite on human bone marrow cell adhesion, proliferation, differentiation and detachment strength. *Biomaterials* **2000**, *22* (1), 87-96.
215. Lampin, M.; Warocquier-Clérout, R.; Legris, C.; Degrange, M.; Sigot-Luizard, M., Correlation between substratum roughness and wettability, cell adhesion, and cell migration. *Journal of biomedical materials research* **1997**, *36* (1), 99-108.
216. Mason, B. N.; Califano, J. P.; Reinhart-King, C. A., Matrix stiffness: A regulator of cellular behavior and tissue formation. In *Engineering Biomaterials for Regenerative Medicine*, Springer: 2012; pp 19-37.
217. Wong, J. Y.; Velasco, A.; Rajagopalan, P.; Pham, Q., Directed movement of vascular smooth muscle cells on gradient-compliant hydrogels. *Langmuir* **2003**, *19* (5), 1908-1913.
218. Zaari, N.; Rajagopalan, P.; Kim, S. K.; Engler, A. J.; Wong, J. Y., Photopolymerization in microfluidic gradient generators: microscale control of substrate compliance to manipulate cell response. *Advanced Materials* **2004**, *16* (23-24), 2133-2137.

219. Peyton, S. R.; Raub, C. B.; Keschrumus, V. P.; Putnam, A. J., The use of poly (ethylene glycol) hydrogels to investigate the impact of ECM chemistry and mechanics on smooth muscle cells. *Biomaterials* **2006**, *27* (28), 4881-4893.
220. Rogers, S.; Mandelkern, L., Glass transitions of the poly-(n-alkyl methacrylates). *The Journal of Physical Chemistry* **1957**, *61* (7), 985-991.
221. Lan, T.; Torkelson, J. M., Methacrylate-based polymer films useful in lithographic applications exhibit different glass transition temperature-confinement effects at high and low molecular weight. *Polymer* **2014**, *55* (5), 1249-1258.
222. Peleg, M., Mapping the stiffness-temperature-moisture relationship of solid biomaterials at and around their glass transition. *Rheologica Acta* **1993**, *32* (6), 575-580.
223. Smith, K. E.; Parks, S. S.; Hyjek, M. A.; Downey, S. E.; Gall, K., The effect of the glass transition temperature on the toughness of photopolymerizable (meth) acrylate networks under physiological conditions. *Polymer* **2009**, *50* (21), 5112-5123.
224. Zeng, H.; Huang, J.; Tian, Y.; Li, L.; Tirrell, M. V.; Israelachvili, J. N., Adhesion and Detachment Mechanisms between Polymer and Solid Substrate Surfaces: Using Polystyrene–Mica as a Model System. *Macromolecules* **2016**, *49* (14), 5223-5231.
225. Amiri, B.; Ghollasi, M.; Shahrousvand, M.; Kamali, M.; Salimi, A., Osteoblast differentiation of mesenchymal stem cells on modified PES-PEG electrospun fibrous composites loaded with Zn 2 SiO 4 bioceramic nanoparticles. *Differentiation* **2016**, *92* (4), 148-158.
226. Kurtz, S. M.; Devine, J. N., PEEK biomaterials in trauma, orthopedic, and spinal implants. *Biomaterials* **2007**, *28* (32), 4845-4869.
227. Bandyopadhyay, A.; Sengupta, S.; Das, T., *Hyperbranched Polymers for Biomedical Applications*. Springer: 2017.
228. Khalyavina, A.; Häußler, L.; Lederer, A., Effect of the degree of branching on the glass transition temperature of polyesters. *Polymer* **2012**, *53* (5), 1049-1053.
229. Parhi, P.; Golas, A.; Vogler, E. A., Role of proteins and water in the initial attachment of mammalian cells to biomedical surfaces: a review. *Journal of Adhesion Science and Technology* **2010**, *24* (5), 853-888.
230. Harnett, E. M.; Alderman, J.; Wood, T., The surface energy of various biomaterials coated with adhesion molecules used in cell culture. *Colloids and surfaces B: Biointerfaces* **2007**, *55* (1), 90-97.
231. Lim, J. Y.; Liu, X.; Vogler, E. A.; Donahue, H. J., Systematic variation in osteoblast adhesion and phenotype with substratum surface characteristics. *Journal of Biomedical Materials Research Part A* **2004**, *68* (3), 504-512.
232. Liu, X.; Lim, J. Y.; Donahue, H. J.; Dhurjati, R.; Mastro, A. M.; Vogler, E. A., Influence of substratum surface chemistry/energy and topography on the human fetal osteoblastic cell

- line hFOB 1.19: phenotypic and genotypic responses observed in vitro. *Biomaterials* **2007**, *28* (31), 4535-4550.
233. Lee, J. H.; Lee, H. B., A wettability gradient as a tool to study protein adsorption and cell adhesion on polymer surfaces. *Journal of Biomaterials Science, Polymer Edition* **1993**, *4* (5), 467-481.
234. Lee, J. N.; Jiang, X.; Ryan, D.; Whitesides, G. M., Compatibility of mammalian cells on surfaces of poly (dimethylsiloxane). *Langmuir* **2004**, *20* (26), 11684-11691.
235. Wang, Y.-W.; Wu, Q.; Chen, G.-Q., Reduced mouse fibroblast cell growth by increased hydrophilicity of microbial polyhydroxyalkanoates via hyaluronan coating. *Biomaterials* **2003**, *24* (25), 4621-4629.
236. Valamehr, B.; Jonas, S. J.; Polleux, J.; Qiao, R.; Guo, S.; Gschweng, E. H.; Stiles, B.; Kam, K.; Luo, T.-J. M.; Witte, O. N., Hydrophobic surfaces for enhanced differentiation of embryonic stem cell-derived embryoid bodies. *Proceedings of the National Academy of Sciences* **2008**, *105* (38), 14459-14464.
237. Bauer, S.; Park, J.; von der Mark, K.; Schmuki, P., Improved attachment of mesenchymal stem cells on super-hydrophobic TiO₂ nanotubes. *Acta Biomaterialia* **2008**, *4* (5), 1576-1582.
238. Geckeler, K. E.; Wacker, R.; Aicher, W. K., Biocompatibility correlation of polymeric materials using human osteosarcoma cells. *Naturwissenschaften* **2000**, *87* (8), 351-354.
239. Lee, J. H.; Khang, G.; Lee, J. W.; Lee, H. B., Interaction of different types of cells on polymer surfaces with wettability gradient. *Journal of colloid and interface science* **1998**, *205* (2), 323-330.
240. Hao, L.; Lawrence, J., *Laser surface treatment of bio-implant materials*. John Wiley and Sons: 2005.
241. Gentleman, M. M.; Gentleman, E., The role of surface free energy in osteoblast–biomaterial interactions. *International Materials Reviews* **2014**, *59* (8), 417-429.
242. Birdi, K., Adherence of bacteria to solid surfaces and the surface forces. *Journal of dentistry* **1979**, *7* (3), 230-234.
243. Bellon-Fontaine, M.-N.; Rault, J.; Van Oss, C., Microbial adhesion to solvents: a novel method to determine the electron-donor/electron-acceptor or Lewis acid-base properties of microbial cells. *Colloids and Surfaces B: Biointerfaces* **1996**, *7* (1), 47-53.
244. Bren, L.; English, L.; Fogarty, J.; Policoro, R.; Zsidi, A.; Vance, J.; Drelich, J.; Istephanous, N.; Rohly, K., Hydrophilic/electron-acceptor surface properties of metallic biomaterials and their effect on osteoblast cell activity. *Journal of adhesion science and technology* **2004**, *18* (15-16), 1711-1722.
245. Grassie, N.; MacCallum, J., Thermal and photochemical degradation of poly (n-butyl methacrylate). *Journal of Polymer Science Part A: Polymer Chemistry* **1964**, *2* (2), 983-1000.

246. Manring, L. E.; Sogah, D. Y.; Cohen, G. M., Thermal degradation of poly (methyl methacrylate). 3. Polymer with head-to-head linkages. *Macromolecules* **1989**, *22* (12), 4652-4654.
247. Bhagat, R.; Madras, G., Thermal and sonochemical degradation kinetics of poly (n-butyl methacrylate-co-alkyl acrylates): Variation of chain strength and stability with copolymer composition. *Polymer Engineering & Science* **2013**, *53* (7), 1542-1553.
248. Daraboina, N.; Madras, G., Thermal and photocatalytic degradation of poly (methyl methacrylate), poly (butyl methacrylate), and their copolymers. *Industrial & Engineering Chemistry Research* **2008**, *47* (18), 6828-6834.
249. Kyremateng, S. O.; Amado, E.; Kressler, J., Synthesis and characterization of random copolymers of (2, 2-dimethyl-1, 3-dioxolan-4-yl) methyl methacrylate and 2, 3-dihydroxypropyl methacrylate. *European polymer journal* **2007**, *43* (8), 3380-3391.
250. Elshereksi, N. W.; Mohamed, S. H.; Arifin, A.; Ishak, Z. A. M., Thermal characterisation of poly (methyl methacrylate) filled with barium titanate as denture base material. *Journal of Physical Science* **2014**, *25* (2), 15.
251. OHYAMA, A.; IMAI, Y., Differential scanning calorimetric study of acrylic resin powders used in dentistry. *Dental materials journal* **2000**, *19* (4), 346-351.
252. Maciejewska, M., Thermal properties of TRIM–GMA copolymers with pendant amine groups. *Journal of Thermal Analysis and Calorimetry* **2016**, *126* (3), 1777-1785.
253. Özlem, S.; Hacıoğlu, J., Thermal degradation of poly (n-butyl methacrylate), poly (n-butyl acrylate) and poly (t-butyl acrylate). *Journal of analytical and applied pyrolysis* **2013**, *104*, 161-169.
254. Behera, G. C.; Saha, A.; Ramakrishnan, S., Hyperbranched copolymers versus linear copolymers: A comparative study of thermal properties. *Macromolecules* **2005**, *38* (18), 7695-7701.
255. Kim, Y. H.; Beckerbauer, R., Role of end groups on the glass transition of hyperbranched polyphenylene and triphenylbenzene derivatives. *Macromolecules* **1994**, *27* (7), 1968-1971.
256. Sam Zhang, L. L., Ashok Kumar, *Materials Characterization Techniques*. 1 ed.; CRC press: Boca Raton, FL33487-2742, 2008; p 334.
257. Nuriel, S.; Liu, L.; Barber, A.; Wagner, H., Direct measurement of multiwall nanotube surface tension. *Chemical Physics Letters* **2005**, *404* (4), 263-266.
258. Rudawska, A.; Jacniacka, E., Analysis for determining surface free energy uncertainty by the Owen–Wendt method. *International Journal of Adhesion and Adhesives* **2009**, *29* (4), 451-457.
259. Katsikogianni, M.; Amanatides, E.; Mataras, D.; Missirlis, Y., Staphylococcus epidermidis adhesion to He, He/O₂ plasma treated PET films and aged materials: contributions

- of surface free energy and shear rate. *Colloids and Surfaces B: Biointerfaces* **2008**, *65* (2), 257-268.
260. Van Oss, C., Hydrophobicity of biosurfaces—origin, quantitative determination and interaction energies. *Colloids and Surfaces B: Biointerfaces* **1995**, *5* (3), 91-110.
261. Van Oss, C.; Chaudhury, M.; Good, R., Monopolar surfaces. *Advances in colloid and interface science* **1987**, *28*, 35-64.
262. Mittal, K. L., *Physicochemical aspects of polymer surfaces*. Springer: 1983; Vol. 1.
263. Chen, J.; Shen, L.; Zhang, M.; Hong, H.; He, Y.; Liao, B.-Q.; Lin, H., Thermodynamic analysis of effects of contact angle on interfacial interactions and its implications for membrane fouling control. *Bioresource technology* **2016**, *201*, 245-252.
264. Chevalier, S.; Chaudhury, M. K., Further Reflections on the Geometric Mean Combining Rule for Interfacial Tension. *Langmuir* **2015**, *31* (41), 11296-11304.
265. Grant, C. A.; Thomson, N. H.; Savage, M. D.; Woon, H. W.; Greig, D., Surface characterisation and biomechanical analysis of the sclera by atomic force microscopy. *Journal of the mechanical behavior of biomedical materials* **2011**, *4* (4), 535-540.
266. Tranchida, D.; Kiflie, Z.; Acierno, S.; Piccarolo, S., Nanoscale mechanical characterization of polymers by atomic force microscopy (AFM) nanoindentations: viscoelastic characterization of a model material. *Measurement Science and Technology* **2009**, *20* (9), 095702.
267. Childs, A.; Li, H.; Lewittes, D. M.; Dong, B.; Liu, W.; Shu, X.; Sun, C.; Zhang, H. F., Fabricating customized hydrogel contact lens. *Scientific reports* **2016**, *6*.
268. Thomson, L.; Law, F.; James, K.; Matthew, C.; Rushton, N., Biocompatibility of particulate polymethylmethacrylate bone cements: a comparative study in vitro and in vivo. *Biomaterials* **1992**, *13* (12), 811-818.
269. Langer, K.; Mutschler, E.; Lambrecht, G.; Mayer, D.; Troschau, G.; Stieneker, F.; Kreuter, J., Methylmethacrylate sulfopropylmethacrylate copolymer nanoparticles for drug delivery: Part III: Evaluation as drug delivery system for ophthalmic applications. *International journal of pharmaceutics* **1997**, *158* (2), 219-231.
270. Sun, Y.; Maughan, J.; Haigh, R.; Hopkins, S.; Wyman, P.; Johnson, C.; Fullwood, N.; Ebdon, J.; MacNeil, S.; Rimmer, S. In *Polymethacrylate networks as substrates for cell culture*, Macromolecular Symposia, Wiley Online Library: 2007; pp 137-148.
271. Al-Nasiry, S.; Geusens, N.; Hanssens, M.; Luyten, C.; Pijnenborg, R., The use of Alamar Blue assay for quantitative analysis of viability, migration and invasion of choriocarcinoma cells. *Human reproduction* **2007**, *22* (5), 1304-1309.
272. Rampersad, S. N., Multiple applications of Alamar Blue as an indicator of metabolic function and cellular health in cell viability bioassays. *Sensors* **2012**, *12* (9), 12347-12360.

273. Forsey, R. W.; Chaudhuri, J. B., Validity of DNA analysis to determine cell numbers in tissue engineering scaffolds. *Biotechnology letters* **2009**, *31* (6), 819-823.
274. Choksakulnimitr, S.; Masuda, S.; Tokuda, H.; Takakura, Y.; Hashida, M., In vitro cytotoxicity of macromolecules in different cell culture systems. *Journal of Controlled Release* **1995**, *34* (3), 233-241.
275. Fischer, D.; Li, Y.; Ahlemeyer, B.; Krieglstein, J.; Kissel, T., In vitro cytotoxicity testing of polycations: influence of polymer structure on cell viability and hemolysis. *Biomaterials* **2003**, *24* (7), 1121-1131.
276. Wolterbeek, H. T.; Van der Meer, A. J., Optimization, application, and interpretation of lactate dehydrogenase measurements in microwell determination of cell number and toxicity. *Assay and drug development technologies* **2005**, *3* (6), 675-682.
277. Cooper, G., *The Cell: A Molecular Approach*, 2nd edn. The Cell: A Molecular Approach. Sunderland, MA. USA: Sinauer Associates: 2000.
278. Liberio, M. S.; Sadowski, M. C.; Soekmadji, C.; Davis, R. A.; Nelson, C. C., Differential effects of tissue culture coating substrates on prostate cancer cell adherence, morphology and behavior. *PloS one* **2014**, *9* (11), e112122.
279. Rimmer, S.; Wilshaw, S.-P.; Pickavance, P.; Ingham, E., Cytocompatibility of poly (1, 2 propanediol methacrylate) copolymer hydrogels and conetworks with or without alkyl amine functionality. *Biomaterials* **2009**, *30* (13), 2468-2478.
280. Bhattacharyya, D.; Xu, H.; Deshmukh, R. R.; Timmons, R. B.; Nguyen, K. T., Surface chemistry and polymer film thickness effects on endothelial cell adhesion and proliferation. *Journal of Biomedical Materials Research Part A* **2010**, *94* (2), 640-648.
281. Bisson, I.; Kosinski, M.; Ruault, S.; Gupta, B.; Hilborn, J.; Wurm, F.; Frey, P., Acrylic acid grafting and collagen immobilization on poly (ethylene terephthalate) surfaces for adherence and growth of human bladder smooth muscle cells. *Biomaterials* **2002**, *23* (15), 3149-3158.
282. McClary, K. B.; Ugarova, T.; Grainger, D. W., Modulating fibroblast adhesion, spreading, and proliferation using self-assembled monolayer films of alkylthiolates on gold. *Journal of Biomedical Materials Research Part A* **2000**, *50* (3), 428-439.
283. De Luca, I.; Di Salle, A.; Alessio, N.; Margarucci, S.; Simeone, M.; Galderisi, U.; Calarco, A.; Peluso, G., Positively charged polymers modulate the fate of human mesenchymal stromal cells via ephrinB2/EphB4 signaling. *Stem cell research* **2016**, *17* (2), 248-255.
284. Xu, Y.; Takai, M.; Ishihara, K., Protein adsorption and cell adhesion on cationic, neutral, and anionic 2-methacryloyloxyethyl phosphorylcholine copolymer surfaces. *Biomaterials* **2009**, *30* (28), 4930-4938.
285. Drury, J. L.; Mooney, D. J., Hydrogels for tissue engineering: scaffold design variables and applications. *Biomaterials* **2003**, *24* (24), 4337-4351.

286. El-Sherbiny, I. M.; Yacoub, M. H., Hydrogel scaffolds for tissue engineering: Progress and challenges. *Global Cardiology Science and Practice* **2013**, 38.
287. Tsou, Y.-H.; Khoneisser, J.; Huang, P.-C.; Xu, X., Hydrogel as a bioactive material to regulate stem cell fate. *Bioactive Materials* **2016**, 1 (1), 39-55.
288. Lee, T. T.; García, J. R.; Paez, J. I.; Singh, A.; Phelps, E. A.; Weis, S.; Shafiq, Z.; Shekaran, A.; Del Campo, A.; García, A. J., Light-triggered in vivo activation of adhesive peptides regulates cell adhesion, inflammation and vascularization of biomaterials. *Nature materials* **2015**, 14 (3), 352-360.
289. Sun, Y.; Collett, J.; Fullwood, N. J.; Mac Neil, S.; Rimmer, S., Culture of dermal fibroblasts and protein adsorption on block copolymers of poly (butyl methacrylate-block-(2, 3 propanediol-1-methacrylate-stat-ethandiol dimethacrylate)). *Biomaterials* **2007**, 28 (4), 661-670.
290. Poole, J.; MacNeil, S.; Rimmer, S., Semicontinuous Emulsion Polymerization of Butyl Methacrylate and 1, 3-Butadiene in the Presence of Cyclodextrins and Cytocompatibility of Dicarboxylic Acid Telechelic Oligo (butyl Methacrylate) s Derived from Ozonolysis of the Latexes. *Macromolecular Chemistry and Physics* **2011**, 212 (18), 2043-2051.
291. Greenberg, C. S.; Birckbichler, P. J.; Rice, R. H., Transglutaminases: multifunctional cross-linking enzymes that stabilize tissues. *The FASEB Journal* **1991**, 5 (15), 3071-3077.
292. Folk, J., Transglutaminases. *Annual review of biochemistry* **1980**, 49 (1), 517-531.
293. Priglinger, S. G.; Alge, C. S.; Neubauer, A. S.; Kristin, N.; Hirneiss, C.; Eibl, K.; Kampik, A.; Welge-Lüssen, U., TGF- β 2-Induced Cell Surface Tissue Transglutaminase Increases Adhesion and Migration of RPE Cells on Fibronectin through the Gelatin-Binding Domain. *Investigative ophthalmology & visual science* **2004**, 45 (3), 955-963.
294. Eckert, R. L.; Kaartinen, M. T.; Nurminskaya, M.; Belkin, A. M.; Colak, G.; Johnson, G. V.; Mehta, K., Transglutaminase regulation of cell function. *Physiological reviews* **2014**, 94 (2), 383-417.
295. Zhu, Y.; Zhang, X.; Zhu, J.; Zhao, Q.; Li, Y.; Li, W.; Fan, C.; Huang, Q., Cytotoxicity of phenol red in toxicity assays for carbon nanoparticles. *International journal of molecular sciences* **2012**, 13 (10), 12336-12348.
296. Thomas, M. G.; Marwood, R. M.; Parsons, A. E.; Parsons, R. B., The effect of foetal bovine serum supplementation upon the lactate dehydrogenase cytotoxicity assay: important considerations for in vitro toxicity analysis. *Toxicology in Vitro* **2015**, 30 (1), 300-308.
297. Ren, T.; Yu, S.; Mao, Z.; Gao, C., A complementary density gradient of zwitterionic polymer brushes and NCAM peptides for selectively controlling directional migration of Schwann cells. *Biomaterials* **2015**, 56, 58-67.
298. Wightman, L.; Kircheis, R.; Rössler, V.; Carotta, S.; Ruzicka, R.; Kursá, M.; Wagner, E., Different behavior of branched and linear polyethylenimine for gene delivery in vitro and in vivo. *The journal of gene medicine* **2001**, 3 (4), 362-372.

299. Godbey, W.; Wu, K. K.; Mikos, A. G., Size matters: molecular weight affects the efficiency of poly (ethyleneimine) as a gene delivery vehicle. *Journal of biomedical materials research* **1999**, *45* (3), 268-275.
300. Nociari, M. M.; Shalev, A.; Benias, P.; Russo, C., A novel one-step, highly sensitive fluorometric assay to evaluate cell-mediated cytotoxicity. *Journal of immunological methods* **1998**, *213* (2), 157-167.
301. Quent, V.; Loessner, D.; Friis, T.; Reichert, J. C.; Hutmacher, D. W., Discrepancies between metabolic activity and DNA content as tool to assess cell proliferation in cancer research. *Journal of cellular and molecular medicine* **2010**, *14* (4), 1003-1013.
302. Ng, K. W.; Leong, D. T.; Hutmacher, D. W., The challenge to measure cell proliferation in two and three dimensions. *Tissue Engineering* **2005**, *11* (1-2), 182-191.
303. Bacakova, L.; Filova, E.; Parizek, M.; Ruml, T.; Svorcik, V., Modulation of cell adhesion, proliferation and differentiation on materials designed for body implants. *Biotechnology advances* **2011**, *29* (6), 739-767.
304. Van Wachem, P.; Beugeling, T.; Feijen, J.; Bantjes, A.; Detmers, J.; Van Aken, W., Interaction of cultured human endothelial cells with polymeric surfaces of different wettabilities. *Biomaterials* **1985**, *6* (6), 403-408.
305. Van Wachem, P.; Hogt, A.; Beugeling, T.; Feijen, J.; Bantjes, A.; Detmers, J.; Van Aken, W., Adhesion of cultured human endothelial cells onto methacrylate polymers with varying surface wettability and charge. *Biomaterials* **1987**, *8* (5), 323-328.
306. Lee, J. H.; Lee, S. J.; Khang, G.; Lee, H. B., The effect of fluid shear stress on endothelial cell adhesiveness to polymer surfaces with wettability gradient. *Journal of colloid and interface science* **2000**, *230* (1), 84-90.
307. Perumal, O.; Khandare, J.; Kolhe, P.; Kannan, S.; Lieh-Lai, M.; Kannan, R. M., Effects of Branching Architecture and Linker on the Activity of Hyperbranched Polymer– Drug Conjugates. *Bioconjugate chemistry* **2009**, *20* (5), 842-846.
308. Fomine, S.; Fomina, L.; Guadarrama, P. In *Synthesis, properties and molecular modeling of functional hyperbranched polymers and dendrimers*, Macromolecular Symposia, Wiley Online Library: 2003; pp 43-62.